

Technical University of Denmark (DTU)

Heterogeneously Catalysed Chemical Reactions in Carbon Dioxide Medium

Nikolai E. Musko

PhD-thesis

Supervisors: Georgios M. Kontogeorgis (DTU)
 Anker Degn Jensen (DTU)
 Jan-Dierk Grunwaldt (Karlsruhe Institute of Technology)

Department of Chemical and Biochemical Engineering

Combustion and Harmful Emission Control Research Centre

Centre for Energy Recourses Engineering

Lyngby, Denmark, 2012

Моим родителям посвящаю...

Preface

The present PhD-thesis summarises the results of research activities carried out at the Department of Chemical and Biochemical Engineering (The Technical University of Denmark, DTU) from July 2009 till September 2012.

This work has been supervised by prof. Jan-Dierk Grunwaldt (DTU, later Karlsruhe Institute of Technology, KIT, Germany), prof. Georgios M. Kontogeorgis from the Centre for Energy Recourses Engineering (DTU-CERE) and prof. Anker Degn Jensen from the Combustion and Harmful Emission Control Research Centre (DTU-CHEC), both centres at the Department of Chemical and Biochemical Engineering at DTU. A large part of the experimental work has been performed at the Institute of Catalysis Research and Technology and at the Institute for Technical Chemistry and Polymer Chemistry (KIT, Germany). Complementary studies were performed at the Institute for Chemical and Bioengineering (Swiss Federal Institute of Technology, Zurich, Switzerland) in the group of prof. Alfons Baiker.

The financial support was granted by The Danish Research Council for Technology and Production Sciences, project “Exploring new catalytic reactions in supercritical carbon dioxide as innovative and non-flammable reaction medium”, and the Technical University of Denmark. Experimental facilities at the Institute of Catalysis Research and Technology were established with the support by Karlsruhe Institute of Technology, Germany.

Some parts of the present thesis have been published in the following articles:

- Chapter 3 - N.E. Musko, A.D. Jensen, A. Baiker, J.-D. Grunwaldt, G.M. Kontogeorgis, *Fluid phase equilibria of the reaction mixture during the selective hydrogenation of 2-butenal in dense carbon dioxide*, Applied Catalysis A: General 443-444 (2012) 67-75.
- Chapter 4 - N.E. Musko, J.-D. Grunwaldt, *Heterogeneously Catalysed Aldol Reactions in Supercritical Carbon Dioxide as Innovative and Non-Flammable Reaction Medium*, Topics in Catalysis 54 (16-18) (2011) 1115-1123.
- Chapter 5 - L. Gharnati, N.E. Musko, A.D. Jensen, G.M. Kontogeorgis, J.-D. Grunwaldt, *Fluid phase equilibria during propylene carbonate synthesis from propylene oxide in carbon dioxide medium*, Journal of Supercritical Fluids (2012) submitted.

Summary

In this PhD-study the different areas of chemical engineering, heterogeneous catalysis, supercritical fluids, and phase equilibrium thermodynamics have been brought together for selected reactions. To exploit the beneficial properties of supercritical fluids in heterogeneous catalysis, experimental studies of catalytic chemical reactions in dense and supercritical carbon dioxide have been complemented by the theoretical calculations of phase equilibria using advanced thermodynamic models.

In the recent years, the use of compressed carbon dioxide as innovative, non-toxic and non-flammable, cheap, and widely available reaction medium for many practical and industrial applications has drastically increased. Particularly attractive are heterogeneously catalysed chemical reactions. The beneficial use of CO₂ is attributed to its unique properties at dense and supercritical states (at temperatures and pressures above the critical ones), i.e. when it combines both gas-like and liquid-like properties. In terms of practical use it means that CO₂ can be used as an effective solvent for reactants, while the viscosity and diffusion coefficients are close to those for gases, which minimises heat and mass transport limitations in case of heterogeneous catalysis.

Previous reports and the studies in the present thesis have shown that phase behaviour can play a crucial role in chemical reactions, especially when they are performed near the supercritical region of the reaction mixture. Experimental monitoring and determination of phase equilibria is very time consuming, expensive, and very often reveals very little information. However, these problems can be overcome when thermodynamic modelling is applied. The Cubic-Plus-Association Equation of State (CPA) was used throughout this study; therefore this model is discussed more extensively.

Heterogeneously catalysed hydrogenation reactions are considered to be quite well studied and established. However, the catalyst performance can alter significantly when

the reaction is performed in carbon dioxide medium. This effect was studied with the example of the selective hydrogenation of 2-butenal over palladium catalyst. It was found that the maximum conversion of 2-butenal is achieved when the reaction mixture exists in the near-critical region, or the so-called “expanded-liquid” phase. Some possible reasons for that have been proposed.

Aldol reactions are the complex processes that are very important for the chemical industry. Furthermore, multistep reactions performed in “one-pot” using multifunctional catalysts attract a lot of interest. Thus, a part of this thesis was devoted to performing the aldol reaction and the “one-pot” synthesis of aldol products starting from the selective hydrogenation of unsaturated aldehydes in carbon dioxide medium. It was found that supported tungstosilicic acid catalysts and acidic resin Amberlyst-15 are very effective for performing aldol reactions. The positive influence of temperature and CO₂-content on catalyst activity was studied. Furthermore, the “one-pot” synthesis with 2-butenal was performed using bifunctional and mixed catalysts. The reactions were studied in different reactor types and reaction conditions were optimised using CPA calculations. Extensive catalyst characterisation was carried out in order to understand the catalyst structure.

Carbon dioxide can play a dual role in some chemical reactions, i.e. as reaction medium and as one of the reactants. An example of this reaction is the synthesis of propylene carbonate from propylene oxide and CO₂. The study of the phase equilibrium in this case is more complex not only because the composition changes due to the chemical reaction, but also due to the constantly decreasing amount of solvent. Furthermore, organic carbonates have significantly lower solubility in CO₂ than reacting epoxides. In this part of the study, the influence of CO₂-content on the performance of the immobilized 1-hydroxyethyl-9-propyl-cyclicguanidinium bromide on SBA-15 (HEPCGBr/SBA-15) catalyst was investigated. The maximum conversion was observed in the transition region from the two- to one-phase state. This finding was supported by previous experimental studies. Thermodynamic calculations were shown to be extremely useful for the phase behaviour investigations.

The direct synthesis of dimethyl carbonate from methanol and CO_2 has been investigated for quite a long time, however hardly any sufficiently active catalysts have been found so far. Nevertheless, optimisation of the phase equilibria of the reaction mixture can make the process economically more feasible. Many different thermodynamic models of different capability and applicability have been applied for this task. The CPA model is an advanced model that accounts for complex interactions between associating molecules like water and methanol. It has been shown that CPA can satisfactorily describe any type of phase equilibria for the quaternary reaction mixture as well as ternaries and binaries that comprise it. This makes CPA a universal and very useful model for many practical applications.

All aforementioned studies have shown that supercritical fluids in heterogeneous catalysis complemented by thermodynamic modelling have an immense potential for further investigations.

Resumé på Dansk

I dette Ph.D.-studium blev de forskellige kemiteknikområder - heterogen katalyse, superkritiske væsker og fase­lige­vægtstermodynamik bragt sammen for udvalgte reaktioner. For at udnytte de gavnlige egenskaber af superkritiske væsker i heterogen katalyse blev eksperimentelle studier af katalytiske kemiske reaktioner i tæt og superkritisk kuldioxid suppleret med teoretiske beregninger af fase­lige­vægte ved hjælp af avancerede termodynamiske modeller.

I de seneste år er brugt af komprimeret kuldioxid som et innovativt, ugiftigt, ubrændbart, billigt og nemt tilgængeligt reaktionsmiddel for mange praktiske og industrielle anvendelser øget markant. Især attraktiv er heterogent katalyseret kemiske reaktioner. Fordelen ved kuldioxid ligger i de unikke egenskaber som den besidder i den tætte og superkritiske tilstand (ved temperaturer og tryk over det superkritiske punkt) idet dens gasagtige og væskeagtige egenskaber bliver kombineret. Fra den praktiske synsvinkel betyder det at kuldioxid kan bruges som opløsningsmiddel for reaktanter, samtidig med at dens viskositet og diffusionskoefficienter er tætte på dem for gasser og derved er varme- og massetransportbegrænsninger (relevante i den heterogene katalyse) minimeret.

Tidligere rapporter såvel som det nuværende arbejde har vist at faseforhold kan spille en afgørende rolle i kemiske reaktioner, især når de udføres i nærheden af reaktionsblandingens superkritiske faseområde. Eksperimentelle overvågning og bestemmelse af fase­lige­vægte er meget tidskrævende, dyrt og afslører tit meget lidt information. Dog kan disse problemer løses når termodynamisk modellering anvendes. Cubic-Plus-Association tilstandsligningen (CPA) blev anvendt i hele studiet; derfor er denne model diskuteret mere udførligt.

Heterogent katalyserede hydrogeneringsreaktioner anses for at være velundersøgt og -etableret. Katalysatorens ydeevne kan dog ændres væsentligt når reaktionen udføres i

kuldioxid som reaktionsmedium. Denne effekt blev undersøgt på den selektive hydrogenering af 2-butenal over en palladium-katalysator. Man har fundet at den maksimale omdannelse af 2-butenal opnås i en reaktionsblandingen i den nær-kritiske region eller den såkaldte "ekspanderede-flydende" fase. Mulige årsager til dette er blevet foreslået.

Aldolreaktioner er komplekse processer og de er meget vigtige for den kemiske industri. Desuden tiltrækker flertrins reaktioner, udført over multifunktionelle katalysatorer ved "one-pot" ("enkeltholder") tilgang, meget interesse. Således fokuserer en del af denne afhandling på udførelsen af aldolreaktionen og "one-pot"-syntesen af aldolprodukter, med udgangspunkt i den selektive hydrogenering af umættede aldehyder, i kuldioxid-medium. Det blev fundet, at bårne siliciumwolframsyre katalysatorer og den sure harpiks Amberlyst-15 er meget effektive til at udføre aldolreaktioner. Indflydelsen af temperatur og kuldioxidindhold på katalysatorydeevnen blev undersøgt. Desuden blev "one-pot"-syntesen med 2-butenal forskellige reaktortyper og reaktionsbetingelserne blev optimeret ved hjælp af CPA-beregninger. Omfattende katalysator karakterisering blev udført for at forstå katalysatorernes struktur.

Kuldioxid kan spille en dobbeltrolle i visse kemiske reaktioner, nemlig som reaktionsmedium og som en af reaktanterne. Et eksempel er syntesen af propylencarbonat fra propylenoxid og kuldioxid. Undersøgelsen af fase ligevægten i dette tilfælde er mere kompleks fordi udover ændringerne i sammensætningen er der en stadigt faldende mængde opløsningsmiddel. Udover det har organiske carbonater betydeligt lavere opløselighed i kuldioxid end epoxidet (reaktanten). I denne del af studiet blev indflydelsen af kuldioxidindhold undersøgt på ydeevnen af den SBA-15-immobiliserede 1-hydroxyethyl-9-propylcycloguanidiniumbromid (HEPCGBr/SBA-15) katalysator. Den maksimale omdannelse blev iagttaget i overgangen fra en to- til én-fasetilstand. Dette resultat blev støttet af tidligere eksperimentelle studier. Termodynamiske beregninger viste sig at være særdeles nyttige for undersøgelsen af faseforhold.

Den direkte syntese af dimethylcarbonat ud fra methanol og kuldioxid er blevet undersøgt i længere tid, men næppe tilstrækkeligt aktive katalysatorer er blevet fundet indtil nu. Ikke desto mindre kan optimering af reaktionsblandingerne fasevægte gøre processen økonomisk mere gennemførlig. Mange termodynamiske modeller med forskellige evner og anvendelighed er blevet anvendt til denne opgave. CPA-modellen er en avanceret model der tager komplekse vekselvirkninger mellem associerende molekyler som vand og methanol i betragtning. Det er blevet vist at CPA-modellen kan tilfredsstillende beskrive enhver type fasevægt for kvaternære reaktionsblandinger, såvel som de ternære og binære der udgør dem. Dette gør CPA-modellen til en universel og meget brugbar model for mange praktiske anvendelser.

Alle de nævnte studier har vist at superkritiske væsker i heterogen katalyse sammen med termodynamisk modellering har et potentiale for yderligere undersøgelser.

Table of Contents

	Chapter 1. General Introduction	1
1.1	Foreword	2
1.2	Supercritical fluids and their properties	2
1.3	Application of supercritical fluids in heterogeneous catalysis	3
1.4	Carbon dioxide in catalysis	5
1.5	Scope of the present PhD-project	7
1.6	References	9
	Chapter 2. Thermodynamic Modelling	11
2.1	Introduction	12
2.2	The classical models	14
2.3	Advances association models	18
2.4	The Cubic-Plus-Association Equation of State	21
2.5	Concluding Remarks	24
2.6	References	25
	Chapter 3. Selective Hydrogenation of 2-Butenal in Carbon Dioxide Reaction Medium	27
3.1	Introduction	28
3.2	Experimental	31
3.2.1	Catalyst preparation	31
3.2.2	Catalyst characterisation	31
3.2.3	Catalytic hydrogenation of 2-butenal	33
3.2.4	Phase behaviour measurements	33
3.3	Experimental results	35

3.3.1	Catalyst performance	35
3.3.2	Phase behaviour measurements	36
3.4	Modelling with the CPA equation of state	36
3.4.1	Pure fluids	36
3.4.2	Binary mixtures	37
3.4.3	CPA predictions for the multicomponent reaction system	41
3.5	Discussion	44
3.6	Conclusion	48
3.7	References	49

Chapter 4. Aldol Reactions in Dense and Supercritical Carbon

	Dioxide Reaction Medium	53
4.1	Introduction	54
4.2	Experimental	57
4.2.1	Materials	57
4.2.2	Catalyst preparation	57
4.2.3	Catalyst characterisation	59
4.2.4	Catalytic reactions	61
4.2.4.1	View cell	61
4.2.4.2	Batch reactors	62
4.2.4.3	Continuous-flow apparatus	62
4.2.5	Thermodynamic modelling with CPA	65
4.3	Results	66
4.3.1	Catalyst characterisation	66
4.3.2	Catalytic studies	73
4.4.	Discussion	82
4.5	Conclusion	88
4.6	References	89

Chapter 5. Fluid Phase Equilibria During the Synthesis of		
	Propylene Carbonate from Propylene Oxide and CO ₂	93
5.1	Introduction	94
5.2	Experimental	96
5.2.1	Catalyst preparation	96
5.2.1.1	Preparation of the mesoporous carrier SBA-15	96
5.2.1.2	Synthesis of [HEPCG]Br supported on SBA-15	97
5.2.2	Catalyst characterisation	98
5.2.3	Catalytic synthesis of propylene carbonate	99
5.3	Experimental results	99
5.3.1	Catalyst characterisation	99
5.3.2	Catalyst performance	102
5.4	Modelling with the CPA equation of state	102
5.4.1	Pure Fluid Parameters	103
5.4.2	Binary interaction parameters	104
5.4.3	CPA predictions for multicomponent reaction systems	105
5.5	Discussion	109
5.6	Conclusion	112
5.7	References	113
 Chapter 6. Experimental Determination and Modelling of the		
	Phase Behaviour for the Direct Synthesis of Dimethyl Carbonate	
	from Methanol and Carbon Dioxide	117
6.1	Introduction	118
6.2	Experimental	123
6.2.1	Setup description	123
6.2.2	Experimental procedure	123
6.3	Experimental results	124
6.4	Modelling with the CPA equation of state	125

6.4.1	Pure Fluids	125
6.4.2	Binary Mixtures	126
6.4.3	Prediction of the phase behaviour of ternary and multicomponent systems	131
6.4.4	Application	133
6.5	Discussion	135
6.6	Conclusion	139
6.7	References	139
	Chapter 7. General conclusions and outlook	143
	List of Symbols	147
	Acknowledgements	149
	Appendices: published papers	

Chapter 1

General Introduction

Abstract

The present PhD-thesis is devoted to the use of dense and supercritical carbon dioxide in heterogeneously catalysed reactions. The interest to supercritical fluids in catalysis has increased dramatically over the past decades. This is due to the unique combination of physicochemical properties of substances at the critical state, i.e. they behave both like liquids and gases. These properties, as well as other features of highly compressed phases, are discussed in this chapter. Furthermore, multiple effects can arise when supercritical fluids are used in chemical reactions over heterogeneous catalysts, which significantly affect the reaction. Most of the time it brings about elevated yield and conversion, however, in some cases the use of sc-fluids should be avoided, as it is discussed here. Immense interest is drawn to carbon dioxide as a very promising substance for the use in the supercritical state. Therefore, its properties, advantages and limitations for heterogeneous catalysis are presented in more detail. Carbon dioxide can also be used as a C1-building block in chemical syntheses while being the reaction medium in the same process, which increases its value. The final part of the chapter is focused on the aims of the present study, namely, reactions and processes that this PhD-project has been built upon.

1.1 Foreword

Dense and supercritical fluids have found their widespread applications in various processes in the chemical, pharmaceutical, and other industries. These processes involve not only physical transformations (like separation, extraction, etc.) [1-3], but also chemical reactions where supercritical medium can be both solvent and one of the reactants, e.g. Ref. [4]. A large number of review articles have been published so far summarising the recent advances in this area [1-23]. All the works highlight a huge potential for the further use of supercritical fluids in catalysis.

1.2 Supercritical fluids and their properties

The critical state of matter is achieved at the so-called critical temperature T_c and pressure P_c . Above these values the supercritical fluid exists only in one phase and it cannot be transformed into two non-solid phases by compressing or expanding it at a constant temperature. In other words, at the critical point the difference between gas and liquid phases disappears.

Dense and supercritical fluids, i.e. compounds at the near-critical point conditions, attract a lot of attention due to their unique physical properties. Namely, they combine both gas-like and liquid like properties, which are very tuneable, especially close to the critical point. As liquids sc-fluids possess similar values of density which depend on temperature and pressure. By changing the density of the fluid, its dissolution power can also be also changed dramatically. This makes sc-fluids attractive and effective solvents and reaction medium for many processes. Very often co-solvents may also be involved.

On the other hand, some properties of supercritical fluids resemble those for gases. For instance, dynamic and kinematic viscosities are normally lower than for the gaseous state, whereas diffusivity coefficients lie between those for gases and liquids, e.g. Ref. [18, 23].

Multiple phenomena occur during the transition from the multiphase to the critical and supercritical state. The most interesting one is the so-called clustering or local

density enhancement, which occurs when attractive forces rearrange the molecules locally to energetically favourable positions at low cost of free energy [23]. This brings about density fluctuations in the liquid and the frequency of such fluctuations are close to the visible light, which is visually observed as opalescence. When mixtures of different components are used, these effects become much more complex.

1.3 Application of supercritical fluids in heterogeneous catalysis

When substances in their critical state are used in heterogeneously catalysed reactions, the effects that arise are very different from those in conventional gas – liquid – solid catalyst reactions, due to the properties described above.

Firstly, all reactions in the near- and supercritical state occur at high pressures, and pressure in turn has a great impact on the chemical equilibrium. This can happen in two forms – the so-called thermodynamic and kinetic effects of pressure, Eq. 1.1 and 1.2, respectively [22].

$$\left(\frac{\partial \ln K_x}{\partial P}\right)_{T,x} = -\frac{\Delta V_r}{RT} \quad (1.1)$$

$$\left(\frac{\partial \ln k_x}{\partial P}\right)_{T,x} = -\frac{\Delta V^\ddagger}{RT} \quad (1.2)$$

In the first case, the reaction equilibrium constant, expressed in mole fractions, is dependent on the difference in the reaction volume before and after the reaction (Eq. 1.1). Elevated pressures may also affect the reaction rate constant in terms of the transition state theory (Eq. 1.2). According to this theory, the rate equilibrium constant of an elementary reaction, expressed via mole fractions, is dependent on the activation volume, which is expressed as the difference between the partial molar volume of the complex and the sum of those for the reactants. The partial molar volumes of the

components in the near-critical region can change dramatically, affecting thereby the reaction quite significantly.

Furthermore, the density fluctuations occurring at the critical point may significantly activate the intermolecular forces not only between the reactants and solvents, but also between the reaction mixture molecules, the catalyst surface, and active sites. This can lead to substantial intensification of chemical reactions [17].

As it was discussed above, the diffusivity and viscosity of supercritical fluids makes transport phenomena processes much more favourable compared to those in gases or liquids. Reactant molecules get easier access to active sites of a porous heterogeneous catalyst, whereas reactants are easily removed from the surface. Moreover, heat transfer also increases. Therefore the concentration and heat borders in supercritical fluids are minimised, as it is shown in Fig. 1.1.

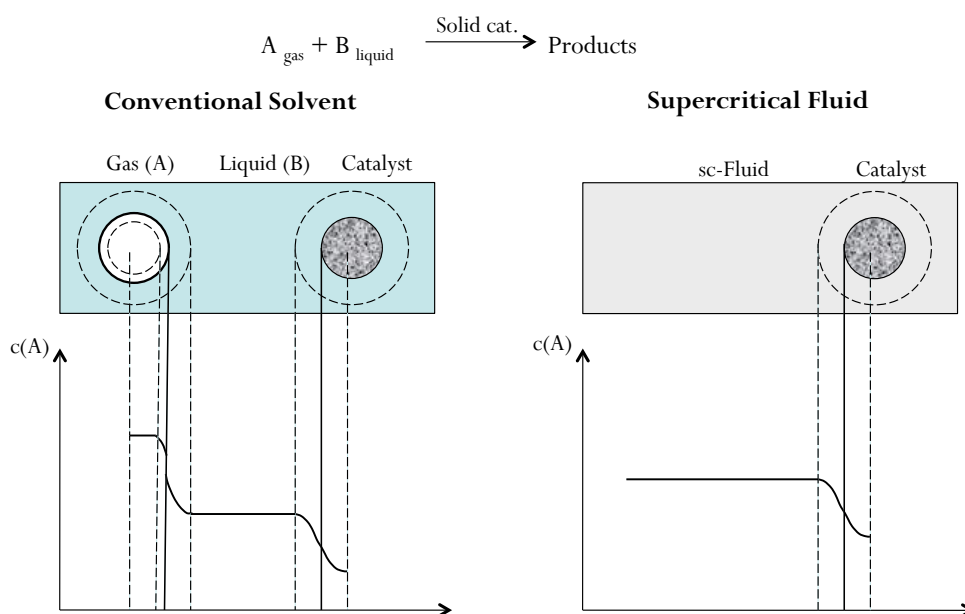


Fig. 1.1. Schematic representation of concentration profiles for the three phase reaction - between A in the gas phase and B in the liquid phase over a solid catalyst. On the left, there is a conventional way of performing this reaction with the concentration limitations at the gas-liquid border and at the liquid-solid catalyst border, including internal diffusion of reactants to the centre of a catalyst grain. On the right the same reaction is performed in the supercritical region, where the concentration of the gaseous reactant A is even in the reaction mixture and decreases only towards the centre of the catalyst grain.

Therefore, chemical processes can be effectively intensified due to the minimised mass and heat transfer limitations, due to the possible positive effect of pressure on the reaction equilibrium and kinetics, and the increased solubility of reactants in supercritical medium. Furthermore, heavy coke precursors or other side-products do not remain on the catalyst surface and block active sites – the reaction medium constantly removes them exposing the catalyst surface to new portions of the reactant. This significantly increases catalyst lifetime. Furthermore, the consequent separation processes become easier and much cheaper, compared to distillation, evaporation, etc., because for the majority of fluids simple depressurising and/or cooling are sufficient for phase splitting.

1.4 Carbon dioxide in catalysis

A number of fluids at the near and supercritical conditions have found their application for multiple purposes. Among the most widely used are carbon dioxide, ethane, ethene, propane, ammonia, methanol, ethanol, and water [4, 7, 17, 18]. However, CO₂ has attracted the particular attention in the recent years.

Carbon dioxide is a unique substance from many viewpoints. The liquid-like and gas-like properties of CO₂ in the condensed and supercritical phases are complemented by the fact that it is a non-toxic, cheap, widely available, inert, non-flammable, and environmentally benign substance. Its critical point ($T_c = 304.15$ K and $P_c = 73.8$ bar), unlike for instance for water ($T_c = 647.15$ K and $P_c = 220.6$ bar), is located at mild conditions, which is also beneficial from the economical perspective. The phase diagram of carbon dioxide is presented in Fig. 1.2.

As it was mentioned above, carbon dioxide has been used in numerous reactions, which include homogeneous catalysis [9], biocatalysis [10, 15], and heterogeneous catalysis [6, 7, 13, 24], as well as the reactions where it is one of the reactants. Almost all studies have shown that the use of carbon dioxide improves conversion and selectivity of the reactions compared to the conventional conditions.

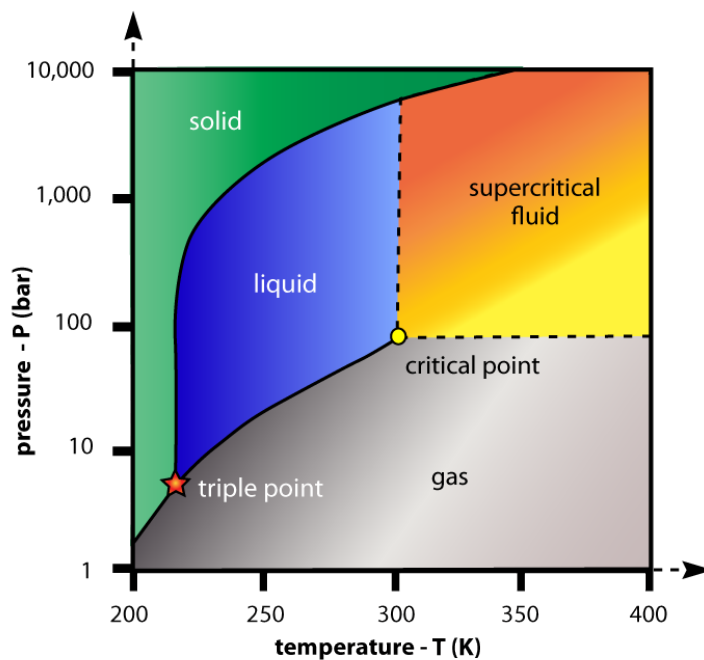


Fig. 1.2. Phase diagram of carbon dioxide [25], with the critical point at $T_c = 304.15$ K and $P_c = 73.8$ bar.

Nevertheless, the use of CO_2 in catalysis is limited by a number of factors, which also stem from its properties. Carbon dioxide molecules are non-polar, however they have a positively polarised carbon atom and two negatively polarised oxygen atoms. This fact explains the slightly acidic properties of CO_2 when interacting with other molecules. These interactions become especially well pronounced with the substances bearing base properties, like amines, NH_3 , etc. It may result in strong solvation of reactants, which impedes the reaction, and such acid-base interactions may block the active centres of base catalysts, depending on the conditions, e.g. Ref. [24]. Furthermore, since CO_2 is non-polar, it can be an effective solvent only for non-polar substances with low molecular weight. Its dissolution power for heavy, very polar, and associating components sometimes can be improved by the use of co-solvents, or simply extremely high concentrations of CO_2 can be used, but this is not always reasonable for practical applications.

Furthermore, generally speaking carbon dioxide is a very inert and stable substance, however, under certain conditions and in the presence of precious metals in

reducing atmosphere, it can react with other substances forming side products, e.g. carbon monoxide, water, etc., that can poison the catalyst [26-28].

1.5 Scope of the present PhD-project

As it was previously outlined, heterogeneous catalysis complemented by the use of carbon dioxide as reaction medium may result in extremely effective processes. For catalytic reactions in supercritical fluids the phase behaviour plays a very important role. There are quite a number of experimental techniques to investigate the phase equilibrium during chemical reaction [29], however, thermodynamic models [30] can be successfully used for the same purpose, which is further discussed in Chapter 2.

Amongst numerous catalytic reactions, particular interest cause multistep reactions performed over multifunctional catalysts in one reactor, like, for instance, the “one-pot” synthesis of 2-ethyl-2-hexenal from 2-butenal [31, 32]. This synthesis includes two consequent steps – selective hydrogenation of 2-butenal to butanal and its aldol reaction, which are performed with a bifunctional catalyst.

Firstly, the product that is yielded in this synthesis, 2-ethylhexanal, is of great practical importance [33, 34]. Secondly, the conventional technologies for aldol reactions are not very effective [35], and the use of active heterogeneous catalysis as well as supercritical fluids has been shown to have a great potential for process intensification [31, 32]. However, this has not been studied in detail. Therefore, this reaction has been chosen for the case study in this project.

Selective hydrogenation is the first step of the “one-pot” synthesis, and, in general, this reaction is extremely important and widespread in the fine chemical industry. Many attempts have been done to perform the hydrogenation of different substances over numerous catalysts in carbon dioxide medium, e.g. reviews [18, 23, 36]. A large number of catalysts have been developed so far for different hydrogenation reactions and they are very well established. However, the influence of the reaction media on the reaction performance as well as the mechanism were not always clear, therefore, in the present

study the selective hydrogenation of 2-butenal was investigated with respect to the influence of CO₂ medium and phase behaviour on catalyst performance.

As it was noted above, the aldol reaction technology has a lot of room for optimisation and improvement. Therefore, this study was further devoted to investigations of new types of catalysts for this reaction, as well as bifunctional catalysts for the “one-pot” synthesis.

Organic carbonates (dimethyl carbonate and propylene carbonate) are extremely important for the chemical industry and their synthesis from carbon dioxide is very attractive, though it has a lot of difficulties [37]. Here carbon dioxide is not only the reaction medium, but also a reactant. Furthermore, organic carbonates have very low solubility in CO₂. Consequently, the phase behaviour is extremely complex and very important. Hence, it was decided to study the influence of phase behaviour on the synthesis of propylene carbonate from propylene oxide and CO₂.

A similar reaction, the direct synthesis of dimethyl carbonate from methanol and CO₂, has many limitations, one of which is phase equilibrium [38]. In order to optimise the reaction conditions an advanced thermodynamic model is required. Therefore, the aim of this piece of study was to validate the Cubic-Plus-Association model for the synthesis of dimethyl carbonate.

In summary, the scope of the this PhD-thesis includes heterogeneously catalysed selective hydrogenation reactions of unsaturated aldehydes and aldol reactions in dense and supercritical carbon dioxide reaction medium, as well as the reactions where CO₂ is one of the reactants with the examples of the synthesis of propylene carbonate and dimethyl carbonate. In addition to catalytic investigations, thermodynamic modelling is applied in order to get insight into the phase equilibria during the reactions, and the effects that it causes.

1.6 References

- [1] D.A. Morgenstern, R.M. LeLacheur, D.K. Morita, S.L. Borkowsky, S. Feng, G.H. Brown, L. Luan, M.F. Gross, M.J. Burk, W. Tumas, ACS Symp. Ser. 626 (1996) 132-151.
- [2] S. Pereda, S.B. Bottini, E.A. Brignole, Appl. Catal., A 281 (2005) 129-137.
- [3] M. Nunes da Ponte, J. Supercrit. Fluids 47 (2009) 344-350.
- [4] P.G. Jessop, W. Leitner, Chemical Synthesis Using Supercritical Fluids, Wiley-VCH: Weinheim, 1999.
- [5] H. Hugl, M. Nobis, Top. Organomet. Chem. 23 (2008) 1-17.
- [6] X. Han, M. Poliakoff, Chem. Soc. Rev. 41 (2012) 1428-1436.
- [7] A. Kruse, H. Vogel, Chem. Eng. Technol. 31 (2008) 1391-1395.
- [8] P.G. Jessop, Drugs Pharm. Sci. 138 (2004) 461-495.
- [9] P.G. Jessop, J. Supercrit. Fluids 38 (2006) 211-231.
- [10] Y. Ikushima, Adv. Colloid Interface Sci. 71-72 (1997) 259-280.
- [11] P. Licence, J. Ke, M. Sokolova, S.K. Ross, M. Poliakoff, Green Chem. 5 (2003) 99-104.
- [12] W. Leitner, Acc. Chem. Res. 35 (2002) 746-756.
- [13] R. Ciriminna, M.L. Carraro, S. Campestrini, M. Pagliaro, Adv. Synth. Catal. 350 (2008) 221-226.
- [14] L.A. Blanchard, G. Xu, M.A. Stadtherr, J.F. Brennecke, Phase Behavior and Its Effects on Reactions and Processing in Green Chemistry Using Liquid and Supercritical Carbon Dioxide (eds. J. M. Desimone and W. Tumas), Oxford University Press Inc., 2003, pp. 3-16.
- [15] T. Matsuda, T. Harada, K. Nakamura, Curr. Org. Chem. 9 (2005) 299-315.
- [16] B. Subramaniam, C.J. Lyon, V. Arunajatesan, Appl. Catal., B 37 (2002) 279-292.
- [17] C.A. Eckert, K. Chandler, The 4th International Symposium on Supercritical Fluids, Sendai, Japan (1997) 799 - 806.
- [18] A. Baiker, Chem. Rev. 99 (1999) 453-473.

- [19] C. Smith, *Chem. Rev.* 16 (2007) 14-16.
- [20] B. Subramaniam, M.A. McHugh, *Ind. Eng. Chem. Proc. Des. Dev.* 25 (1986) 1-12.
- [21] R.A. Sheldon, *Green Chem.* 7 (2005) 267-278.
- [22] H. Tiltscher, H. Hofmann, *Chem. Eng. Sci.* 42 (1987) 959-977.
- [23] R. Wandeler, A. Baiker, *Cat. Tech.* 4 (2000) 34-50.
- [24] T. Seki, M. Onaka, *Catal. Surv. Asia* 10 (2006) 138-150.
- [25] Obtained from "<http://kb.eng-software.com/questions/426/Modeling+Systems+that+Contain+Supercritical+Fluids>", last accessed on 04.09.2012.
- [26] M. Burgener, D. Ferri, J.D. Grunwaldt, T. Mallat, A. Baiker, *J. Phys. Chem. B* 109 (2005) 16794-16800.
- [27] D. Ferri, T. Buergi, A. Baiker, *Phys. Chem. Chem. Phys.* 4 (2002) 2667-2672.
- [28] B. Minder, T. Mallat, K.H. Pickel, K. Steiner, A. Baiker, *Catal. Lett.* 34 (1995) 1-9.
- [29] J.-D. Grunwaldt, R. Wandeler, A. Baiker, *Catal. Rev. Sci. Eng.* 45 (2003) 1-96.
- [30] G.M. Kontogeorgis, G.K. Folas, *Thermodynamic Models for Industrial Applications: from classical and advanced mixing rules to association theories*, Wiley, 2010.
- [31] T. Seki, J.D. Grunwaldt, A. Baiker, *Chem. Commun.* (2007) 3562-3564.
- [32] J.G. Stevens, R.A. Bourne, M. Poliakoff, *Green Chem.* 11 (2009) 409-416.
- [33] H. Bahrmann, H.-D. Hahn, M. D., *Ullmann's Encyclopedia of Industrial Chemistry*, Wiley-VCH Verlag GmbH & Co. KGaA, Weinheim (2012) 579-583.
- [34] R. Mestres, *Green Chem.* 6 (2004) 583-603.
- [35] G. Duembgen, D. Neubauer, *Chemie Ing.-Tech.* (1969) 974-980.
- [36] T. Seki, J.-D. Grunwaldt, A. Baiker, *Ind. Eng. Chem. Res.* 47 (2008) 4561-4585.
- [37] T. Sakakura, J.C. Choi, H. Yasuda, *Chem. Rev.* 107 (2007) 2365-2387.
- [38] N. Keller, G. Rebmann, V. Keller, *J. Mol. Catal. A: Chem.* 317 (2010) 1-18.

Chapter 2

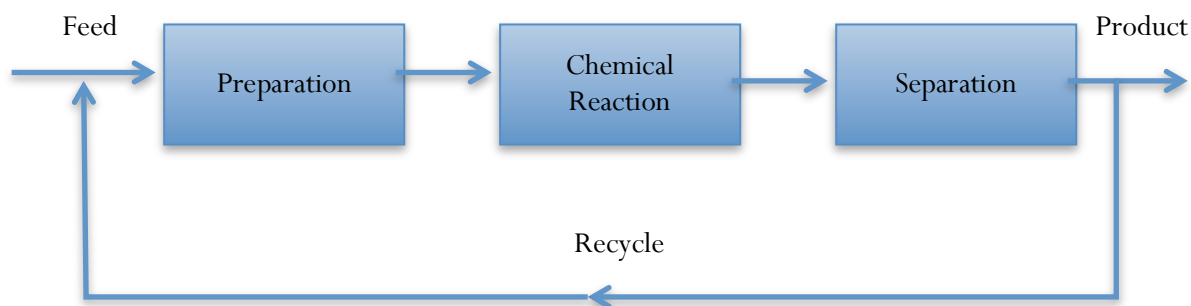
Thermodynamic Modelling

Abstract

In this chapter the importance of thermodynamics for industrial applications is covered, with the emphasis on modelling. It starts with a brief introduction to the problem of thermodynamic phase equilibria and continues with an overview of existing models that have been developed so far in order of their complexity, applicability, and capability, which often coincides with the historical order of their appearance. Equations of state are the core of the following discussion. Their main features, theoretical bases, limitations, etc. are presented. A brief discussion of other models, i.e. the activity coefficient models and the EoS/ G^E mixing rules, is also provided. At the end, the most advanced and powerful models are discussed together with their main characteristics. A large experimental part of the present PhD-project is complemented by thermodynamic calculations that have been made using the advanced model Cubic-Plus-Association Equation of State (CPA EoS), which is therefore presented here. The analysis of the literature has shown that there is no “universal” model that predicts any kind of phase equilibria and any thermodynamic properties for every mixture. Furthermore, depending on the purpose of modelling, type of systems, conditions, etc. “simple” models can be also successfully applied.

2.1 Introduction

Any industrial process can be divided into three basic steps: (i) feed preparation, (ii) chemical reaction, and (iii) product separation, sometimes including recycling, as it is shown in Scheme 2.1. Every step can include different types of processes involving various kinds of thermodynamic equilibria: vapour-liquid VLE (distillation, evaporation, absorption, etc.), liquid-liquid LLE (extraction), vapour-liquid-liquid VLLE (extractive, azeotropic distillation), solid-gas VSE (adsorption), solid-liquid LSE (leaching, crystallization, dissolution), etc. The number and complexity of the components that are often involved in the equilibrium can vary from inert gases to liquid hydrocarbons, polar protic and aprotic solvents (like pyridine, water, alcohols, organic acids, etc.), electrolytes, polymers, ionic liquids, biomolecules, and many other very complex compounds. The range of the conditions under which the aforementioned processes are performed can vary from ambient to supercritical, which normally exist at high temperatures and pressures.



Scheme 2.1. Typical industrial process.

Thermodynamics is the essential basis upon which the rest of any chemical technology is built. Regardless of the branch of industry, i.e. oil and gas, electrolytes, bulk and fine chemistry, pharmaceuticals, polymers, etc., the knowledge of thermodynamic data is crucial in order to design any technological scheme. Very often separation processes can make up the biggest part of the final cost. Therefore, the knowledge and the quality of the initial thermodynamic data are very important for the efficient process and product design, as well as the thermodynamic model applied for this purpose. Nowadays, there are many

thermodynamic models that can fulfil very different tasks. They are based on different principles, which will be discussed later, and very often their capabilities are limited only to certain types of tasks, systems, equilibria, components, etc.

Regardless of the type of equilibria, the number and complexity of components involved, there is the fundamental phase equilibria equation, which is used for solving any phase equilibria problem. The fugacities \hat{f} of all components in all phases α , β , γ , etc. in equilibria are equal: $\hat{f}_i^\alpha = \hat{f}_i^\beta = \hat{f}_i^\gamma = \dots$, where $i = 1, 2, \dots$ - the number of components. This basic equation may be written in many different forms depending on the type of phase equilibria and thermodynamic model employed for calculating fugacities, i.e. equations of state or activity coefficient models.

Equations of state (EoS) are thermodynamic models that can be expressed in form of functions $P = f(V, T)$ or $V = f(P, T)$. In principle, they can be used for any fluid phase, any number of components, and in a very wide range of temperature, pressure and concentration. First classical EoS together with van der Waals one-fluid mixing rules were suitable only for describing vapour-liquid equilibria of relatively simple systems. However, for complex types of equilibria, like liquid-liquid, solid-liquid, etc., a large number of activity coefficient models have been developed, and in many cases they are more convenient to use than cubic EoS since they were developed specifically for condensed phases. Furthermore, the use of activity coefficients is a very reasonable way of describing the non-ideality of mixtures. Ideal systems are formed by components with similar size and shape of the molecules, and intermolecular forces between like-components are similar to those between unlike-ones. Indeed, ideal systems are extremely scarce in real life and an overwhelming majority of mixtures used in the industry are non-ideal.

There are two classical approaches to solving the phase equilibria problem – the *gamma-phi* ($\gamma - \phi$) and *phi-phi* ($\phi - \phi$). The first approach implies the use of an activity coefficient model for liquid and/or solid phases and an EoS for vapour, whereas in the second approach an EoS is used for both.

Intermolecular interactions at given temperature and pressure are a decisive factor for a certain type of phase behaviour of the system, therefore, for its better understanding and for a reasonable choice of an appropriate thermodynamic model, it is important to consider the nature and main features of intermolecular forces between molecules in mixtures.

In order to represent intermolecular forces, different intermolecular potential functions $\Gamma(r)$ can be used. Very often these functions are directly introduced into thermodynamic models. The simplest one is the *hard sphere* potential, where attractive forces are ignored, and in many models this function is used as a purely repulsive potential. The most frequently used, however, are the *square-well* and *Lennard-Jones* potentials, where the distance dependency of potential energy is expressed in the same way as in the potential for van der Waals forces. All three potentials are summarised in Fig. 2.1.

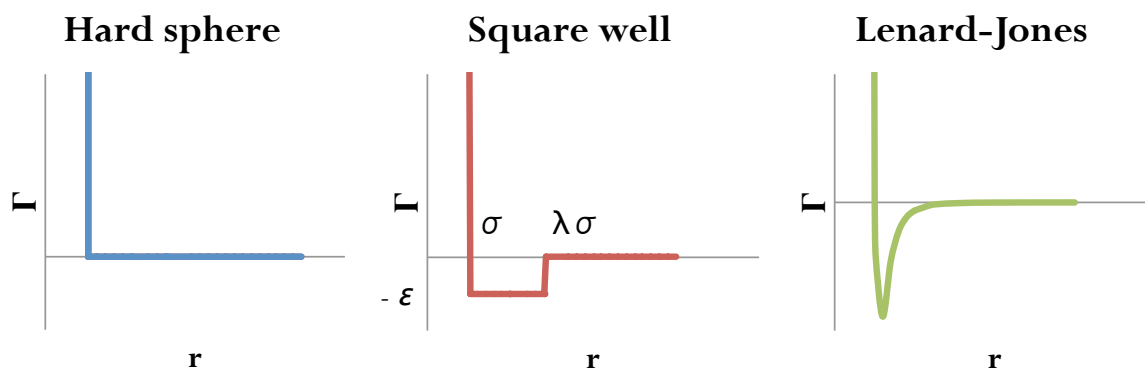


Fig. 2.1. Geometric profiles of different intermolecular potential functions.

2.2 The classical models

The classical thermodynamic models can be divided into three main groups – *equations of state*, the *activity coefficient* models, and the so-called *EoS/G^E* models, which combine the advantages of the first two.

Cubic Equations of State can predict thermodynamic properties at high pressures, i.e. pressures that significantly affect the properties of the system, normally higher than 15 – 20 bar. At high pressures interactions between molecules significantly increase,

therefore, the system becomes more and more non-ideal, especially this is the case for condensed phases.

The most well-known and widely applied models in engineering calculations are the van der Waals (vdW) [1], the Soave-Redlich-Kwong (SRK) [2], and Peng-Robinson (PR) [3] equations, which are presented in Table 2.1. These models typically use critical temperature T_c and critical pressure P_c as pure fluid parameters, while SRK and PR also use an additional parameter – acentric factor ω , which shows how far the molecule shape is from spherical one.

Table 2.1. Classical equations of state with the parameters.

Van der Waals	Soave-Redlich-Kwong	Peng-Robinson
$P = \frac{RT}{V-b} - \frac{a}{V^2}$	$P = \frac{RT}{V-b} - \frac{a(T)}{V(V+b)}$	$P = \frac{RT}{V-b} - \frac{a(T)}{V(V+b) + b(V-b)}$
Parameters		
$a = \frac{27}{64} \frac{(RT_c)^2}{P_c}$	$a_c = 0.42748 \frac{(RT_c)^2}{P_c}$	$a_c = 0.45724 \frac{(RT_c)^2}{P_c}$
$b = \frac{1}{8} \frac{RT_c}{P_c}$	$b = 0.08664 \frac{RT_c}{P_c}$	$b = 0.07780 \frac{RT_c}{P_c}$
	$a(T) = a_c [1 + m(1 - \sqrt{T_r})]^2$	$a(T) = a_c [1 + m(1 - \sqrt{T_r})]^2$
	$m = 0.48 + 1.574\omega - 0.176\omega^2$	$m = 0.37464 + 1.54226\omega - 0.26992\omega^2$
	$T_r = T/T_c$	$T_r = T/T_c$

Cubic equations of state can be expressed in terms of third power with respect to volume. The largest value of V represents the molar volume of the vapour phase and the smallest one is the liquid phase volume. All equations of state include attractive and repulsive terms, and they are built upon the *corresponding state principle*, which states that all fluids at the same reduced temperature and pressure have the same compressibility factor $Z = PV/RT$.

Equations in Table 2.1 represent a classical way of estimating the pure fluid parameters, which is based on critical pressure and temperature and acentric factor of components. In order to extend cubic EoS to mixtures, mixing rules have to be employed.

The *van der Waals one-fluid* (vdW1f) mixing rules are quite widely used for many practical applications, Table 2.2. They imply quadratic composition dependency for both energy and co-volume parameters in EoS, and the classical combining rules for the cross-energy (the geometric mean rule) and cross-co-volume (the arithmetic mean rule) parameters are often used.

Table 2.2. Van der Waals one-fluid mixing and combining rules.

Mixing rules	Combining rules
$a = \sum_{i=1}^N \sum_{j=1}^N x_i x_j a_{ij}$	$a_{ij} = \sqrt{a_i a_j} (1 - k_{ij})$
$b = \sum_{i=1}^N \sum_{j=1}^N x_i x_j b_{ij}$	$b_{ij} = \frac{b_i + b_j}{2} (1 - l_{ij})$

In the aforementioned mixing rules there are two adjustable interaction parameters k_{ij} and l_{ij} , however, very often only k_{ij} is sufficient, whereas l_{ij} is set to 0. The convenient way of obtaining k_{ij} and l_{ij} by fitting the model to experimental phase equilibrium data, however, for some relatively simple mixtures they can be also correlated [4]. Interaction parameter k_{ij} is temperature dependent and it decreases with temperature, since interatomic forces become less important at elevated temperatures. It also indirectly reflects the non-ideality of the mixture for which it was estimated. In most cases k_{ij} has positive values, which means that molecules of the same kind tend to interact between themselves rather than with the other kind (e.g. methanol – water), whereas negative values of k_{ij} reflect strong interactions between the molecules of different kind (e.g. chloroform – acetone).

Equations of state with parameters estimated using critical temperature and pressure together with classical mixing and combining rules (vdW1f) are quite simple thermodynamic models and applicable for many practical tasks. For simple systems of gases and hydrocarbons they give very good predictions for multicomponent VLE in a

wide range of temperature and pressure [5]. Nevertheless, there are a number of limitations for Cubic EoS [6]. For example, they fail to predict complex VLE, LLE for multicomponent systems with polar compounds. Almost always an interaction parameter is required and sometimes two adjustable parameters k_{ij} and l_{ij} are required for obtaining satisfactory correlation of VLE, and in some cases k_{ij} has to be temperature-dependent. Classical EoS cannot be easily used for complex molecules e.g. electrolytes and biomolecules. Cubic EoS can predict well vapour-liquid equilibria (VLE) for many mixtures. Such models perform less satisfactorily for liquid densities but VLE is determined by accurate vapour pressures and these are described well by cubic equations of state.

In chemical engineering there are a huge number of multicomponent mixtures (including highly polar compounds), which work at low pressures. The *activity coefficient* models are far more convenient for such systems compared to equations of state. There are two types of activity coefficient models – the so-called “*random-mixing*” and the theoretically based *local composition (LC)* models [6]. The second type is far more widely used, and includes models like Wilson [7], NRTL [8], UNIQUAC [9], and UNIFAC [10].

Equations of state and activity coefficient models have their own limits of applicability. In this regard, cubic equations of state can predict equally well systems at low and high pressures, whereas activity coefficient models work only for low-pressure equilibria. Multicomponent mixtures with polar compounds, very often LLE, are much better described using activity coefficient models. Moreover, they can make predictions (e.g. UNIFAC) using group contribution methods, which is not the case for equations of state.

The combined approach, i.e. EoS/G^E , uses advantages of both types of models, i.e. this type of models appear to be very suitable for phase equilibria of multicomponent mixtures of polar and non-polar compounds at low and high pressures [6]. Basically this is just another type of mixing rules for the energy parameter in equations of state, which introduces the expression for the excess Gibbs energy g^E via an activity coefficient model into an equation of state. The EoS/G^E models have been very successful since they

broadened the range of applicability of EoS to polar components and multicomponent mixtures and they extended activity coefficient models to high pressures. Still, there are systems where even this advanced approach does not perform satisfactorily – associating components, complex multiphase equilibria, solids, LLE, etc.

2.3 Advances association models

As mentioned, there are numerous thermodynamic models which are applicable only for a certain range of conditions (low or high pressures), types of equilibria (VLE, LLE, etc.), phases (vapour, liquid, solid), number and type of components (polar or non-polar), etc. However, even the most sophisticated among those, the so-called EoS/ G^E models, have problems predicting complex phase equilibria for multicomponent mixtures of polar components, especially those that are prone to association.

The reason lies in the nature of intermolecular interactions. The aforementioned models account directly for van der Waals interactions, however, the presence of quasi-chemical forces, i.e. hydrogen bonds, can significantly affect phase behaviour. The complexity of mixtures also goes beyond of what classical models are capable of. Industrially important mixtures very often contain tens, hundreds and even thousands of components (e.g. in the oil industry). Therefore, there is a need for approaches, theories, new terms and mathematical expressions in thermodynamic models, etc. that can take into account quasi-chemical interactions between components.

A large number of such models actually have been developed [11, 12], and they are called *association models* since they describe phase equilibria of mixtures of highly polar and/or strongly associating components prone to self- and cross-association, i.e. association with the same kind molecules (e.g. water-water) and between different molecules (e.g. water-methanol), respectively.

Many association models have two basic parts, i.e. the physical term accounting for physical interactions between molecules and the association term that considers

association. In practice, however, it is not always possible to separate these interactions. In terms of compressibility factor it can be expressed as $Z = Z^{\text{physical}} + Z^{\text{association}}$.

The association contribution, that describes the formation of hydrogen bonds between molecules, can be based on one of the three theories:

1. *Chemical Theories* [13] which are based on the assumption that interacting molecules form oligomers with the same properties that monomers have, and the extent of oligomerisation depends on density, temperature, and composition.
2. *Lattice Theories* [14] built upon the idea that molecules (their certain parts) in two adjacent layers can form bonds with each other. The number of these bonds reflects the extent of association.
3. *Perturbation Theories* [15] which account for number of association sites per one molecule and the total association energy (energy of hydrogen bonding) is calculated from statistical mechanics.

The most frequently used advanced models like SAFT models and CPA, which will be discussed later, use the association terms based on the perturbation theory. These association terms are based on the Wertheim's theory [16-19], which is basically a model for systems with a repulsive core and attractive sites that can form chains and closed rings. The key relation in this theory is between the residual Helmholtz energy due to association and the fraction of molecules not bonded at a specific site X^A , which is related to the association strength Δ^{AB} , where A and B indicate two different sites.

In the perturbation theory the activity of each site is independent of bonding at other sites on the same molecule. The repulsive cores prevent bonding of two molecules on the same site. The strength of association Δ^{AB} is represented by a square-well potential (like the one in Fig. 2.2), which has two characteristics – the association energy $\epsilon^{A_i B_j}$ (the well depth) and the association volume $\kappa^{A_i B_j}$ or $\beta^{A_i B_j}$ (the well width).

As it was mentioned above, the key property in association theories is the fraction of molecules, present as monomers, not bonded to any association site. If there are two association sites A and B in a molecule and their activity is assumed to be independent of

bonding at the other sites of the same molecule, the fraction of monomers will be $X_1 = X^A X^B = (X^A)^2$, if $X^A = X^B$. The general expression for the monomer mole fraction (i.e. of non-bonded molecules) is $X_1 = \prod_K X^K$, where K is the number of sites. Equation 2.24 is valid for example for alcohols, which have two association sites. In the case of water that has four equal sites, the monomer fraction is $X_1 = X^A X^B X^C X^D = (X^A)^4$. Therefore, depending on the number and type of association sites, different *association schemes* and, therefore, different expressions for monomer fractions can be used [20].

The monomer mole fraction, as discussed above, is a key property when it comes down to interpreting association processes in fluids, and the validity of the theories has been also tested against experimental spectroscopic data [6]. Different kinds of spectroscopy (infrared, nuclear magnetic resonance, etc.) can be used in order to determine experimentally the number of monomers in associating fluids and compare it with theoretical predictions.

The first theoretically derived model successfully taking into account association between molecules and based on the perturbation theory was the Statistical Associating Fluid Theory SAFT [16-19] Equation of State with its original form presented in Ref. [20, 21].

In the SAFT model any molecule is presented as a particle consisting of chain and associating sites. At the first step each fluid is seen as a hard-sphere fluid. Then, attractive forces and chain sites are added, thereby forming the molecules. At a next step, association sites appear on the molecules and associates are formed through the association sites. At each step a contribution to the residual Helmholtz energy is made, i.e. $a^{\text{res}} = a^{\text{seg}} + a^{\text{chain}} + a^{\text{assoc}}$, where a^{seg} is the Helmholtz energy of the initial segments (hard spheres), a^{chain} is the contribution from the chain formation, and a^{assoc} - the contribution from the formation of the associates.

Every pure component in SAFT is characterised by the length of chains m (the number of segments in the molecule), the size σ and energy ϵ parameters of a segment.

There are two additional parameters in the case of association – the association energy $\epsilon^{A_i B_j}$ and volume $\kappa^{A_i B_j}$. The last two parameters could be estimated from molecular quantum-mechanics calculations or based on the enthalpy and entropy of hydrogen bonding. All five parameters of SAFT are usually fitted to experimental vapour pressure and liquid density data.

Therefore, the SAFT models can be treated as models accounting for hydrogen bonding in a theoretically derived and correct way. The SAFT models provide often excellent results when describing complex multicomponent equilibria of polar and associating components (like water, alcohols, organic acids) [6]. Low and high pressure VLE, VLLE, LLE, etc. can be described satisfactorily. Still, for electrolytes, biomolecules and certain other complex molecules, changes in the model and/or additional terms may be required.

2.4 The Cubic-Plus-Association Equation of State

The CPA EoS [15, 22] combines two terms – the Soave-Redlich-Kwong EoS (Table 2.1) and the association term similar to that in the SAFT models, discussed above. In terms of compressibility factor it can be expressed as $Z^{CPA} = Z^{SRK} + Z^{assoc}$, where $Z = PV/RT$.

The idea was to extend a classical model like SRK, which had found widespread applications for important industrial systems, to more complex associating mixtures, using the theoretically correct association term taken from SAFT.

CPA can be written in terms of pressure for mixtures:

$$P = \frac{RT}{V - b} - \frac{a(T)}{V(V + b)} - \frac{1}{2} \frac{RT}{V} \left(1 + \rho \frac{\partial \ln g}{\partial \rho} \right) \sum_i x_i \sum_{A_i} (1 - X_{A_i}) \quad (2.1)$$

where X_{A_i} is the fraction of sites A on molecule i that do not form bonds with other association sites, x_i – is the mole fraction of component i and ρ is molar density (i.e.

1/V). Furthermore, X_{A_i} can be determined as follows:

$$X_{A_i} = \frac{1}{1 + \rho \sum_j X_j \sum_{B_j} X_{B_j} \Delta^{A_i B_j}} \quad (2.2)$$

where $\Delta^{A_i B_j}$ is the association strength which includes the association energy $\varepsilon^{A_i B_j}$ and volume $\beta^{A_i B_j}$:

$$\Delta^{A_i B_j} = g(\rho) \left[\exp\left(\frac{\varepsilon^{A_i B_j}}{RT}\right) - 1 \right] b_{ij} \beta^{A_i B_j} \quad (2.3)$$

$b_{ij} = (b_i + b_j)/2$, $g(\rho) = (1 - 1.9\eta)^{-1}$ - the radial distribution function with $\eta = 0.25b\rho$. The energy parameter a in the physical term of CPA is temperature dependent:

$$a(T) = a_0 \left(1 + c_1 \left(1 - \sqrt{T/T_c} \right) \right)^2 \quad (2.4)$$

From equations 2.1 – 2.4 it can be seen that the physical term of CPA has three pure fluid parameters - a_0 , b , and c_1 and together with two parameters from the association term – association energy $\varepsilon^{A_i B_j}$ and volume $\beta^{A_i B_j}$ they constitute the five pure fluid parameters for the CPA model. If all components in the mixture are unable to form hydrogen bonding, the association energy $\varepsilon^{A_i B_j}$ and volume $\beta^{A_i B_j}$ are equal to zero, which eliminates the association term and CPA is reduced to the simple SRK EoS.

The five pure fluid parameters of CPA can be estimated by fitting the model to experimental saturated vapour pressure and liquid density data. The pure fluid parameters in the physical term a_0 , b , and c_1 can be also calculated in a conventional manner using critical parameters T_c , P_c , and acentric factor ω , Table 2.1.

Furthermore, mixing and combining rules are required for mixtures. For the energy and co-volume terms in the SRK EoS the conventional mixing rules are employed for both parameters and the geometric mean rule is used for the cross energy parameter:

$$a = \sum_i \sum_j x_i x_j a_{ij}, \text{ where } a_{ij} = \sqrt{a_i a_j} (1 - k_{ij}) \quad (2.5)$$

$$b = \sum_i x_i b_i$$

k_{ij} - the only adjustable parameter of CPA.

In the association term in Eq. 2.1 no mixing rules are required, however when two associating components are present in the system, combining rules are needed to account for the cross-association energy $\epsilon^{A_i B_j}$ and volume $\beta^{A_i B_j}$. The CR-1 combining rules are among the most frequently used combining rules for many practical applications, however, if one of the components is non-associating, the modified CR-1 combining rules are used [23]. The cross-association energy is just a half of the association energy of the associating component, whereas the cross association volume is fitted to experimental data, Table 2.3.

In CPA the only adjustable binary interaction parameter (for non-solvating mixtures) is typically k_{ij} and it is normally obtained by fitting to experimental phase equilibria data (VLE, LLE, etc.) for mixtures. However, prior to parameter estimation an appropriate association scheme should be chosen.

Table 2.3. Combining rules for the cross-association energy and volume.

CR-1 combining rules	Modified CR-1 combining rules
$\epsilon^{A_i B_j} = \frac{\epsilon^{A_i B_i} + \epsilon^{A_j B_j}}{2}$	$\epsilon^{A_i B_j} = \frac{\epsilon^{\text{associating component}}}{2}$
$\beta^{A_i B_j} = \sqrt{\beta^{A_i B_i} \beta^{A_j B_j}}$	$\beta^{A_i B_j}$ (fitted)

Using the CPA EoS excellent results have been achieved for many types of equilibria (VLE, LLE, SLE, VLLE, etc.) for multicomponent mixtures containing associating components like water, alcohols, glycols, acids, etc. For many mixtures temperature independent interaction parameters were used, and often satisfactory results are obtained even when $k_{ij} = 0$. CPA has also found applications in multiple industrial projects [6, 24, 25].

2.5 Concluding Remarks

The chemical, oil and gas, and other branches of the industry operate with thousands mixtures that contain many different components. Many types of processes are involved, many types of phase equilibria are performed, and, therefore many types of thermodynamic properties become important for successful operation and design. The situation is complicated even further by the severe lack of experimental data, especially for new types of systems, or very complex ones, like polymers, ionic liquids, electrolytes, etc. And all these issues are normally addressed by thermodynamic models which are thus useful for optimum design of industrial processes.

As it was outlined in this chapter, there are many different thermodynamic models which all have their own range of applicability and problems. Nowadays several advanced and powerful models exist, like SAFT and CPA. However, depending on the system (number of the components, complexity, association, etc.) and the properties of interest, sometimes even classical and relatively simple cubic EoS can provide entirely satisfactory results. Many industrially important liquid mixtures are easily handled by activity coefficient models like UNIQUAC and UNIFAC, which were developed specifically for liquid phases at low pressures.

The increasing demand for advanced models appeared when older models could not cope with the tasks because too complex components were involved (e.g. hydrogen bonding ones), or severe conditions were employed (vapour-liquid-liquid equilibria, high temperatures, pressures, supercritical conditions, etc.). Even now, not all components

and mixtures can be successfully modelled with the abovementioned and other models [6]. Mixtures with electrolytes, ionic liquids, polymers, etc. present challenges for most existing models. Such mixtures require different terms, or approaches, or completely different models, in order to achieve appropriate predictions. Therefore, thermodynamic model development does not stop at this point.

2.6 References

- [1] J.D. Van der Waals, On the continuity of the gas and liquid state, Doctoral Thesis, 1873.
- [2] G. Soave, Chem. Eng. Sci. 27 (1972) 1197-1203.
- [3] D.-Y. Peng, D.B. Robinson, Ind. Eng. Chem., Fundam. 15 (1976) 59-64.
- [4] A. Kordas, K. Tsoutsouras, S. Stamataki, D. Tassios, Fluid Phase Equilib. 93 (1994) 141-166.
- [5] D.P. Tassios, Applied chemical engineering thermodynamics, Springer-Verlag, 1993.
- [6] G.M. Kontogeorgis, G.K. Folas, Thermodynamic Models for Industrial Applications: from classical and advanced mixing rules to association theories, Wiley, 2010.
- [7] G.M. Wilson, J. Am. Chem. Soc. 86 (1964) 127-130.
- [8] H. Renon, J.M. Prausnitz, AIChE J. 14 (1968) 135-144.
- [9] D.S. Abrams, J.M. Prausnitz, AIChE J. 21 (1975) 116-128.
- [10] A. Fredenslund, R.L. Jones, J.M. Prausnitz, AIChE J. 21 (1975) 1086-1099.
- [11] I.G. Economou, M.D. Donohue, AIChE J. 37 (1991) 1875-1894.
- [12] I.G. Economou, M.D. Donohue, Fluid Phase Equilib. 116 (1996) 518-529.
- [13] R.A. Heidemann, J.M. Prausnitz, Proc. Natl. Acad. Sci. USA 73 (1976) 1773-1776.
- [14] C. Panayiotou, I.C. Sanchez, J. Phys. Chem. 95 (1991) 10090-10097.
- [15] G.M. Kontogeorgis, E.C. Voutsas, I.V. Yakoumis, D.P. Tassios, Ind. Eng. Chem. Res. 35 (1996) 4310-4318.

- [16] M.S. Wertheim, J. Stat. Phys. 35 (1984) 19.
- [17] M.S. Wertheim, J. Stat. Phys. 35 (1984) 35.
- [18] M.S. Wertheim, J. Stat. Phys. 42 (1986) 459.
- [19] M.S. Wertheim, J. Stat. Phys. 42 (1986) 477.
- [20] S.H. Huang, M. Radosz, Ind. Eng. Chem. Res. 29 (1990) 2284-2294.
- [21] Y.-H. Fu, S.I. Sandler, Ind. Eng. Chem. Res. 34 (1995) 1897-1909.
- [22] G.M. Kontogeorgis, I.V. Yakoumis, H. Meijer, E. Hendriks, T. Moorwood, Fluid Phase Equilib. 158-160 (1999) 201-209.
- [23] G.K. Folas, G.M. Kontogeorgis, M.L. Michelsen, E.H. Stenby, Ind. Eng. Chem. Res. 45 (2006) 1527-1538.
- [24] G.M. Kontogeorgis, M.L. Michelsen, G.K. Folas, S. Derawi, N. von Solms, E.H. Stenby, Ind. Eng. Chem. Res. 45 (2006) 4855-4868.
- [25] G.M. Kontogeorgis, M.L. Michelsen, G.K. Folas, S. Derawi, N. von Solms, E.H. Stenby, Ind. Eng. Chem. Res. 45 (2006) 4869-4878.

Chapter 3

Selective Hydrogenation of 2-Butenal in Carbon Dioxide Reaction Medium

Abstract

Knowledge of the phase behaviour and composition is of paramount importance for understanding multiphase reactions. In this part of the project the effect of the phase behaviour in the palladium-catalysed selective hydrogenation of 2-butenal to saturated butanal in dense carbon dioxide has been investigated. The reactions were performed using 5 wt% Pd on activated carbon in custom-designed high-pressure autoclaves at 323 K. The Cubic-Plus-Association (CPA) equation of state was employed to model the phase behaviour of the experimentally studied systems. CPA binary interaction parameters were estimated based on the experimental vapour-liquid or liquid-liquid equilibria data available in the literature. No experimental data for the CO₂–2-butenal binary were found in the literature; therefore, the bubble points of this mixture of varying composition at three different temperatures were measured in a high-pressure view cell. The results of the catalytic experiments have showed that small amounts of carbon dioxide added to the system significantly decrease the conversion, whereas at higher loadings of CO₂ the reaction rate gradually increases reaching a maximum. The CPA calculations revealed that this maximum is achieved in the so-called expanded liquid region, which is located near the critical point of the reacting mixture. It was also found that in this point the hydrogen concentration achieved its maximum in the CO₂-expanded phase. Furthermore, the pressure – temperature regions where the multicomponent reaction system exists in one single phase and where it is multiphase were calculated.

3.1 Introduction

Hydrogenation reactions in general are widely used in the chemical industry [1]. Particularly, the selective hydrogenation of α,β -unsaturated aldehydes has been extensively studied over the past decades, because the products - saturated aldehydes and α,β -unsaturated alcohols – have many applications, especially in the synthesis of various fine chemicals [2]. The scope of the present study comprises the selective hydrogenation of 2-butenal to butanal (Scheme 3.1). Recent findings on bifunctional catalysts have shown that it is the first step of the “one-pot” synthesis with the consecutive second step of the aldol reaction of the saturated aldehydes [3]. The present study is planned to be extended to those systems as well, and some exploration in that direction has already been done [4-6], which will be discussed in the next chapters of the present thesis.



Scheme 3.1. Selective hydrogenation of 2-butenal in dense carbon dioxide.

In molecules of α,β -unsaturated aldehydes with two types of double bonds, C=C and C=O, the former unsaturated bond is thermodynamically more prone to hydrogenation than the latter. However, depending on the catalyst used in the process one or the other product can be selectively produced. Platinum catalysts doped with different additives favour mainly C=O hydrogenation [7-15], whereas palladium catalysts are typically used for C=C hydrogenation. For example, using a 10 wt% Pd/C catalyst, 2-butenal was easily hydrogenated into butanal with almost 100% selectivity [16]. Also over 1 wt% Pd/Amberlyst-15 and 1 wt% Pd/C in carbon dioxide as reaction medium selective hydrogenation of the double bond was found [3]. Similarly, the C=C double bond in 2-hexenal is selectively converted with hydrogen on a 1 wt% Pd/Amberlyst-15 catalyst [17].

As it was discussed in the previous chapters, heterogeneous catalysis combined with the use of dense and/or supercritical carbon dioxide provides additional opportunities to optimise and intensify the process [18-21]. This is particularly interesting for gas-liquid reactions like selective hydrogenation [22, 23]. Thus, it has been shown that the reaction rate of the selective hydrogenation of 2-butenal to butanal is higher in supercritical fluids than in conventional liquid phase with or without an addition of solvent [3, 16, 17]. Burgener *et al.* [24] studied the hydrogenation of citral in supercritical CO₂ and conventional solvents in continuous and batch reactors. It was shown that the reaction rate and selectivity were greatly influenced by the type of the reactor, solvent, total pressure, and feed composition. In many cases both conversion and selectivity were higher than those in conventional solvents, and both depended on CO₂ pressure, whereas hydrogen pressure mainly accelerated the reaction rate [24]. An interesting trend was observed when different H₂ : feed ratios were used. The highest conversion was observed when the system was changing from single phase to two phases at a moderate H₂ concentration. All aforementioned reactions have been performed in carbon dioxide media but the phase behaviour during the reaction progress with its changing composition was not studied systematically. Note, however, that the phase behaviour for a number of other systems has been investigated experimentally [25].

Phase behaviour plays an important role in chemical reactions in dense and/or supercritical carbon dioxide media. It is very demanding to study it experimentally, especially *in situ* during the reaction, however theoretical thermodynamic calculations can be very useful in this regard. A large number of thermodynamic models have been developed in order to predict many thermodynamic properties of mixtures, including their phase behaviour with satisfactory accuracy [26]. The challenge for applying them to catalysis is to provide examples that demonstrate that they are capable of predicting multicomponent mixtures at varying composition, as occurring during reaction.

For this purpose, an advanced thermodynamic model, the Cubic-Plus-Association (CPA) Equation of State [27], is used in the present study. CPA is one of the models that takes into account strong cross-association between components, i.e. hydrogen bonding;

and it has been proven to be a powerful tool for predicting various properties of complex multicomponent systems at elevated temperatures and pressures [28, 29]. The CPA equation of state consists of two parts – the Soave-Redlich-Kwong (SRK) equation of state and an association term based on Wertheim’s first order thermodynamic perturbation theory [30]. In the case when no hydrogen-bonding components are present in the mixture, the association term vanishes and CPA reduces to the SRK functionality.

In the present reaction, all the components comprising the reaction mixture – 2-butenal, hydrogen, butanal and carbon dioxide – are non-associating, i.e. they do not form hydrogen bonds between themselves and/or each other. For such a simple system the original Soave-Redlich-Kwong equation of state might be used [31], instead of CPA. However, the original SRK uses critical temperature T_c , critical pressure P_c , and acentric factor ω as pure fluid parameters. On the other hand, the estimation of pure fluid parameters for CPA is based on experimental vapour pressure and liquid density data, which means that the temperature dependency of those important properties is captured by the model. Therefore, CPA gives better results when describing vapour pressure dependencies with temperature.

In order to account for intermolecular interactions one interaction parameter k_{ij} is typically used in the model. It is estimated on the basis of experimental VLE, LLE or VLLE data for the binary mixtures of the components comprising the reaction system. In many cases such data are available in the literature for binary systems; however, no experimental data were found for the CO_2 – 2-butenal binary system. Therefore, the bubble point pressures of the CO_2 – 2-butenal binary mixture of various compositions at different temperatures were measured experimentally. Based on the obtained data the binary interaction parameter of CPA for this system was estimated.

In summary, the present study aims at the following aspects: (1) the elucidation of the influence of the carbon dioxide amount on the catalyst performance, (2) the measurement of the phase equilibrium of the CO_2 – 2-butenal binary mixture, and finally, (3) the application of the CPA equation of state and the parameters obtained for predicting the phase equilibrium of the multicomponent reaction systems.

3.2 Experimental

3.2.1 Catalyst preparation

A 5 wt% Pd/C catalyst was prepared using the incipient wetness impregnation technique as follows. 0.1282 g of $[\text{Pd}(\text{NH}_3)_4]\text{Cl}_2$ (Sigma-Aldrich) as a precursor was dissolved in 1.69 ml of deionised water - the amount required for the complete impregnation of 0.988 g of activated carbon (Sigma-Aldrich, ground fraction 125 – 250 μm). The sample was dried at room temperature overnight, then in an oven at 373 K for 24 hours, and subsequently activated in nitrogen flow containing 10 vol% of hydrogen at 383 K for two hours. The final catalyst sample was stored in dry atmosphere.

3.2.2 Catalyst characterisation

The specific surface area of the as-prepared 5 wt% Pd/C catalyst was determined using BET isotherms recorded on a BEL Japan surface area analyser at a nitrogen adsorption temperature of 77 K. The specific surface of the sample was measured to be 994 m^2/g .

The as-prepared catalyst was analysed using X-ray diffraction (Bruker D8-Advance Diffractometer with a Cu $K\alpha$ -Anode source, $\lambda=1,54$ nm, angle range 20 - 80° 2 θ). The obtained diffractograms did not reveal any significant reflections, which indicates that the palladium particles are well dispersed and fairly small.

In order to support this finding, the transmission electron microscopy images (TEM) were obtained on a FEI Technai TEM operating at 200 kV (Centre for Electron Nanoscopy, DTU). A typical TEM image is depicted in Fig. 3.1. It can be seen that the palladium particles are evenly distributed on the carbon surface, and the average particle size falls below 4 nm.

Temperature-programmed reduction (TPR) of the impregnated catalyst was performed as follows: 500 mg of the fresh sample was placed into a quartz tube (10 mm in diameter) heated in flowing N_2 (Air Liquid, 50 mL/min) to 393 K, and held for 10

min. The tube was then cooled in flowing nitrogen to room temperature, N₂ was replaced by the carrier gas, and the TPR run was started using the following conditions: carrier gas 5 vol% H₂ in N₂ (Air Liquid) with a flow rate of 50 mL/min; initial temperature 308 K; ramp 5 K/min; and final temperature 433 K.

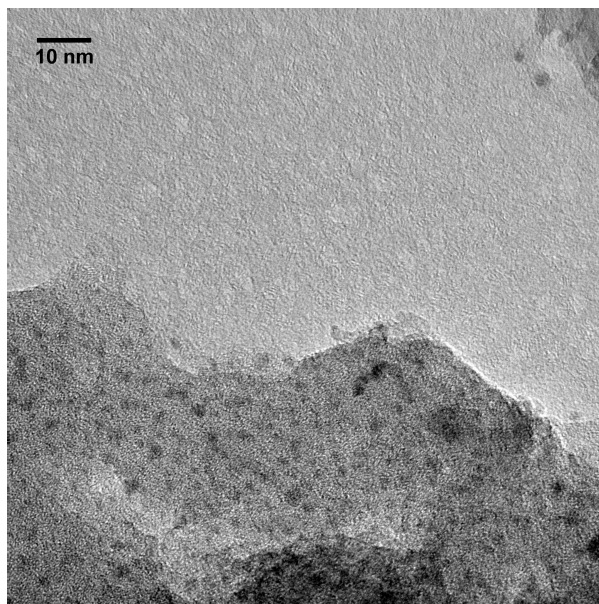


Fig. 3.1. Typical TEM image of 5 wt% Pd/C catalyst.

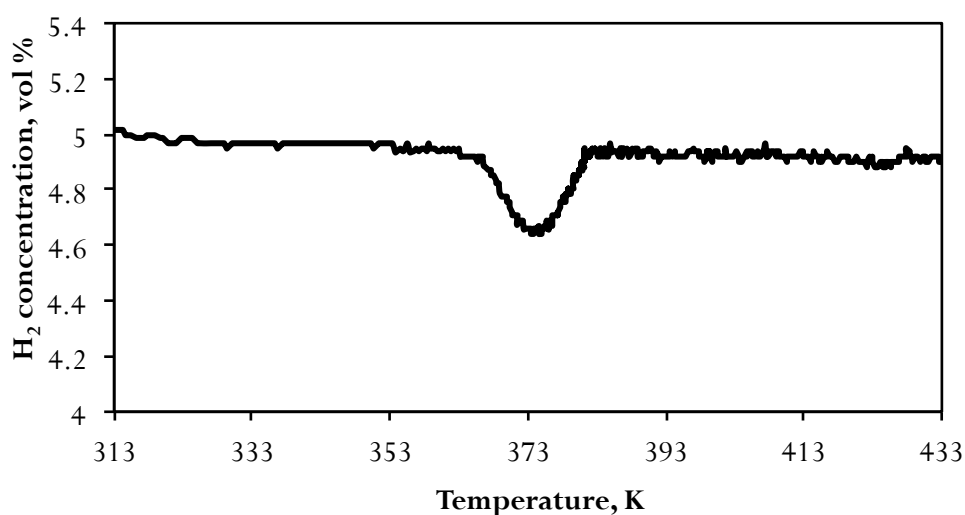


Fig. 3.2. Temperature-programmed reduction of the 5wt.% Pd/C.

The concentration of hydrogen was detected with a GC-14A chromatograph (Shimadzu GmbH). The obtained TPR profile is shown in Fig. 3.2. The TPR experiments indicate

that the palladium constituent of the catalyst was reduced to metallic palladium in the temperature range between 363 and 383 K.

3.2.3 Catalytic hydrogenation of 2-butenal

The catalyst performance was tested in the selective hydrogenation of 2-butenal using homemade stainless steel autoclaves with magnetic stirring bars ($T_{\max} = 250\text{ }^{\circ}\text{C}$, $P_{\max} = 200\text{ bar}$, inner volume $\sim 125\text{ ml}$). Before use, the reactors were thoroughly washed with organic solvents and dried with compressed air. Required amounts of the catalyst and 2-butenal were loaded into the autoclaves which then were tightly closed. After that, the reactors were carefully flushed with hydrogen several times and pressurised up to the desired pressure. Hydrogen was supplied directly from the hydrogen cylinder via an interconnected reduction valve. As a next step, carbon dioxide was added using a CO_2 -compressor (NWA, PM-101, Lörrach, Germany), and its amount was measured by weighing the autoclaves before and after loading. Pressure and temperature were monitored with installed manometers and thermocouples, respectively.

After the reaction, the autoclaves were quickly cooled down to room temperature in a water bath, slowly and carefully depressurised, and opened. Samples of the reaction mixture were taken out, diluted with toluene and analysed employing a gas chromatograph (Shimadzu, GC 2010+, polar column), which had been previously calibrated for the reactant and possible products.

All catalytic experiments were performed at least twice. The conversion of 2-butenal in two identical experiments by maximum deviated by 7% relative.

3.2.4 Phase behaviour measurements

Phase behaviour was visually monitored in a high-pressure view cell (15-65 ml, SITEC, Switzerland) with a sapphire window (26 mm diameter). The pressure was adjusted by changing the volume of the cell by means of a screw-type manual pump. The setup principle is based on the so-called synthetic method [32], where the phase

transition is directly observed through the window without taking samples. The flow chart and the setup description can be found in Ref. [33-35]. Temperature and pressure were monitored with a thermocouple and a Dynisco pressure sensor, respectively. Stirring was performed by a magnetic stirrer with a stirring bar placed inside the cell. Temperature was controlled by means of an oil-containing heating jacket connected to a thermo/cryostat.

Before every experiment the view cell was thoroughly cleaned with acetone and CO₂, dried with an air jet, and left open heated up to 323 K in the air for a minimum of 2 hours. After cooling down to room temperature, the desired amount of 2-butenal (Aldrich, 99.8%+) was loaded into the cell. Its mass was determined by weighing the syringe before and after loading. After charging the cell with the liquid, it was closed, tightened, and flushed slowly and carefully with gaseous CO₂ in order to substitute the air. CO₂ was added using a CO₂-compressor (NWA, PM-101, Lörrach, Germany), and its quantity was measured by a mass flow transmitter (Rheonik Messgeräte GmbH, Germany) at a constant pressure of 100 bar, which was controlled by means of an interconnected reduction valve. The view cell was further heated up to a desired temperature and pressurised to a pressure higher than the expected bubble point pressure. At this stage the cell was left for equilibrating for at least 2 hours. A first rough estimation of the bubble point was made by stepwise depressurising the system (4 – 6 bar). After the first bubbles appeared in the top part of the cell, it was pressurised again and left for equilibration. Small stepwise pressure drop (0.2 – 1 bar) with subsequent equilibration after each step was applied to determine the bubble point pressure of the specific system. Since the first bubble of gas phase usually appeared in the highest point of the cell, the latter was slightly tilted to make this point more visible. The pressure at which the first bubble of the second phase appeared was noted.

All experimental points were measured at least three times. The difference between these points was generally less than 0.2 - 0.4 bar, which was within the accuracy range of the pressure gauge. The temperature was measured with a precision of 0.5 K.

3.3 Experimental results

3.3.1 Catalyst performance

A series of catalytic experiments was carried out in order to investigate the influence of the carbon dioxide content on the catalytic performance. Blind tests without a catalyst were also performed, and no detectable catalytic activity was observed. The results are presented in Table 3.1.

Table 3.1. Selective hydrogenation of 2-butenal to butanal over 5 wt% Pd/C catalyst.

Amount of CO ₂ , g	CO ₂ : 2-butenal mole ratio	Pressure, bar	Conversion, %	TOF, h ⁻¹ ^a
0	0.0 : 1	22	34.3	730
4	2.3 : 1	34	27.6	580
10	5.7 : 1	50	10.7	230
28	15.9 : 1	70	14.6	310
34	19.3 : 1	98	17.1	360
45	25.6 : 1	111	20.2	430
60	34.1 : 1	126	39.1	840
70	39.8 : 1	138	39.7	840
82	46.6 : 1	150	26.6	560
92	52.3 : 1	185	24.6	520

Conditions: substrate 0.04 mol, H₂: 2-butenal mole ratio 2.5 : 1 (corresponding to a pressure of 20 bar at room temperature), m_{cat} = 0.01 g, temp. 323.2 K, reaction time 60 min.

^a TOF[h⁻¹] = $\frac{n_{\text{sub}} \times \text{Conv.}}{\left(\frac{m_{\text{cat}} \times \text{wt}_{\text{Pd}}}{M_{\text{rPd}}}\right) \times t}$, where n_{sub} - amount of 2-butenal, mol; Conv. - conversion of 2-butenal, %; m_{cat} - catalyst mass, g; wt_{Pd} - palladium loading, wt%; M_{rPd} - molecular weight of Pd, g/mol; t - time, hour.

The results showed that the conversion, and corresponding turnover frequency (TOF) reached a minimum when the amount of carbon dioxide approached 10 g, i.e. when the mole ratio CO₂ : 2-butenal was 5.7:1. When this ratio was increased, the

conversion also went up reaching a maximum of almost 40% at a mole ratio CO_2 : substrate of 35 – 40 : 1. The total pressure of the reaction system was almost linearly dependent on the amount of CO_2 used in the reaction. Note that in the present study the turnover frequency was referred to the total number of Pd atoms: in reality only the surface palladium atoms or even special sites contribute to the reaction.

3.3.2 Phase behaviour measurements

The bubble point pressures for the CO_2 – 2-butenal binary mixture at four different compositions were measured at three different temperatures using the aforementioned setup and experimental procedure. The results are presented in Table 3.2.

Table 3.2. Experimental bubble point pressures for CO_2 – 2-butenal.

CO ₂ mole fraction	Pressure, bar		
	313.2 K	331.9 K	350.2 K
0.3899	28.8	38.2	48.4
0.4580	34.9	46.5	59.2
0.5429	41.5	55.2	70.3
0.7081	57.4	77.6	98.8

3.4 Modelling with the CPA equation of state

3.4.1 Pure fluids

The CPA pure fluid parameters (\mathbf{a}_0 , \mathbf{b} , \mathbf{c}_1) were estimated using saturated liquid volume V^{liq} and vapour pressure P^{sat} data from DIPPR [36] or, when it was possible, they were obtained from the literature. Due to the fact that all the components are non-associating, the association energy and volume ($\epsilon^{\text{A}_i\text{B}_j}$ and $\beta^{\text{A}_i\text{B}_j}$) are equal to zero. The pure fluid parameters are presented in Table 3.3.

Table 3.3. CPA parameters for pure fluids.

T_c , K	a_0 , L ² bar mol ⁻²	b , L mol ⁻¹	c_1	%AAD ^a in P ^{sat}	%AAD in V ^{liq}	Ref.
<i>Carbon dioxide</i> ($T_r = 0.65 - 0.9$)						
304.2	3.5079	0.0272	0.7602	0.2	0.8	[37]
<i>Hydrogen</i> ($T_r = 0.5 - 0.9$)						
33.19	0.2664	0.0194	0.0474	1.6	4.4	This work
<i>2-Butenal</i> ($T_r = 0.4 - 0.9$)						
565.0	18.9939	0.0728	0.8140	4.8	1.9	This work
<i>Butanal</i> ($T_r = 0.4 - 0.9$)						
537.2	16.6777	0.0758	0.8803	2.2	0.8	This work

^a %AAD = $\frac{1}{n} \sum_i \left| \frac{X_i^{\text{cal}} - X_i^{\text{exp}}}{X_i^{\text{exp}}} \right| \times 100$, where X stands for P^{sat} or V^{liq} and n is the number of experimental data points.

3.4.2 Binary mixtures

The reaction mixture consists of four components (CO₂, hydrogen, 2-butenal, and butanal); therefore, six interaction parameters are required for the six binaries occurring in the system. As it was previously mentioned, for estimating k_{ij} parameters some experimental data are required.

Unfortunately, the experimental data were not available for all the binaries, specifically, for the binaries with 2-butenal no data were found in the literature. However, due to the strong similarities between the structure of 2-butenal and butanal, the following assumptions were made: (1) the k_{ij} for the hydrogen – 2-butenal binary was assumed to be equal to that of hydrogen – butanal, and (2) for the 2-butenal – butanal system k_{ij} was set to zero. The binary interaction parameters are presented in Table 3.4.

The CPA model describes quite satisfactorily the phase behaviour of the CO₂ – hydrogen binary mixture, however, slight deviations between the model predictions and experimental data are observed at higher hydrogen concentrations, as shown in Fig. 3.3.

Table 3.4. CPA binary interaction parameters for binary mixtures. All k_{ij} are independent of temperature.

System	Temperature range, K	k_{ij}	%AAD in P	%AAD in y_1	Experimental data ref.
CO ₂ – H ₂	278.15 – 290.15	-0.0323	6.9	17.9	[38]
CO ₂ – butanal	303.2 – 313.2	-0.2859	10.0	0.6	[39]
CO ₂ – 2-butenal	313.2 – 350.2	-0.0180	1.4	- ^a	This work
H ₂ – butanal	293.15 – 393.15	-0.0436	7.3	- ^a	[40]
H ₂ – 2-butenal	-	-0.0436 ^b	-	-	No lit. data
2-butenal – butanal	-	0	-	-	No lit. data

^a Calculations based on experimental P – x – T data, therefore, %AAD in y_1 were not estimated

^b The interaction parameter for this mixture is set equal to the interaction parameter of the H₂ – butanal binary.

For the CO₂ – butanal binary mixture a temperature independent k_{ij} parameter was estimated based on the experimental VLE data. The first attempt to measure and predict the phase behaviour of this system was made by Vazquez da Silva *et al.* [39]. In their work the authors used the SRK and Peng – Robinson (PR) equations of state, in both cases employing the quadratic mixing rules with two adjustable parameters, i.e. k_{ij} for the energy parameter and l_{ij} for the co-volume. The authors report that the employed equations of state quite accurately described the experimental data. However, at higher concentrations of carbon dioxide in the mixture (0.9 – 1.0 CO₂ molar fraction) a large difference between the model prediction and experimental data is observed. This might be due to the fact that the experimental data in this range are not accurate enough. One of the sets of data was measured at a temperature of 303.2 K, which is very close to the critical temperature of pure CO₂ (304.2 K [36]). This means that at high concentrations of CO₂ the vapour pressure of the mixtures should be close to its critical pressure (73.83 bar [36]), however, it is nearly 20 bar lower than that. Moreover, the second data set was measured at 313.2 K, which is 9 K higher than the critical point of

CO₂, but the vapour pressures of the mixtures with a significant excess of CO₂ are still lower than its critical pressure.

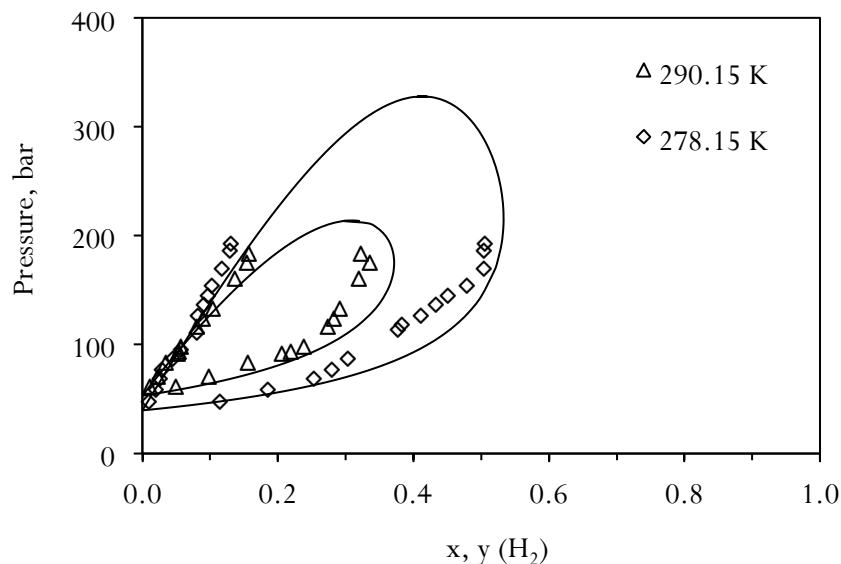


Fig. 3.3. Hydrogen – CO₂ VLE. Experimental data (points) at different temperatures and CPA calculations (lines) with a temperature independent $k_{ij} = -0.0323$.

Note, however, that the CPA model predictions account for this behaviour and show reasonable vapour pressures for the CO₂-rich mixtures. This is due to the fact that the CPA pure fluid parameters are fitted to the pure compound vapour pressure. In the present work only one adjustable parameter k_{ij} is considered for the CO₂ – butanal binary, as shown in Fig. 3.4.

The temperature independent binary interaction parameter was estimated for the CO₂ – 2-butenal system based on the P – x – T experimental data obtained in the present study. The CPA model predictions are in good agreement with the bubble point pressures of the binary mixtures of different composition at three different temperatures, as shown in Fig. 3.5.

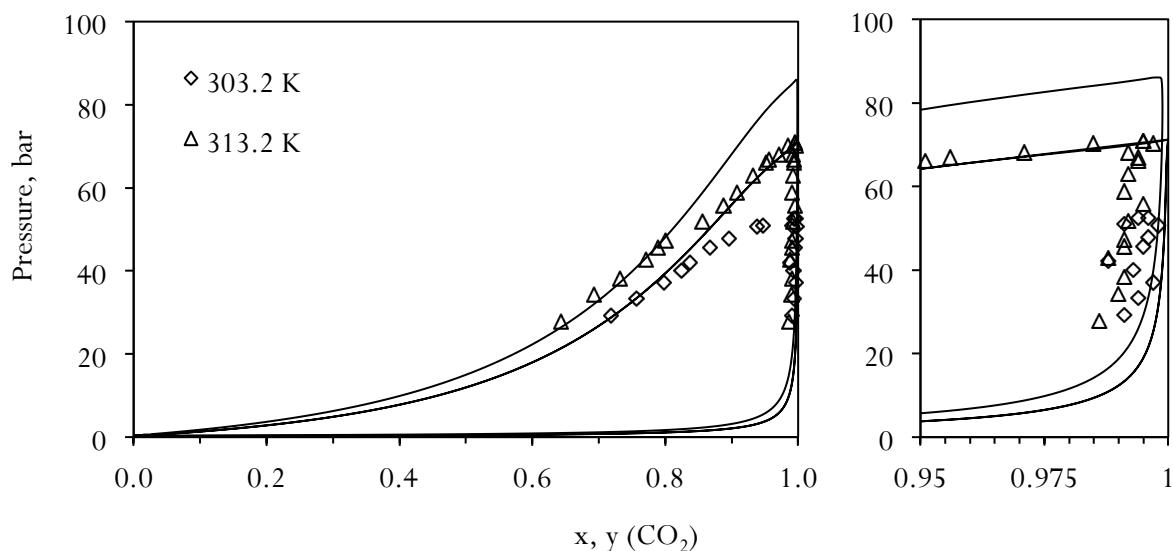


Fig. 3.4. CO₂ – butanal VLE. Experimental data (points) at different temperatures and CPA calculations (lines) with a temperature independent $k_{ij} = -0.2859$. On the right: carbon dioxide – butanal VLE in the CO₂-rich region.

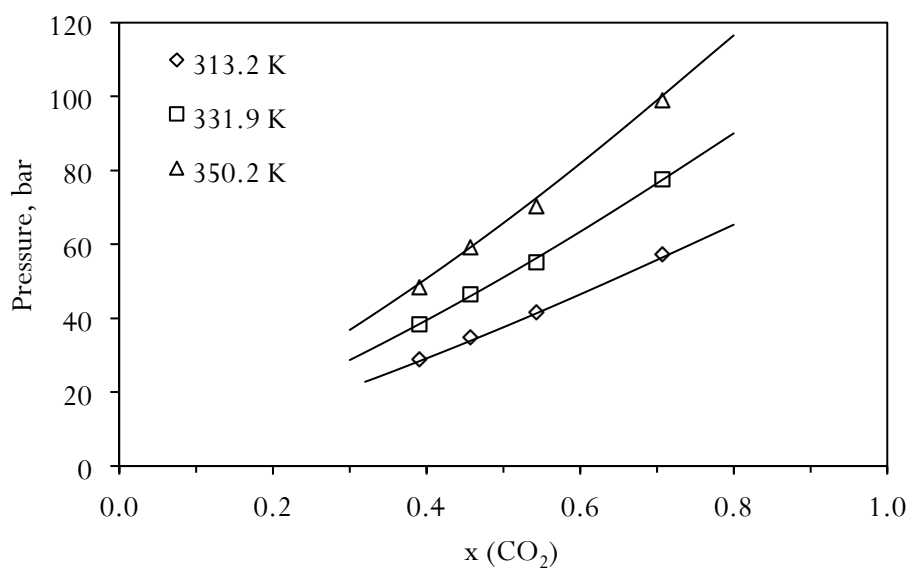


Fig. 3.5. CO₂ – 2-butenal VLE. Experimental data (points) at different temperatures and CPA calculations (lines) with a temperature independent $k_{ij} = -0.0180$.

The phase behaviour of CO₂ – 2-butenal resembles that of the CO₂ – butanal binary mixture. However, the vapour pressures of the CO₂ binaries with butanal are lower than those with 2-butenal at the same composition. This might be explained by the fact that 2-butenal is more polar than butanal, dipole moment 3.66 versus 2.72 D,

respectively [36]. Carbon dioxide, in turn, is a non-polar compound, and therefore, less polar components, such as butanal, are more soluble in it, which explains the lower vapour pressures of binary mixtures.

The k_{ij} parameter for the hydrogen – butanal system was estimated using available $P - x - T$ data at different temperatures. The $H_2 -$ butanal mixture had been previously investigated by Ke *et al.* [41], where the authors used the Peng – Robinson equation of state which required a temperature dependent k_{ij} . However, due to its small value they set it to zero in their further calculations. When using the CPA model one temperature independent parameter is sufficient, as shown in Fig. 3.6. Again, due to the similarity of CPA with SRK for non-associating components, this improvement is attributed to the inclusion of vapour pressure data in the pure compound parameter estimation.

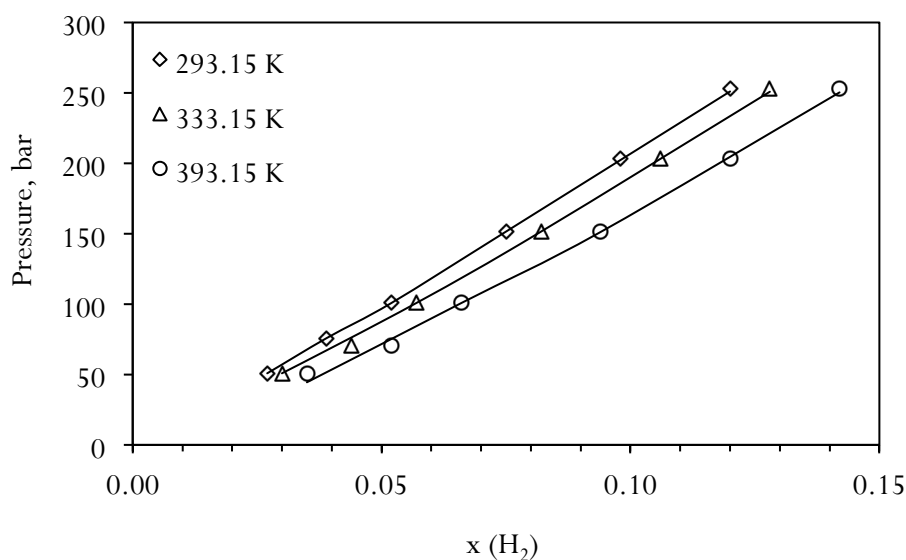


Fig. 3.6. Hydrogen – butanal VLE. Experimental data (points) at different temperatures and CPA calculations (lines) with a temperature independent interaction parameter $k_{ij} = -0.0436$.

3.4.3 CPA predictions for the multicomponent reaction system

The catalytic results have shown that the conversion of 2-butenal is dependent on the amount of CO_2 loaded into the reactor (Table 3.1). There are multiple effects caused by the addition of CO_2 to the system. Firstly, the more carbon dioxide is used in a batch

autoclave the higher the reaction pressure is. The partial pressures of the reacting components, however, do not change and, therefore, the thermodynamic equilibrium is not affected by the increasing pressure, as seen in Scheme 3.1. What possibly happens in reality is that the amount of CO₂ determines the number and composition of the phases co-existing in the reactor as well as the dissolution power of hydrogen in the CO₂-expanded liquid reactant phase. The liquid (or more general, the denser phase) is of a particular interest, because it is in direct contact with the solid catalyst at the bottom of the autoclave and, therefore, the reaction occurs in this dense fluid.

In order to determine the initial concentrations of the components in the 2-butenal hydrogenation reaction, the CPA equation of state together with the binary interaction parameters estimated in the present work were used. The concentrations of the components and the number of phases present in the reactor before reaction are presented in Table 3.5 and underline the presence of a CO₂-expanded reactant phase. The amount of CO₂ in this phase increases with pressure, whereas for hydrogen it only increases between 70 and 138 bar. Table 3.5 shows that in most cases the reaction started at biphasic conditions and only when a large excess of CO₂ was used, the reaction ran in the single-phase regime.

However, at this point another question arises – whether the number of phases changes as the reaction proceeds. In this regard, P – T regions where the multicomponent reaction mixture exists in one or two phases depending on the conversion were calculated with CPA. It was assumed that the mole ratio of the components in the initial mixture was CO₂ : H₂ : 2-butenal = 25 : 2.5 : 1. No conversion, 20, 40, 60, 80% and full conversion were considered. The corresponding compositions of the mixtures are presented in Table 3.6, and the obtained P – T diagrams are shown in Fig. 3.6. According to this figure, if the mentioned above initial reaction mixture starts to react, for instance, at 313 K and 175 bar, it means that before the reaction ($t = 0$) it exists in one single phase, and it will stay in one phase even after all 2-butenal has converted.

Table 3.5. Phase composition of the reaction mixture before reaction.

T, K	P, bar	Feed composition, mol			Number of phases	Composition of the liquid (dense) phase, mole fraction		
		CO ₂	H ₂	2-Butenal		CO ₂	H ₂	2-Butenal
323	22	0.00	0.1	0.04	2	0.000	0.007	0.993
323	34	0.09	0.1	0.04	2	0.178	0.006	0.816
323	50	0.23	0.1	0.04	2	0.367	0.006	0.627
323	70	0.64	0.1	0.04	2	0.604	0.006	0.390
323	98	0.77	0.1	0.04	2	0.770	0.014	0.216
323	111	1.02	0.1	0.04	2	0.817	0.021	0.162
323	126	1.36	0.1	0.04	2	0.911	0.043	0.045
323	138	1.59	0.1	0.04	1	0.919	0.057	0.024
323	150	1.86	0.1	0.04	1	0.930	0.050	0.020
323	185	2.09	0.1	0.04	1	0.937	0.045	0.018

Table 3.6. Composition of a reaction mixture with a given (CO₂ : H₂ : 2-butenal : butanal) ratio at different conversion.

Mixture	Conversion, %	Composition of the reaction mixture, mol			
		CO ₂	H ₂	2-Butenal	Butanal
1	0	25	2.5	1.0	0
2	20	25	2.3	0.8	0.2
3	40	25	2.1	0.6	0.4
4	60	25	1.9	0.4	0.6
5	80	25	1.7	0.2	0.8
6	100	25	1.5	0.0	1.0

If the reaction occurs under the same conditions but at a pressure in the system of around 130 bar, this will mean that the initial system is bi-phasic, however, as the reaction proceeds, at some point the phase transition will occur and the system will become

mono-phasic. Finally, if the reaction pressure is 90 bar, the reaction will begin in the two phase region and it will stay like this even after all substrate has reacted.

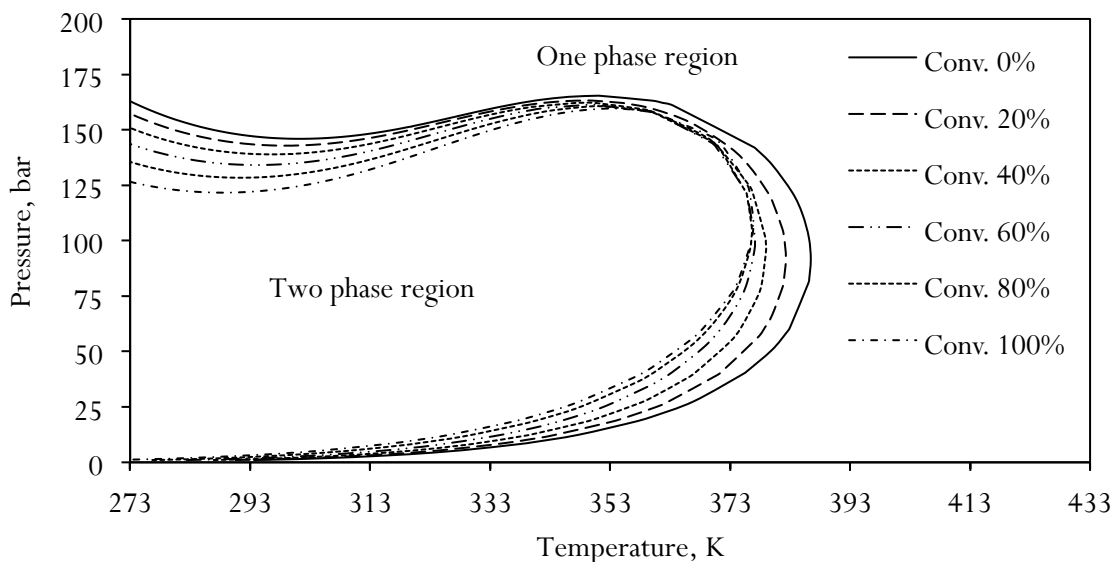


Fig. 3.7. CPA predictions of the bubble and dew point curves for the reaction mixtures during the selective hydrogenation of 2-butenal in carbon dioxide. The composition of every mixture is shown in Table 3.6.

3.5 Discussion

The results of the catalytic studies (Table 3.1) show that the presence of small amounts of carbon dioxide in the reacting system deteriorates catalytic performance; however, higher amounts of carbon dioxide added to the system lead to higher conversion. As mentioned above, this might be due to the concentration and phase behaviour effects arising when more CO_2 is added to the system. The calculations performed with CPA show that the amount of CO_2 used in the reaction determines the number of phases, their composition and total pressure in the reaction, as shown in Table 3.5.

Most of the time, the reactions occurred in the biphasic region. This means that the initial reaction kinetics was determined by the initial concentrations of the components in the liquid phase, which is in direct contact with the catalyst. The reaction pathway in the biphasic region might be easily impeded by mass transfer limitations, i.e. diffusion of

the components (particularly hydrogen) from the gas phase to the liquid and further to the catalyst surface. Under single-phase conditions, the concentration of all the components was constant in the whole volume of the reaction mixture due to intense stirring, therefore, possible external mass transfer limitations were minimised. However, as it was shown by the calculations the maximum catalyst activity was observed at a CO₂ : 2-butenal ratio near the critical point of the reaction mixture, where the phase transition occurred. Further dilution of the system with CO₂ caused a decrease of catalytic activity. In other words, even though the reaction conditions were in favour of higher conversion, i.e. minimised mass transfer effects, the opposite was observed.

A similar observation was made by Burgener *et al.* [24], where they found that at higher hydrogen concentrations the catalytic performance decreased, which was against the expectation from reaction thermodynamics and kinetics. A significant change occurred when the system moved to an expanded liquid where maximal conversion was obtained. Unlike in the present study, this phase transition occurred due to the fact that hydrogen decreased the dissolution power of carbon dioxide, and as a consequence, the one phase system split into two phases. Furthermore, in an earlier study by Tschan *et al.* [42], the authors investigated the selective semi-hydrogenation of propargyl alcohol in supercritical carbon dioxide. They concluded that in the two-phase region excessive amounts of hydrogen are required in order to maintain a sufficient supply through the liquid layer to the catalyst surface, whereas when working in a single phase lower hydrogen concentrations are needed for the selective semi-hydrogenation of propargyl alcohol due to the minimised mass transport limitations. In both studies the concentrations of hydrogen in the reaction phase was speculated to be crucial.

In the present study, thermodynamic calculations were used to provide insight into the behaviour during the hydrogenation of 2-butenal. Table 3.5 suggests that the concentration of 2-butenal gradually decreased when more CO₂ was added to the system, whereas the concentration of hydrogen was more or less stable at the very beginning and after a certain point it started to rise to the point where the phase

transition occurred, as shown in Fig. 3.8. At this point the concentration of hydrogen in the dense layer was maximal, and then it started to decrease gradually.

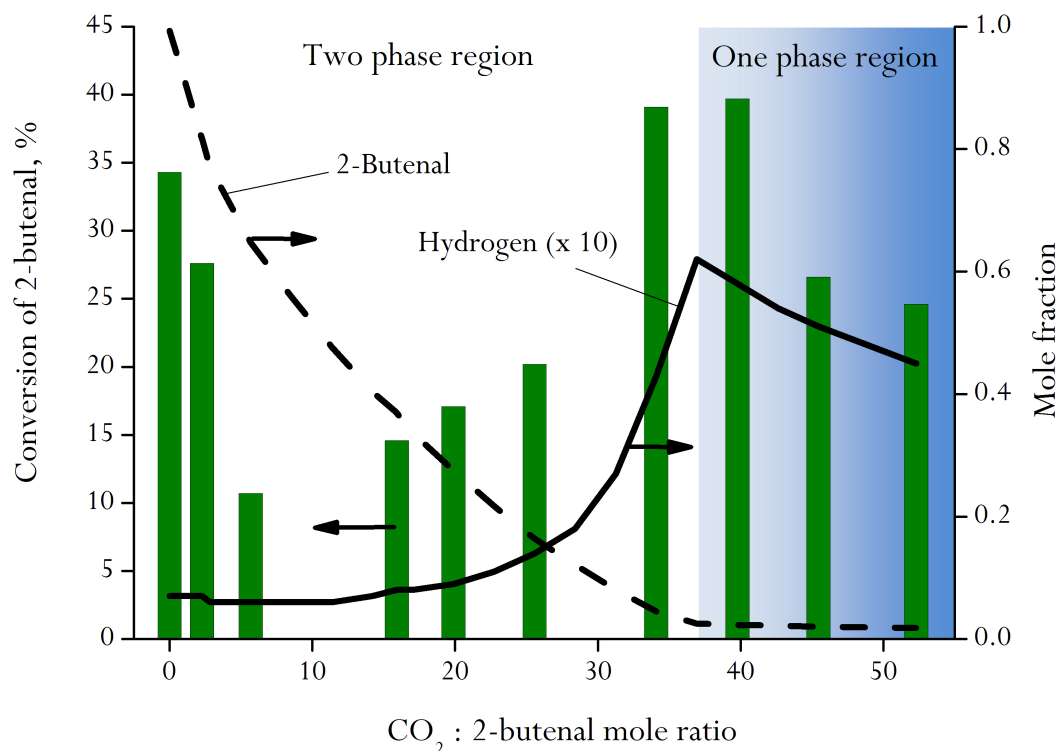


Fig. 3.8. Mole fractions (CPA lines) of hydrogen and 2-butenal in the **liquid (dense) phase** which is in contact with the catalyst and conversion of 2-butenal (bars) depending on the initial CO₂ : 2-butenal mole ratio. *Conditions:* 2-butenal 0.04 mol, H₂ : 2-butenal mole ratio 2.5 : 1, m_{cat} = 0.01 g, T = 323.2 K, reaction time 60 min. Shaded area – one phase region.

The maximum concentration of hydrogen coincides with the maximum catalytic activity. Therefore, due to the fact that the concentration of 2-butenal was decreasing at the beginning while the concentration of hydrogen in the liquid layer was constant the reaction rate was decreasing as well. After the point where the concentration of hydrogen started to increase, the reaction rate increased as well. These observations are in line with the conclusions for the abovementioned reactions studied by Burgener *et al.* [24] and Tschan *et al.* [42]. Figure 3.8 further shows that in the one phase region the concentration of hydrogen decreases while the concentration of the substrate stays almost unchanged; thereby possibly explaining the decrease in the catalytic activity.

Furthermore, the excessive amounts of carbon dioxide at high reaction pressures may cause its strong adsorption on the catalyst surface, which competes with the adsorption of hydrogen and 2-butenal. In addition, both Zhao *et al.* [43] and Burgener *et al.* [44] found reaction of CO₂ and hydrogen under single phase conditions on noble metal particles.

Most of the time carbon dioxide is considered as an inert reaction medium, however, some recent findings revealed that under certain conditions, i.e. in the presence of hydrogen and noble metals at relatively low temperatures, CO₂ can react with hydrogen in the so-called reverse water-gas shift reaction and form carbon monoxide and water [44, 45]. The former acts as an active catalyst poison [46], and sometimes changes the route of the reaction by changing the catalyst selectivity [47]. Catalyst poisoning by CO might be the case in the present study; however, this is hardly the main reason for a significant drop in conversion when excessively large amounts of CO₂ were used. As it was pointed out by Burgener *et al.* [44], the reverse water-gas shift reaction takes place in many hydrogenation reactions and under hydrogenation conditions metal surfaces are partially covered with CO, however, this effect is weakly pronounced and carbon dioxide could be considered as a relatively inert reaction medium.

However, another type of intermolecular interactions can play an important role when reactions are performed in scCO₂. Carbon dioxide, possessing electron-accepting properties, can easily interact with other functional groups in organic molecules, such as aldehydes, ketones, esters, etc. Such interactions and their pressure dependency have been studied using high-pressure FT-infrared spectroscopy [48, 49]. It was found that CO₂ is capable of activating of carbonyl groups in organic aldehydes and this effect is different for saturated and unsaturated ones [49]. Thus, in the hydrogenation of benzaldehyde the conversion into benzyl alcohol is merely decreasing with increasing CO₂ pressure due to dilution of the system, whereas for cinnamaldehyde conversion reaches a maximum. The authors attribute it to the activation of C=O bond in cinnamaldehyde by CO₂ at low pressures, and at elevated pressures this effect disappears

and conversion decreases due to the dilution of the system. In the present study another type of hydrogenation is relevant, i.e. C=C bond saturation, however the presence of intermolecular forces between CO₂ and aldehydes is indirectly indicated by the binary interaction parameter k_{ij} (Table 3.4), which provides insight into the non-ideality of the system due to the presence of intermolecular forces between the components. The significance of such interactions is in their ability to determine the phase behaviour of the system, which in turn affects the catalyst performance as it was discussed above.

Further CPA calculations of the P – T regions of co-existing phases (Fig. 3.7) showed that the system phase transition at a constant temperature and elevated pressures decreases towards lower pressures as the reaction proceeds. This means that if the initial reaction mixture (at $t = 0$) was in a single phase it stayed in one phase even after all the 2-butenal had reacted. However, depending on the composition, T and P, in some cases the reaction may begin in the two-phase region, but at a certain conversion the phase transition may occur and the system will become single phase. These changes of the phase behaviour as a result of concentration changes during reaction have to be considered for proper interpretation of reaction kinetics and the CPA calculations proved to be an elegant tool for this task.

3.6 Conclusion

The influence of the phase behaviour on the palladium-catalysed selective hydrogenation of 2-butenal to butanal was investigated. For this purpose the CPA equation of state was successfully used and directly provided a correlation between the concentrations of the reactants in the fluid phase and the reaction rate. The interaction parameters for three binaries were estimated using experimental data from the literature. The binary mixture carbon dioxide – 2-butenal was experimentally studied in order to find the bubble point pressures at different temperatures. Based on this experimental data the binary interaction parameter was obtained.

The CPA model is shown to be a powerful tool allowing thermodynamic calculations with high precision and accuracy. Using CPA the number of co-existing phases was predicted, and the concentrations of the reacting components in coexisting phases were calculated. These data are very important and useful for further kinetic studies where knowledge of concentrations in individual phases is a key element.

Furthermore, calculations using CPA gave insight into the phase behaviour during the reaction, showing that the pressures and temperatures at which the one phase region exists are decreasing as the reaction proceeds.

The catalytic studies showed that maximum conversion was achieved when the reaction mixture changed from the one-phase to the two-phase regions, near the critical point of the system. The concentrations of the components in the reaction mixture, calculated with CPA, were shown to cause such behaviour.

3.7 References

- [1] B. Chen, U. Dingerdissen, J.G.E. Krauter, H.G.J.L. Rotgerink, K. Mobus, D.J. Ostgard, P. Panster, T.H. Riermeier, S. Seebald, T. Tacke, H. Trauthwein, *Appl. Catal., A* 280 (2005) 17-46.
- [2] P. Gallezot, D. Richard, *Catal. Rev.: Sci. Eng.* 40 (1998) 81-126.
- [3] T. Seki, J.D. Grunwaldt, A. Baiker, *Chem. Commun.* (2007) 3562-3564.
- [4] N.E. Musko, J.D. Grunwaldt, *Top. Catal.* 54 (2011) 1115-1123.
- [5] J.G. Stevens, R.A. Bourne, M. Poliakoff, *Green Chem.* 11 (2009) 409-416.
- [6] K. Matsui, H. Kawanami, Y. Ikushima, H. Hayashi, *Chem. Commun.* (2003) 2502-2503.
- [7] L. Tian, Q.Y. Yang, Z. Jiang, Y. Zhu, Y. Pei, M.H. Qiao, K.N. Fan, *Chem Commun.* 47 (2011) 6168-6170.
- [8] E. Gebauer-Henke, J. Farbotko, R. Touroude, J. Rynkowski, *Kinet. Catal.* 49 (2008) 574-580.
- [9] A.M. Ruppert, T. Paryjczak, *Appl. Catal., A* 320 (2007) 80-90.

- [10] B.A. Riguetto, C.E.C. Rodrigues, M.A. Morales, E. Baggio-Saitovitch, L. Gengembre, E. Payen, C.M.P. Marques, J.M.C. Bueno, *Appl. Catal., A* 318 (2007) 70-78.
- [11] J.C.S. Wu, T.S. Cheng, C.L. Lai, *Appl. Catal., A* 314 (2006) 233-239.
- [12] W.X. Tu, H.F. Liu, *Chin. J. Polym. Sci.* 23 (2005) 487-495.
- [13] F. Ammari, J. Lamotte, R. Touroude, *J. Catal.* 221 (2004) 32-42.
- [14] M. Abid, G. Ehret, R. Touroude, *Appl. Catal., A* 217 (2001) 219-229.
- [15] B.M. Bhanage, Y. Ikushima, M. Shirai, M. Arai, *Catal. Lett.* 62 (1999) 175-177.
- [16] F. Zhao, Y. Ikushima, M. Chatterjee, M. Shirai, M. Arai, *Green Chem.* 5 (2003) 76-79.
- [17] T. Seki, J.D. Grunwaldt, N. van Vegten, A. Baiker, *Adv. Synth. Catal.* 350 (2008) 691-705.
- [18] A. Baiker, *Chem. Rev. (Washington, DC, U. S.)* 99 (1999) 453-473.
- [19] W. Leitner, P.G. Jessop, *Chemical Synthesis Using Supercritical Fluids*, Wiley-VCH, 1999.
- [20] C.A. Eckert, D. Bush, J.S. Brown, C.L. Liotta, *Ind. Eng. Chem. Res.* 39 (2000) 4615-4621.
- [21] X. Han, M. Poliakoff, *Chem. Soc. Rev.* 41 (2012) 1428-1436.
- [22] T. Seki, J.D. Grunwaldt, A. Baiker, *Ind. Eng. Chem. Res.* 47 (2008) 4561-4585.
- [23] J.R. Hyde, P. Licence, D. Carter, M. Poliakoff, *Appl. Catal., A* 222 (2001) 119-131.
- [24] M. Burgener, R. Furrer, T. Mallat, A. Baiker, *Appl. Catal., A* 268 (2004) 1-8.
- [25] J.D. Grunwaldt, R. Wandeler, A. Baiker, *Catal. Rev.: Sci. Eng.* 45 (2003) 1-96.
- [26] G.M. Kontogeorgis, G.K. Folas, *Thermodynamic Models for Industrial Applications: from classical and advanced mixing rules to association theories*, Wiley, 2010.
- [27] G.M. Kontogeorgis, E.C. Voutsas, I.V. Yakoumis, D.P. Tassios, *Ind. Eng. Chem. Res.* 35 (1996) 4310-4318.

- [28] G.M. Kontogeorgis, M.L. Michelsen, G.K. Folas, S. Derawi, N. von Solms, E.H. Stenby, *Ind. Eng. Chem. Res.* 45 (2006) 4855-4868.
- [29] G.M. Kontogeorgis, M.L. Michelsen, G.K. Folas, S. Derawi, N. von Solms, E.H. Stenby, *Ind. Eng. Chem. Res.* 45 (2006) 4869-4878.
- [30] M.S. Wertheim, *J. Stat. Phys.* 42 (1986) 477-492.
- [31] G. Soave, *Chem. Eng. Sci.* 27 (1972) 1197-1203.
- [32] R. Dohrn, S. Peper, J.M.S. Fonseca, *Fluid Phase Equilib.* 288 (2010) 1-54.
- [33] C. Crampon, G. Charbit, E. Neau, *J. Supercrit. Fluids* 16 (1999) 11-20.
- [34] I. Tsvintzelis, M.J. Beier, J.D. Grunwaldt, A. Baiker, G.M. Kontogeorgis, *Fluid Phase Equilib.* 302 (2011) 83-92.
- [35] R. Wandeler, N. Kunzle, M.S. Schneider, T. Mallat, A. Baiker, *J. Catal.* 200 (2001) 377-388.
- [36] D. DIADEM, The DIPPR information and Data Evaluation Manager for the Design Institute for Physical Properties. Version 1.1.0 (2006).
- [37] I. Tsvintzelis, G.M. Kontogeorgis, M.L. Michelsen, E.H. Stenby, *Fluid Phase Equilib.* 306 (2011) 38-56.
- [38] K. Bezanehtak, G.B. Combes, F. Dehghani, N.R. Foster, D.L. Tomasko, *J. Chem. Eng. Data* 47 (2002) 161-168.
- [39] M.V. da Silva, D. Barbosa, *Ind. Eng. Chem. Res.* 39 (2000) 4427-4430.
- [40] I.I. Vasileva, A.A. Naumova, A.A. Polyakov, T.N. Tyvina, V.V. Fokina, *J. Appl. Chem-USSR* 62 (1989) 1755-1757.
- [41] J. Ke, B.X. Han, M.W. George, H.K. Yan, M. Poliakov, *J. Am. Chem. Soc.* 123 (2001) 3661-3670.
- [42] R. Tschan, R. Wandeler, M.S. Schneider, M. Burgener, M.M. Schubert, A. Baiker, *Appl. Catal., A* 223 (2002) 173-185.
- [43] F. Zhao, Y. Ikushima, M. Arai, *J. Catal.* 224 (2004) 479-483.
- [44] M. Burgener, D. Ferri, J.D. Grunwaldt, T. Mallat, A. Baiker, *J. Phys. Chem. B* 109 (2005) 16794-16800.
- [45] D. Ferri, T. Buergi, A. Baiker, *Phys. Chem. Chem. Phys.* 4 (2002) 2667-2672.

- [46] B. Minder, T. Mallat, K.H. Pickel, K. Steiner, A. Baiker, *Catal. Lett.* 34 (1995) 1-9.
- [47] S. Ichikawa, M. Tada, Y. Iwasawa, T. Ikariya, *Chem. Commun.* (Cambridge, U. K.) (2005) 924-926.
- [48] F. Zhao, S. Fujita, S. Akihara, M. Arai, *J. Phys. Chem. A.* 109 (2005) 4419-4424.
- [49] Y. Akiyama, S. Fujita, H. Senboku, C.M. Rayner, S.A. Brough, M. Arai, *J. Supercrit. Fluids* 46 (2008) 197-205.

Chapter 4

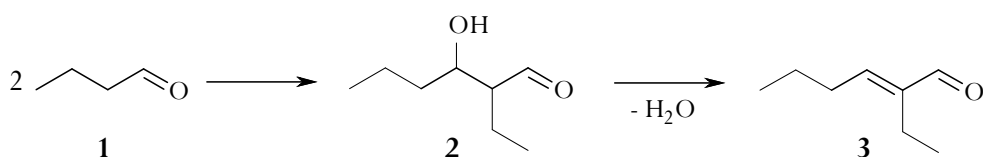
Aldol Reactions in Dense and Supercritical Carbon Dioxide Reaction Medium

Abstract

Aldol reactions of a number of aldehydes have been investigated over acidic and basic catalysts in CO₂ medium at various temperatures and pressures in three modes using: (i) a view cell/batch reactor with adjustable volume which allows phase behaviour monitoring, (ii) homemade batch autoclaves, and (iii) a newly established plug-flow setup. Among other tested catalysts, Amberlyst-15 showed the highest conversion based on the catalyst mass, while supported tungstosilicic acid (TSA)-based catalysts were significantly better if the rates were related to the number of acidic sites. It was found that small and linear aldehydes, such as pentanal react more efficiently than the branched 3-methylbutanal. Furthermore, regardless of the catalyst in the aldol reaction of butanal conversion increases with temperature. In contrast, higher CO₂-content improves the selectivity and yield of the product only for Amberlyst-15. Further catalytic results showed that the conversion of 2-butenal in the “one-pot” synthesis of 2-ethyl-2-hexenal-2 in CO₂ medium in the continuous-flow mode is much higher when one catalyst bed (a physical mixture of 5 wt% Pd/C for the hydrogenation step and 45 wt% TSA/MCM-41 for the aldol reaction) is used compared to the case with two separate beds (hydrogenation catalyst first followed by 45 wt% TSA/MCM-41). The reaction conditions were optimised using thermodynamic calculations performed with the Cubic-Plus-Association (CPA) model. Every reaction was performed in the transition region between the one- and two phases. Extensive catalyst characterisation was performed in order to reveal the structure and properties of the catalysts used in the study.

4.1 Introduction

The aldol reaction, an example of which is presented in Scheme 4.1, plays an important role in chemical syntheses as it leads to C-C bond formation and yields products that can be used as solvents, flavours, additives, etc. [1]. Traditionally, aldol reaction is carried out in liquid phase with stoichiometric amounts of the aqueous solution of inorganic bases (NaOH, Ca(OH)₂, etc.) or acids [2, 3]. Therefore, huge amounts of wastes are produced, whereas conversion and selectivity are usually quite low. Complicated separation and low overall effectiveness of traditional processes require improvements, i.e. the use of heterogeneous catalysts and the development of “green technology” for the aldol reactions. In 2004 Mestres published a review on “green” aldol reaction processes which showed the potential of heterogeneous catalysts, ionic liquids and supercritical fluids [3], but only very little had been done in that direction.



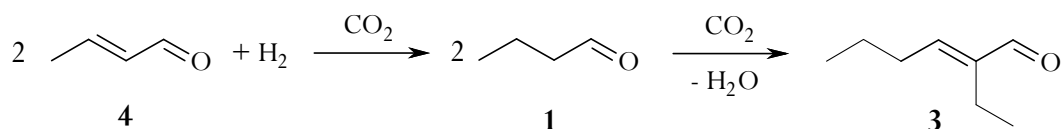
Scheme 4.1. Aldol reaction of butanal (1) to 2-ethyl-2-hexenal (3) via an intermediate product 3-hydroxy-2-ethylhexanal (2).

As it was outlined in earlier chapters, the use of dense and supercritical carbon dioxide in heterogeneous catalysis provides a number of opportunities due to the fact that it combines both gas-like and liquid-like properties [4-6]. Gas-like properties significantly decrease heat and mass transfer limitations, and the relatively high density, which is determined by liquid-like properties, leads to increased solubility and allows the use of CO₂ as an alternative to conventional solvents. The properties of scCO₂ are strongly dependent on temperature and pressure in the system, especially near the critical point, which makes both chemical and separation processes quite tuneable. Besides, the use of carbon dioxide in connection with a solid catalyst makes the whole

technology much “greener” due to the fact that it can be recycled and the amount of waste can be minimised [7].

The aldol cross-condensation of acetone and benzaldehyde over hydrotalcite can be considered as the first reaction performed in the presence of a heterogeneous catalyst [8]. In later work, Matsui *et al.* studied the aldol reaction of propanal in scCO₂ over basic MgO catalysts of different particle size in the presence or absence of water [9, 10]. They found that elevated pressures of CO₂ in batch processing decrease conversion and yield of the products. In related works, a number of bifunctional catalysts have been developed for the synthesis of methylisobutylketone (MIBK) [11-17], which comprises two subsequent steps: (i) the aldol reaction of acetone and dehydration to an unsaturated keton, and (ii) the subsequent hydrogenation of the unsaturated keton to MIBK.

A successful attempt to use the bifunctional catalyst 1 wt% Pd on acidic resin Amberlyst-15 was made by Seki *et al.* [18]. In their work they synthesised 2-ethyl-2-hexenal directly from 2-butenal, as it is shown in Scheme 4.2. In this case, the hydrogenation step precedes the aldol reaction, but the whole process occurs in “one-pot”. Extending this work also by the use of different characterisation techniques a first reaction mechanism was proposed [19]. The active site for 1 wt% Pd/Amberlyst-15 catalyst was considered [Pd-H]⁺, both hydrogenation and aldol condensation steps are taking place on the same active site without an intermediate migration from a palladium particle to an acidic site and back. They also studied the reaction of 2-hexenal in the same synthesis and obtained satisfactory results.



Scheme 4.2. “One-pot” synthesis of 2-ethyl-2-hexenal (3) from 2-butenal (4) in carbon dioxide reaction medium over 1 wt% Pd/Amberlyst-15.

Later Stevens *et al.* studied the aldol reaction of propanal over a number of acidic and basic catalysts in scCO₂, using an automated continuous-flow reactor [20]. These results support that Amberlyst-15 and γ -Al₂O₃ are the promising catalysts for aldol reactions. The authors also performed the “one-pot” synthesis of 2-methylpentenal-2 from propanal using a mixture of hydrogenation and acidic catalysts. Their findings revealed that aldol reactions and scCO₂ reaction medium have a great potential for further investigations.

Nevertheless, only a couple of active catalysts for this process have been found so far. They give good results at temperatures 343 – 373 K, however this temperature range is quite far from the critical point of CO₂ (304.6 K) and it is desirable to shift the reaction temperature range towards this point. The “one-pot” synthesis and the aldol reaction itself in compressed carbon dioxide are not studied in detail yet, and the reaction mechanism is still a matter of discussion. *In situ* spectroscopic investigations of heterogeneous catalysts and reaction media at high pressures could be useful for that purpose as it was done in Ref. [21]. Furthermore, the aldol reaction occurs alongside with the formation of relatively heavy products the solubility of which in CO₂ is lesser compared to the reactants. Therefore, monitoring and controlling the phase behaviour is crucial in the study.

Although bifunctional catalysis is an attractive tool for the reaction improvement, however, hydrogenation and aldol reaction steps are quite different in the sense that the saturation of C=C double bond with hydrogen over noble metal catalysts is a quite easy and well established step [5], unlike aldol reactions which are usually much slower and reasonable conversions are achieved at elevated (compared to hydrogenation) temperatures. In addition, the hydrogenation of 2-butenal to butanal in carbon dioxide medium over the 5 wt% Pd/C catalyst was studied and discussed in the previous chapter. The study revealed that the amount of CO₂ in the system determines the phase behaviour, and thereby affects the catalyst performance. The maximum conversion is achieved in the transient state between the one- and two-phase regions. The optimal CO₂ : 2-butenal ratio may not be optimal for the aldol reaction step.

The role of thermodynamic modelling in chemical reactions has been outlined in previous Chapters 1, 2, and 3, and will be discussed further in this thesis. The reaction conditions for the aldol reaction of butanal and two butanal were optimised using an advanced model the Cubic-Plus-Association (CPA) Equation of State [22], which was discussed in detail in Chapter 2.

Therefore, this part of the thesis was aimed at: (i) screening a number of acidic and base catalysts for aldol reactions of aldehydes with different chemical structure, (ii) investigating the influence of temperature and CO₂-content on the catalyst performance during the aldol reaction of butanal over the best catalysts, and (iii) investigations into the “one-pot” synthesis of 2-ethylhexenal from 2-butanal in CO₂ medium in different reaction modes.

4.2 Experimental

4.2.1 Materials

All substances used in the present study such as solvents, reactants, catalyst precursors, carriers, were purchased from Sigma-Aldrich, unless otherwise stated. The following organic materials were used without further purification: propanal ($\geq 97\%$), butanal ($\geq 99\%$), pentanal ($\geq 97\%$), hexanal (98%), 3-methylbutanal (97%), 2-butanal (99.5%), toluene (99.5%), and acetone (99.5%).

4.2.2 Catalyst preparation

A number of different acidic and basic catalysts were chosen for catalyst screening. HZSM-5(15) (from Zeolyst), γ -Al₂O₃ and SiO₂ (from Haldor Topsøe) and Amberlyst-15 (16-50 mesh, number of acid sites - 4.7 meq/g by dry weight) were received commercially and directly used for the catalytic tests. A 5 wt% Pd/C catalyst was prepared according to the description presented in Chapter 3.

Tungstosilicic acid (TSA) supported catalysts (10, 20, 40 and 45 wt% TSA on SiO₂ or MCM-41) were prepared by incipient wetness impregnation. 0.22, 0.50, 1.33, and

1.50 g of TSA ($\text{H}_4\text{SiW}_{12}\text{O}_{40}\cdot\text{H}_2\text{O}$, $\geq 99.9\%$) correspondingly were dissolved in 1.2 ml for SiO_2 or 2 ml for MCM-41 (specific surface area 940-1000 m^2/g , 1.0 cm^3/g pore volume, 2.5 – 3 nm pore size) of deionised water. The amounts were calculated from the pore volumes of the carriers. 2.0 g of each carrier were impregnated by the solutions; the samples were subsequently dried in air until visually dry, at 373 K overnight, and calcined at 573 K for 5 hours.

Hydrotalcite (HT) preparation was carried out by the procedure described in Ref. [23]: solution A was prepared by dissolving 25.6 g of $\text{Mg}(\text{NO}_3)_2\cdot 6\text{H}_2\text{O}$ (0.1 mol, purity 97%) and 18.6 g of $\text{Al}(\text{NO}_3)_3\cdot 9\text{H}_2\text{O}$ (0.05 mol, purity 98%) in 70 ml distilled water. Solution B was prepared by dissolving 28.0 g of 50% NaOH (14.0 g of NaOH pellets, in 14 ml distilled water, purity 98%) and 10.0 g of Na_2CO_3 (purity 99%) in 100 ml distilled water. The hydrotalcite was prepared by adding solution A to solution B in 3-4 h with constant stirring. The resulting gel was transferred to an autoclave (250 ml inner volume with a Teflon cup and magnetic stirrer inside) and allowed to crystallize at 323 K for 18 h. The sample was filtered off and washed with hot distilled water until the pH of the filtrate was neutral and also to remove any free sodium ions that may present. The sample was dried in an oven for 12 h at 373 K and then calcined at 723 K in air for 18 h to obtain the hydrotalcite.

A 1 wt% Pd/Amberlyst-15 sample was prepared strictly in accordance with the recipe presented in Ref. [18, 19]. 0.0532 g of $[\text{Pd}(\text{NH}_3)_4]\text{Cl}_2$ were dissolved in 20 ml of deionised water and 2.02 g of Amberlyst-15 were added to this solution in a 50 ml flask. The obtained heterogeneous mixture was left for constant stirring at 353 K for 24 hours. The saturated material was later filtered off, washed with 20 ml of deionised water, and dried first in air until visually dry, and in an oven at 383 K overnight. The obtained sample was then activated in N_2 flow containing 10 vol% of hydrogen at 383 K for two hours.

A 0.5 wt% Pd/45 wt% TSA/MCM-41 catalyst was prepared using the incipient wetness impregnation technique. As a carrier 45 wt% TSA/MCM-41 was used which had been previously prepared according to the procedure described above. In this regard,

0.0128 g of $[\text{Pd}(\text{NH}_3)_4]\text{Cl}_2$ were dissolved in 0.8 ml of deionised water, and 0.9987 g of 45 wt% TSA/MCM-41 were impregnated with the obtained solution. It was dried in air until visually dry, and at 373 K in an oven overnight. The sample was activated in N_2 flow containing 10 vol% of hydrogen at 383 K for two hours. The final catalyst was stored in dry atmosphere.

Using a similar technique, a 0.5 wt% Pd/45 wt% WO_3 /MCM-41 sample was prepared. 1.0390 g of $(\text{NH}_4)_6\text{W}_{12}\text{O}_{40}$ (99.5% pure) were dissolved in 1.21 ml of deionised water and this solution was used for the impregnation of 1.19 g of MCM-41. The obtained material was dried in air until visually dry, then at 373 K overnight, and subsequently calcined in an oven at 623 K for 5 hours. After that 0.0063 g of $[\text{Pd}(\text{NH}_3)_4]\text{Cl}_2$ were dissolved in 0.4 ml of deionised water, and 0.4903 g of 45 wt% WO_3 /MCM-41 (pore volume approx. $0.8 \text{ cm}^3/\text{g}$) were impregnated with the obtained solution. The sample was dried in air, at 373 K in an oven overnight, and subsequently activated in N_2 flow containing 10 vol% of hydrogen at 383 K for two hours. The final sample was stored in dry atmosphere.

Finally, a 0.2 wt% Pd/ MCM-41 sample was obtained using the incipient wetness impregnation technique as well as the previous samples. In this regard, 0.0063 g of $[\text{Pd}(\text{NH}_3)_4]\text{Cl}_2$ were dissolved in 1.94 ml of deionised water, and 0.9994 g of MCM-41 were impregnated with this solution. The product was dried in air until visually dry, and at 373 K in an oven overnight. The sample was activated in N_2 flow containing 10 vol% of hydrogen at 383 K for two hours. The final material was stored in dry atmosphere.

4.2.3 Catalyst characterisation

The specific surface area of the prepared catalysts was determined using BET isotherms recorded on a BEL Japan surface area analyser at a liquid N_2 temperature of 77 K.

The number of acidic sites on surface for the samples were estimated using ammonia temperature-programmed desorption (NH_3 -TPD). The experimental procedure was as follows. A catalyst sample (0.2 – 0.3 g) was fixed with glass wool in a

glass reactor with two thermocouples inside for controlling the temperature. At the beginning of the experiments the reactor with the sample was flushed with N₂ flow (510 ml/min) and heated up to 623 K (with a ramp of 10 K/min) for desorbing light components and gases from the catalyst surface. After that the system was cooled down to 328 K, and the gas flow was switched to the NH₃ flow (600 ppm NH₃ in N₂, total flow 510 ml/min). The saturation occurred at a constant temperature of 327 – 328 K. The amount of NH₃ in the outlet line after the reactor was detected by a non-dispersive infrared (NDIR) detector, which had been previously calibrated. When NH₃ concentration reached a plateau, the flow was switched back to the pure nitrogen to flush out an excess amount of the adsorptive. When the concentration of NH₃ came to a steady minimum the system was heated up to 753 K (with a ramp of 10 K/min). Thereby, the desorption profile was recorded from which the number of acidic sites was estimated.

Transmission electron microscopy (TEM, FEI Technai TEM operating at 200 kV, Centre for Electron Nanoscopy, DTU) was used for determining the morphology and particle size on the catalyst surfaces.

Crystalline structure of obtained catalysts was studied using the X-Ray Diffraction (XRD) technique on Bruker D8-Advance Diffractometer with a Cu K α -Anode source, $\lambda=1,54$ nm, angle range 20 - 80° 2 θ .

X-ray absorption spectroscopy (XAS) data were collected at the tungsten L₃-edge in transmission mode at the synchrotron radiation facilities ANKA (Karlsruhe, Germany) at the ANKA-XAS beamline and HASYLAB (Hamburg, Germany) at the beamline X1. For these experiments the catalysts were pressed to pellets with cellulose as additive. The edge jumps (defined by difference in pre-edge and post-edge sections at the edge) were 0.4-0.7. The raw data were energy calibrated, background corrected and normalized using the ifeffit-code [24]. After extraction of the $\chi(k)$ function from the EXAFS data, Fourier transformation was performed on the k^3 -weighted data in the interval $k = 2.0 - 12.0 \text{ \AA}^{-1}$.

4.2.4 Catalytic reactions

4.2.4.1 View cell

Aldol reactions and “one-pot” syntheses with different reactants were carried out in a batch reactor/view cell with adjustable volume (inner volume 23 – 64 ml, $T_{\max} = 300$ °C, $P_{\max} = 300$ bar, NWA analytics, Lörrach, Germany) and a sapphire window for *in situ* monitoring of the phase behaviour of the reaction mixture. The temperature was controlled by a J-type thermocouple connected to a Eurotherm 2216e controller, and the pressure was monitored by a standard manometer. For safety reasons, the cell was equipped with a burst plate (Swagelok, 300 bar). The cell construction was similar to the phase equilibria monitoring cell described in Chapter 3.

Before the experiments the cell was thoroughly cleaned, washed with organic solvents, and subsequently dried with pressurised nitrogen. First, the required amount of catalyst was loaded into the batch reactor and the lid was tightened. The liquid substrate was added with a syringe through a hole in the upper part of the cell. Then it was sealed and flushed several times with gaseous carbon dioxide in order to replace all the air inside by CO₂. After that the batch reactor was charged with CO₂, adjusted by the pressure in the system. When carrying out “one-pot” syntheses, it was previously charged with the required amount of hydrogen. After pressure charging the whole system underwent leakage testing. Then the reactor was heated up to a desired temperature with constant stirring. The pressure was adjusted to the working conditions by the means of an oil-pump pushing the piston in the cell, thereby changing the reactor volume. Typical reaction conditions were 373 K, 180 bar and 2 h reaction time. After the reaction the cell was cooled down to room temperature and slowly depressurised down to atmosphere pressure. The batch reactor was opened and a sample was taken with a syringe, diluted with acetone and analysed by GC-analysis described below.

Prior to every experiment blind tests for hydrogenation and aldol reactions without catalysts were performed. No detectable catalytic activity was observed under the typically applied reaction conditions.

Product analysis was performed using a gas chromatograph (Agilent 6890 N) with a 7683 B series autosampler with a polar capillary column (HP INNOWAX, 30 m length and 0.25 mm diameter) and a flame ionisation detector (FID). Column temperature conditions were 323 K (10 min) – heating with a ramp of 20 K/min – 523 K (10 min). The products were identified by comparing the GC retention times with those of commercially available authentic samples. Before the analyses the GC was calibrated for the reactants and possible products.

4.2.4.2 Batch reactors

The aldol reaction of butanal and the “one-pot” synthesis were also performed in conventional homemade stainless steel autoclaves with magnetic stirring bars ($T_{\max} = 250$ °C, $P_{\max} = 200$ bar, inner volume ~ 125 ml), which were also used for catalytic studies in Chapter 3 of the present thesis with a similar experimental procedure. Before use, the reactors were thoroughly washed with isopropanol and acetone and dried with air. Desired amounts of catalysts and butanal were loaded into the reactors which were tightly closed afterwards. Carbon dioxide was added using a CO₂-compressor (NWA, PM-101, Lörrach, Germany), and its amount was measured by weighing the autoclaves before and after loading. Pressure and temperature were monitored with installed manometers and thermocouples, respectively.

After the reaction, the autoclaves were quickly cooled down to room temperature in a water bath, consequently depressurised, and opened. Samples of the reaction mixture were taken out, diluted with toluene and analysed using a gas chromatograph (Shimadzu, GC 2010+, HP INNOWAX, 30 m length and 0.25 mm diameter), which had been previously calibrated for the reactant and possible products. The typical column conditions were 343 K (5 min) – heating with a ramp of 20 K/min – 543 K (5 min).

4.2.4.3 Continuous-flow apparatus

The continuous-flow setup design was similar to the one described in Ref. [25, 26], with the difference in the view cell that is missing in the presented here version, Fig. 4.1.

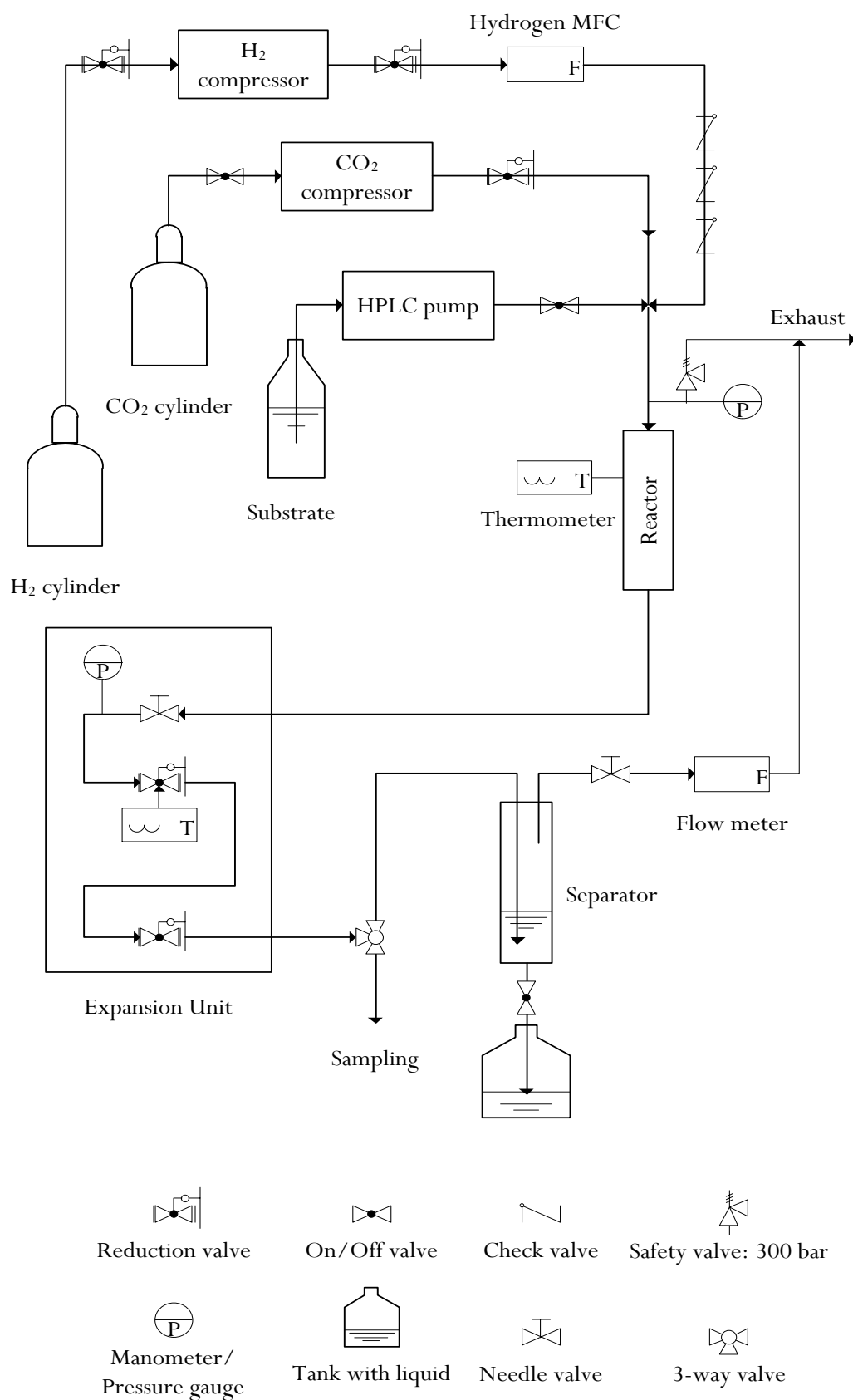


Fig. 4.1. Scheme of the experimental setup for continuous-flow reactions in dense and supercritical carbon dioxide.

All tubes and valves were purchased from Swagelok. Carbon dioxide pressurised with a compressor (NWA, PM-101, Lörrach, Germany) up to 120 bar was supplied to the system via an interconnected reduction valve (TESCOM, stainless steel, P/N 44-1165-24), which reduced the pressure down to the required one, typically 90 bar. Hydrogen from a cylinder via a reduction valve installed on the hydrogen bottle with a pressure of around 50 bar was transported to a H₂-compressor (NWA, CU105, Lörrach, Germany), where it was pressurised up to 110 – 120 bar. Via an interconnected reduction valve (TESCOM, stainless steel, P/N 44-1165-24) the pressure was reduced to that one slightly higher than the pressure in the system, i.e. typically 2 – 3 bar higher than the reaction pressure. The hydrogen flow was regulated by a high-pressure mass flow controller (Bronkhorst, F-230M-RGD-33-K), and the risk of the back-flow of liquid and other substances was minimised by three consequently connected check-valves. Liquid substrates were introduced to the reactor by a GILSON 305 HPLC pump (10 ml pump head volume) connected to the system via an on/off valve.

The reactor comprised a 220 mm long Swagelok tube (8 mm OD, 5 mm ID) with a heating jacket and a Eurotherm 2216e temperature controller, together with a pressure gauge (OEM Pressure Transmitter Type C-10, WIKA, Germany). For safety reasons it was also equipped with a burst plate ($P_{\max} = 300$ bar). The reactor was filled with the desired amount of catalyst (fraction 250 – 500 μm) with inert quartz wool at the top and bottom of the catalyst bed.

The reaction mixture coming out of the reactor was consequently depressurised by two reduction valves, the first of which was heated by a Eurotherm 2216e temperature controller in order to avoid crystallisation in the lines due to the Joule-Thompson effect. The product was collected in a separator where phase splitting occurred and the gas phase was connected to an exhaust line via a needle valve and a flow meter. The separator was connected to the system via a three-way valve, which was also used for taking samples.

Prior to every experiment the reactor with catalyst was flushed with CO₂ and the pressure was regulated as required, after which the desired hydrogen flow was set. At a next step, the reactor was heated up to the required temperature and the desired flow of the liquid substrate was introduced with the HPLC pump. The gaseous flow of CO₂ was measured at the outlet of the reactor (accounting as well for the hydrogen flow) and controlled manually with a needle valve on the gas line after the separator. The samples were taken after the conversion became stable. An average of 5 – 7 samples per experimental point was taken and analysed using a GC-analysis exploiting exactly the same procedure as described in section 4.2.3.2.

4.2.5 Thermodynamic modelling with CPA

The importance of phase behaviour during heterogeneously catalysed chemical reactions has been outlined in Chapter 1 of this thesis. The difficulties connected to experimental determination of the phase behaviour may be overcome by the use of thermodynamic models. In the present study the advanced CPA EoS was used (cf. section 2.4).

The reaction mixture included the following components: 2-butenal, butanal, hydrogen, carbon dioxide and aldol reaction products. For the first four components the CPA pure fluid and binary interaction parameters were estimated in Chapter 3, Tables 3.3 and 3.4. The literature data for aldol reaction products, i.e. 3-hydroxy-2-ethylhexanal and 2-ethyl-2-hexenal, are extremely scarce due to the complexity of the components.

For the catalytic studies it was decided to stick to one type of phase equilibria, namely to the transition from the two-phase region to the one single phase. In other words, it was decided to perform experiments when reaction mixtures experience similar phase equilibria. Since in Chapter 3 it was found that the phase transition region gives the highest conversion, the same assumption was applied here as well. Therefore, the corresponding amounts of CO₂ were calculated using CPA in order to achieve phase transition of a given system at given reaction temperature and pressure. Note, however,

that the assumption that the phase transition conditions are the best for the aldol reaction may not be generally valid. Nevertheless, it unifies the phase equilibria of different reactions and helps to minimise its influence on the catalytic results. This will be further discussed in the Results section.

Since only the fluid composition of the initial state was taken into account, the CPA parameters for aldol reaction products were not estimated and were not used in this study. However, note that due to large molecular weight and volume these components have lower solubility in CO₂ than the initial components. In other words, if the reaction starts in the one phase region, the reaction mixture may easily split into two phases under certain conditions.

The reaction conditions were optimised using SPECS software – a program for phase equilibrium calculations developed at the Centre for Energy Resources Engineering (CERE), Department of Chemical and Biochemical Engineering, Technical University of Denmark. The calculations were made using the two-phase flash algorithm integrated into the software. The reaction temperature and pressure were fixed, whereas the feed composition, i.e. CO₂ : butanal or CO₂ : H₂ : 2-butenal mole ratio, was varied manually. By running the code the number and the composition of co-existing vapour and liquid phases were obtained. The feed composition, at which the phase splitting occurs, i.e. the desired reaction conditions, was found by stepwise approximation.

4.3 Results

4.3.1 Catalyst characterisation

The BET surface areas of the catalysts and carriers and the numbers of their acid sites are presented in Table 4.1 from which it is clearly seen that loading TSA significantly decreases the total surface area of the carriers which it is deposited on. Thus, the surface area of pure MCM-41 is 980 m²/g and after loading 40 wt% of H₄SiW₁₂O₄₀ it dropped more than twice, down to 372 m²/g. Similarly, the surface area of silica decreased after loading the acid, considering that the BET surface area of pure silica is 91

m²/g. Hence, higher loading of TSA causes a decrease of the sample surface area probably due to the deposition on narrow pores or particle coagulation. Nevertheless, the surface area remains relatively high.

It was previously reported that TSA deposited on MCM-41 forms separate particles on the carrier surface [27]. Assuming that the average surface occupied by one TSA molecule is 1.44 nm², only 120 m²/g is covered with the acid in the 40 wt% TSA/MCM-41 catalyst, which is just 12.3% of the total surface of MCM-41. It was further previously reported that above 6 wt% TSA the Keggin cluster remained intact [28] and that TSA deposited on SiO₂ forms layers with different uniform thickness depending on the loading of the acid. Theoretically, 10, 20 and 40 wt% loadings of TSA form 1.8, 4.6, and 8.7 layers on the silica surface [29]. W. Kuang *et al.* [30] suggested based on calculations by XRD results using the Scherrer's equation that silica-supported tungstophosphoric acid with 40 wt% loading mainly deposited on the silica surface in a form of small particles of about 26 nm in diameter.

An interesting trend was observed when measuring the number of acid sites of the samples using NH₃-TPD. The TSA samples were prepared using the incipient wetness impregnation; therefore, it was additionally possible to calculate the theoretical number of acid sites. Assuming that tungstosilicic acid H₄SiW₁₂O₄₀ with Keggin structure forms a monolayer on the carrier surface, and that all active sites are equally accessible one can calculate the number of acidic sites. With only the four protons of the Keggin cluster, as the origin of the acidity, the acidity of the 10% wt. catalyst is approximately 0.14 mmol/g. The theoretical numbers of acid sites of the samples containing 20, 40, and 45 wt% of TSA are 0.27, 0.55, and 0.62 mmol/g, respectively. The results are presented in Table 4.1.

Table 4.1 shows that the experimentally determined acidity of TSA catalyst was almost 3 – 4 times higher than calculated, depending on the type of the carrier. This could mean that the assumption that only the four protons possess acidity in tungstosilicic acid molecules was incorrect. Obviously, some other parts of the molecules have certain acidity. Furthermore, it should be kept in mind that the carriers also possess Brønsted

and Lewis acid sites. Thus, MCM-41 has significantly higher number of acid sites than silica. This could partly explain the higher deviation of experimental acidity from the theoretical in case of the 40 wt% TSA/MCM-41 sample compared to 40 wt% TSA/SiO₂ (2.32 vs. 3.62 mmol/g). Another reason for that deviation could be the difference in surface areas of two carriers. Presumably, the TSA molecules are spread more evenly on the MCM-41 surface than on the silica, therefore, they are more accessible for NH₃ molecules during adsorption-desorption processes.

Table 4.1. BET surface area and number of acid sites of the catalysts and carriers.

Catalyst	S_{BET} , m ² /g	Number of acid sites, mmol/g	
		Experimental	Calculated
SiO ₂	91	0.02	-
MCM-41	980	0.78	-
10 wt% TSA/SiO ₂	79	0.37	0.14
20 wt% TSA/SiO ₂	66	0.99	0.27
40 wt% TSA/SiO ₂	60	2.32	0.55
40 wt% TSA/MCM-41	372	3.62	0.55
γ -Al ₂ O ₃	215	1.88	-
HZSM-5 (15)	400	4.18	-
Hydrotalcite ^a	37	-	-

^a basic catalyst.

Furthermore, the results in Ref. [27] suggest that measuring acidity of heteropolyacids using ammonia as a probe molecule is not absolutely correct. Heteropolyacids may behave in some respects like liquids in the sense that under certain conditions light polar molecules like water, ethanol, etc. may easily penetrate the Keggin's structure and react inside the bulk material. This results in higher adsorption of ammonia, which is not only due to the acidic sites. Hence, the data given in Table 4.1 should be taken as a trend only. As an alternative, the temperature-programmed

desorption of benzonitrile can be used for the determination of the surface acidity of heteropolyacids [27].

Tungstosilicic acid catalysts and their carriers were studied using XRD, and the obtained diffractograms are presented in Fig. 4.2. The XRD patterns of pure materials, i.e. MCM-41, SiO₂ and tungstosilicic acid are shown in Fig. 4.2 (a) and reveal absence of any reflections in the area of large angles and by a broad peak at the beginning of the diffractogram ($2\theta = 25 - 27$ deg). For MCM-41 this is explained by the fact that it is a crystalline mesoporous material, which gives reflections only at small 2θ angles, i.e. 1 – 5 degrees [31]. Whereas for SiO₂ the absence of reflections in XRD might indicate its amorphous structure. The TSA pattern with well-defined reflections, in turn, shows the crystalline structure of the acid. The reflections for TSA resembles very much those reported in Ref. [27], where the highest peaks are obtained at 2θ angles of 26, 34, 53, and 63. Other reflections also coincide. The XRD diffractograms of 10, 20, and 40 wt% TSA/SiO₂ are shown in Fig. 4.2 (b), and indicate that with the increase in TSA content on SiO₂ surface the crystallinity of the acid is also increasing, together with the average particle size. Considering the relatively small surface area of silica TSA forms large particles and agglomerates on its surface when the TSA content increases. This is not the case, however, for highly loaded TSA on MCM-41 catalysts, Fig. 4.2 (c). Furthermore, the reflections from the 40 wt% TSA/SiO₂ strongly resemble those of the pure TSA. Here it can be concluded that silica surface hosts large TSA particles especially for the samples with high TSA loadings.

Since the TSA dispersion on the catalyst surface plays an important role in catalysis two samples were further investigated by transmission electron microscopy. Due to the fact that MCM-41 is a mesoporous material it was difficult to obtain clear TEM images of the sample. Some of the images are depicted in Figure 4.3.

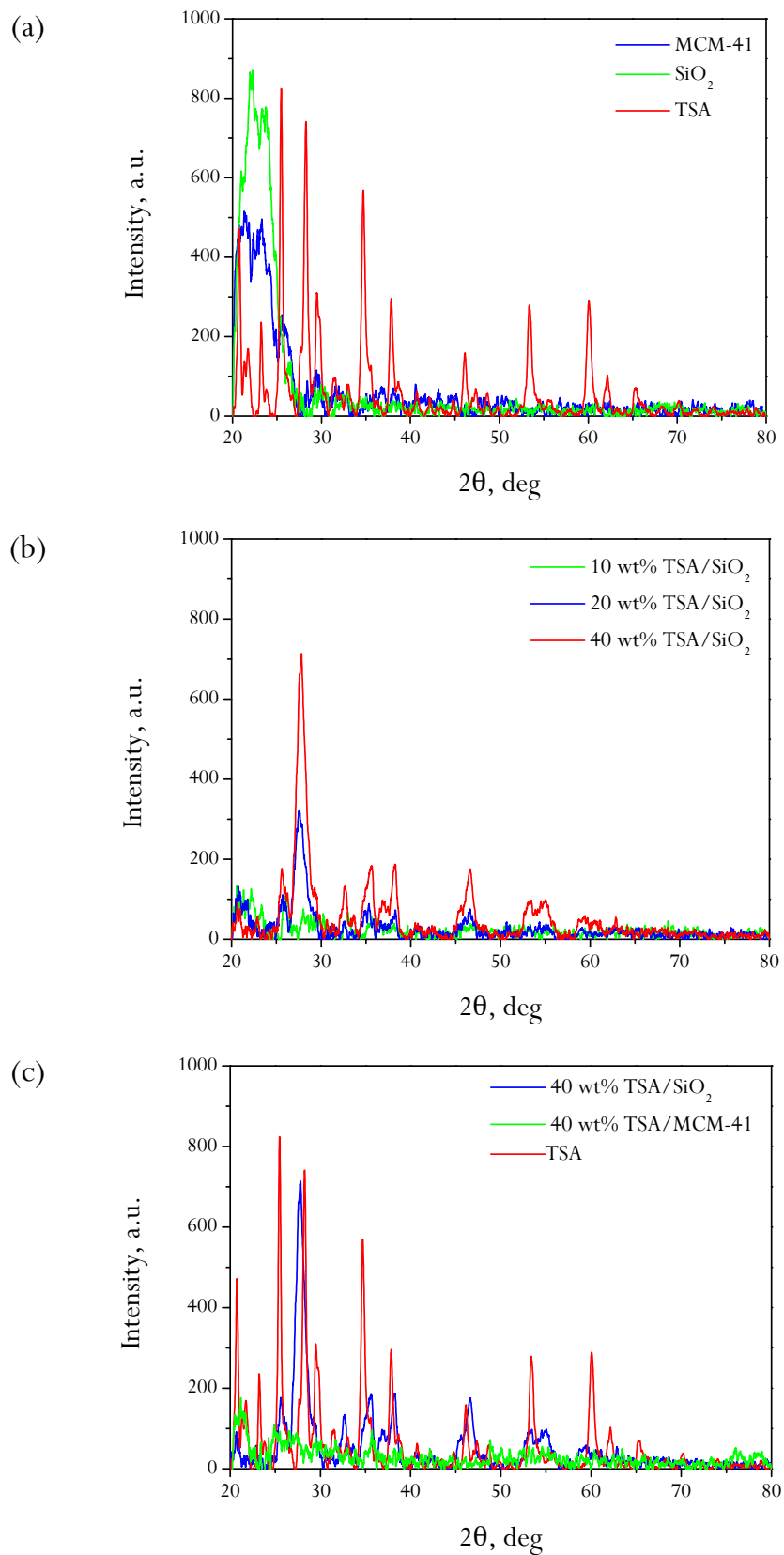
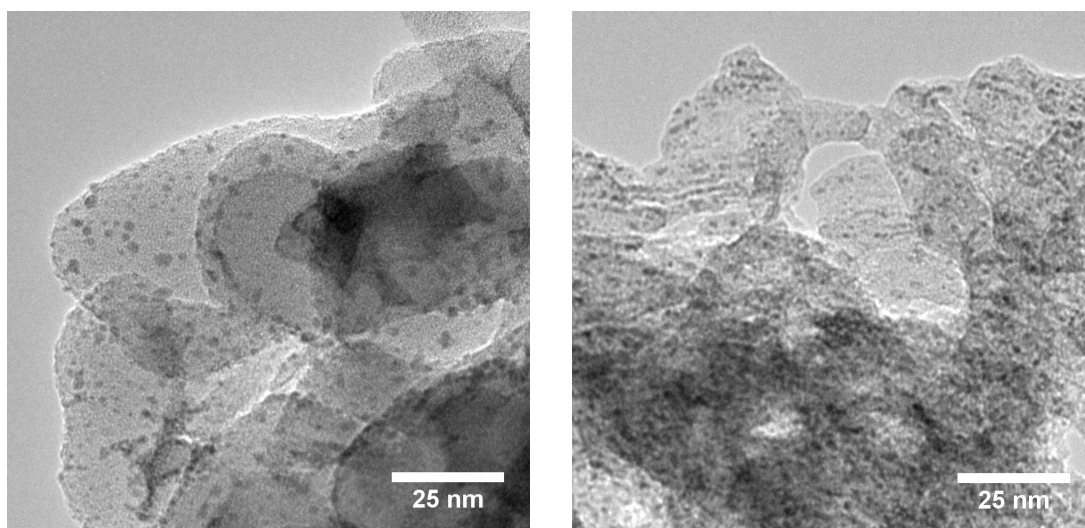


Fig. 4.2. XRD patterns of tungstosilicic acid (TSA), two carriers - MCM-41 and SiO₂, and supported TSA catalysts – 10, 20, 40 wt% TSA on MCM-41 and SiO₂.

From the TEM images of TSA on MCM-41 catalyst alone it is difficult to conclude about the dispersion of the acid. However, the comparison of the TEM images of the 40 wt% TSA/MCM-41 sample with those of 40 wt% TSA/SiO₂ at the same magnification reveals that the dispersion of the acid is higher on the MCM-41 as the particles on the surface appear to be smaller. From the image of the 40 wt% TSA/SiO₂ sample it can be seen that the acid is finely dispersed on the carrier surface, and mainly forms agglomerates of several molecules of TSA. However, according to Kuang *et al.* [30] silica-supported tungstophosphoric acid with 40 wt% loading mainly deposited on the silica surface in a form of small particles about 26 nm in diameter. In the obtained TEM images for 40 wt% TSA/SiO₂ it is seen that the particles are much smaller than 25 nm. This might indicate that TSA is unevenly deposited on silica, i.e. it forms large particles, which give reflections in XRD, as well as smaller ones like those on Fig. 4.3. However, for 40 wt% TSA on MCM-41 the distribution shown on the TEM images can be reasonable, since no reflections for TSA are observed in the XRD patterns for this catalyst.



40 wt% TSA/SiO₂

40 wt% TSA/MCM-41

Fig. 4.3. Typical TEM images of tungstosilicic catalysts.

X-ray absorption spectroscopy techniques were applied to get an insight into catalysts structure. The spectra were obtained for TSA catalysts at the W L₃-edge in

transmission geometry. As indicated by the white line intensity (Fig. 4.4), which is determined by the absorption maximum at the edge, the tungsten in all catalyst samples is very similar to the TSA reference sample, but due to the higher whiteness more ionic, i.e. more oxidized. Note also that in the pure TSA self-absorption effects may play a stronger role. The k^3 -weighted EXAFS spectra and the corresponding Fourier transforms (k -range 0-6 \AA^{-1}) are shown in Fig. 4.5. The two coordination shells in the Fourier transformed data are presumably W–O at 1.6 \AA and W–O–W at 3.3 \AA (not phase-corrected) shells. The spectrum of pure TSA is very similar but exhibits slightly lower signals for both shells than the 10 – 40 wt% TSA catalysts, supporting the conclusion in Ref. [32] that at loadings of 10 wt% and higher mostly Keggin clusters are formed during the impregnation process on silica. Note that the structure both on silica and MCM-41 is the same.

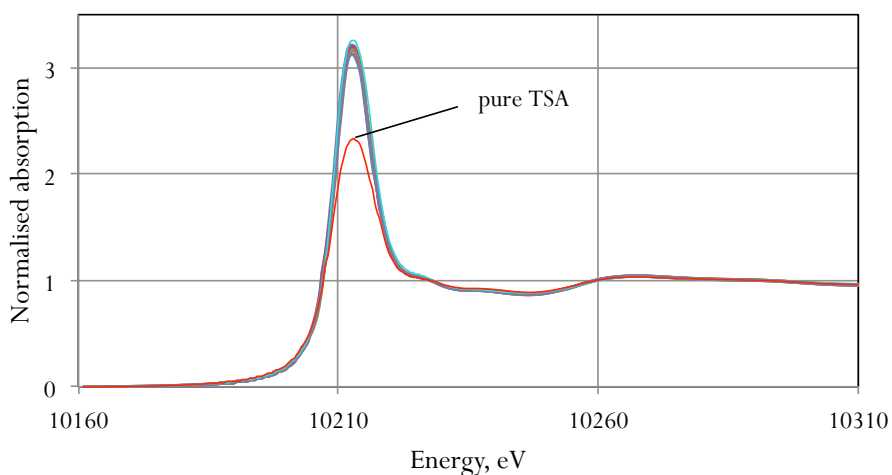


Fig. 4.4. XANES spectra of pure tungstosilicic acid (TSA) and the TSA catalysts: 10 wt% TSA/SiO₂, 20 wt% TSA/SiO₂, 40 wt% TSA/SiO₂, and 40 wt% TSA/MCM-41.

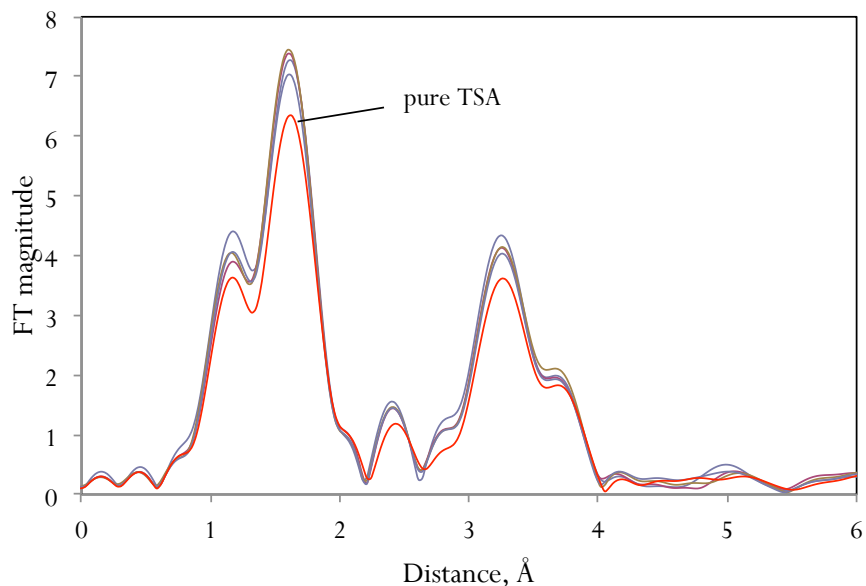


Fig. 4.5. Fourier transformed EXAFS spectra (k -range 2-12Å, k^3 -weighted) of pure tungstosilicic acid (TSA) and the TSA catalysts: 10 wt% TSA/SiO₂, 20 wt% TSA/SiO₂, 40 wt% TSA/SiO₂, and 40 wt% TSA/MCM-41.

Newman *et al.* [33] reported EXAFS analysis on H₃PW₁₂O₄₀/SiO₂ catalysts with an acid loading between 3.6 and 62.5 %wt. It was found that for all catalysts the Keggin's structure remains intact, even at the low loadings. However, in the same work it was also mentioned that there are some strong interactions between –OH groups of the silica support and the acid, which may cause a destruction of tungstophosphoric acid. The formation of species like $(\equiv\text{SiOH}_2)^+(\text{H}_2\text{PW}_{12}\text{O}_{40})^-$ was reported [34], but note that the loadings in the present work were kept rather high.

4.3.2 Catalytic studies

A number of catalysts were tested in the aldol reaction of butanal in a view-cell autoclave with adjustable volume according to the abovementioned experimental procedure. The phase behaviour was monitored during the reactions, which were carried out under the same reaction conditions for all catalysts and occurred in one single phase without phase splitting even after the reactions were terminated. The results of the experiments are shown in Table 4.2.

Table 4.2. Aldol reaction of butanal over different catalysts in scCO₂ in a view cell with adjustable volume.

Catalyst	Conversion, %	Selectivity, %	Reaction rate, mol/(g _{cat} ·h)
Amberlyst-15	51	100	5.1
Hydrotalcite	14	100	1.4
HZSM-5 (15)	13	100	1.3
γ-Al ₂ O ₃	11	100	1.1
MCM-41	9	100	0.9
10 wt% TSA/SiO ₂	9	100	0.9

Conditions: substrate 0.02 mol, $m_{\text{cat}} = 0.1$ g, temp. 373 K, $m_{\text{CO}_2} = 10$ g, total pressure 180 bar, reaction time 120 min, single phase reaction.

All the catalysts showed 100% selectivity and 2-ethylbutenal-2 was observed as the only product. The most active catalyst in terms of the mass of the used catalyst was Amberlyst-15, giving by far the highest conversion. Surprisingly, the second active catalyst was hydrotalcite with base properties, because carbon dioxide is known to inhibit the performance of base catalysts due to its weak acidic properties [4]. Also other acidic catalysts showed reasonable catalytic performance considering that the number of acidic sites is much smaller compared to Amberlyst-15.

As Amberlyst-15 turned out to be the most active catalyst for the aldol reaction of butanal, it was also tested in the reactions with other saturated aldehydes under identical conditions, the results are presented in Fig. 4.6. Note that all the reactions occurred in a single phase, even for hexanal with the highest molecular weight only one phase was observed at the end of the reaction, which means that the dissolution power due to the sufficient density of carbon dioxide was able to maintain the system in one phase. The results have shown that the reaction rate decreased with the increasing complexity of the reactant structure. The selectivity was decreasing as well, but only slightly. This trend can be explained by the increased steric hindrance.

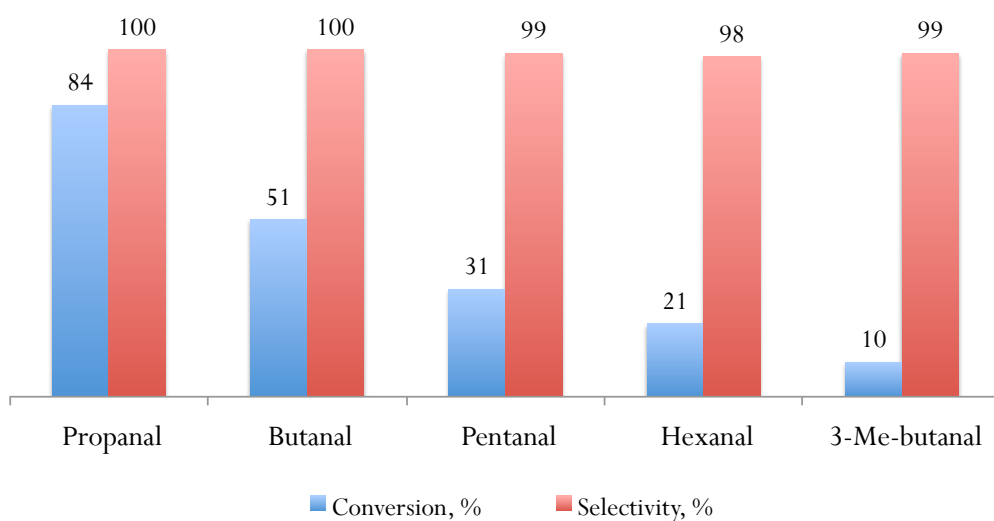


Fig. 4.6. Aldol reaction of different saturated aldehydes over Amberlyst-15 in $scCO_2$ in a view cell with adjustable volume. *Conditions:* substrate 0.02 mol, $m_{cat} = 0.1$ g, temp. 373 K, $m_{CO_2} = 10$ g, total pressure 180 bar, reaction time 120 min.

The number of acid sites of Amberlyst-15 is known to be 4.70 mmol/g, therefore, reaction rates can also be expressed as turnover frequency (TOF) considering that all acidic sites are accessible. The catalyst sample of 10 wt% TSA/SiO₂ was prepared synthetically, therefore it is also possible to calculate its number of acid sites with the assumption that one mole of tungstosilicic acid has 4 moles of protons and TSA forms a monolayer on the surface of silica, which was already discussed. However, several layers could form on the surface, therefore, the calculated number can be seen as the theoretical maximum. The estimated number of acid sites of 10 wt% TSA/SiO₂ is 0.14 mmol/g. The calculated TOF for butanal is 64 h⁻¹, which is almost 5.7 times higher compared to that of Amberlyst-15 (11 h⁻¹). Therefore, TSA can be potentially used as an active and selective catalyst for the process, especially at lower temperature near the critical point of carbon dioxide.

At a next step, a number of different TSA supported catalysts were prepared. These samples were tested in the aldol reaction of butanal under the same conditions as in the case of Amberlyst-15. Two types of carriers were used – silica oxide with a BET surface area of 91 m²/g and mesostructured MCM-41 with a surface area of 980 m²/g

(Table 4.1). The results of catalytic experiments together with the reaction rates and TOF's are presented in Table 4.3. It is seen that higher loadings of the acid give higher magnitudes of conversion at almost 100% selectivity. When the same TSA loadings were used, the catalyst with higher surface area, i.e. 40 wt% TSA/MCM-41, showed almost doubled conversion, compared to 40 wt% TSA/SiO₂ with lower surface.

Since it was observed that Amberlyst-15 and tungstosilicic acid supported on a high surface material like MCM-41 are effective catalysts for aldol reactions, they were tested in the aldol reaction of butanal in batch autoclaves. The amount of CO₂ as well as the reaction temperature was varied. The results are presented in Table 4.4. It was observed that with increasing temperature the conversion of butanal over 45 wt% TSA/MCM-41 is also increasing (entries 1, 2, and 3). This is also true for the selectivity and, correspondingly, the yield of 2-ethyl-2-hexenal, which is the target product. Conversely, at lower temperatures the formation of 2,4,6-tripropyl-1,3,5-trioxan from butanal predominates, according to Scheme 4.3, therefore elevated yields of the trimer of butanal are observed at lower temperatures.

Table 4.3. Aldol reaction of butanal over different tungstosilicic catalysts in scCO₂ in a view cell with adjustable volume.

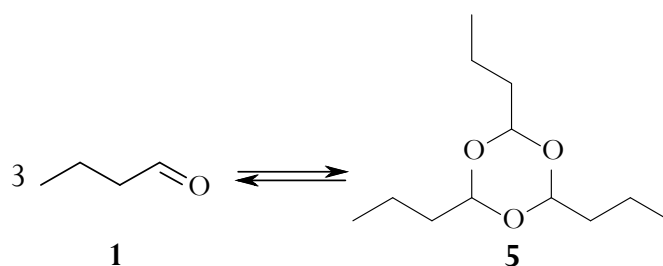
Catalyst	Calculated acidity, mmol/g	Conv., %	Select., %	Reaction rate, mol/(g _{cat} ·h)	TOF, h ⁻¹
10 wt% TSA/SiO ₂	0.14	9	100	0.9	64
20 wt% TSA/SiO ₂	0.27	11	99	1.1	41
40 wt% TSA/SiO ₂	0.55	13	99	1.3	24
40 wt% TSA/MCM-41	0.55	27	99	2.7	49

Conditions: substrate 0.02 mol, m_{cat} = 0.1 g, temp. 373 K, m_{CO₂} = 10 g, total pressure 180 bar, reaction time 120 min.

^a TOF = $\frac{10 \times n_{\text{sub}} \times \text{Conv.}}{m_{\text{cat}} \times A \times t}$, where n_{sub} - amount of butanal, mol; Conv. – conversion of butanal, %;

m_{cat} - catalyst mass, g; A – calculated acidity of the catalysts, mmol/g; t – time, hour.

Table 4.4 further shows that the amount of carbon dioxide added to the system at a constant temperature has almost no effect on the product distribution (selectivity) when the reaction was performed over 45 wt% TSA/MCM-41 at 323 K (entries 3, 4, 5). However, the conversion of butanal and the yield of 2-ethyl-2-hexenal achieved a minimum when a moderate amount of CO₂ was used for the reaction. Overuse of carbon dioxide leads to increased reaction pressures and excessive formation of 2,4,6-tripropyl-1,3,5-trioxan.



Scheme 4.3. Trimerisation of butanal (1) to 2,4,6-tripropyl-1,3,5-trioxan (5) over acidic catalysts.

Table 4.4. Aldol reaction of butanal over different catalysts in batch autoclaves.

No.	Catalyst	T, K	m _{CO₂} , g	P, bar	Conv., %	Selectivity, %		Yield, %	
						3 ^a	5 ^b	3	5
1	TSA cat. ^c	373	0	1	41	63	28	26	11
2	TSA cat.	353	0	1	45	46	47	21	21
3	TSA cat.	323	0	1	58	11	88	6	51
4	TSA cat.	323	20	68	48	9	90	4	43
5	TSA cat.	323	100	150	69	9	90	6	62
6	Amb.-15 ^d	323	0	1	60	10	88	6	53
7	Amb.-15	323	94	140	21	50	43	11	9

Conditions: substrate 0.02 mol, m_{cat} = 0.1 g, reaction time 60 min.

^a 2-ethyl-2-hexenal, ^b 2,4,6-tripropyl-1,3,5-trioxan, ^c 45 wt% TSA/MCM-41, ^d Amberlyst-15.

Under identical conditions without the use of CO₂ two catalysts 45 wt% TSA/MCM-41 and Amberlyst 15 give very similar results, see entries 3 and 6 in Table 4.4. However, when similar amounts of carbon dioxide are added to the system, entries

5 and 7, two catalysts behave differently. Amberlyst-15 gives lower conversion of substrate at an increased selectivity, which eventually results in higher total yield of 2-ethyl-2-hexenal. In contrast, the 45 wt% TSA/MCM-41 catalyst becomes more active in the presence of CO₂, however, the selectivity towards the target product falls sharply and results in a very high yield of the undesired side-product, i.e. 2,4,6-tripropyl-1,3,5-trioxan.

At a next step the 45 wt% TSA/MCM-41 catalyst was tested in the aldol reaction of butanal in a continuous-flow setup according to the procedure described in the experimental part (cf. Section 4.2.4.3). Pressure, temperature and composition are one of the most important factors that affect both chemical reactions and the phase equilibria. Moreover, these parameters are interconnected, i.e. if the temperature is increased it affects both the reaction rate and the phase behaviour (i.e. phase transition may occur), which complicates interpreting the results.

In this study the aforementioned reaction was studied at three different temperatures, however, in order to maintain similar phase behaviour, the amount of CO₂ was also changed. This transition region was chosen as the reference phase behaviour for the aldol reaction of butanal in the continuous-flow apparatus. In other words, using the CPA model, the amount of CO₂, which is required for performing the reaction in the transient region, was calculated taking into account the reaction conditions (T, P, butanal flow). The results of catalytic experiments are presented in Table 4.5, and they show that the conversion of butanal is increasing with the temperature, as well as the selectivity to 2-ethyl-2-hexenal. Therefore, the higher the reaction temperature the higher is the yield of the target product. The yield of the undesired trimer also increases but very insignificantly. The selectivity and the yield of intermediate 3-hydroxy-2-ethylhexanal reach maximums when moderate temperatures are applied.

Table 4.5. Aldol reaction of butanal over 45 wt% TSA/MCM-41 in a continuous-flow apparatus.

T, K	CO ₂ : butanal mole ratio	Conv., %	Selectivity, %			Yield, %		
			3 ^a	2 ^b	5 ^c	3	2	5
323	15 : 1	17	81	8	11	14	1	2
353	5 : 1	51	82	14	4	42	7	2
373	3 : 1	60	89	3	8	53	2	5

Conditions: $m_{\text{cat}} = 0.5300$ g (≈ 1 ml), butanal flow 4.02 ml/h (0.045 mol/h), total pressure 90 bar, ^a 2-ethyl-2-hexenal, ^b 3-hydroxy-2-ethylhexanal, ^c 2,4,6-tripropyl-1,3,5-trioxan. The reaction conditions were calculated using CPA, see part 4.2.5.

In order to compare the performance of the 45 wt% TSA/MCM-41 in two different reaction modes, i.e. in batch reactors and continuous-flow apparatus, the corresponding turnover frequencies (TOF) should be evaluated. They must be calculated for the reactions under similar conditions, i.e. temperatures, pressures, concentrations, etc. In this regard, the TOF obtained in the batch reactor was calculated based on Entry 4 in Table 4.4, i.e. at 323 K, reaction pressure 68 bar, CO₂ : butanal mole ratio 23 : 1. For the continuous-flow setup, TOF was calculated at 323 K, reaction pressure 90 bar, and CO₂ : butanal mole ratio 15 : 1. Despite the fact that the reaction conditions in the two modes differed only slightly, the calculated TOF showed that 45 wt% TSA/MCM-41 was almost 6 times less active in the continuous-flow mode with a TOF of 23 h⁻¹ compared to 155 h⁻¹ in the batch reactor.

Since the aldol reaction was quite successful it was decided to perform the “one-pot” reaction with 2-butenal using two different catalysts in the continuous-flow setup. For the hydrogenation step a 5 wt% Pd/C catalyst was used and 45 wt% TSA/MCM-41 was exploited for the second aldol reaction step. Two types of experiments were performed. In the first experimental mode the two catalyst layers were placed separately, i.e. 2-butenal flow first went through 5% wt Pd/C and then through acidic catalyst. In the second case both catalysts were mechanically mixed together and one single catalyst bed was placed into the reactor. This was done in order to verify the need for a bifunctional catalyst for the “one-pot” synthesis and find the optimal catalyst

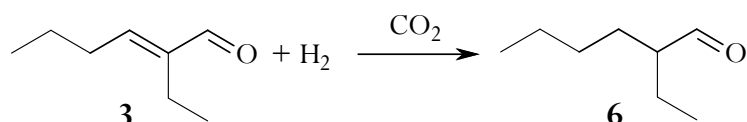
placement. The hydrogenation and aldol reaction steps are quite different and, therefore, require different catalysts and reaction conditions. In this regard, the hydrogenation step requires much lower temperatures and pressures; however, higher CO₂-content is needed since hydrogen decreases the density and therefore the dissolution power of CO₂. The aldol reaction, in turn, requires lower concentrations of CO₂ and higher temperatures. Sometimes, when two reaction steps are too different it is economically more efficient to perform them in different reactors. However, the experiments have shown that the mixture of two different catalysts gives much better results compared to the case with two different catalyst beds. The results are presented in Table 4.6. Note that for these experiments the CO₂ : 2-butenal mole ratio was not calculated with CPA but it was chosen in the same way as for the aldol reaction experiments with butanal (Table 4.5). In this case, the reaction started in the two-phase reaction region because of the presence of hydrogen in the system and due to lower solubility of 2-butenal in CO₂ compared to butanal (cf. Chapter 3). Since the reaction products have high molecular weight and water is one of the products, one can implicitly suggest that the resulting reaction mixture existed in the two-phase state as well.

As Table 4.6 shows, the mixed catalyst bed gives much higher magnitudes of 2-butenal conversion compared to two separate beds. In both cases temperature positively affected the conversion of 2-butenal, i.e. it increased. The same is true for the yields of 2-ethyl-2-hexenal and the intermediate 3-hydroxy-2-ethylhexanal. The yield of the undesired butanal trimer in the first case was constant, whereas when one catalyst bed was used it decreased with the temperature as it was observed in the batch reactor experiments. The main difference between these two types of experiments is the formation of 2-ethylhexanal in the case when mixed catalyst bed was used, Scheme 4.4. This product was not detected when two different layers were loaded into the reactor. With temperature, the yield of 2-ethylhexanal increases, which explains the decreased yield of unsaturated 2-ethyl-2-hexenal.

Table 4.6. “One-pot” reaction with 2-butenal over two catalysts – 5 wt% Pd/C and 45 wt% TSA/MCM-41 in a continuous-flow setup.

T, K	CO ₂ : 2-butenal mole ratio	Conv., %	Yield, %				
			1 ^a	3 ^b	2 ^c	6 ^d	5 ^e
Separate 5 wt% Pd/C and 45 wt% TSA/MCM-41 catalyst beds							
323	15 : 1	18	16	1	1	0.0	1
353	5 : 1	38	33	4	1	0.0	1
373	3 : 1	85	70	12	2	0.0	1
One mixed bed of 5 wt% Pd/C and 45 wt% TSA/MCM-41							
323	15 : 1	59	36	15	3	1	6
353	5 : 1	93	69	13	3	4	4
373	3 : 1	97	60	16	5	14	3

Conditions: m_{cat} (45 wt% TSA/MCM-41) = 0.1055 g (\approx 0.25 ml), m_{cat} (5 wt% Pd/C) = 0.5310 g (\approx 1 ml), 2-butenal flow 3.66 ml/h (0.045 mol/h), H₂ : 2-butenal mole ratio 2.5 : 1, total pressure 90 bar, ^a butanal, ^b 2-ethyl-2-hexenal, ^c 3-hydroxy-2-ethylhexanal, ^d 2-ethylhexanal, ^e 2,4,6-tripropyl-1,3,5-trioxan. The reaction conditions were calculated using CPA, see part 4.2.5.



Scheme 4.4. Hydrogenation of 2-ethyl-2-hexenal (**3**) to 2-ethylhexanal (**6**) over Pd catalyst in CO₂ medium.

The last run of catalytic experiments was devoted to investigations into bifunctional catalysis for the “one-pot” reaction of 2-butenal. In this regard, 1 wt% Pd/Amberlyst-15 and 0.5 wt% Pd/45 wt% TSA/MCM-41 catalysts were prepared and tested in the batch reactors under similar conditions. In order to elucidate the significance of acidic properties of tungstosilicic acid and support in general, 0.5 wt% Pd/45 wt% WO₃/MCM-41 and 0.2 wt% Pd/MCM-41 samples were prepared and also tested in the aforementioned reaction. The reaction conditions and catalytic results are presented in Table 4.7.

It can be seen that 0.5 wt% Pd/45 wt% TSA/MCM-41 is the most active catalyst among the other tested with nearly 100% conversion of 2-butenal, however, 1 wt% Pd/Amberlyst-15 provided the highest but still comparatively low yield of 2-ethyl-2-hexenal, which is the target product. Furthermore, the comparison between these two catalyst shows that the latter catalyst is more selective towards the desired product. As it was expected, the 0.5 wt% Pd/45 wt% WO₃/MCM-41 and 0.2 wt % Pd/MCM-41 catalysts were very active in the hydrogenation reaction, with the former being more active probably due to a higher Pd-content. However, the latter catalyst provided trace amounts of butanal trimer, due to a higher acidity of the support, whereas the MCM-41 acid surface is almost totally covered inert tungsten oxide (VI) in the 0.5 wt% Pd/45 wt% WO₃/MCM-41 sample.

Table 4.7. “One-pot” synthesis of 2-ethyl-2-hexenal from 2-butenal **without** CO₂ medium.

Catalyst	Conv., %	Yield, %		
		1 ^a	3 ^b	5 ^c
1 wt% Pd/Amberlyst-15	55	38	2.2	13.8
0.5 wt% Pd/45 wt% TSA/MCM-41	99	59	0.2	39.6
0.5 wt% Pd/45 wt% WO ₃ /MCM-41	55	55	0.0	0.0
0.2 wt % Pd/MCM-41	26	26	0.0	0.1

Conditions: 2-butenal 0.02 mol, H₂ : substrate mole ratio = 2.5 : 1, m_{cat} = 0.1 g, temp. 323 K, reaction pressure 20 bar, reaction time 60 min, ^a butanal, ^b 2-ethyl-2-hexenal, ^c 2,4,6-tripropyl-1,3,5-trioxan.

4.4 Discussion

Catalyst screening has shown that Amberlyst-15 is the most active catalyst among other tested in the aldol reaction of butanal in a batch reactor with an adjustable volume, with the results presented in Table 4.2. It was found that the catalytic activity and the acidity of the catalysts (see Table 4.1) decrease in the row: Amberlyst-15, HZSM-5, γ -Al₂O₃, MCM-41, 10 wt% TSA/SiO₂, i.e. catalytic activity correlates with acidity. Hydrotalcite is a base material, however, it turned out to be quite active in the aldol

reaction of butanal. Previously, it was reported on successful base catalysed aldol reactions in carbon dioxide [9, 10, 20], even though slightly acidic CO₂ molecules can strongly adsorb on basic sites of the catalysts thereby deactivating them [4].

Further experiments with different saturated aldehydes over Amberlyst-15 have shown that the conversion is dependent on the molecular weight and chemical structure of the reactants. The heavier and more complex reactants are – the lower are the reaction rates, Fig. 4.6. Interestingly, the dissolution power of carbon dioxide that was used as reaction medium was sufficient to maintain the system in one single phase regardless of the molecular weight and structural complexity of the components. Unfortunately, it was not possible to estimate the density of the reaction mixture due to the specific design of the cell.

Since it was found that tungstosilicic acid catalysts are also active in the aldol reaction of butanal, a series of supported TSA catalyst was prepared and tested in this reaction in carbon dioxide medium, Table 4.3. It was found that the reaction rate increases with the loading of TSA on carrier, however, not to the same extent. This can be explained by the fact that higher concentrations of TSA cause strong agglomeration of the particles on the carrier surface [27, 30, 33], which is also supported by the XRD patterns obtained for the tested catalysts. Higher surface area provides smaller particles while the acid loading is maintained the same. This can indirectly be seen from the catalyst performance of two samples with the same loading of TSA but on different carriers: 40 wt% TSA/MCM-41 gives twice as high conversion compared to the 40 wt% TSA/SiO₂ catalyst, Table 4.3. Smaller particles of TSA expose more acid sites to the reactant, which increases reaction rates. The complex of characterisation techniques used in the present study, i.e. XRD, TEM, EXAFS, and the results compared with the literature lead to a conclusion that the acidic material deposited on silica and MCM-41 is very probably tungstosilicic acid. XRD reflections of pure TSA and TSA supported on silica are very similar to those reported in Ref. [27]. However, more investigations are required to reveal its real structure, for which purpose other techniques like IR-spectroscopy, EXAFS, XRD, etc. must be employed. Furthermore, the acidity of the

TSA samples was not estimated accurately enough, and TPD of benzonitrile or pyridine can be very useful in this regard.

Supported TSA on MCM-41 was tested in the aldol reaction of butanal in the batch reactor system. At first, the influence of temperature on the aldol reaction was investigated in the absence of carbon dioxide. As expected, the yield of desired 2-ethyl-2-hexenal increased with the temperature, although the conversion of butanal decreased, as seen in Table 4.4 (entries 1, 2, and 3). This is due to the fact that at lower temperatures the formation of 2,4,6-tripropyl-1,3,5-trioxine becomes more pronounced, which is in accordance with the chemical equilibrium for this reaction [35]. Therefore, at low temperatures the reaction rate decreases, and it is also constrained by the competitive trimerisation of the substrate. This issue to our knowledge has not been addressed in previous studies.

Next, the influence of carbon dioxide media on catalyst performance was tested, Table 4.4 (entries 3, 4, 5). When using the TSA catalyst CO_2 almost does not change the product distribution, i.e. the selectivity to 2-ethyl-2-hexenal was around 10% vs. 90% to trimer, regardless of the amount of CO_2 used in the reaction. Moreover, with the increase in CO_2 -content, conversion of butanal increased. However, the yield of the product did not change significantly, whereas the yield of butanal trimer raised quite a lot. Interestingly, when the same trend was investigated for Amberlyst-15, it was observed that carbon dioxide significantly improves the selectivity towards the product, Table 4.4 (entries 6 and 7).

Further catalytic experiments showed that carbon dioxide affects different catalysts differently. In this regard, entries 3 and 6 in Table 4.4 show that Amberlyst-15 and 45 wt% TSA/MCM-41 have a very similar activity when no CO_2 is used. The performance of Amberlyst-15 significantly improves when carbon dioxide is added (the yield of 2-ethyl-2-hexenal increases by 5% with the simultaneous drop in the undesired trimer yield by 44%), entry 6 vs. entry 7. The same amount of CO_2 added to the 45 wt% TSA/MCM-41 catalyst did not change the product yield, but only increased the yield of the trimer by 11% (entry 3 vs. entry 5).

45 wt% TSA/MCM-41 has much stronger active sites compared to Amberlyst-15, which is indirectly seen from catalyst performance, i.e. TOF numbers for tungstosilicic acid catalysts which are higher. However, the number of acid sites is almost 7.5 times higher for Amberlyst-15. Secondly, multiple effects occur when carbon dioxide is added to the reaction system in the batch regime. Carbon dioxide adsorbs on the catalyst surface, and it also interacts with butanal, this issue was discussed in Chapter 3. The higher pressure and CO₂-content are – the stronger these interactions can become. This causes the formation of the solvation layer of CO₂ around butanal molecules, which decreases their reactivity and also it decreases the accessibility of the active centres for the reactants. Furthermore, both aldol reaction and trimerisation of butanal occur in the liquid phase and, therefore, pressure effects should not be significant when carbon dioxide is used. Finally, when more CO₂ is added the reaction mixture becomes diluted in the phase which is in contact with the catalyst.

For extremely active acid sites of tungstosilicic acid all the aforementioned effects apparently do not play any important role, and the reaction equilibrium is achieved very quickly. Since the temperature is constant, the yields of the product and trimer remains almost constant regardless of CO₂-content. Again for Amberlyst-15 the amount of carbon dioxide changes the catalyst performance quite a lot. This might be due to the fact that the acid sites are blocked by adsorbed layers, and they are not strong enough to “break” the solvation layers of CO₂ around butanal, therefore, the yield of butanal trimer significantly drops when carbon dioxide is used.

Catalytic reactions over 45 wt% TSA/MCM-41 showed that this catalyst is quite active in the aldol reaction of butanal in the continuous-flow regime. The reaction was performed in the regime where the reaction mixture exists in the transition phase between the one- and two-phase regions. In this case the effects on catalyst performance due to phase splitting were minimised. This was achieved by the simultaneous change of temperature and CO₂-flow through the system. On the other hand, the interpretation of the results might be somewhat ambiguous since two parameters were changed at a time. The catalytic data in Table 4.5 show that elevated temperatures positively affect the

catalyst performance. Conversion as well as the yield of 2-ethyl-2-hexenal increased with temperature, as expected. Interestingly, the yield of 2,4,6-tripropyl-1,3,5-trioxan was relatively small and almost independent of temperature and CO₂-content.

The continuous-flow experiments with two catalysts showed that the use of a physical mixture is way more reasonable for performing the “one-pot” synthesis with 2-butenal, compared to two different beds, Table 4.6. In the latter case two beds are considered independent and in both catalysts corresponding reactions are limited by the theoretical equilibria. When a mixture of the two catalysts was used, the equilibrium of the first step, i.e. hydrogenation of 2-butenal, was shifted by the consequent aldol reaction, whose equilibrium, in turn, was pulled by the hydrogenation of 2-ethyl-2-hexenal. Similar experiments with propanal were performed by Stevens *et al.* [20] over a mixture of Amberlyst-15 and 2 wt% Pd on silica/alumina. However, the palladium catalyst was used only for 2-methyl-2-pentenal hydrogenation. They observed elevated conversion and selectivity to the aldol reaction product, and concluded that this might be due to the fact that hydrogenation reaction to some extent drives the preceding aldol reaction.

Therefore, the mixed catalyst bed is very promising, but it needs to be further optimised. In the upper layers basically only hydrogenation reaction takes place, therefore, the 45 wt% TSA/MCM-41 catalyst does not work there efficiently enough, but still is needed to drive the hydrogenation. Therefore, an increased content of the hydrogenation catalyst is desired in the upper layer. In the middle of the bed, the aldol reaction prevails, and hydrogenation catalyst works there only for driving this step by hydrogenating the aldol reaction products. In the bottom layer only final hydrogenation reactions are of importance, therefore, the whole catalyst bed can be finished with pure hydrogenation catalyst.

Looking from this perspective, the use of the physical mixture of two catalysts seems more useful for the preparation of such a catalyst distribution. The use of bifunctional catalysts certainly saves the reactor volume, since no additional support is used for the hydrogenation particles.

Catalytic studies in the present chapter were finalised with the comparison of Pd supported catalysts in the “one-pot” synthesis with 2-butenal in batch reactors without carbon dioxide medium, Table 4.7. In this regard, 0.5 wt% Pd/45 wt% TSA/MCM-41 was the most active catalyst with almost 100% conversion of 2-butenal. However, the biggest part of saturated butanal was converted to trimer, but not to 2-ethyl-2-hexenal. In contrast, 1 wt% Pd supported on Amberlyst-15 converted only 55% of the substrate, however, the yield of the product was by 2% higher, and the amount of trimer was about three times smaller.

Even though the aldol reaction step was not very well pronounced, the role of acidic sites was significant. The 0.5 wt% Pd/45 wt% WO₃/MCM-41 catalyst has very similar composition and structure as the TSA catalysts, however, it gave only 55% conversion of 2-butenal with 100% selectivity to butanal. The lack of acidic sites explains the absence of aldol reaction and trimerisation products. This difference in performance between WO₃ and TSA catalysts confirms the finding that in multistep reactions following steps pull the chemical equilibria of the preceding ones. At this stage the real nature and structure of the active sites becomes extremely important. Perhaps, hydrogen atoms included into the TSA structure not only catalyse the aldol reaction step, but also directly facilitate the hydrogenation step, being hydrogenation centres, like it was suggested by Seki *et al.* [18, 19].

The catalytic results for 0.2 wt% Pd/MCM-41 shows that small acidity of the support can catalyse butanal trimer formation, however, it is insufficient for the formation of 2-ethyl-2-hexenal. Interestingly, the number of acid sites for MCM-41 is comparable with those for 45 wt% TSA/MCM-41, i.e. 0.78 mmol/g vs. 0.62 (calc.), however, MCM-41 possesses mainly Lewis type of acid sites, whereas tungstosilicic acid has basically Brønsted acidity. Therefore, the strength (type) of acid sites is perhaps more important than their number.

4.5 Conclusion

In this study a number of active catalysts for the aldol reaction of saturated aldehydes in supercritical carbon dioxide have been found after screening basic and acidic materials. In fact, both acidic and basic catalyst materials are active in this reaction. Particularly, tungstosilicic acid based catalysts have a great potential, and further efforts shall be made in this direction.

The 45 wt% TSA/MCM-41 catalyst was tested in different types of reactors in the aldol reaction of butanal and as an acidic catalyst in the “one-pot” reaction. It was observed that elevated temperatures positively influence the yield of target product, whereas at lower temperatures a side reaction, the trimerisation of butanal, prevails. Reactions performed in the continuous-flow regime showed that in this regime the formation of the undesired trimer can be minimised. The presence of carbon dioxide only slightly changes the performance of 45 wt% TSA/MCM-41 catalyst, whereas its use increases the yield of the target product when Amberlyst-15 is used.

All reactions in this study have been performed in a certain phase regime. The conditions were calculated with the help of the Cubic-Plus-Association model. The use of this model simplified the search for the reaction conditions and helped to interpret some catalytic results.

Clearly, a bifunctional catalyst for the two-step reaction should be developed and extensively studied, as well as the composition of the catalyst bed should be optimised. Perhaps, some other acidic and basic properties possess much higher catalytic activity in the studied reactions. The experimental evidence shows that tungstosilicic acid supported on silica and MCM-41 generally remains intact, however, extensive catalyst characterisation is required to elucidate not only the real catalyst structure, but also the reaction mechanism. In this regard, the “one-pot” reaction is of particular interest, namely, the structure of active sites, and the necessity of the hydrogenation component. A number of characterisation techniques, such as EXAFS, TEM, XRD, IR, benzonitrile TPD, could be employed, including multiple *in situ* methods.

Furthermore, the influence of the presence of CO₂, and phase behaviour in general, on the catalyst performance has not been extensively studied. This may reveal some ideas as to how to intensify and optimise the reaction conditions. Furthermore, the hydrogenation and aldol reaction steps require quite different conditions, but when combined in one reactor an optimum had to be found.

4.6 References

- [1] M.M. Green, H.A. Wittcoff, *Organic Chemical Principles and Industrial Practice*, Wiley-VCH, Weinheim, 2003.
- [2] G.J. Kelly, F. King, M. Kett, *Green Chem.* 4 (2002) 392-399.
- [3] R. Mestres, *Green Chem.* 6 (2004) 583-603.
- [4] A. Baiker, *Chem. Rev. (Washington, D. C.)*. 99 (1999) 453-473.
- [5] J.-D. Grunwaldt, R. Wandeler, A. Baiker, *Catal. Rev. - Sci. Eng.* 45 (2003) 1-96.
- [6] W. Leitner, P.G. Jessop, *Chemical Synthesis Using Supercritical Fluids*, Wiley-VCH, 1999.
- [7] P. Licence, J. Ke, M. Sokolova, S.K. Ross, M. Poliakoff, *Green Chem.* 5 (2003) 99-104.
- [8] F. Figueras, J. Lopez, in: R.A. Sheldon, H. van Bekkum (Eds.), *Fine Chemicals through Heterogeneous Catalysis*, Wiley-VCH, Weinheim, 2001, p. 327.
- [9] K. Matsui, H. Kawanami, H. Hayashi, *Stud. Surf. Sci. Catal.* 153 (2004) 363-368.
- [10] K. Matsui, H. Kawanami, Y. Ikushima, H. Hayashi, *Chem. Commun. (Cambridge, U. K.)* (2003) 2502-2503.
- [11] Kirk-Othmer, *Encyclopaedia of Chemical Technology*, Wiley-VCH, New York, 1991.
- [12] M. Takao, Japanese Patent JP63068539, 1988.
- [13] T. Yasuhiko, Japanese Patent JP62258335, 1987.
- [14] M. Takao, Japanese Patent JP63068538, 1988.

- [15] Y. Higashio, T. Nakayama, *Catalysis Today*. 28 (1996) 127-131.
- [16] Y.Z. Chen, B.J. Liaw, H.R. Tan, K.L. Shen, *Applied Catalysis A: General*. 205 (2001) 61-69.
- [17] G. Waters, O. Richter, B. Kraushaar-Czarnetzki, *Ind. Eng. Chem. Res.* 45 (2006) 5701-5707.
- [18] T. Seki, J.-D. Grunwaldt, A. Baiker, *Chem. Commun. (Cambridge, U. K.)* (2007) 3562-3564.
- [19] T. Seki, J.-D. Grunwaldt, V.N. van, A. Baiker, *Adv. Synth. Catal.* 350 (2008) 691-705.
- [20] J.G. Stevens, R.A. Bourne, M. Poliakoff, *Green Chem.* 11 (2009) 409-416.
- [21] J.-D. Grunwaldt, A. Baiker, *Phys. Chem. Chem. Phys.* 7 (2005) 3526-3539.
- [22] G.M. Kontogeorgis, G.K. Folas, *Thermodynamic Models for Industrial Applications: from classical and advanced mixing rules to association theories*, Wiley, 2010.
- [23] W.T. Reichle, *J. Catal.* 94 (1985) 547-557.
- [24] B. Ravel, M. Newville, *J. Synchrotron Radiat.* 12 (2005) 537-541.
- [25] M.J. Beier, J.-D. Grunwaldt, I. Tsvintzelis, A.D. Jensen, G.M. Kontogeorgis, A. Baiker, *The Journal of Supercritical Fluids*. 63 (2012) 199-207.
- [26] G. Jenzer, M.S. Schneider, R. Wandeler, T. Mallat, A. Baiker, *J. Catal.* 199 (2001) 141-148.
- [27] Y. Kamiya, T. Okuhara, M. Misono, A. Miyaji, K. Tsuji, T. Nakajo, *Catal. Surv. Asia*. 12 (2008) 101-113.
- [28] M.V. Joshi, C.S. Narasimhan, *J. Catal.* 120 (1989) 282-286.
- [29] J. Regalbuto, *Catalyst Preparation: Science and Engineering*, CRC Press, 2007.
- [30] W. Kuang, A. Rives, M. Fournier, R. Hubaut, *Appl. Catal., A*. 250 (2003) 221-229.
- [31] C.Y. Chen, H.X. Li, M.E. Davis, *Microporous Mater.* 2 (1993) 17-26.
- [32] M.V. Joshi, S. Vaidya, R. Pandey, D. Mukesh, *J. Catal.* 183 (1999) 102-106.

- [33] A.D. Newman, D.R. Brown, P. Siril, A.F. Lee, K. Wilson, *Phys. Chem. Chem. Phys.* 8 (2006) 2893-2902.
- [34] F. Lefebvre, *J. Chem. Soc., Chem. Commun.* (1992) 756-757.
- [35] A.L. Ogorodnikov, M.G. Katsnel'son, V.V. Pinson, Y.V. Levin, *Zh. Prikl. Khim.* (Leningrad). 63 (1990) 1340-1343.

Chapter 5

Fluid Phase Equilibria During the Synthesis of Propylene Carbonate from Propylene Oxide and CO₂

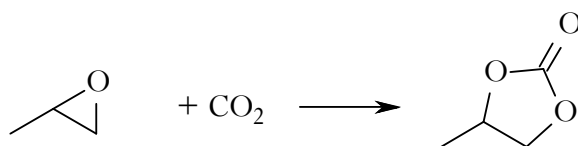
Abstract

In this part of the present PhD-study the influence of the amount of carbon dioxide on the catalytic performance during the propylene carbonate synthesis from propylene oxide and CO₂ was investigated. The reaction was performed in high-pressure batch autoclaves using immobilized 1-hydroxyethyl-9-propyl-cyclicguanidinium bromide on SBA-15 (HEPCGBr/SBA-15) as catalyst in the absence of any co-catalyst. It was found that the yield was strongly dependent on the amount of CO₂ added to the system and that the phase behavior strongly changes along the reaction pathway. The Cubic-Plus-Association (CPA) equation of state was used to predict the phase behaviour during the reaction and the number and composition of coexisting phases in the multicomponent reaction system were determined. In accordance with the experimental data, the maximum conversion was achieved in the transition region between the two- and the one-phase region where a CO₂-expanded reactant/product phase is present. Optimal conditions for performing the reaction have been derived which requires consideration not only of the phase behavior of the starting phase, but also of the mixture during the reaction.

5.1 Introduction

The production of many industrially important chemicals is based on hazardous and toxic C1 building blocks like phosgene or cyanides. However, carbon dioxide has a high potential of being an environmentally benign and safe alternative, which is available in high purity at low cost. Thus, it can be used in the synthesis of organic carbonates from epoxides [1], which find widespread applications in science and industry [2]. The unique physical properties of dense and supercritical CO₂, such as high miscibility with gases and liquids, and high diffusivity and mass transfer coefficients, can be beneficial for chemical reactions. Consequently, reactions with CO₂ can be potentially performed without the use of conventional solvents [3].

Nevertheless, the main challenge in the synthesis of organic carbonates remains in the molecular design of novel catalysts to efficiently activate carbon dioxide and to overcome its intrinsic thermodynamic stability. Several research groups have pursued this path on developing both homogeneous and heterogeneous catalysts for CO₂ fixation to produce valuable chemicals like propylene carbonate (PC) from propylene oxide (PO) and carbon dioxide (Scheme 5.1); most of them with high conversion and selectivity in the temperature range of 253 – 473 K, and reaction pressures of 40 - 140 bar [4-11]. The mole feed ratio (PO : CO₂) varies from 1 : 2 to 1 : 10. Most reactions reported so far have been carried out in batch reactors with reaction times of 4 - 24 hours. Very few attempts have been made to perform the reaction in a continuous-flow system [12].



Scheme 5.1. Catalytic propylene carbonate synthesis from propylene oxide and CO₂.

Supported catalysts working in the continuous-flow mode are particularly attractive, since they exploit the advantages of heterogeneous catalytic systems together

with the high activity of homogeneous catalysts. With respect to catalyst design for cyclic carbonates synthesis, organic salts like imidazolium halides or guanidinium derivatives on silica have been developed [13-15]. Park and co-workers developed active catalysts based on imidazolium bromide supported on different types of silica (99% PC yield). Zhang *et al.* [16] achieved similar results with a cyclic guanidine base (1,5,7-Triazabicyclo[4.4.0]dec-5-ene on silica TBD/SiO₂, 99% PC yield) with the use of a special ultrasonic technique to optimize porosity for CO₂ activation. Obviously, the presence of a guanidinium cation in the molecular structure of the catalyst positively influences the reaction mechanism. Xie *et al.* [17] employed an acyclic guanidinium salt (*N,N,N',N'*-Tetrabutyl,*N''*propyl,*N''-H*-guanidinium chloride ([TBPHG]Cl/SiO₂)) with higher BET surface area (627 m²/g versus 258 m²/g for TBD/SiO₂), but lower activity, although the presence of a halide anion was expected to increase the PC yield. In the present study 1-(hydroxyethyl)-9-propyl-cyclicguanidinium bromide ([HEPCG]Br) as a linker for the investigated immobilized catalyst on SBA-15 was chosen.

Phase behaviour plays an important role during the propylene carbonate synthesis. A number of experimental studies have been devoted to this issue [3, 10, 18, 19]. Interestingly, it was found that maximum conversion was achieved when the reaction occurred in a CO₂-expanded reaction phase, i.e. the two-phase region close to the one phase region. Moreover, the lowest reaction rates were observed in the one phase region, which is contradictory to many other reactions in carbon dioxide media, which perform much better when carried out in a single phase [20, 21].

Experimental phase behaviour measurements are expensive and time consuming, despite the large number of techniques that are currently available [22]. However, thermodynamic modelling can be a reliable alternative [23]. In the present study the Cubic-Plus-Association (CPA) Equation of State (EoS) [24] was exploited for thermodynamic calculations, since it has been proven to be very powerful when predicting various properties of complex multicomponent mixtures at elevated temperatures and pressures [25, 26].

The present study was aimed at (i) the synthesis and characterization of an active catalyst for the propylene carbonate synthesis, (ii) the experimental determination of the influence of carbon dioxide amount on catalyst performance, and (iii) modelling the phase behaviour of the reacting system using the CPA model in order to investigate its influence on the reaction and predict optimal reaction conditions.

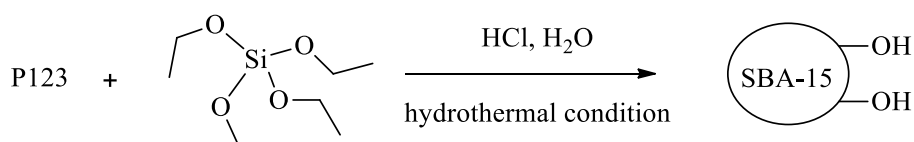
5.2 Experimental

5.2.1 Catalyst preparation

The first step of the catalyst preparation was the synthesis of the support, which is the mesoporous nanoparticles of SBA-15 (Scheme 5.2). The latter was fused to the organic linker to yield the target catalyst – immobilized [HEPCG]Br on SBA-15 (Scheme 5.3). The synthesis route, based on a combination of known steps [27, 28], is described below.

5.2.1.1 Preparation of mesoporous carrier SBA-15

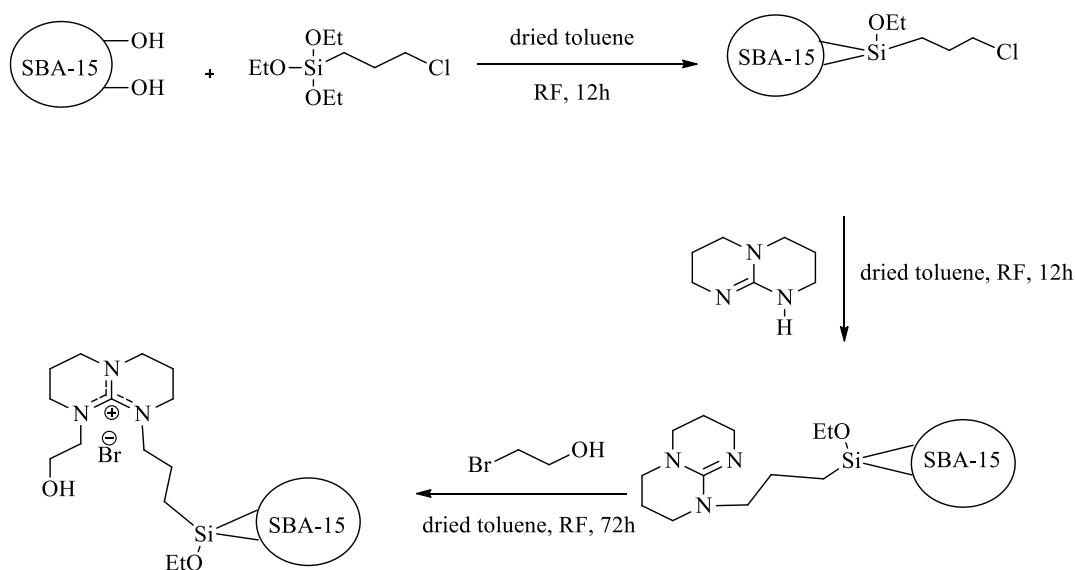
In a three necked flask 20.0 g of the surfactant Pluronic P123 (Sigma-Aldrich; $M_n \sim 5.800$) were dissolved in 500 ml deionized water and 120 ml aq. HCl (32%, Sigma-Aldrich) were added dropwise within 1.5 h. The homogeneous solution was heated to 313 K, followed by the dropwise addition of tetraethylorthosilicate (Scheme 5.2) (ABCR), and the reaction mixture was stirred for 12 h at the same temperature. The emulsion was transferred into a stainless steel autoclave with a Teflon inlay and kept at 393 K for 24 h under static and hydrothermal conditions. The final product was filtered, washed several times with deionized water and dried at 393 K for 12 h. The organic template was removed from the SBA-15 by refluxing for 48 h in 180 ml ethanol. The white suspension was filtered, washed with 300 ml ethanol and dried at 393 K for 24 h. The yield of the target SBA-15 was 14.6 g (white powder).



Scheme 5.2. Preparation of SBA-15.

5.2.1.2 Synthesis of [HEPCG]Br supported on SBA-15

In a 100 ml flask 3.00 g SBA-15 (Scheme 5.3) in 60.0 g water were boiled for 2 h at 393 K and dried in the oven at 453 K for 12 h. 2.80 g of the white powder were added to 2.45 g (10.0 mmol) 3-chloropropyltriethoxysilane dissolved in 80 ml dry toluene and the mixture was refluxed for 12 h.



Scheme 5.3. Preparation of [HEPCG]Br supported on SBA-15.

The grafted material was cooled to room temperature, filtered, washed with 2 x 30 ml dry toluene and 2 x 10 ml dry diethyl ether, and dried in an oven to provide 3.29 g as fine white powder. 1.38 g (10 mmol) 1,5,7-Triazabicyclo[4.4.0]dec-5-ene (TBD) dissolved in 80 ml dry toluene were added and the mixture was refluxed for 13 h. The pale yellow solid was filtered off, washed with 3 x 20 ml dry toluene, 3 x 20 ml

diethyl ether and dried in the oven (temperature ramp 50 K/h to 473 K, kept for 2 h) to yield 4.29 g of the semi-product. 1.54 g (10 mmol) 2-bromoethanol dissolved in 80 ml dry toluene were added to the grafted guanidine on SBA-15 and the mixture was refluxed for 72 h. The target product (catalyst) was filtered off, washed as before and dried in the oven for 12 h. The final product was obtained after mild calcination at 423 K for 4 h (temperature ramp 50 K/h).

5.2.2 Catalyst characterisation

The morphology of the catalyst and the carrier SBA-15 were thoroughly examined using a Hitachi S570 scanning electron microscope, equipped with a Noran EDX-Analyzer (Oxford Instruments). Prior to SEM, the samples were mounted on aluminum holders covered with conductive carbon tabs and then coated with gold in an "Ions Sputter" Balzers, SCD-040 (Balzers Union Limited, Liechtenstein) using the following coating parameters: Argon (sputtering gas) with pressure = 0.05 mbar, time $t = 20$ s, current = 30 mA.

The specific surface area of the catalyst and its carrier were determined using the nitrogen adsorption-desorption technique, by means of recording BET isotherms (423 K for 2 h under vacuum) on a BELSORP-mini II (Rubotherm) surface area analyser at a nitrogen adsorption temperature of 77 K.

XAS measurements in terms of X-ray Absorption Near Edge Structure (XANES) and Extended X-ray Absorption Fine Structure (EXAFS) were carried out at the ANKA-XAS beamline (ANKA synchrotron radiation source, Karlsruhe, Germany) using a Si(111) double crystal monochromator detuned to 60% of the maximum intensity. The storage ring was operated at electron energy of 2.5 GeV with an injection current of 80 – 140 mA. XAS spectra were recorded around the Br K-edge (13474 eV) in transmission geometry. The obtained spectra were energy corrected, background corrected and normalized using the IFEFFIT-package [29].

5.2.3 Catalytic synthesis of propylene carbonate

The catalytic activity in the synthesis of propylene carbonate was investigated in home-built stainless steel autoclaves ($T_{\max} = 250\text{ }^{\circ}\text{C}$, $P_{\max} = 300\text{ bar}$, inner volume $\sim 125\text{ ml}$) with magnetic stirrers, integrated manometers and thermocouples. Before reaction, the reactors were thoroughly washed with organic solvents and dried with a stream of compressed air. The autoclaves were loaded with 20 mg catalyst and 5.0 ml PO. The cells were flushed several times with CO_2 in order to remove air. Subsequently the desired amount of carbon dioxide was added using a CO_2 -compressor (NWA, PM-101, Lörrach, Germany) and an interconnected reduction valve. The total amount of CO_2 was measured by weighing the autoclaves before and after loading. After reaction the autoclaves were quickly cooled down to 291 K in ice-water bath, carefully depressurised and opened. The catalyst was filtered off and 20 mg of the reaction mixture were diluted in d_6 -benzene for NMR analysis (250 MHz, Bruker). The yields were determined with ^1H -NMR spectroscopy by comparing the peak areas of the carbonate to the sum of the peak areas of epoxide and carbonate. All catalytic experiments were performed at least twice and conversion of PO within two identically performed experiments did not deviate by more than 5% relative.

5.3 Experimental results

5.3.1 Catalyst characterisation

The SEM images of SBA-15 at different magnifications (Fig. 5.1, 400x (A), 2200x (B), 5000x (C), and 10000x (D) show channel character. The SEM-EDX measurement confirmed that the predominant elements in the sample are Si and O. The measured BET surface area S_{BET} was $781\text{ m}^2/\text{g}$ and slightly higher than in the examples from the literature ($731\text{ m}^2/\text{g}$) [28].

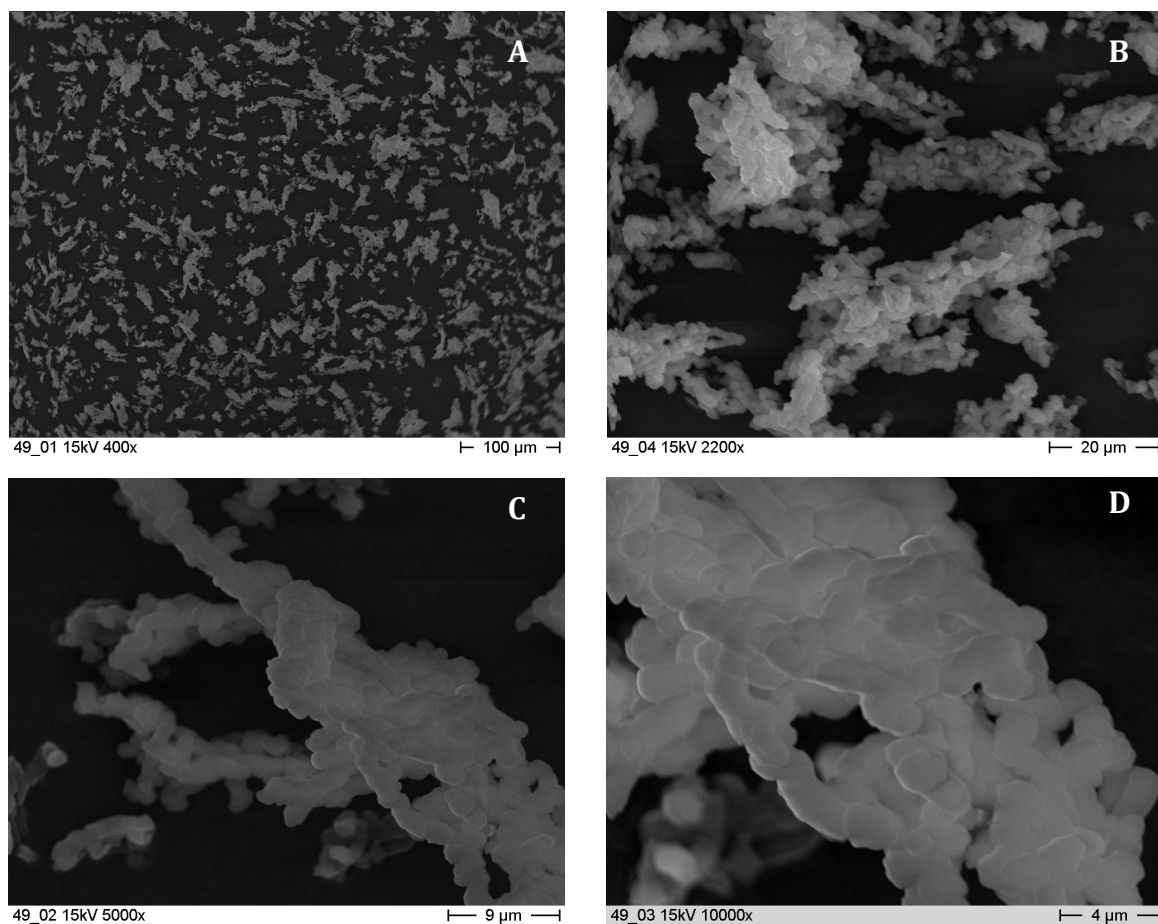


Fig. 5.1. Typical SEM images of SBA-15 with magnifications of 400x (A), 2200x (B), 5000x (C) and 10000x (D).

The supported catalyst was analysed with SEM-EDX to identify the structure morphology and the statistic element diversion. Furthermore, the specific surface area was measured and compared with the one without organic linker (Fig. 5.2). For every enlarged section the element distribution on the catalyst was almost equal to the statistic element diversion (C % 22.32, N % 7.93, O % 35.78, Si % 21.63, Br % 11.40). The channel-morphology of the carrier did not change after the reaction with the organic linker. Notably, the immobilized catalyst has a lower specific surface area than the pure carrier ($S_{\text{BET}} = 122$ vs. $781 \text{ m}^2/\text{g}$).

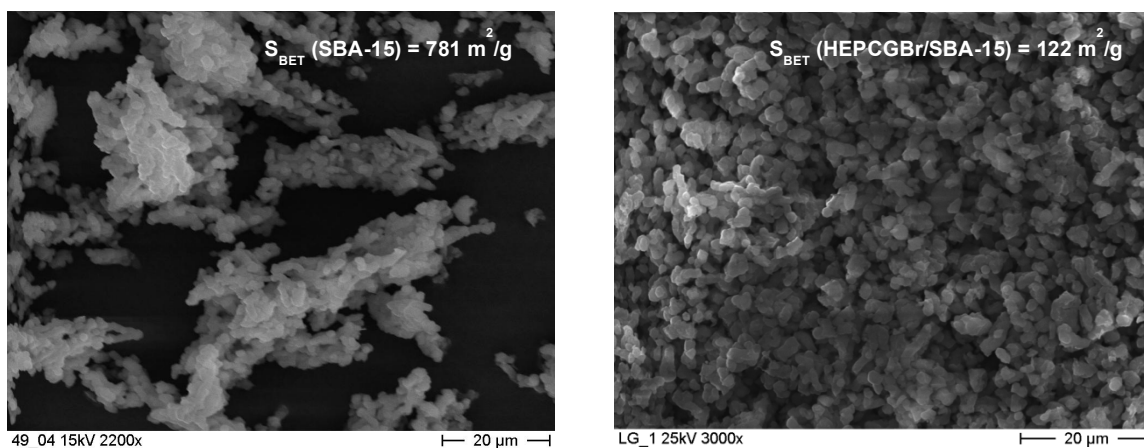


Fig. 5.2. Typical SEM pictures from SBA-15 pure and after reaction with the organic layer (3000x).

For the same reaction Ramin *et al.* [30] used immobilized zinc bromide on silica as catalyst and measured *in situ* XAS at the Br K-edge and Zn K-edge both on the solid catalyst and the liquid phase. During the reaction the bromide species dissolved in the liquid phase, which led to catalyst deactivation when the catalyst was used again. After the reaction no bromide was found in the immediate neighbourhood of Zn and it could not be regenerated by adding ammonium bromide.

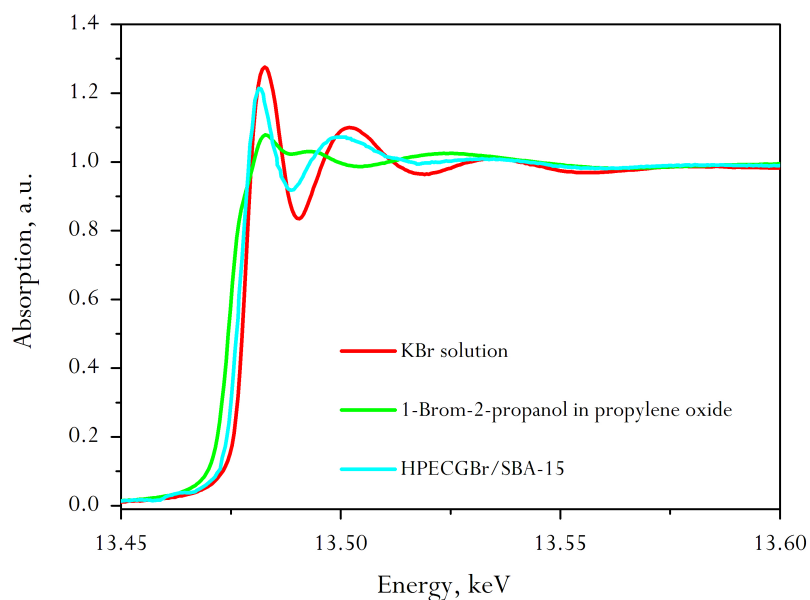


Fig. 5.3. EXAFS spectra at the Br K-edge: KBr solution, 1-bromo-2-propanol in propylene oxide and immobilized catalyst in its as prepared form.

Hence, also in the present study, the bromide content and structure of the supported catalyst was measured with X-ray absorption spectroscopy (Fig. 5.3). The intensity of the white line features of the XANES spectra at the Br K-edge were compared with those of the reference substances (1-bromo-2-propanol and liquid potassium bromide) and confirmed that bromine is mainly present as bromide species on the carrier as outlined in Scheme 5.3.

5.3.2 Catalyst performance

A series of catalytic experiments were performed in order to investigate in what way the amount of CO₂ affects the catalytic activity and the results are presented Table 5.1. Blind tests in the setup without a catalyst showed no detectable catalytic activity.

The catalytic experiments show that the maximum conversion of propylene oxide (22%) and the corresponding turnover frequency (ca. 527 h⁻¹) were achieved when the molar ratio CO₂ : PO was around 4 : 1. With the increase of CO₂-content the yield of PC decreased steadily. Notably, the total pressure of the reaction system as a function of the amount of CO₂ in the reaction was nearly linear.

5.4 Modelling with the CPA equation of state

As it was discussed in the previous chapters, in the case when no hydrogen-bonding components are present in the mixture, the CPA EoS reduces to SRK functionality but with the parameters fitted to the vapour pressures and liquid densities of pure components. In the present study all the three components – propylene oxide, carbon dioxide, and propylene carbonate – are non-associating. None of these components can form hydrogen bonds between each other, i.e. they are incapable of self- or cross-association. For such systems the original SRK equation of state [31] could be used instead of CPA. SRK typically uses the critical temperature T_c , the critical pressure P_c , and the acentric factor ω as pure fluid parameters. However, the estimation of pure fluid parameters for CPA is based on experimental vapour pressure and liquid density data,

which means that the temperature dependency of those important properties is taken into account by the model. Therefore, CPA provides superior results when describing vapour pressure and density dependencies with temperature.

Table 5.1. Propylene carbonate synthesis from propylene oxide PO and CO₂ over HEPCGBr/SBA-15.

Amount of CO ₂ , g	Mole ratio CO ₂ : PO	Pressure, bar	PC yield, %	TOF ^a , h ⁻¹
6.5	2.1	34	14.0	355
9.0	2.9	45	16.0	392
12.0	3.8	54	21.5	527
24.0	7.6	90	9.0	213
45.0	14.3	138	5.0	123
61.5	19.6	190	4.5	103
77.0	24.4	239	4.0	88

Conditions: 0.07 mol PO, 20 mg catalysts corresponding to the mole of immobilized catalyst of $n_{\text{cat}} = 6.55 \times 10^{-5}$ mol, 383 K, 60 min.

^a TOF = $\frac{n_{\text{prod.}}}{n_{\text{cat.}} \times t}$, where n – amount of product and immobilized catalyst in moles and t – reaction time in hours.

5.4.1 Pure Fluid Parameters

The CPA model requires the knowledge of three pure fluid parameters for the physical interactions (a_0 , b , c_1) and two additional parameters for self-association interactions ($\epsilon^{A_i B_j}$ and $\beta^{A_i B_j}$). In this work, the pure fluid parameters for propylene oxide and propylene carbonate were estimated using the saturated liquid molar volume V^{liq} and vapour pressure P^{sat} data from the Design Institute for Physical Properties (DIPPR) database [32]. For carbon dioxide they were obtained from literature [33]. Due to the fact that all the components are non-associating, the association energy and volumes were neglected. The pure fluid parameters are presented in Table 5.2.

Table 5.2. CPA parameters for pure fluids.

T_c , K	a_0 , L ² bar mol ⁻²	b , L mol ⁻¹	c_1	%AAD ^a in P ^{sat}	%AAD in V ^{liq}	Ref.
<i>Carbon dioxide</i> ($T_r = 0.65 - 0.9$)						
304.2	3.5079	0.0272	0.7602	0.2	0.8	[33]
<i>Propylene oxide</i> ($T_r = 0.4 - 0.9$)						
482.25	12.1015	0.0568	0.7676	2.2	0.7	This work ^b
<i>Propylene carbonate</i> ($T_r = 0.4 - 0.9$)						
778.0	30.0907	0.0851	0.8891	1.4	3.5	This work ^b

$$^a \text{\%AAD} = \frac{1}{n} \sum_i \left| \frac{X_i^{\text{cal}} - X_i^{\text{exp}}}{X_i^{\text{exp}}} \right| \times 100, \text{ where } X \text{ stands for } P^{\text{sat}} \text{ (vapour pressure) or } V^{\text{liq}} \text{ (saturated}$$

liquid molar volume) and n is the number of experimental data points.

^b Estimated based on the experimental data from DIPPR [32].

5.4.2 Binary interaction parameters

The reaction mixture consists of three components; hence, the knowledge of the interaction parameters for three binary systems is required. All interaction parameters k_{ij} were estimated based on experimental VLE data found in the literature. The results are presented in Table 5.3.

Table 5.3. Binary interaction parameters.

System	Temperature range, K	k_{ij}	%AAD in P	%AAD in y_1	Exp. data ref.
CO ₂ – propylene oxide	323.15 – 448.15	-0.0057	3.8	5.2	[34]
CO ₂ – propylene carbonate	298.15 – 373.15	-0.0182	10.0	0.8	[35, 36]

Due to the lack of experimental data for the propylene oxide – propylene carbonate system, the interaction parameter for this mixture was neglected. The CPA model quite satisfactorily describes the VLE of the CO₂ – propylene oxide binary system

in the whole range of temperatures with one temperature independent interaction parameter k_{ij} , as shown in Fig. 5.4.

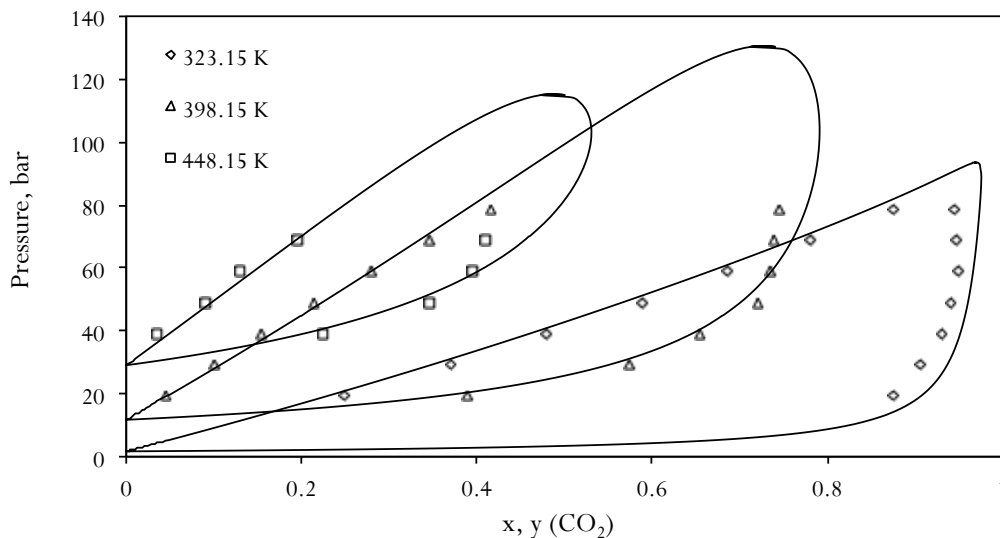


Fig. 5.4. CO₂ – propylene oxide VLE. Experimental data (points) at different temperatures and CPA calculations (lines) with a temperature independent $k_{ij} = -0.0057$.

Two experimental VLE data sets were available in the literature [35, 36] for the CO₂–propylene carbonate system. The CPA model describes well the VLE; however, with occasionally moderate deviations in vapour pressure at lower temperatures, as shown in Fig. 5.5.

5.4.3 CPA predictions for multicomponent reaction systems

The catalytic experiments have shown that the yield of propylene carbonate is strongly dependent on the amount of carbon dioxide added to the system. There are multiple effects that might cause this behaviour. Firstly, excessive amounts of CO₂ should shift the reaction equilibrium towards the formation of products, which is in accordance with Scheme 5.1. In fact, such behaviour is observed only when small amounts of CO₂ are added to the reaction mixture and it adds up to a threshold after which the catalyst performance deteriorates.

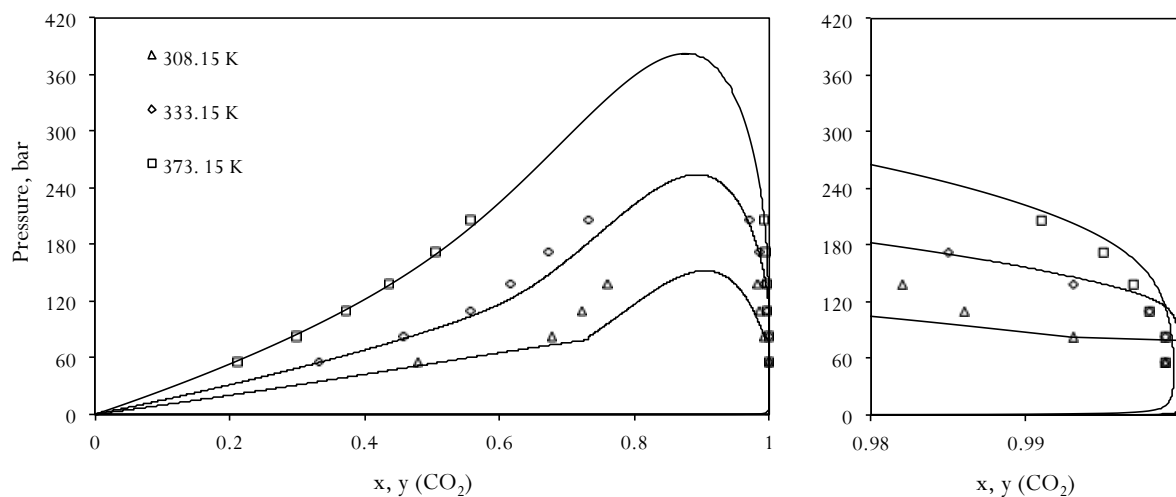


Fig. 5.5. CO₂– propylene carbonate VLE. Experimental data (points) at different temperatures and CPA calculations (lines) with a temperature independent $k_{ij} = -0.0182$.

Another possible reason for the observed dependency on the CO₂ content is the number and the composition of the phases co-existing in the reactor. In propylene carbonate synthesis, carbon dioxide is not only one of the reactants but it also acts as reaction medium. The more CO₂ is added to the system, the easier it becomes to dissolve PO and PC in the solvent, especially, and keep the system in one phase. However, propylene carbonate has very low miscibility with CO₂ compared to propylene oxide. This means, that even if the reaction started in a one phase region, under certain conditions, it is possible that the system at some degree of conversion will split into two phases. This is because (i) some CO₂ has participated in the reaction, therefore the amount of solvent has been reduced, and (ii) some of the relatively insoluble product has been formed.

In order to study the phase behaviour during the reaction, the bubble and dew point curves were predicted using the CPA equation of state. It was assumed that the initial reaction mixture (CO₂ : PO) molar composition was 3 : 1. Six mixtures were considered, assuming 0, 20, 40, 60, 80 and 100% conversion of the substrate. The mixture compositions are presented in Table 5.4, and the calculated P – T diagrams are shown in Fig. 5.6.

Table 5.4. Composition of the reaction mixture with initial CO₂ : propylene oxide (PO) ratio 3 : 1 as function of conversion degree.

Mixture	Conversion, %	Composition of the reaction mixture, moles		
		CO ₂	Propylene oxide	Propylene carbonate
1	0	3	1	0
2	20	2.8	0.8	0.2
3	40	2.6	0.6	0.4
4	60	2.4	0.4	0.6
5	80	2.2	0.2	0.8
6	100	2	0	1

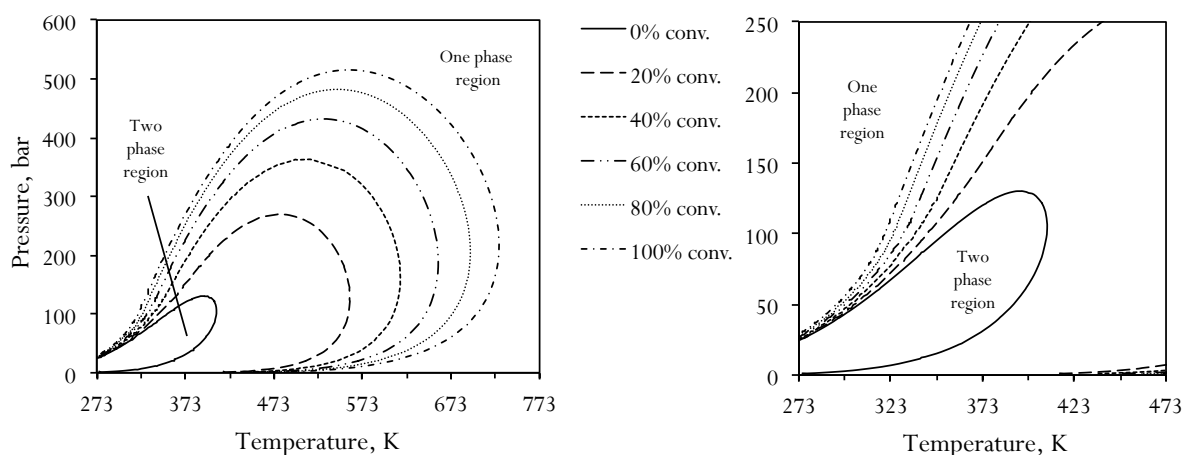


Fig. 5.6. CPA predictions of the bubble and dew point curves for the reaction mixtures during the propylene carbonate synthesis from propylene oxide and CO₂.

As shown in Fig. 5.6 the two-phase region significantly broadens as the reaction proceeds. This means that if the initial reaction starts in the one phase region, at some point (at a certain degree of conversion) a phase transition is likely to occur and the system becomes biphasic. This phase transition may significantly affect the reaction rate. It is remarkable that the phase transition may already be caused by very low degrees of conversion, and the higher the temperature the more pronounced this effect becomes. This observation can be explained by the very low solubility of propylene carbonate in carbon dioxide. Furthermore, propylene oxide has a stronger affinity to propylene

carbonate than to CO₂, which means, that PC that is formed during the reaction, serves as an intermediate solvent for PO, extracting it from the gaseous phase to the liquid. Therefore, the liquid phase mainly contains reactant and product molecules and some amount of dissolved CO₂, which was shown in a detailed experimental study [18]. The calculations in the present work not only give faster access to these data and therefore allow to determine the best reaction conditions; they can also predict the phase compositions.

For the experiments performed in the present study, the numbers of co-existing phases in the reactor before and after the synthesis were calculated using CPA and the parameters were estimated. Furthermore, it was calculated at which conversion every particular mixture splits into two phases and whether the reaction starts in the one-phase region or not. The results are presented in Table 5.5.

Table 5.5. Phase composition during propylene carbonate synthesis as function of the CO₂ : propylene oxide (PO) ratio at 383 K including the observed conversion after 1 hour (0.07 mol PO, 20 mg catalyst).

No.	P _{Tot} , bar	Mole feed ratio CO ₂ : PO	Conv., %	Number of phases		Trans. conv., % ^a
				Before	After	
1	34	2.1	14.0	2	2	0
2	45	2.9	16.0	2	2	0
3	54	3.8	21.5	2	2	0
4	90	7.6	9.0	1	2	1
5	138	14.3	5.0	1	2	4
6	190	19.6	4.5	1	1	15
7	239	24.4	4.0	1	1	34

^a Conversion degree at which the phase splitting (from one single to two phases) occurs.

As Table 5.5 suggests, when only small amounts of carbon dioxide were added to the system, the conversion was steadily increasing while the system before and, consequently, after the reaction was bi-phasic. When moderate amounts of CO₂ were used, the reacting system was monophasic at the beginning, however after a certain

degree of conversion a phase transition occurred (see entries 4 and 5 in Table 5.5). Notably, when the molar ratio was 7.6 (entry 4) the reaction started in the one-phase region. However, after only 1% conversion it became biphasic and the remaining of the reaction was running in the two-phase region, i.e. most of the time the reaction was biphasic. In contrast, with twice the amount of CO₂ (feed ratio 14.3 – entry 5), the reaction system was most of the time monophasic and above 4% conversion the mixture split into two phases. Furthermore, as it is seen from Table 5.5, excessive amounts of carbon dioxide push the reaction system into the one-phase region and it remains in that state until the end of the reaction. Thus, the more CO₂ is used in the reaction, the higher the degree of conversion is necessary for phase splitting.

Further calculations have shown that the initial system becomes monophasic at reaction conditions when the initial mole ratio CO₂ : PO is around 4.1 : 1. Therefore, the concentrations of reactants in the liquid layer, which were in direct contact with the catalyst, were calculated (Table 5.6). At low concentrations of CO₂ the reaction began in the two-phase region and at higher CO₂ contents the reactant concentration in the liquid phase was decreasing with the total pressure of the system.

Table 5.6. Phase composition of the initial reaction mixture of CO₂ and propylene oxide ($t = 0$) in the propylene carbonate synthesis at 383 K.

No.	Pressure, bar	Feed composition, mol		Liquid phase composition, mole fractions	
		CO ₂	PO	CO ₂	PO
1	34	0.036	0.017	0.173	0.827
2	45	0.049	0.017	0.243	0.757
3	54	0.065	0.017	0.299	0.701

5.5 Discussion

The performance of the supported guanidinium-based catalyst is strongly affected by the carbon dioxide content and pressure. With small amounts of carbon dioxide the

yield of propylene carbonate is steadily increasing, as it is shown in Fig. 5.7. Generally, higher concentrations of CO₂ are favourable for product formation (Scheme 5.1) and the higher reaction pressure due to additional CO₂, shifts the reaction equilibrium towards PC formation. The CPA calculations revealed that for a relatively small CO₂ : PO ratio (less than 4.0) the reaction system is biphasic, and gaseous CO₂ dissolves in the liquid layer of propylene oxide, resulting in a CO₂-expanded reactant phase. This means that as long as the system exists in the two-phase region, an increase in CO₂ content causes an increase in the CO₂ concentration in the liquid layer, where the reaction occurs, which kinetically favours the reaction (Table 5.6). Therefore, with increasing pressure and CO₂ content in the two-phase region, higher conversions are achieved.

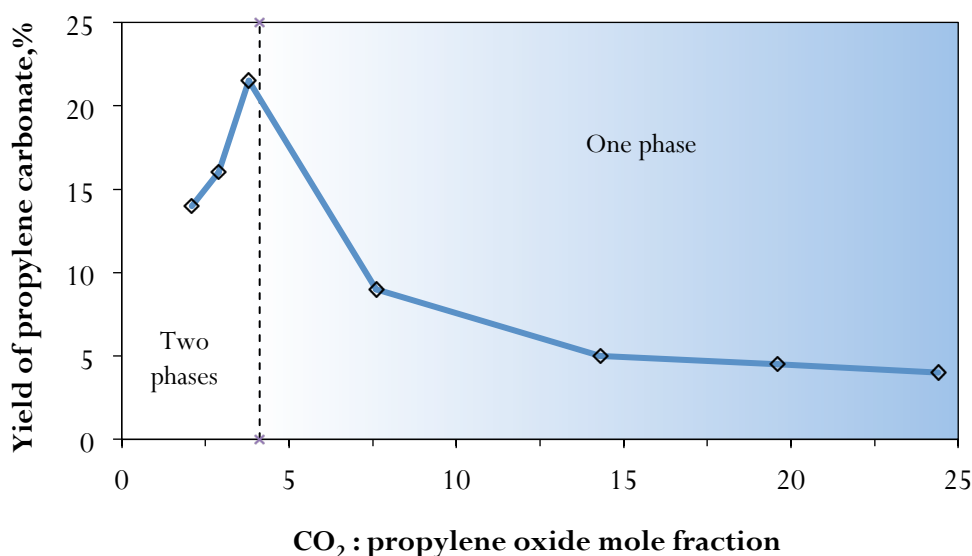


Fig. 5.7. Propylene carbonate yield as function of the initial CO₂ : propylene oxide (PO) ratio. The points are the experimental values of PC yield, with the correlation line (solid). The dashed line indicates the beginning of the one-phase region (shaded area) at CO₂ : PO = 4.1.

However, when exceedingly large amounts of CO₂ were used, the conversion significantly dropped (Fig. 5.7) even though this should favour reaction from both a thermodynamic (equilibrium) point of view as well as kinetically, since the high CO₂ concentrations and elevated pressures improve the mass transfer properties. Furthermore, since this is a heterogeneously catalysed reaction, the mass transfer

limitations both at the dense fluid phase and in the porous catalyst are expected to be minimised in the supercritical region, which will accelerate the reaction [20, 21]. Nevertheless, the conversion of PO in this region was greatly smaller than expected.

The CPA calculations revealed that the excessive amounts of CO₂ push the reaction to the single-phase region, which clearly has a negative effect on the PC yield. The same was observed in experimental studies [18, 37], where the phase behavior was determined by a view cell or infrared spectroscopy. A possible explanation for this behaviour is catalyst poisoning, i.e. an over exposition of the catalyst surface with CO₂, substrate and/or product that deteriorates its performance. Elevated pressures and CO₂ concentrations might further block available active sites on the surface and compete with PO adsorption, thereby decreasing the reaction rate [10, 19, 38]. The beneficial use of CO₂-expanded liquid has recently also been observed in a number of further reactions, cf. Ref. [39-41].

The basicity of the catalyst plays a significant role in the conversion of PO with CO₂. In the present design, the catalyst is bifunctional with a basic (guanidine and alcohol groups) and a nucleophilic site (bromide). Here, the molecular geometry of the catalyst might be crucial for the adsorption of PO, CO₂ and PC and also for the nucleophilic attack of PO by the bromide anion to form 1-bromo-propan-alcoholate, which is probably the first step of this reaction. This intermediate may be stabilised and solvated by the guanidinium cation at the solid/liquid interphase and here the higher solvation power of the CO₂-expanded reaction/product phase may be advantageous. The alcoholate-like bromoalkane species attacks the CO₂, forms the carbonate and subsequently closes the ring by eliminating the bromide anion. Similar studies with immobilized Zn(py)₂Br₂ on SiO₂ demonstrated that the bromide dissolved into the liquid phase during the reaction, which deactivated the catalyst [42]. The applied catalyst system therefore behaves similarly to those observed during phase transfer catalysis in multiphase reactions using quaternary ammonium salts as catalyst [43, 44].

According to the experimental results and the CPA calculations, the highest yield of PC was achieved when the system resides in the transient region (CO₂-expanded

phase) close to the conditions where the reaction phase becomes monophasic, as shown in Fig. 5.7.

Further CPA calculations showed that the optimal conditions for performing propylene carbonate synthesis from propylene oxide and CO₂ is the CO₂-expanded reaction phase, where the biphasic system has a high volume and is close to convert into a single-phase system. This is in agreement with experimental results by Ramin *et al.* [18]. They considered three reaction regimes in a batch reactor: (i) biphasic (vapour–liquid equilibrium VLE, where a minimum amount of carbon dioxide was used), (ii) CO₂-expanded regime (with the use of moderate amounts of CO₂), and (iii) a single-phase reaction (elevated pressures and an excess of CO₂). Despite the fact that the catalyst was significantly different to the one reported here, also in this case, the best reaction regime was the CO₂-expanded reaction phase.

5.6 Conclusion

In the present part of the study an efficient catalyst for the synthesis of propylene carbonate was synthesised and successfully tested in the cyclic carbonate synthesis from propylene oxide and carbon dioxide. The immobilised catalyst is acting in a resembling way to phase transfer catalysts, which work most efficiently in the two-phase region. Several effects can bring about the lower activity in the single-phase region, in particular, the lower dissolution power, the slower extraction of the product and the lower efficiency in the nucleophilic attack of the bromide. Although the mass transfer in one-phase systems is better than in two-phase systems, herein it was shown that a phase interface or a phase with higher dissolution power in a biphasic regime can lead to improved catalytic performance.

The CPA equation of state proved to be a powerful tool for calculating the number and composition of phases coexisting in the reactor during the synthesis. Thus, the concentrations of reactants were calculated, which is the first step towards a rational design and a basis for optimisation of the reaction conditions for the kinetic studies. Furthermore, with CPA it was shown that as the reaction progresses, the system will stay

biphasic if it starts biphasic and it will, in many cases, become biphasic upon reaction progress due to the formation of the highly insoluble product – propylene carbonate.

In general, this case study shows that thermodynamic modelling can aid by effectively predicting the range of reaction conditions. Using the CPA EoS it becomes possible to predict an optimal CO₂-expanded region for any given temperature and pressure.

5.7 References

- [1] T. Sakakura, J.C. Choi, H. Yasuda, *Chem. Rev.* 107 (2007) 2365-2387.
- [2] A.A.G. Shaikh, S. Sivaram, *Chem. Rev.* (1996) 951-976.
- [3] Y. Du, F. Cai, D.L. Kong, L.N. He, *Green Chem.* 7 (2005) 518-523.
- [4] H.S. Kim, J.J. Kim, H.N. Kwon, M.J. Chung, B.G. Lee, H.G. Jang, *J. Catal.* 205 (2002) 226-229.
- [5] S. Fujita, B.M. Bhanage, Y. Ikushima, M. Shirai, K. Torii, M. Arai, *Catal. Lett.* 79 (2002) 95-98.
- [6] H. Yasuda, L.N. He, T. Sakakura, *J. Catal.* 209 (2002) 547-550.
- [7] M. Tu, R.J. Davis, *J. Catal.* 199 (2001) 85-91.
- [8] K. Yamaguchi, K. Ebitani, T. Yoshida, H. Yoshida, K. Kaneda, *J. Am. Chem. Soc.* 121 (1999) 4526-4527.
- [9] R. Srivastava, D. Srinivas, P. Ratnasamy, *Catal. Lett.* 89 (2003) 81-85.
- [10] H. Yasuda, L.N. He, T. Takahashi, T. Sakakura, *Appl. Catal., A* 298 (2006) 177-180.
- [11] M. Ramin, N. van Vegten, J.D. Grunwaldt, A. Baiker, *J. Mol. Catal. A: Chem.* 258 (2006) 165-171.
- [12] A.V. Ufimtsev, I.E. Kuzova, *Khimicheskaya Promyshlennost (Moscow, Russian Federation)* (1993) 555-557.
- [13] W.L. Dai, S.F. Yin, R. Guo, S.L. Luo, X. Du, C.T. Au, *Catal. Lett.* 136 (2010) 35-44.

- [14] L. Han, H.J. Choi, S.J. Choi, B.Y. Liu, D.W. Park, *Green Chem.* 13 (2011) 1023-1028.
- [15] L. Han, S.W. Park, D.W. Park, *Energy Environ. Sci.* 2 (2009) 1286-1292.
- [16] X. Zhang, N. Zhao, W. Wei, Y. Sun, *Catal. Today* 115 (2006) 102-106.
- [17] H.B. Xie, H.F. Duan, S.H. Li, S.B. Zhang, *New J. Chem.* 29 (2005) 1199-1203.
- [18] M. Ramin, J.D. Grunwaldt, A. Baiker, *Appl. Catal., A* 305 (2006) 46-53.
- [19] R.L. Paddock, S.T. Nguyen, *J. Am. Chem. Soc.* 123 (2001) 11498-11499.
- [20] A. Baiker, *Chem. Rev.* 99 (1999) 453-473.
- [21] J.D. Grunwaldt, R. Wandeler, A. Baiker, *Catal. Rev.* 45 (2003) 1-96.
- [22] R. Dohrn, S. Peper, J.M.S. Fonseca, *Fluid Phase Equilib.* 288 (2010) 1-54.
- [23] G.M. Kontogeorgis, G.K. Folas, *Thermodynamic Models for Industrial Applications: from classical and advanced mixing rules to association theories*, Wiley, 2010.
- [24] G.M. Kontogeorgis, E.C. Voutsas, I.V. Yakoumis, D.P. Tassios, *Ind. Eng. Chem. Res.* 35 (1996) 4310-4318.
- [25] G.M. Kontogeorgis, M.L. Michelsen, G.K. Folas, S. Derawi, N. von Solms, E.H. Stenby, *Ind. Eng. Chem. Res.* 45 (2006) 4855-4868.
- [26] G.M. Kontogeorgis, M.L. Michelsen, G.K. Folas, S. Derawi, N. von Solms, E.H. Stenby, *Ind. Eng. Chem. Res.* 45 (2006) 4869-4878.
- [27] D. Ballivet-Tkatchenko, F. Bernard, F. Demoisson, L. Plasseraud, S.R. Sanapureddy, *ChemSusChem* 4 (2011) 1316-1322.
- [28] W.L. Dai, L. Chen, S.F. Yin, S.L. Luo, C.T. Au, *Catal. Lett.* 135 (2010) 295-304.
- [29] B. Ravel, M. Newville, *J. Synchrotron Radiat.* 12 (2005) 537-541.
- [30] M. Ramin, J.D. Grunwaldt, A. Baiker, *J. Catal.* 234 (2005) 256-267.
- [31] G. Soave, *Chem. Eng. Sci.* 27 (1972) 1197-1203.
- [32] D. DIADEM, The DIPPR information and Data Evaluation Manager for the Design Institute for Physical Properties. Version 1.1.0 (2006).

- [33] I. Tsivintzelis, G.M. Kontogeorgis, M.L. Michelsen, E.H. Stenby, *Fluid Phase Equilib.* 306 (2011) 38-56.
- [34] S.F. Shakhova, O.L. Rutenber, M.N. Targansk, *Zh. Fiz. Khimii* 47 (1973) 1581-1583.
- [35] H.L. Li, R.J. Zhu, W. Xu, Y.F. Li, Y.J. Su, Y.L. Tian, *J. Chem. Eng. Data* 56 (2011) 1148-1157.
- [36] L.L. Williams, E.M. Mas, J.B. Rubin, *J. Chem. Eng. Data* 47 (2002) 282-285.
- [37] F. Jutz, J.-D. Grunwaldt, A. Baiker, *J. Mol. Catal. A: Chem.* 297 (2009) 63-72.
- [38] H. Kawanami, Y. Ikushima, *Chem. Commun.* (2000) 2089-2090.
- [39] M. Arai, S.-i. Fujita, M. Shirai, *J. Supercrit. Fluids* 47 (2009) 351-356.
- [40] B. Subramaniam, C.J. Lyon, V. Arunajatesan, *Appl. Catal., B* 37 (2002) 279-292.
- [41] P.G. Jessop, B. Subramaniam, *Chem. Rev.* 107 (2007) 2666-2694.
- [42] M. Ramin, F. Jutz, J.-D. Grunwaldt, A. Baiker, *J. Mol. Catal. A: Chem.* 242 (2005) 32-39.
- [43] S.D. Naik, L.K. Doraiswamy, *AIChE J.* 44 (1998) 612-646.
- [44] C.M. Starks, *J. Am. Chem. Soc.* 93 (1971) 195-199.

Chapter 6

Experimental Determination and Modelling of the Phase Behaviour for the Direct Synthesis of Dimethyl Carbonate from Methanol and Carbon Dioxide

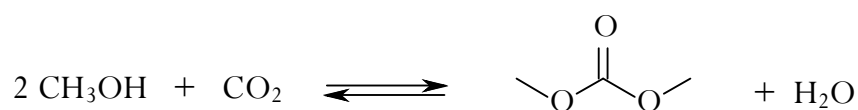
Abstract

This study is focused on the investigation of the phase behaviour of the mixtures relevant to the direct synthesis of dimethyl carbonate from methanol and carbon dioxide. The bubble pressure points of corresponding quaternary mixtures (methanol – CO₂ – dimethyl carbonate – water) of different composition were experimentally determined, and the Cubic-Plus-Association (CPA) Equation of State was employed to predict the phase behaviour of the quaternaries. In this regard, the CPA binary interaction parameters were estimated based on the experimental vapour-liquid or liquid-liquid equilibria data available in the literature, and the phase behaviour of the multicomponent systems was predicted. It was shown that CPA is a powerful model capable of predicting the complex phase behaviour of systems containing polar and associating components, such as methanol and water, at elevated temperatures and pressures. The pressure – temperature regions where the system can exist in one single phase and where it is multiphase were also predicted. This provided some useful information for further optimisation not only of the chemical reaction itself but also consequent product separation processes.

6.1 Introduction

In the past decade, dimethyl carbonate (DMC) has attracted considerable attention as it has found applications in various ways. DMC is widely used as an effective painting solvent, active and selective reacting agent in many chemical syntheses [1]. Due to its good anti-detonating properties, DMC is also used as a high-octane fuel additive [2].

Being itself a non-toxic, environmentally benign, and biodegradable substance, DMC is produced from quite toxic and dangerous components, using rather ineffective technologies with serious safety and waste utilisation problems [1]. In recent years, the number of papers and patents on the direct dimethyl carbonate synthesis from methanol and carbon dioxide (Scheme 6.1) has significantly increased. The given process meets many requirements for a “greener” technology as it uses and produces environmentally friendly substances. Furthermore, the starting materials for the synthesis are cheap and widely available.



Scheme 6.1. The direct synthesis of dimethyl carbonate from methanol and carbon dioxide.

The decisive and the most difficult reaction step is the activation of quite inert CO₂ molecules and the attack of methanol; therefore, a very active and selective catalyst is required for the synthesis. As it is reported in a review by Keller *et al.* [3], quite a number of catalytic systems have been studied up to now, however, only a few of them turned out to be sufficiently active.

The theoretical yield of DMC is very limited by the reaction equilibrium. Under typical reaction conditions (373 – 473 K, 50 – 100 bar) the theoretical yield based on methanol barely exceeds few per cents, practically it is about 0.3 – 2.0%. Moreover, water forming in the process has a very negative impact. Firstly, it deactivates many catalytic systems; secondly, it actively hydrolyses DMC, i.e. if not removed it shifts the

equilibrium towards the reactants. On top of that, phase behaviour, i.e. the number and composition of co-existing phases, during the reaction also causes some effects.

The use of carbon dioxide in the synthesis both as a reacting agent and reaction medium allows to a great extent to overcome the thermodynamic and catalytic challenges and significantly improve the technology. A large number of papers and reviews have been devoted to the beneficial use of supercritical fluids (carbon dioxide particularly) in heterogeneously catalysed chemical reactions; see for example Ref. [4]. Phase behaviour during the process plays a very important role, although its experimental monitoring is very elaborating, time consuming, and expensive. However, using advanced thermodynamic models, the task becomes achievable [5]. These issues have already been discussed in the previous chapters of the present thesis.

The first attempt to model the phase behaviour of the methanol – CO₂ – DMC – water quaternary system using the Soave-Redlich-Kwong (SRK) equation of state with the Huron and Vidal mixing rules modified by Michelsen (MHV2) was made by Camu *et al.* [6]. The excess Gibbs energy at zero pressure was obtained using the UNIQUAC activity coefficient model. The model requires the knowledge of two binary interaction parameters A_{ij} and A_{ji} per one binary. They were obtained by fitting experimental $P - x - y$, $T - x - y$, and/or $P - x$ data. For all binaries temperature independent interaction parameters were used, except for the DMC – CO₂ mixture, for which the temperature dependencies of A_{ij} and A_{ji} were introduced.

The authors reported that the model correlates satisfactorily the experimental data for the binary mixtures, with some occasional deviations, which were not evaluated quantitatively. However, from the plots presented in Ref. [6], it can be seen that high deviations were observed for the CO₂ – methanol VLE in the CO₂-rich phase (the greatest discrepancy in pressure of 3 – 5 bar); for the methanol – water VLE mainly at high temperature and in the methanol-rich phase (deviation in pressure of 0.04 – 0.05 bar); and for the methanol – DMC VLE in the methanol-rich phase (deviation in pressure of 0.02 – 0.05 bar). A relatively good agreement between the experiment and

calculations was observed for the DMC – CO₂ VLE with occasional deviations in pressure of 5 – 7 bar in the DMC-rich phase, as well as for the DMC – water VLE, where the model predicts quite satisfactorily the azeotropic point of the mixture with a discrepancy of 5% from the experiment. Taking into account the range of T and P of the experimental data, the abovementioned deviations can be considered satisfactory for further calculations.

Using the interaction parameters from the correlations of the experimental data for binaries, the high-pressure VLE for the methanol – CO₂ – water ternary at 313.15 K and three different pressures of 70, 100, and 120 bar was predicted. The obtained plots showed that the predictions matched closely the experimental data with the highest deviations in the vapour phase compositions; however, the values of the deviations were not reported.

Furthermore, in their work Camu *et al.* [6] predicted the number of phases existing in the reactor depending on temperature and pressure, and they concluded that the supercritical region is the most favourable for performing the dimethyl carbonate synthesis.

Two other thermodynamic models were used in order to describe the phase behaviour during the DMC synthesis [7]. The Patel-Teja (PT) and Peng-Robinson-Stryjek-Vera (PRSV) equations of state together with the van der Waals one-fluid (vdW1f) mixing rules performed quite nicely. Two binary interaction temperature-dependent parameters in the mixing rules, k_{ij} and l_{ij} , were used in the PRSV model, and one temperature-dependent k_{ij} in PT. These parameters were obtained by fitting experimental VLE data. The calculations showed that PRSV correlates the binaries VLE better than PT. Namely, for all binaries with CO₂ the deviations in pressure ($\Delta P/P$) were in the range of 1 – 3% for the PRSV model, and 2 – 4% for PT. For the DMC – methanol mixture the deviations both in pressure ($\Delta P/P$) and in the vapour phase composition ($\Delta y/y$) were relatively high, around 3 – 4% for PRSV and 4 – 5% for PT, respectively. For methanol – water, the discrepancies between the model correlations

and experimental data were the highest, i.e. $\Delta P/P$ of around 5 – 9% and $\Delta y/y$ of 7 – 10% for PRSV versus 15 – 23% and 2 – 3% for PT, respectively.

Like in the previous study the obtained parameters were used for predicting the VLE of the CO₂ – methanol – water ternary at 313.15 K and three different pressures. Although the values of the deviations between the model predictions and experimental data were not reported, the ternary plots showed that the PRSV and PT models perform quite satisfactorily. They were also used for predicting P – T diagrams for the CO₂ – methanol – water mixture. The obtained plots showed that the predictions matched closely the experimental data.

When the reaction mixture comes out of the reactor it undergoes a series of separation procedures, which very often include depressurising and eliminating CO₂ from the system. The remaining methanol, DMC, and water, depending on the composition (conversion), T and P, can participate in the liquid-liquid equilibria. The ternary mixtures of these three components were experimentally studied and modelled by J. de la Torre *et al.* [8]. The authors measured LLE for the methanol – DMC – water ternaries of different composition in a wide range of temperatures, and correlated the obtained data using the NRTL and UNIQUAC models. Both models use temperature dependent binary interaction parameters A_{ij} and A_{ji} , one pair per each binary. In other words, for correlation of the LLE of one ternary, six temperature dependent parameters were employed. For the NRTL model an additional non-randomness parameter α was used, one per every binary. Both models excellently correlated the experimental data, the root-mean-square deviation (RMSD) in the phase composition varied in the range of 0.32 – 0.50% for UNIQUAC and 0.54 – 0.89% for NRTL. However, when the optimised temperature-independent binary interaction parameters were employed, the RMSD increased to 1.79 and 2.04% for UNIQUAC and NRTL, respectively.

Bustamante *et al.* [9] have very recently published an extensive study on the thermodynamic aspects of this reaction. They studied the vapour-liquid equilibria of the direct synthesis of DMC from methanol and CO₂ under moderate conditions, and for

this purpose they exploited the $\gamma - \phi$ thermodynamic approach, i.e. activity coefficient for the liquid phase using UNIQUAC and fugacity coefficient for the vapour phase using the Peng-Robinson-Stryjek-Vera EoS with the van der Waals one-fluid mixing rules (PRSV-vdW1f). The authors considered the theoretical chemical equilibrium of the reaction at given temperatures and pressures, and consequently, they introduced reasonable reaction mixture compositions when calculating the phase behaviour equilibria. However, the modelling approach itself has disadvantages. Firstly, two different models are used for vapour and liquid phases and each of them requires a set of parameters, many of which are temperature dependent. Secondly, the use of an activity coefficient model restricts extrapolation to supercritical regions and high pressures (70 bar maximum for mixtures with CO₂). Nevertheless, the described above approach turned out to be reasonable and effective when predicting the VLE for the binary mixtures comprising the four-component reaction mixture. The authors further concluded that the methanol conversion increases with the increase in pressure and the decrease in temperature. They also assumed that the best region for the most effective performance of the reaction is the gas phase. Based on this assumption they calculated the T – P regions, where this condition can be fulfilled.

To the best of our knowledge there have not been any attempts to measure experimental data for the quaternary mixtures corresponding to the reaction system. Quite a number of thermodynamic models were used to correlate only specific types of equilibrium, e.g. SRK, PT, and PRSV were used for predicting VLE of only some mixtures, as well as NRTL and UNIQUAC models were tested only for describing LLE of one ternary mixture. This makes the aforementioned studies quite limited in use for the applications of interest here. Having a model that is capable of describing any type of equilibrium (VLE, LLE, etc.) at any T, P, concentrations, could simplify the prediction of the thermodynamic properties of the reaction mixture.

Therefore, the purpose of this part of the PhD-project is to (i) model the phase behaviour of the quaternary system, corresponding to the DMC synthesis, using an advanced thermodynamic model such as the Cubic-Plus-Association Equation of State

(CPA EoS), (ii) validate the model predictions by measuring experimental data for four component mixtures, and (iii) provide an insight into possible ways of process optimisation.

6.2 Experimental

6.2.1 Setup description

Phase behaviour was monitored in a high-pressure view cell (15-65 ml, SITEC, Switzerland) with changeable volume, which is adjusted by a screw-type manual pump. The details are described in Chapter 3 of the present thesis. The setup principle is based on the so-called synthetic method [10], where phase transition is directly observed visually through a sapphire window (26 mm diameter), with no need for sampling. The flow chart and the setup description may be found in Ref. [11-13]. Temperature and pressure were monitored by a J-type thermocouple and a Dynisco pressure sensor (MDT422H-1/2-2C-15/46), respectively. Stirring was performed by a magnetic stirrer (Heidolph MR 2002) with a stirring bar placed inside the cell. Temperature was controlled by means of an oil-containing heating jacket connected to a thermo-/cryostat (Julabo F25 HD). A bright light source was applied to the cell for better optical monitoring of phase transition.

6.2.2 Experimental procedure

Prior to every experiment the view cell was thoroughly cleaned with acetone and CO₂, dried with an air jet, and left open heated to 323 K in the air for a minimum of 2 hours. After cooling it down to a room temperature, the desired amounts of methanol (Fluka, 99.8%+), dimethyl carbonate (Aldrich, 99%+, anhydrous), and water (Fluka, >2 μ S/cm) were loaded into the cell. The masses of the components were calculated by weighting syringes with the substances before and after loading. After charging the cell with liquids, it was closed, tightened, and flushed carefully with CO₂ to substitute the air in the cell. CO₂ was added using a CO₂-compressor (NWA, Lörrach, Germany),

and its quantity was measured by a mass-flow transmitter (Rheonik Messgeräte GmbH, Germany) at a constant pressure of 100 bar, which was achieved by an interconnected reducing valve. The view cell was further heated up to a desired temperature and pressurised to a pressure higher than expected bubble point pressure. At this stage the cell was left for equilibrating for a minimum of 2 hours. A first rough estimation of the bubble point was made by means of stepwise depressurising the system (4 – 6 bar). After appearing first bubbles in the top part of the cell, it was pressurised again and left for equilibration. Small stepwise pressure drop (0.2 – 1 bar) was applied to find the bubble point pressure of the desired system. First bubble of gas phase usually appeared in the highest point of the cell, therefore, the latter was slightly tilted to make this point more visible. The pressure at which first bubble of the second phase appeared was noted. All the experimental points were measured at least three times. The difference between these points was in most cases no more than 0.1 - 0.3 bar, which is within the tolerance of the pressure gauge. The temperature was measured with a precision of 0.5 K.

6.3 Experimental results

Using the setup and experimental procedure described above a number of bubble points were measured for two quaternary systems of different composition at various temperatures. The results are presented in Table 6.1.

Table 6.1. Bubble points for six quaternary systems at different temperatures.

Mixture	Composition, mol%				Temperature, K	Pressure, bar
	CO ₂	Methanol	DMC	Water		
1	27.19	53.33	11.44	8.04	323.7	41.9
					342.7	53.9
					364.7	67.9
2	41.23	42.24	8.23	8.30	323.7	59.3
					342.7	76.7
					364.7	97.6

6.4 Modelling with the CPA equation of state

6.4.1 Pure Fluids

As it was outlined in Chapter 2 of this thesis, the CPA model requires the knowledge of three pure fluid parameters for the physical interactions (\mathbf{a}_0 , \mathbf{b} , \mathbf{c}_1) and two additional parameters for self-association interactions ($\epsilon^{A_i B_j}$ and β^{cross}). In this work, all the parameters were estimated using saturated liquid density and vapour pressure data from DIPPR [14] or, when it was possible were obtained from the literature. The pure fluid parameters are presented in Table 6.2.

Table 6.2. CPA parameters for pure fluids.

Association Scheme	\mathbf{a}_0 L ² bar mol ⁻²	\mathbf{b} L mol ⁻¹	\mathbf{c}_1	ϵ L bar mol ⁻¹	β	%AAD ^a in P ^{sat}	%AAD in V ^{liq}
<i>Carbon dioxide</i> ($T_r = 0.65 - 0.9$) ^b							
n/a ^c	3.5079	0.0272	0.7602	0	0	0.2	0.8
<i>Methanol</i> ($T_r = 0.43 - 0.93$) ^b							
2B	4.0531	0.0310	0.4310	245.91	0.0161	0.6	0.5
<i>Dimethylcarbonate</i> ($T_r = 0.5 - 0.9$) ^d							
n/a	17.5724	0.0731	0.8937	0	0	0.2	0.7
<i>Water</i> ($T_r = 0.5 - 0.9$) ^b							
4C	1.2277	0.0145	0.6736	166.55	0.0692	0.8	0.5

^a %AAD = $\frac{1}{n} \sum_i \left| \frac{X_i^{\text{cal}} - X_i^{\text{exp}}}{X_i^{\text{exp}}} \right| \times 100$, where X stands for P^{sat} or V^{liq} and n is the number of experimental data points

^b parameters obtained from Ref. [15]

^c non associating component

^d parameters estimated in the present study.

Interestingly, the parameters of CPA (\mathbf{a}_0 , \mathbf{b} and \mathbf{c}_1) for different associating and non-associating components plotted against their van der Waals volume V_W give trends which allow to choose the initial parameters for estimation and/or validate the obtained

parameters ([5], pp. 267 – 268). The CPA pure fluid parameters for dimethyl carbonate ($V_W = 46.24 \text{ cm}^3/\text{mol}$ [14]) estimated in the present work are in a very good agreement with these trends.

6.4.2 Binary Mixtures

Calculation for the binaries containing carbon dioxide, methanol, dimethyl carbonate and water were performed in order to obtain the corresponding binary interaction parameters for the CPA model. All interaction parameters in the present study were assumed to be temperature independent. For binary mixtures that include associating components combining rules are required for cross-association energy $\epsilon^{A_i B_j}$ and volume β^{cross} . As it was extensively discussed in Chapter 2, when both compounds are associating the CR-1 combining rules are employed, when one of the components is non-associating – the modified mCR-1 rules are used (cf. section 2.4, Table 2.3).

The quaternary system of interest (methanol – CO_2 – DMC – water) can be divided into six binary sub-systems. For the following four binaries methanol – water, methanol – DMC, water – DMC, and CO_2 – DMC, an extensive literature search was done in order to find experimental VLE and/or VLLE data.

Water and methanol were modelled as self-associating components. Water molecules have two positive and two negative sites, whereas, methanol possesses one positive and one negative site, therefore, 4C and 2B association schemes were considered for these components, respectively. Furthermore, carbon dioxide is quite specific compound. It is widely known that CO_2 molecules may act either as proton acceptor or as electron acceptor depending on the nature of the organic molecule interacting with CO_2 . Such interactions are of Lewis electron donor – acceptor (base – acid) type. As it was shown by Tsivintzelis *et al.* [15], the best results the CPA model provides considering that CO_2 is non self-associating fluid, possessing one positive site (electron acceptor), thereby, being able to cross-associate with water and methanol. This assumption was applied to this work as well. In the same study it was shown that the CO_2 – water and CO_2 – methanol binaries are better correlated when the cross-energy

parameter is set to the one obtained from the experimental FTIR data and corresponding *ab initio* calculations, and the cross-volume parameter is obtained by fitting experimental data.

At last, dimethyl carbonate was modelled as non self-associating fluid, possessing one negative site (electron donor), which is capable of cross-association with other components, i.e. solvation.

Based on these data the binary interaction parameters were estimated. The resulting binary interaction, cross-association energy and volume parameters, together with the deviations from the experimental data are presented in Table 6.3.

Table 6.3. CPA binary interaction parameters for the binaries comprising the DMC reacting system.

Binary	k_{ij}	Parameters for the cross		%AAD ^a in P	%AAD in y_1
		association			
		$\epsilon^{A_i B_j}$, L bar mol ⁻¹	β^{cross}		
CO ₂ – Water ^b	0.1141	Exp: 142.0	0.0162	-	-
CO ₂ – Methanol ^b	0.0479	Exp: 123.8	0.0196	-	-
Methanol – Water ^c	-0.0704	CR-1: 206.2	CR-1: 0.0334	2.82	3.31
Methanol – DMC ^c	-0.0796	mCR-1: 122.96	Fitted: 0.2899	2.97	4.76
Water – DMC ^c	-0.0371	mCR-1: 83.3	Fitted: 0.5054	-	1.19 ^d
CO ₂ – DMC ^c	-0.0240	0	0	2.03	1.00

CR-1 and mCR-1 are the combining rules for the cross-association energy and volume, cf. Chapter 2, Table 2.3.

^a %AAD = $\frac{1}{n} \sum_i \left| \frac{x_i^{\text{cal}} - x_i^{\text{exp}}}{x_i^{\text{exp}}} \right| \times 100$, where X stands for P or y_1 and n is the number of experimental data points

^b parameters obtained from Ref. [15]

^c parameters estimated in the present study

^d %AAD in x_1 since the parameters were estimated using LLE data.

For the CO₂ – water and CO₂ – methanol binaries the parameters were directly obtained from the literature.

For the methanol – water system the k_{ij} -s were initially estimated at different temperatures and a temperature dependency was derived. However, when the interaction coefficient k_{ij} was estimated over the whole temperature range, the deviations from the experimental data were quite small with exceptions at elevated temperatures 523.15 and 548.15 K, as it is shown in Fig. 6.1. These high deviations, however, could be related to the low quality of the experimental data, i.e. insufficient number of experimental points. Therefore, the k_{ij} was assumed temperature independent for further calculations.

CPA using the estimated k_{ij} and β^{cross} parameters for the methanol – DMC system gave satisfactory results. It was assumed that k_{ij} is temperature independent over the whole temperature range. However, as it is shown in Fig. 6.2, at high temperatures the model predictions slightly deviate from the experimental data.

For the water – DMC binary system two types of experimental data were available in the literature – VLE [6] and VLLE [8]; however, the data for the vapour phase were slightly different. The interaction parameter k_{ij} for this binary was estimated based on the LLE data, and then VLE was predicted using the obtained parameters, as shown in Fig. 6.3. The CPA model describes the LLE of the water – DMC system quite accurately. The predicted azeotropic point ($T_{\text{az}}^{\text{pred}} = 352.7 \text{ K}$, $x_{\text{DMC}}^{\text{pred}} = 0.545$) is located very closely to the experimental one. However, for VLE some deviations from the experimental data are observed, especially for the DMC-rich phase.

For the CO_2 – DMC system $P - x - y - T$ data were available in literature [16]. The calculations based on the data were quite accurate with insignificant discrepancies between the experimental data and model predictions at elevated temperatures, as it is shown in Fig. 6.4.

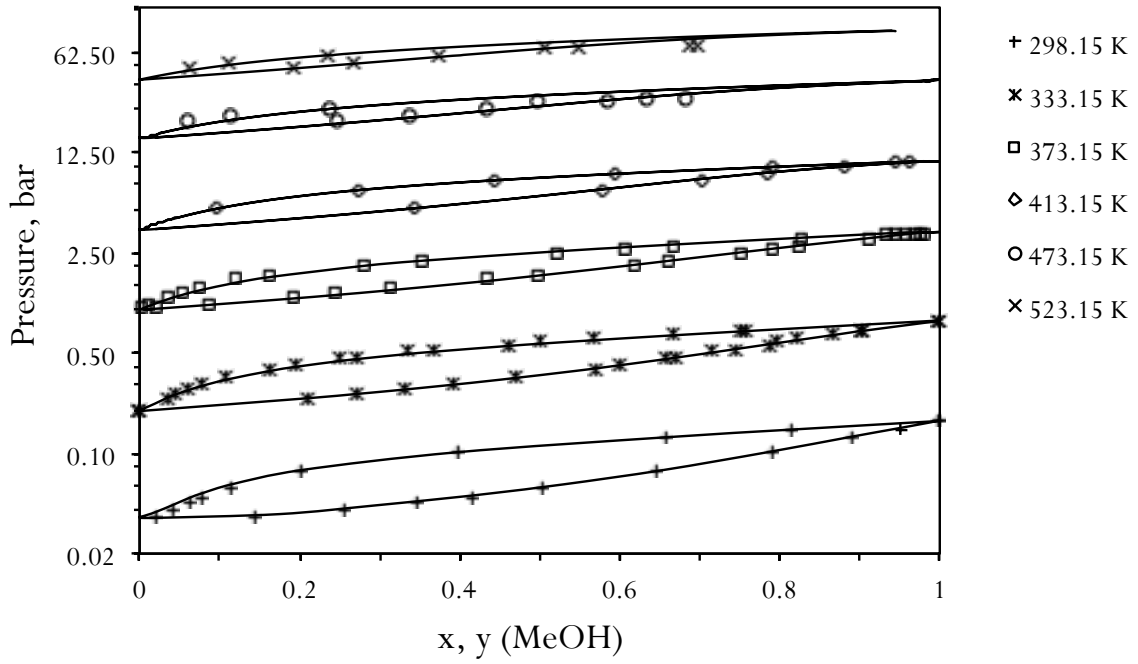


Fig. 6.1. Methanol – water VLE. Experimental data [17-25] (points) and CPA calculations (lines) with a temperature independent $k_{ij} = -0.0704$.

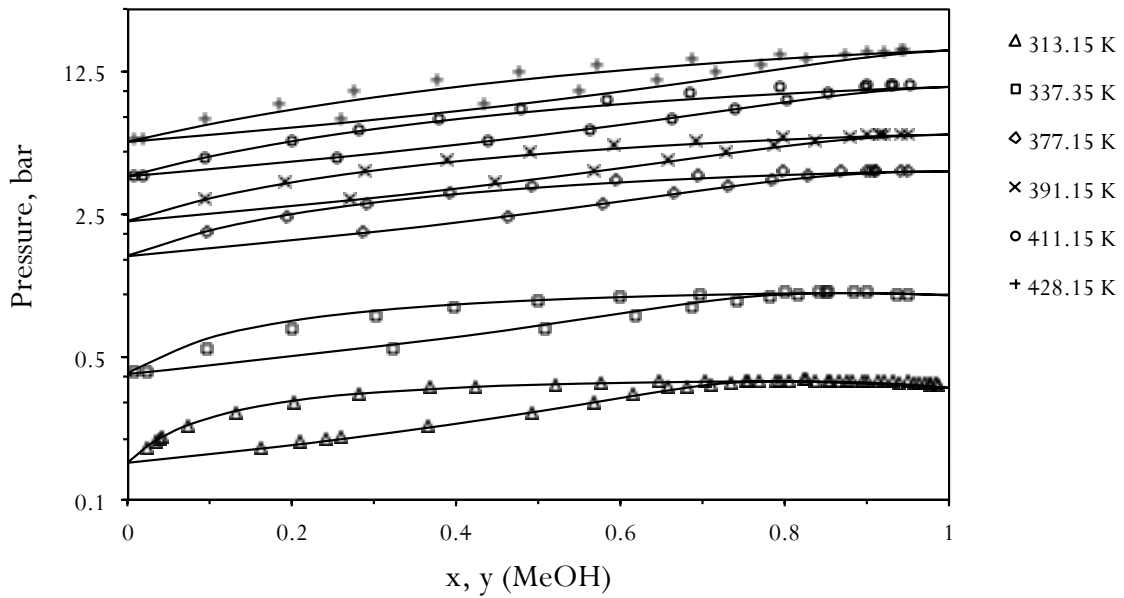


Fig. 6.2. Methanol – DMC VLE. Experimental data [26, 27] (points) and CPA calculations (lines) with temperature independent $k_{ij} = -0.0796$ and $\beta^{\text{cross}} = 0.2899$.

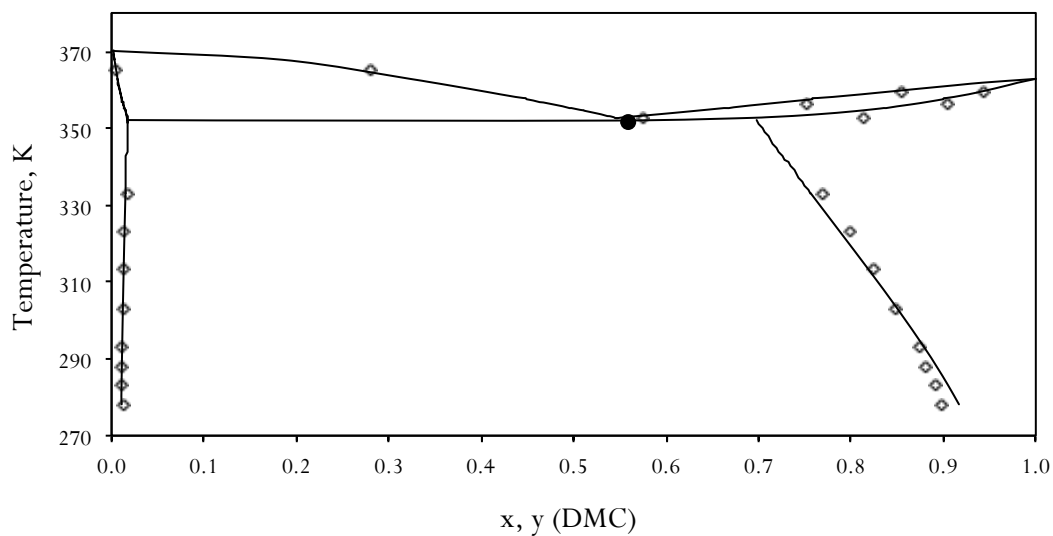


Fig. 6.3. Water – DMC VLE at 1.01325 bar. \diamond - experimental data [8], \bullet - experimental azeotropic point ($T_{\text{az}} = 351.53$ K, $x_{\text{DMC}} = 0.559$ [28]), and CPA calculations (lines) with temperature independent $k_{ij} = -0.0371$ and $\beta^{\text{cross}} = 0.5054$.

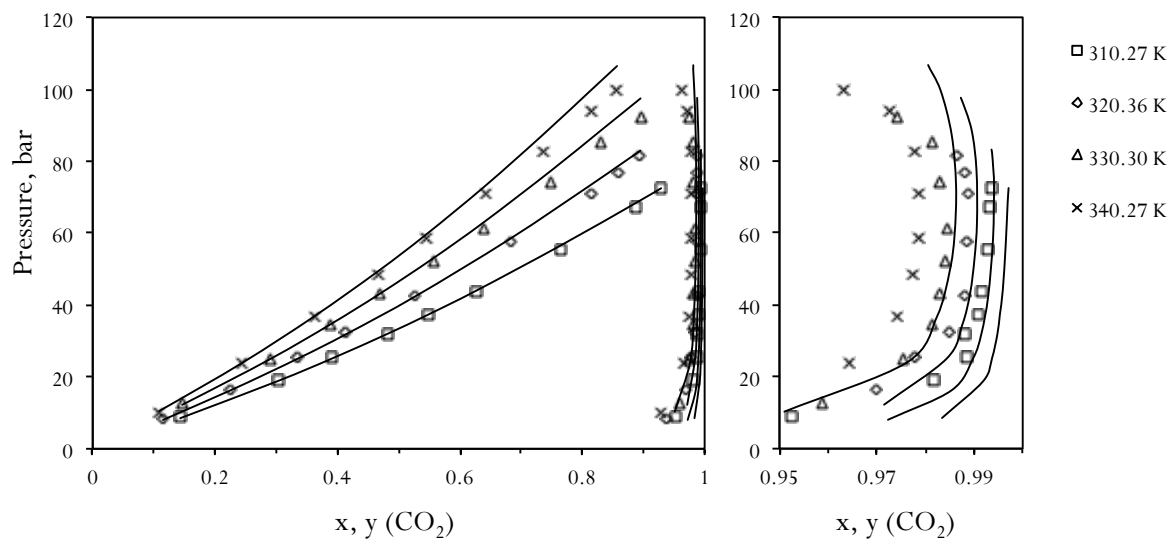


Fig. 6.4. CO_2 – DMC VLE. Experimental data [16] (points) and CPA calculations (lines) with temperature independent $k_{ij} = -0.0240$.

6.4.3 Prediction of the phase behaviour of ternary and multicomponent systems

Having obtained the pure fluid parameters for the components and the interaction parameters for the corresponding binaries, the CPA model was used to predict the phase behaviour of ternary and quaternary systems.

In this regard, it was shown that CPA satisfactorily predicts the VLE for the CO₂ – methanol – water ternary system at high pressures. As it is shown in Fig. 6.5, there are some deviations from the experimental data, however, CPA with the binary parameters obtained in the present study provides a good insight into the phase behaviour of this ternary and can be used for preliminary calculations and rough estimations.

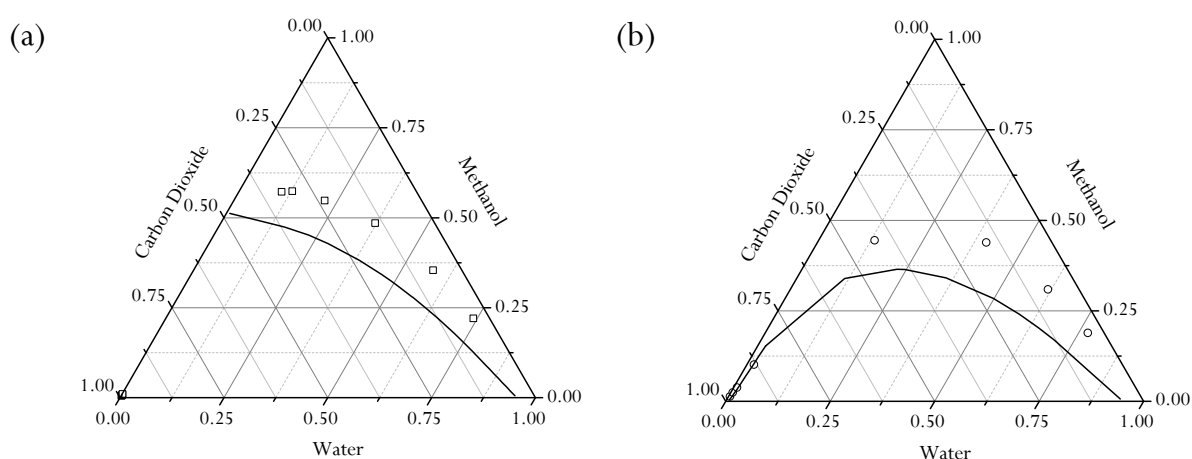


Fig. 6.5. Methanol – CO₂ – water VLE at 313.15 K and two different pressures (a) 70 and (b) 120 bar, respectively. Points represent the experimental data [29], lines are the CPA predictions.

For the CO₂ – methanol – DMC ternary mixture a number of bubble and dew points were measured at near supercritical conditions and a P – T diagram for this system was obtained [7]. The CPA model was used in order to predict dew and bubble point lines for this mixture. The results are presented in Fig. 6.6 and show that the CPA predictions match very closely the experimental data.

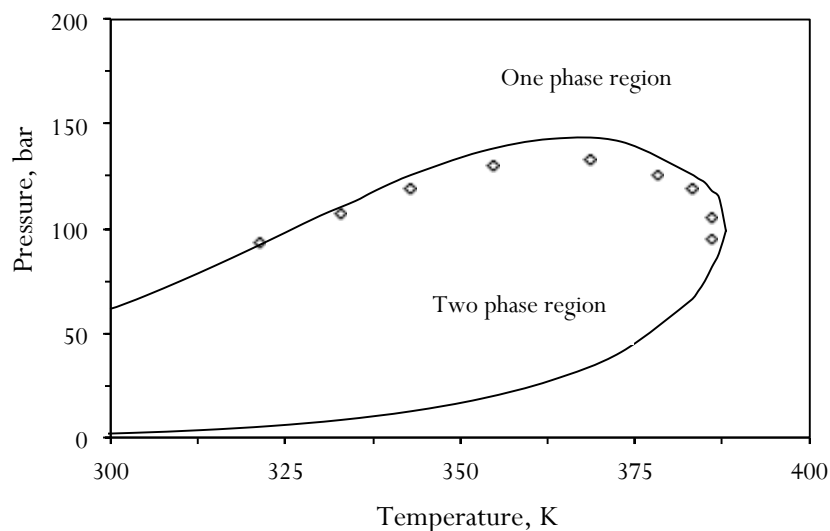


Fig. 6.6. P – T diagram for the CO₂ – methanol – DMC system. Symbols represent experimental data [7], solid lines – CPA predictions.

Furthermore, the liquid-liquid equilibria of the methanol – DMC – water ternary system were predicted with CPA at different temperatures. The experimental data was obtained from Ref. [8]. The CPA predictions deviate from the experimental points, as it is shown in Fig. 6.7. However, for rough estimations the CPA performance might be considered satisfactory.

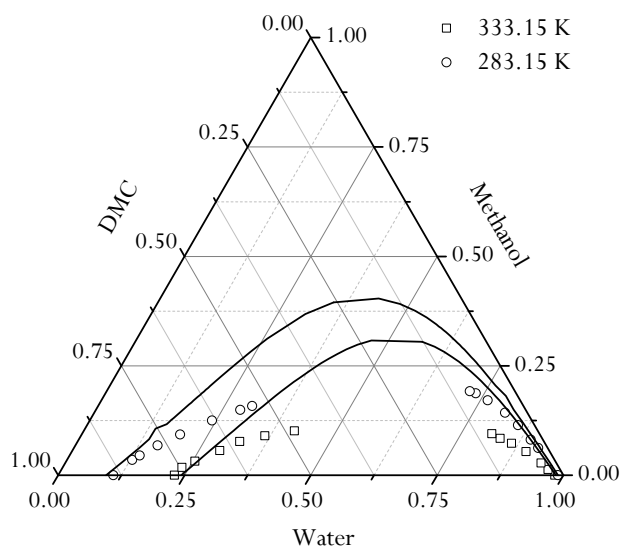


Fig. 6.7. Methanol – DMC – water LLE at three temperatures. Points - experimental data [8], solid lines – CPA predictions.

In order to verify the model capabilities, the phase behaviour was calculated for different quaternary systems at elevated temperatures, the results are shown in Fig. 6.8. The composition of the mixtures is presented in Table 6.1. The CPA predictions quite accurately represent the experimental bubble point pressures obtained for the quaternary systems corresponding to the reaction mixture. The deviations from the experiment, in terms of %AAD, for Mixture 1 was 2.9%, and for Mixture 2 – 9.6%. This confirms the applicability of CPA for predicting the phase behaviour during the direct dimethyl carbonate synthesis from methanol and carbon dioxide.

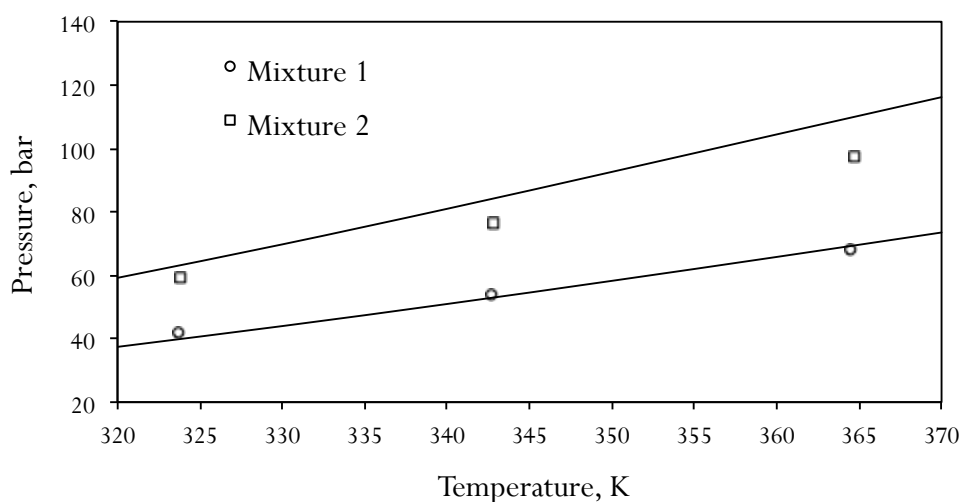


Fig. 6.8. CPA predictions (lines) of bubble points of two quaternary systems and the experimental data (points) measured in the present study with the compositions presented in Table 6.1.

6.4.4 Application

The knowledge of the phase behaviour can provide some useful information as to how to optimise the reaction conditions. Up to now there has been no solid evidence on whether the reaction performs better in a one-phase or many-phase regions. The experimental and theoretical studies on a similar reaction discussed in the previous Chapter 5, i.e. the synthesis of propylene carbonate, has shown that the best region for performing this reaction is the “expanded CO₂”-region. However, this might not be the case for the synthesis of DMC. Nevertheless, for further catalytic studies it might be crucial to know precisely how many phases coexist in the reactor and how the system

behaves with conversion. The importance of this has been previously discussed in the present thesis.

In order to find the one- and two-phase regions where the reaction may occur, the dew point lines were calculated using CPA and the parameters obtained in the present study. The calculations have shown that these regions shift significantly depending on the conversion and feed composition in a reasonable range of temperature and pressure.

Firstly, it was assumed that the mole feed compositions was constant (methanol : $\text{CO}_2 = 1 : 2$). While the reaction is occurring, the total mixture composition is changing, thereby affecting the phase behaviour of the system. As it is shown in Fig. 6.9, the one phase region shifts towards higher temperatures and lower pressures (in the chosen region of T and P), while the system accumulates the products.

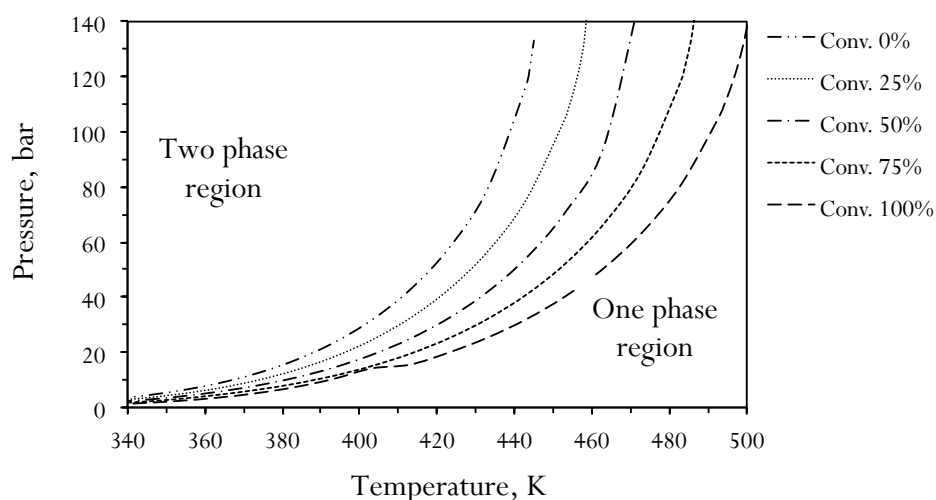


Fig. 6.9. The dew point line CPA predictions of the methanol - CO_2 - DMC - water quaternary system with the initial mole feed composition $\text{MeOH} : \text{CO}_2 = 1 : 2$ and different conversion.

The next step was to study the influence of an excess amount of carbon dioxide on the phase behaviour of the system. The composition of the system was calculated taking into account a constant conversion of 10%. The calculations have revealed that the dilution of the reacting mixture with CO_2 allows to carry out the reaction in one phase at significantly lower temperatures, Fig. 6.10.

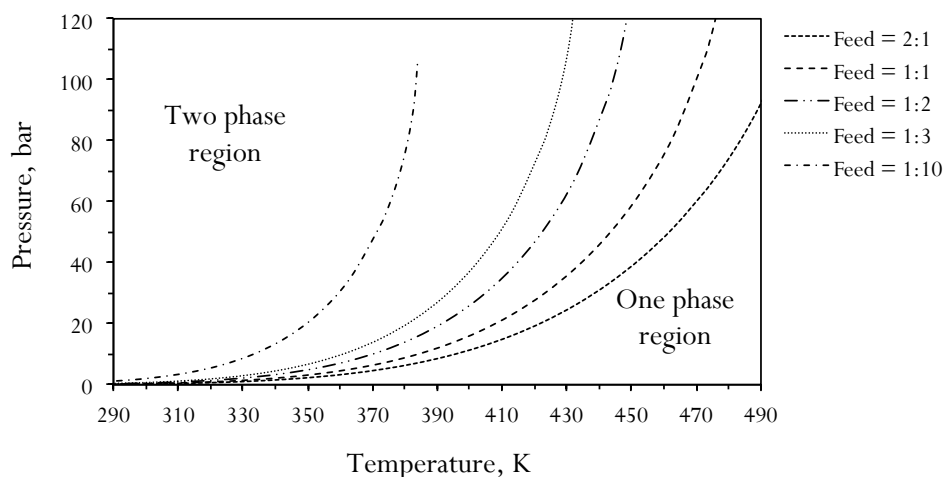


Fig. 6.10. The dew point line CPA predictions of the methanol - CO_2 - DMC - water quaternary system with different feed composition (i.e. methanol : CO_2 mole ratio) and a constant conversion of 10%.

6.5 Discussion

In the present study it has been shown that the CPA EoS is a powerful model that quite satisfactorily predicts the phase behaviour of binary and ternary mixtures comprising the reaction mixture during the direct DMC synthesis. It is capable of predicting not only VLE but also quite complex LLE for some ternary systems. Furthermore, the model was successfully validated by predicting the bubble pressure curves for the quaternary mixtures, the experimental data for which were obtained in the present study.

CPA together with the parameters obtained in this study very nicely describes the binaries that comprise the four-component reaction mixture; however, for ternaries CPA predictions sometimes deviate from the experimental data. This is the case, for instance, for the methanol - CO_2 - water and methanol - DMC - water mixtures. Still in both cases the predictions can be successfully used for preliminary and rough estimations.

The methanol - CO_2 - water ternary mixture had been previously modelled using the gamma-phi $\gamma - \phi$ approach in different variations: (i) the SRK model with the MHV2 mixing rules [6, 29], (ii) the Peng-Robinson-Stryjek-Vera EoS with the vdW1f

mixing rules [7], (iii) the Patel-Teja EoS incorporated with various types of local composition (Wilson and UNIQUAC) and Huron-Vidal mixing rules [29]. The obtained ternary diagrams showed that all models predict the VLE for this ternary satisfactorily, i.e. the predictions match closely the experimental data with some occasional deviations, however, the value of these deviations were not estimated in the abovementioned works.

In general, equations of state describe nicely high-pressure equilibria, such as the one for the methanol – CO₂ – water ternary. The results can be further improved when the equations of state are complemented with the local composition mixing rules, i.e. when the $\gamma - \phi$ approach is used [5]. However, the abovementioned models use multiple adjustable parameters, which are often temperature-dependent.

Models developed specifically for liquid phases, i.e. UNIQUAC and NTRL, were used for describing the LLE of the methanol – DMC – water ternary [8]. Six temperature dependent binary interaction parameters were adjusted when fitting the experimental LLE data of the ternary mixture. Excellent correlations were obtained with a root-mean-square deviation (RMSD) of 0.32 – 0.50% for UNIQUAC and 0.54 – 0.89% for NTRL. However, neither of two models has been used for making predictions of other types of equilibria at different conditions, as well as neither model can be used for high-pressure equilibria.

Unlike UNIQUAC and NTRL, which are the local composition activity coefficient models, CPA is an equation of state, which includes a term for associating components. Accounting for these facts, the CPA performance for the methanol – DMC – water mixture can be considered as very good.

For the methanol – CO₂ – DMC ternary the Peng-Robinson-Stryjek-Vera model with the vdW1f mixing rules was used [7]. Both the PRSV and CPA (in this work) equations of state predicted very well the dew and bubble point curves for this ternary. Apparently, at high pressures and temperatures, and especially in the vapour phase, the effects of association become much less significant than when liquid phase is present. Therefore, the performance of PRSV and CPA are comparable for the methanol – CO₂ – DMC ternary under given conditions.

Further calculations revealed that CPA very nicely represents the bubble point curves of the quaternary mixtures that match very closely the experimental data measured in the present study. The deviation from the experiment on average was 6.7% (%AAD).

The use of multiple parameters, many of which are temperature dependent, as well as the limited range of conditions and types of phase equilibria are the main disadvantages of the models presented in previous studies. In this regard, the CPA EoS appears to be more beneficial. It uses only one temperature independent k_{ij} per binary, i.e. six in total for the quaternary mixture. Its association term is theoretically derived based on the nature of intermolecular interactions between associating components.

From the analysis above it can be seen that CPA, as an equation of state, gives very good predictions for high pressure VLE and satisfactory results for LLE, and its performance could be further improved.

First of all, in CPA the key factor is the monomer fraction X_1 , which in turn is determined by the association scheme that was chosen, as it was discussed in Chapter 2. In the present study both carbon dioxide and dimethyl carbonate were modelled as non self-association components, with the assumption that CO_2 bears one positive site and DMC – one negative. However, different assumptions could have been used and given better results. CO_2 could have been modelled as an inert component (with no sites at all) and for DMC two, three, and more sites could have been assumed, including positively polarised central carbon atom. In general, the CPA calculations showed rather high values for k_{ij} and β^{cross} for the binaries with dimethyl carbonate. It could possibly be explained by the fact that the CPA pure fluid parameters for DMC are high by themselves. Furthermore, sometimes CPA predictions can be improved when a temperature dependency for binary interaction parameters is introduced. However, temperature independent parameters often provide quite satisfactory results.

As it was already mentioned, phase behaviour plays an important role in the reaction, however, it is extremely difficult to say whether the catalytic performance will be better in a supercritical one-phase region, or higher conversions can be achieved when

the reaction is bi-phasic. To answer this question some catalytic data is always required. For example, Camy *et al.* [6] suggested that the most favourable conditions from the catalytic prospective are monophasic. This assumption was based on the fact that heterogeneously catalysed reactions in supercritical medium do not experience any heat and mass-transport limitation in contrast to “gas – liquid – solid catalyst” reactions [30-33]. The same approach was used by Bustamante *et al.* [9], who performed a very extensive theoretical analysis of the reaction equilibria supplemented by phase behaviour calculations, considering that the vapour phase was the desired reaction region.

However, in the case of the propylene carbonate synthesis from propylene oxide and carbon dioxide, which is a very similar reaction to the DMC synthesis, it was experimentally found that the best reaction conditions are located in the so-called “expanded liquid” regime [34]. The phase behaviour modelling presented in Chapter 5 of the present thesis has supported this finding.

Thermodynamic modelling of phase behaviour does not provide an answer to the question in which region the catalyst gives the highest conversion, without running any catalytic experiments. However, as soon as the best region is known, modelling significantly simplifies the search for optimal conditions. In this regard, one and two-phase regions were theoretically predicted, which are shown in Fig. 6.8 and 6.9. The following trends can be captured from them.

Firstly, the two-phase region is expanding as the reaction proceeds. This means, applying the conditions used for the calculations, if the initial feed composition methanol : CO₂ was 1:2, and the reaction began at 60 bar and 440 K, the reaction mixture was monophasic at that moment, according to Fig. 6.9. However, when 35 - 40% of methanol reacted the phase splitting occurred and the system became bi-phasic.

Furthermore, if assumed that the transition state is the best region for the DMC synthesis, some special measures can be taken in order to maintain the system in a certain phase state. Additional amounts of CO₂ can be used in order to prevent the phase splitting or moving the system far away from the phase transition region, i.e. to stay in the “expanded liquid” region. Fig. 6.10 shows how additional carbon dioxide shifts the

phase transition towards lower temperature and pressure. Furthermore, additional amounts of CO₂ move the reaction equilibrium in the direction of DMC formation. All these findings are totally inline with those that had been concluded by Bustamante *et al.* [9].

6.6 Conclusion

In the present study the Cubic-Plus-Association Equation of State was shown to be a powerful and universal model for predicting phase equilibria during the direct synthesis of dimethyl carbonate from methanol and carbon dioxide. It gives quite satisfactory results for low- and high-pressure vapour-liquid and liquid-liquid equilibria of the binaries and ternaries comprising the reaction mixture. Furthermore, CPA was successfully validated by the predicted bubble point pressure curves of quaternary mixtures that matched very closely the experimental data measured in this study.

Some deviations between the CPA predictions for some of the ternary systems and the experimental data have been observed. The reasons are not entirely clear. Some ways to obtain better agreement are to consider different association schemes for carbon dioxide and dimethyl carbonate and/or by incorporating temperature dependent binary interaction parameters.

CPA can predict the one- and two-phase $P - T$ regions where the reaction occurs, as well as the phase behaviour and the composition of co-existing phases. Thermodynamic modelling is a very useful tool for optimising the catalyst performance and separation processes. Some suggestions on optimal reaction conditions can be proposed, however, they must always be complemented by experimental catalytic data.

6.7 References

- [1] Y. Ono, *Appl. Catal., A* 155 (1997) 133-166.
- [2] M. Pacheco, C. Marshall, *Energy & Fuels* (1997) 2-29.
- [3] N. Keller, G. Rebmann, V. Keller, *J. Mol. Catal. A: Chem.* 317 (2010) 1-18.

- [4] J.D. Grunwaldt, R. Wandeler, A. Baiker, *Catal. Rev.* 45 (2003) 1-96.
- [5] G.M. Kontogeorgis, G.K. Folas, *Thermodynamic Models for Industrial Applications: from classical and advanced mixing rules to association theories*, Wiley, 2010.
- [6] S. Camu, J.-S. Pic, E. Badens, J.-S. Condoret, *J. Supercrit. Fluids* 25 (2003) 19 - 32.
- [7] R. Pinero, J. Garcia, M. Sokolova, M.J. Cocero, *J. Chem. Thermodyn.* 39 (2007) 536-549.
- [8] J. de la Torre, A. Chafer, A. Berna, R. Munoz, *Fluid Phase Equilib.* 247 (2006) 40-46.
- [9] F. Bustamante, A.F. Orrego, S. Villegas, A.L. Villa, *Ind. Eng. Chem. Res.* 51 (2012) 8945-8956.
- [10] R. Dohrn, S. Peper, J.M.S. Fonseca, *Fluid Phase Equilib.* 288 (2010) 1-54.
- [11] C. Crampon, G. Charbit, E. Neau, *J. Supercrit. Fluids* 16 (1999) 11-20.
- [12] I. Tsvintzelis, M.J. Beier, J.D. Grunwaldt, A. Baiker, G.M. Kontogeorgis, *Fluid Phase Equilib.* 302 (2011) 83-92.
- [13] R. Wandeler, N. Kunzle, M.S. Schneider, T. Mallat, A. Baiker, *J. Catal.* 200 (2001) 377-388.
- [14] D. DIADEM, *The DIPPR information and Data Evaluation Manager for the Design Institute for Physical Properties. Version 1.1.0* (2006).
- [15] I. Tsvintzelis, G.M. Kontogeorgis, M.L. Michelsen, E.H. Stenby, *Fluid Phase Equilib.* 306 (2011) 38-56.
- [16] J. Im, M. Kim, J. Lee, H. Kim, *J. Chem. Eng. Data* 49 (2004) 243-245.
- [17] J.A.V. Butler, D.W. Thomson, W.H. Maclennan, *J. Chem. Soc.* (1933) 674-686.
- [18] M.L. Mcglashan, A.G. Williamson, *J. Chem. Eng. Data* 21 (1976) 196-199.
- [19] J.B. Ferguson, W.S. Funnell, *J. Phys. Chem.* 33 (1929) 1-8.
- [20] G.A. Ratcliff, K.C. Chao, *Can. J. Chem. Eng.* 47 (1969) 148-153.
- [21] G. Bredig, R. Bayer, *Z. Phys. Chem. Stoch.* 130 (1927) 1-14.

- [22] M. Broul, K. Hlavaty, J. Linek, Collect. Czech. Chem. C. 34 (1969) 3428-3435.
- [23] H. Schuberth, Z. Phys. Chem-Leipzig 255 (1974) 165-179.
- [24] J. Griswold, S.Y. Wong, Chem. Eng. Prog. 48 (1952) 18-34.
- [25] W. Schroeder, Chemie Ingenieur Technik (1958) 523-525.
- [26] F. Comelli, R. Francesconi, J. Chem. Eng. Data 42 (1997) 705-709.
- [27] S. Yunhai, L. Honglai, W. Kun, X. Wende, H. Ying, Fluid Phase Equilib. 234 (2005) 1-10.
- [28] R.F. Gould, Azeotropic Data III, American Chemical Society, 1973.
- [29] J.H. Yoon, M.K. Chun, W.H. Hong, H. Lee, Ind. Eng. Chem. Res. 32 (1993) 2881-2887.
- [30] A. Baiker, Chem. Rev. 99 (1999) 453-473.
- [31] W. Leitner, P.G. Jessop, Chemical Synthesis Using Supercritical Fluids, Wiley-VCH, 1999.
- [32] C.A. Eckert, D. Bush, J.S. Brown, C.L. Liotta, Ind. Eng. Chem. Res. 39 (2000) 4615-4621.
- [33] X. Han, M. Poliakoff, Chem. Soc. Rev. 41 (2012) 1428-1436.
- [34] M. Ramin, J.D. Grunwaldt, A. Baiker, Appl. Catal., A 305 (2006) 46-53.

General Conclusions and Outlook

The present PhD-study has brought together such areas of chemical engineering as heterogeneous catalysis, supercritical fluids, namely dense and supercritical carbon dioxide, as well as thermodynamic modelling of phase behaviour during chemical reactions. It has been shown that phase equilibrium can significantly affect catalyst performance, which opens some ways for the optimisation and intensification of the processes. It has also been highlighted that the use of advanced thermodynamic models, such as CPA, can be particularly useful for this purpose.

Selective hydrogenation reactions are extremely important for the industry, and in many cases the catalytic aspects of the processes are well established. However, when the reactions are performed in the presence of carbon dioxide medium, multiple effects can occur. In this work these effects have been studied with the example of the selective hydrogenation of 2-butenal in carbon dioxide medium. It was experimentally shown that the maximum of conversion is achieved at the critical point of the reaction mixture, i.e. when the reaction system becomes monophasic. The corresponding phase behaviour calculations were made with the CPA model. Complementary measurements of the CO₂ – 2-butenal VLE were carried out in order to obtain the binary interaction parameter for this mixture.

There are multiple explanations for such catalyst performance in the near-supercritical region of the reaction mixture, however, the real one/ones are not clear. Therefore, some *in situ* investigations into the reaction mechanism could be very useful; and the interactions of CO₂ with the reactants and catalyst surface would be particularly interesting. 2-Butenal hydrogenation has been performed only in the batch regime, and the catalyst performance in the continuous mode would be also interesting. In general, the dilution of the reaction system with CO₂ leads to the reduced residence times, which negatively affects conversion; however, the amount of CO₂ determines the phase

behaviour of the system (at a given temperature and pressure). These effects require further investigation.

Aldol reactions yield very valuable products for the industry and they can be significantly improved, compared to the traditional technologies, if heterogeneous catalysis is used together with carbon dioxide reaction medium. The “one-pot” synthesis of aldol reaction products, with the selective hydrogenation of unsaturated aldehydes as the first step, has also attracted a lot of attention.

In this study it has been shown that Amberlyst-15 and tungstosilicic acid (TSA) catalysts have a big potential for performing aldol reactions. TSA loaded on different types of support remains mainly intact, however, its real structure is not entirely clear. Different aldehydes, depending on molecular weight and molecular complexity, react with different reaction rates, which decrease with increasing weight and structure complexity. Furthermore, it was observed that trimerisation of aldehydes is the main side-reaction which significantly decreases the yield of the target product. However, it can be suppressed at elevated temperatures, and/or when large amounts of carbon dioxide are used as reaction medium.

For performing the “one-pot” synthesis in the continuous-flow mode, a bifunctional catalyst is desired. Apparently, the presence of an acidic component pulls the equilibrium of the first hydrogenation step, whereas, the hydrogenation constituent facilitates the aldol reaction step by hydrogenating the aldol reaction product. Moreover, the composition of the bifunctional catalyst along the reactor should also be optimised, since in different parts of the reactor different reactions prevail.

The TSA catalysts can be potentially further improved. However some extensive characterisation will be required in order to understand the reaction mechanism and the nature of active sites. The reaction mechanisms of aldol reaction and especially of the “one-pot” synthesis have to be studied thoroughly, because the latter reaction could be potentially performed without a hydrogenating component. This idea has to be developed further. As it has been shown, the phase behaviour plays an important role

during the reaction; however, the reaction conditions were not optimised. Thermodynamic modelling can be very useful in this regard.

Carbon dioxide, besides being an effective reaction medium, can also be a reactant in many reactions. A good example is the synthesis of propylene carbonate from propylene oxide and CO₂. In this study it has been shown how practical thermodynamic modelling could be. The catalyst performance depending on the phase behaviour of the reaction mixture was studied, and the optimal reaction regime was determined. The highest yield of propylene carbonate was achieved in the near-critical region of the reaction system. The number and the composition of the phases existing in the reactor were calculated with CPA. This finding was supported by the experimental data from the literature. It was shown that thermodynamic modelling is much less time consuming, elaborating, expensive, and dangerous, compared to experimental studies, however, it reveals the same information and sometimes even more.

This study could be continued in the catalyst design direction. The presented here supported homogeneous catalyst is quite active; however, catalyst screening should be performed in order to find more effective and less expensive materials for industrial applications.

The direct synthesis of dimethyl carbonate from methanol and carbon dioxide is another industrially important example of CO₂-fixation reactions. Thermodynamic modelling can help to optimise the reaction conditions, and an advanced model should be used in order to account for the complex interactions of association components, such as methanol and water. In this work it has been shown that the CPA model is a universal and very effective tool for predicting phase behaviour of ternary and quaternary mixtures representing the reaction mixture. Unlike other models, it satisfactorily predicts any type of equilibria (VLE, VLLE, LLE, etc.) and the properties of the system in the sub-, near-, and supercritical state.

The performance of CPA for the synthesis of DMC could be further improved if different association schemes were introduced as well as temperature dependent binary interaction parameters.

List of Symbols

K_x	Equilibrium constant
k_x	Reaction rate constant
x, y	Mole fractions
P, P_c, P^{sat}	Pressure, critical pressure, saturated vapour pressure
T, T_c, T_r	Temperature, critical temperature, reduced temperature ($T_r = T/T_c$)
ω	Acentric factor
V, V^{liq}	Volume or molar volume, saturated liquid molar volume
Z	Compressibility factor
R	Gas constant
G^E, g^E	Excess Gibbs energy
\hat{f}	Fugacity
γ	Activity coefficient
φ	Fugacity coefficient
Γ	Intermolecular potential function
r	Intermolecular distance
N, n, n_{sub}	Number of components in the mixture, experimental points, number of moles
a, a_0	Fluid specific energy parameter in equations of state, CPA fluid specific parameter
b	Fluid specific co-volume parameter in equations of state or CPA fluid specific parameter
c_1	CPA fluid specific parameter
a_{ij}	Cross-energy parameter
b_{ij}	Cross-co-volume parameter

k_{ij}	Adjustable binary interaction parameter in the expression for cross-energy
l_{ij}	Adjustable binary interaction parameter in the expression for cross-volume
i, j	Indices referring to different components
X_{A_i}	Fraction of sites A on molecule i that do not form bonds with other association sites
$\Delta^{A_i B_j}$	Association strength between two sites A and B belonging to molecules i and j , respectively
$\varepsilon^{A_i B_j}$	Association energy
$\beta^{A_i B_j}$	Association volume
$g(\rho)$	Radial distribution function
ρ	Molar density
A_{ij}, A_{ji}	Binary interaction parameters in the activity coefficient models
m_{cat}	Catalyst mass
Mr	Molecular weight
t	Time

Acknowledgements

A PhD study is a big but very exciting challenge with all its ups and downs along this journey. Herewith I would like to thank all people who have been beside me throughout these three years with their advice, support, and nice attitude.

Prof. Jan-Dierk Grunwaldt was the one who initiated this PhD-project and I am very glad and thankful to him for having been offered the position. I have never been dictated from his side what and how to do, however, I always received extensive comments and very useful feedback on everything I did. Prof. Georgios M. Kontogeorgis stepped in as a main advisor at DTU after Jan-Dierk left for Germany. His critical and useful comments on my results have always guided me to the right direction. Prof. Anker Degn Jensen was my co-supervisor at DTU. He helped me to see things at different angles (science and engineering), as well as his feedback helped me to avoid some mistakes.

All three years DTU has been my main Alma Mater, therefore, I would like to thank Prof. Kim Dam-Johansen (Head of the Department of Chemical and Biochemical Engineering) and Prof. Erling H. Stenby (Head of the Department of Chemistry) for creating a very nice working atmosphere.

I would also like to acknowledge The Danish Research Council for Technology and Production Sciences, Institute of Catalysis Research and Technology (IKFT) at Karlsruhe Institute of Technology for financial support. ANKA (Karlsruhe) and DESY (Hamburg) are gratefully acknowledged for beam times, DANSCAT and the EU Contract RII13-CT-2004-506008 for financial support of the synchrotron radiation experiments, as well as all beam line scientists for their help during the experiment. The Centre for Electron Nanoscopy at DTU is acknowledged for the help with TEM measurements. I would like to thank all technicians who have helped me a lot with my experiments at DTU, KIT, and ETH.

A large part of the experimental research has been performed outside DTU at KIT, which has become my second home. I would like to thank Dr. Loubna Gharnati for her help and support in organising experiments at KIT, Dr. Wolfgang Kleist for his valuable advice, Dr. Maria Casapu, Dr. Gian-Luca Chiarello, Dr. Martin Schubert, Dr. Dmitry Doronkin for the lively and fruitful discussions. I have really enjoyed working by your side and learn from you. A piece of research has been carried out in the group of Prof. Alfons Baiker at ETH Zurich in Switzerland. It has been a great pleasure and honour to work with him. I would also like to thank Dr. Jean-Michel Andason for his help with the phase behaviour experiments. Special thanks to Dr. Ioannis Tsivintzelis from DTU, whose invaluable help with thermodynamic calculations can hardly be underestimated.

Furthermore, I would like to highlight the PhD-students that I have had a great pleasure to work with: Matthias J. Beier (who has supported me enormously during my work both in Denmark and in Switzerland and who has received his PhD now), Martin Høj (for measuring some TEM samples for me and translating the summary of this thesis into the Danish language), Alexey Boubnov (for his help with EXAFS analysis and translation the summary into Danish, though “ikke uden hjælp af GoogleTranslate”), Marina Tepluchin (for her help with XRD), Karin Walter (for continuing my work and helping to finalise it), Melanie Leicht (for organising things at KIT), Kirsten Schuh and Tatyana Nesterova. Special regards to Irek Sharafutdinov and Alsu Khusainova who have been very hospitable to me during my frequent trips to Denmark and their enormous support in almost every aspect. I also want to mention Julia Engelke, Elen Ogel, Ilia Maximov, Maxim Artemenko for their support and belief in me. I am very happy to realise that we have become more than just co-workers, but good friends. I would also like to thank my girlfriend and future wife Rimma Zaripova for her patience and understanding. Time and distance mean so little when someone means so much.

At last but by far not least, I would like to express my deepest gratitude, respect and love to my mom and dad, Nina and Evgeny. After all, if it were not for them in the first place, this thesis would never come out.

I have tried not to forget anyone here, and, please, do forgive me if I did so.

Heterogeneously Catalysed Aldol Reactions in Supercritical Carbon Dioxide as Innovative and Non-Flammable Reaction Medium

Nikolai E. Musko · Jan-Dierk Grunwaldt

Published online: 24 August 2011
© Springer Science+Business Media, LLC 2011

Abstract Aldol reactions of several aldehydes have been investigated over acidic and basic catalysts in supercritical carbon dioxide at 180 bar and 100 °C. Both acidic (Amberlyst-15, tungstosilicic acid (TSA) on SiO₂ and MCM-41) and basic (hydrotalcite) materials showed interesting performance in this preliminary study under the entitled reaction conditions. Small and linear aldehydes, such as propanal, butanal, pentanal and hexanal, react more efficiently than the branched 3-methylbutanal, which is converted much slower. Whereas Amberlyst-15 showed the highest conversion based on the catalyst mass, tungstosilicic acid-based catalysts were significantly better if the rates were related to the number of acidic sites ($>1000\text{ h}^{-1}$). The rate depends both on the dispersion and the kind of support. Strikingly, tungstosilicic acid (TSA) on MCM-41 was also an effective catalysts for the selective C=C double bond hydrogenation of 2-butenal and is therefore a potential catalyst for the “one-pot” synthesis of 2-ethyl-2-hexenal and 2-ethylhexenal via combined hydrogenation and aldol reaction from 2-butenal. A number of characterisation techniques, such as temperature-

programmed desorption of ammonia (NH₃-TPD), transmission electron microscopy (TEM), X-ray absorption spectroscopy (XAS), etc. were used to get an insight into the catalyst structure, which support a high dispersion and strong acidity of the tungsten based species on silica and MCM-41.

Keywords Aldol reaction · Supercritical carbon dioxide · 2-Butenal · Selective hydrogenation · Amberlyst-15 · Tungstosilicic acid

1 Introduction

The use of supercritical carbon dioxide in heterogeneous catalysis provides a number of opportunities due to the fact that it combines both gas-like and liquid-like properties [1–3]. Gas-like properties significantly decrease heat and mass transfer limitations, and the relatively high density, which is determined by liquid-like properties, leads to increased solubility and allows the use of CO₂ as an alternative to conventional solvents. The properties of scCO₂ are strongly dependent on temperature and pressure in the system, especially near the critical point, which makes both chemical and separation processes quite tunable. Besides, the use of carbon dioxide makes the whole technology much “greener” due to the fact that it can be recycled and the amount of waste can be minimized [4].

The aldol reaction is one of the most important reactions in chemical syntheses as it leads to C–C bond formation, and yields products that can be used as solvents, flavours, additives, etc. [5]. Traditionally, aldol reaction is carried out in liquid phase with stoichiometric amounts of the aqueous solution of inorganic bases (NaOH, Ca(OH)₂, etc.) or acids [6, 7]. Therefore, huge amount of waste is produced, whereas conversion and selectivity are usually quite

N. E. Musko
Department of Chemical and Biochemical Engineering,
Technical University of Denmark (DTU), Søtofts Plads,
Building 229, 2800 Kgs. Lyngby, Denmark

N. E. Musko · J.-D. Grunwaldt
Institute for Catalysis Research and Technology (IKFT),
Karlsruhe Institute of Technology (KIT),
Herman-Helmholtz-Platz 1, 76344 Eggenstein-Leopoldshafen,
Germany

J.-D. Grunwaldt (✉)
Institute for Chemical Technology and Polymer Chemistry
(ITCP), Karlsruhe Institute of Technology (KIT),
76128 Karlsruhe, Germany
e-mail: grunwaldt@kit.edu

low. Complicated separation and low overall effectiveness of traditional processes require improvements, i.e. the use of heterogeneous catalysts and the development of “green technology” for the aldol reactions. In 2004 Mestres published a review on “green” aldol processes which showed the potential of heterogeneous catalysts, ionic liquids and supercritical fluids [7], but only very little had been done.

The aldol cross-reaction of acetone and benzaldehyde over hydrotalcite can be considered the first reaction performed in the presence of a heterogeneous catalyst [8]. In later work, Matsui et al. studied the aldol reaction of propanal over basic MgO catalysts of different particle size under scCO_2 in the presence or absence of water [9, 10]. In related work, a number of bifunctional catalysts have been developed for the synthesis of methylisobutylketone (MIBK) [11–15], which comprises two subsequent steps: (1) the aldol reaction of acetone and dehydration to an unsaturated ketone; and (2) the subsequent hydrogenation of the unsaturated ketone to MIBK.

A successful attempt to use the bifunctional catalyst 1%Pd on acidic resin Amberlyst-15 was made by Seki et al. [16]. In their work they synthesised 2-ethylhexanal directly from 2-butenal via the hydrogenation and aldol condensation in scCO_2 . In this case, the hydrogenation step precedes the aldol reaction, but the whole process occurs in “one-pot”. Extending this work also by the use of different characterisation techniques a first reaction mechanism was proposed [17]. The active site for 1%Pd/Amberlyst-15 catalyst was considered $[\text{Pd-H}]^+$, both hydrogenation and aldol reaction steps are taking place on the same active site without an intermediate migration from a palladium particle to an acidic site and back. They also studied the reaction of 2-hexenal in the same synthesis and obtained satisfactory results. Very recently Poliakoff et al. [18] studied the aldol reaction of propanal over a number of acidic and basic catalysts in scCO_2 , using an automated continuous-flow reactor. These results support that Amberlyst-15 and $\gamma\text{-Al}_2\text{O}_3$ are promising catalysts for this type of reactions and that the scCO_2 reaction medium has a great potential for further investigations.

However, the “one-pot” synthesis and the aldol reaction itself in supercritical carbon dioxide are not studied in detail yet, the reaction mechanism is still a matter of discussion and they definitely need further investigation. In situ spectroscopic measurements of heterogeneous catalysts and reaction media at high pressures could be useful for that purpose as it was done in [19]. Surprisingly, only a couple of active catalysts for this process have been found so far. They give good results at temperatures 70–100 °C, however this temperature range is quite far from the critical point of CO_2 (31.4 °C) and it is desirable to shift the reaction temperature range towards this point. The aldol reaction and condensation occurs alongside with the

formation of relatively heavy products the solubility of which in carbon dioxide is lesser compared to the reactants. Therefore, monitoring and controlling the phase behaviour is crucial in the study.

The scope of this study comprises (1) screening a number of acidic and base catalysts for aldol reactions of the aldehydes with different chemical structure; and (2) investigations aiming at the realization of the “one-pot” reaction with unsaturated aldehydes over screened catalysts. Note that once an active catalyst for the aldol reaction is found, it shall be possible to develop improved bifunctional catalysts for the “one-pot” reaction because selective hydrogenation reactions are relatively well studied [3].

2 Experimental

2.1 Catalyst Materials

A number of different acidic and basic catalysts were chosen for catalyst screening. HZSM-5 (15) (Zeolyst), $\gamma\text{-Al}_2\text{O}_3$ and SiO_2 (Haldor Topsoe) and Amberlyst-15 (Sigma-Aldrich, 16-50 mesh, number of acid sites—4.7 meq/g by dry weight) were received commercially and directly used for the catalytic tests. In addition, further catalysts were prepared according to the following recipes.

Tungstosilicic acid (TSA) supported catalysts (10, 20, and 40 wt% TSA on SiO_2 or MCM-41) were prepared by incipient wetness impregnation. 0.22, 0.50 and 1.33 g of TSA ($\text{H}_4\text{SiW}_{12}\text{O}_{40}\cdot\text{H}_2\text{O}$, $\geq 99.9\%$, Sigma-Aldrich) correspondingly were dissolved in 1.2 mL (for SiO_2 , received from Haldor Topsoe) or 2 mL (for MCM-41, spec. surface area 940–1000 m^2/g , Sigma-Aldrich, 1.0 cm^3/g pore volume, 2.5–3 nm pore size) of water, which were calculated from the pore volumes of the carriers. 2.0 g of each carrier were impregnated by the solutions; the samples were subsequently dried in air and at 100 °C overnight, and calcined at 300 °C for 5 h.

An equilibrium impregnation technique was used for the preparation of TSA/Carbon sample as follows: 1.0 g of TSA were dissolved in 5 mL of solvent (distilled water and ethanol 1:1 vol.), 1.0 g of carrier-activated charcoal (Sigma-Aldrich, 0.8 mm diam. rods, ground down to 250–500 μm)—was added to the solution and left for 72 h with constant stirring; then the material was filtered off, washed with distilled water, and dried at 100 °C in air overnight.

Hydrotalcite (HT) preparation was carried out by the procedure described in [20]: solution A was prepared by dissolving 25.6 g of $\text{Mg}(\text{NO}_3)_2\cdot 6\text{H}_2\text{O}$ (0.1 mol, Sigma Aldrich, 97%) and 18.6 g of $\text{Al}(\text{NO}_3)_3\cdot 9\text{H}_2\text{O}$ (0.05 mol, Sigma Aldrich, 98%) in 70 mL distilled water. Solution B was prepared by dissolving 28.0 g of 50% NaOH (14.0 g of NaOH pellets, Sigma Aldrich, in 14 mL distilled water,

purity 98%) and 10.0 g of Na_2CO_3 (Sigma Aldrich, 99%) in 100 mL distilled water. The hydrotalcite was prepared by adding solution A to solution B in 3–4 h with constant stirring. The resulting gel was transferred to an autoclave (250 mL inner volume with a teflon cup and magnetic stirrer inside) and allowed to crystallize at 50 °C for 18 h. The sample was filtered off and washed with hot distilled water until the pH of the filtrate was neutral and also to remove any free sodium ions that may present. The sample was dried in an oven for 12 h at 100 °C and then calcined at 450 °C in air for 18 h to obtain the hydrotalcite.

Finally, a 11% WO_3/ZrO_2 sample was obtained by the incipient wetness impregnation of zirconium dioxide using a solution of $(\text{NH}_4)_6\text{H}_2\text{W}_{12}\text{O}_{41}$ (Fluka). The sample was dried overnight at 100 °C. Some of the sample was then impregnated by $\text{Pd}(\text{NO}_3)_2$ solution with subsequent drying overnight at 100 °C and reduction in H_2/N_2 flow at 300 °C. Thereby a 0.8% $\text{Pd}/11\%\text{WO}_3/\text{ZrO}_2$ catalyst sample was obtained.

2.2 Characterisation Techniques

The specific surface areas of the supports and catalysts were determined using BET isotherms recorded on a BELSORB-mini (BEL-Japan inc.) surface area analyser at a nitrogen adsorption temperature of 77 K.

Number of acidic sites on the catalyst surface for all the samples were studied using ammonia temperature-programmed desorption (NH_3 -TPD). The experimental procedure was as follows. A catalyst sample (0.2–0.3 g) was fixed with glass wool in a glass reactor with two thermocouples inside for controlling the temperature. At the beginning of the experiments the reactor with the sample was flushed with nitrogen flow (510 mL/min) and heated up to 350 °C (with a ramp of 10°/min) for desorbing light components and gases from the catalyst surface. After that the system was cooled down to 55 °C, and the gas flow was switched to the ammonia flow (600 ppm NH_3 in nitrogen, total flow 510 mL/min). The saturation occurred at a constant temperature of 54–55 °C. The amount of ammonia in the outlet line after the reactor was detected by a non-dispersive infrared (NDIR) detector, which had been previously calibrated. When the concentration of ammonia reached a plateau, the flow was switched back to the pure nitrogen to flush out an excess amount of the adsorptive. When the concentration of NH_3 came to a steady minimum the system was heated up to 480 °C (with a ramp of 10°/min). Thereby, the desorption profile was recorded from which the number of acidic sites was estimated.

Transmission electron microscopy (TEM) (Technie T20, Center of Nanoscopy, DTU) was used for determining the morphology and particle size on the catalyst surfaces.

X-ray absorption spectroscopy (XAS) data were collected at the W L_3 -edge in transmission mode at the synchrotron radiation facilities ANKA (Karlsruhe, Germany) at the XAS beamline and HASYLAB (Hamburg, Germany) at the beamline X1. For these experiments the catalysts were pressed to pellets with cellulose as additive. The edge jumps (defined by difference in pre-edge and post-edge sections at the edge) were 0.4–0.7. The raw data were energy calibrated, background corrected and normalized using the ifeffit-code [21]. After extraction of the $\chi(k)$ function from the EXAFS data, Fourier transformation was performed on the k^3 -weighted data in the interval $k = 2.0\text{--}12.0 \text{ \AA}^{-1}$.

2.3 Catalyst Test in Aldol Reactions

The aldol condensation and “one-pot” synthesis with different reactants were carried out in a batch reactor with adjustable volume (23–64 mL), potential pressure up to 300 bar and a sapphire window for in situ visualisation of the reaction mixture (NWA analytics, Lörrach, Germany). The temperature was controlled by a J-type thermocouple connected to a Eurotherm 2216e controller and the pressure monitored by a standard manometer. For safety reason, the combined batch reactor/view cell is equipped with a burst plate (Swagelok). The following substrates (all received from Sigma-Aldrich) were used without further purification: propanal ($\geq 97\%$), butanal ($\geq 99\%$), pentanal ($\geq 97\%$), hexanal (98%), 3-methylbutanal (97%), and acetone (99.5%) for GC-analysis.

Before the experiments the cell was thoroughly cleaned, washed with organic solvents, and subsequently dried. First, the required amount of catalyst was loaded into the batch reactor and the lid was tightened. The liquid substrate was added by means of a syringe through a hole in the upper part of the cell. Then it was sealed and flushed several times with gaseous carbon dioxide in order to replace all the air inside by CO_2 . After that the batch reactor was charged with CO_2 , adjusted by the pressure in the system. When carrying out “one-pot” syntheses, it was previously charged with the required amount of hydrogen. The corresponding amounts of the components are given in the “Results and discussion” section. After charging with all the components the whole system underwent leakage testing. Then the reactor was heated up to a desired temperature with constant stirring. The pressure was adjusted to the working conditions by the means of an oil-pump pushing the piston in the cell, thereby changing the reactor volume. Typical reaction conditions were 100 °C, 180 bar and 2 h reaction time. After the reaction the autoclave was cooled down to the room temperature and slowly depressurised to atmosphere pressure. The batch reactor was

opened and a sample was taken with a syringe, diluted with acetone and analysed by GC.

Before all the experiments, blind tests for hydrogenation and aldol condensation reactions without catalysts were performed. No detectable catalytic activity of the autoclave has been found at 100 °C and 180 bar under the typically applied reaction conditions.

Product analysis was performed using a gas chromatograph (Agilent 6890N) with a 7683 B series autosampler with a polar capillary column (HP INNOWAX, 30 m length and 0.25 mm diameter) and a flame ionisation detector (FID). Column temperature conditions were 50 °C (10 min)—heating with a ramp of 20 °C/min–250 °C (10 min). The products were identified by comparing the GC retention times with those of commercially available authentic samples. Before the analyses the GC was calibrated for the reactants and possible products.

3 Results and Discussion

3.1 Catalyst Characterisation

The BET surface areas of the catalysts and carriers and the numbers of their acid sites are presented in Table 1. From the table it is clearly seen that loading TSA significantly decreases the total surface area of the carriers which it is deposited on. Thus, the surface area of pure MCM-41 is 980 m²/g and after loading 40 wt% of tungstosilicic acid it dropped more than twice, down to 372 m²/g. Similarly, the surface area of silica decreased after loading the acid, considering that the BET surface area of pure silica is 91 m²/g. Hence, higher loading of the tungsten based acid causes a decrease of the surface area of the sample probably due to the deposition on narrow pores or particle coagulation. Nevertheless, the surface area remains high.

Table 1 BET surface area and number of acid sites of the catalysts and carriers

Catalyst	S_{BET} (m ² /g)	Number of acid sites (mmol/g)
SiO ₂	91	0.02
10%TSA/SiO ₂	79	0.37
20%TSA/SiO ₂	66	0.99
40%TSA/SiO ₂	60	2.32
MCM-41	980	0.78
40%TSA/MCM-41	372	3.62
γ-Al ₂ O ₃	215	1.88
HZSM-5 (15)	400	4.18
Hydrotalcite ^a	37	–

^a Basic catalyst

Previously, it had been reported that TSA deposited on MCM-41 forms separate particles on the carrier surface [22]. Assuming that the average surface occupied by one TSA molecule is 1.44 nm², only 120 m²/g is covered with the acid in the 40 wt% TSA/MCM-41 catalyst, which is just 12.3% of the total surface of MCM-41. It was further previously reported that above 6 wt% TSA the Keggin cluster remained intact [27] and that TSA deposited on SiO₂ forms layers with different uniform thickness depending on the loading of the acid [23]. Theoretically, 10, 20 and 40 wt% loadings of TSA form 1.8, 4.6, and 8.7 layers on the silica surface. Kuang et al. [24] suggested based on calculations by XRD results using the Scherrer's equation that silica-supported tungstophosphoric acid with 40 wt% loading mainly deposited on the silica surface in a form of small particles about 26 nm in diameter.

An interesting trend was observed when measuring the number of acid sites of the samples using NH₃-TPD. The TSA samples were prepared using the incipient wetness impregnation; therefore, it was additionally possible to calculate the theoretical number of acid sites.

Assuming tungstosilicic acid as H₄SiW₁₂O₄₀ with Keggin structure, that all TSA-entities form a monolayer on the carrier surface and all active sites are equally accessible one can calculate the number of acidic sites. With only the four protons of the Keggin cluster as the origin of the acidity, one can derive that the acidity of the 10 wt% catalyst is approximately 0.14 mmol/g. The theoretical numbers of acid sites of the samples containing 20 and 40 wt% of TSA are 0.27 and 0.55 mmol/g, respectively.

However, the experimental results of NH₃-TPD (Table 1) showed that the catalysts possess almost 3–4 times higher number of acid sites than expected, depending on the type of the carrier. This could mean that the assumption that only the four protons possess acidity in tungstosilicic acid molecules was incorrect. Obviously, some other parts of the molecules have certain acidity. Furthermore, it should be kept in mind that the carriers also possess Brønsted and Lewis acid sites. Thus, MCM-41 has significantly higher number of acid sites than silica. This could partly explain the higher deviation of experimental acidity from the theoretical in case of the 40%TSA/MCM-41 sample compared to 40%TSA/SiO₂ (2.32 vs. 3.62 mmol/g). Another reason for that deviation could be the difference in surface areas of two carriers. Presumably, the TSA molecules are spread more evenly on the MCM-41 surface than on the silica, therefore, they are more accessible for NH₃ molecules during adsorption–desorption process.

Furthermore, the results in Ref. [25] suggest that measuring acidity of heteropolyacids using ammonia as a probe molecule is not absolutely correct. Heteropolyacids may behave in some respects like liquids. It means that under

certain conditions light polar molecules like water, ethanol, etc. may easily penetrate the Keggin's structure and react inside the bulk material. This results in a higher adsorption of ammonia which is not only due to the acidic sites. Hence, the data given in Table 1 should be taken as a trend. Note that alternatively for the determination of the surface acidity of heteropolyacids the temperature-programmed desorption of benzonitrile can be used [25, 26].

Since the TSA dispersion on the catalyst surface plays an important role in catalysis two samples were further investigated by transmission electron microscopy (TEM, Fig. 1). Due to the fact that MCM-41 is a mesoporous material it was difficult to obtain clear TEM images of the sample. Some of the images are depicted in Fig. 1.

From the images of TSA on MCM-41 catalyst alone it is difficult to conclude about the dispersion of the acid. However, the comparison of the TEM images of the 40%TSA/MCM-41 sample with those of 40%TSA/SiO₂ at the same magnification reveals that the dispersion of the acid is higher on the MCM-41 as the particles on the surface appear to be smaller. From the image of the 40%TSA/SiO₂ sample it can be seen that the acid is finely dispersed on the carrier surface, and mainly forms agglomerates of several molecules of TSA.

X-ray absorption spectroscopy techniques were applied to get an insight into catalysts structure. The spectra were obtained for TSA catalysts at the W L₃-edge in transmission geometry.

As indicated by the white line intensity (Fig. 2), which is determined by the absorption maximum at the edge, the tungsten in all the catalyst samples is very similar to the TSA reference sample, but due to the higher whiteness more ionic, i.e. more oxidized. Note also that in the pure TSA self-absorption effects may play a stronger role. The

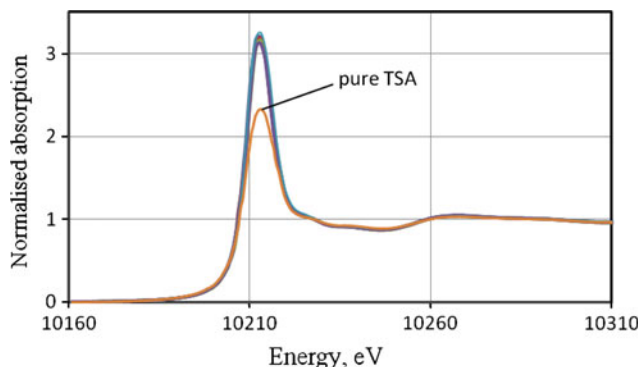


Fig. 2 XANES spectra of pure tungstosilicic acid (TSA) and the TSA catalysts: 10%TSA/SiO₂, 20%TSA/SiO₂, 40%TSA/SiO₂, and 40%TSA/MCM-41

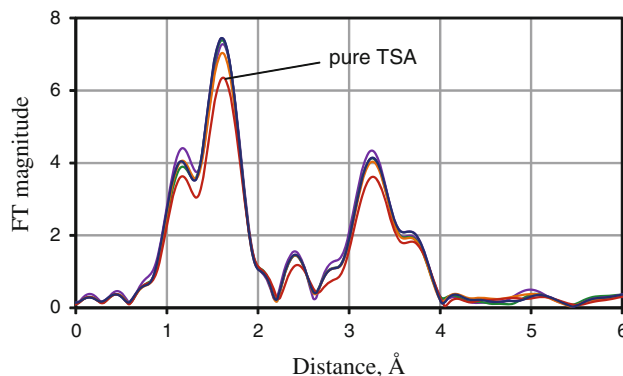


Fig. 3 Fourier transformed EXAFS spectra (k-range 2–12 Å⁻¹, k³-weighted) of pure tungstosilicic acid (TSA) and the TSA catalysts: 10%TSA/SiO₂, 20%TSA/SiO₂, 40%TSA/SiO₂, and 40%TSA/MCM-41

k³-weighted EXAFS spectra and the corresponding Fourier transforms (k-range 2–12 Å⁻¹) are shown in Fig. 3. The two coordination shells in the Fourier transformed data are

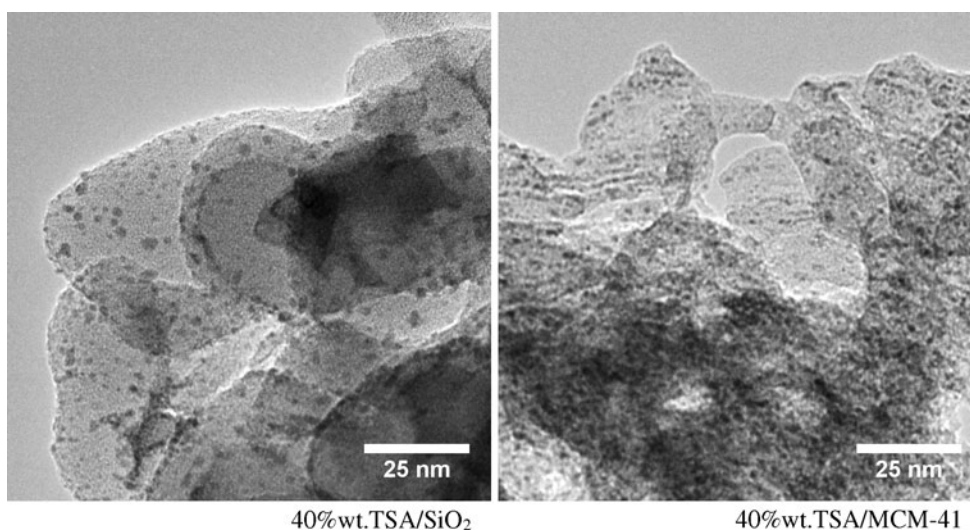


Fig. 1 TEM images of tungstosilicic catalysts

presumably W–O at 1.6 Å and W–W at 3.3 Å (not phase-corrected) shells. The spectrum of pure TSA is very similar but exhibits slightly lower signals for both shells than the 10–40%TSA catalysts, supporting the conclusion in Ref. [27] that at loadings of 10 wt% and higher mostly Keggin clusters are formed during the impregnation process on silica. Note that the structure both on silica and MCM-41 is the same.

Newman et al. [27] reported EXAFS analysis on $H_3PW_{12}O_{40}/SiO_2$ catalysts with an acid loading between 3.6 and 62.5 wt%. It was found that for all the catalysts the Keggin's structure remains intact, even at the low loadings. However, in the same work it was also mentioned that there are some strong interactions between –OH groups of the silica support and the acid, which may cause a destruction of tungstophosphoric acid. The formation of species like $(\equiv SiOH_2)^+(H_2PW_{12}O_{40})^-$ was reported [25], but note that the loadings in the present work were kept rather high.

3.2 Catalyst Performance in Aldol Reaction

In the screening process a series of experiments of the aldol reaction was performed. At the beginning the aldol reaction of butanal was chosen as a model reaction (Fig. 4).

A number of catalysts were tested in the autoclave that served at the same time as a view cell. The phase behaviour was monitored during the experiments, which were carried out under the same reaction conditions for all catalysts and occurred in one single phase. Also after the reaction there was still only one phase according to the visual inspection in the reactor cell which means that there was no separation of aldol reaction and condensation products. This is due to the fact that an excess amount of carbon dioxide (0.25 mol vs. 0.02 mol substrate) was used. The results of the experiments are shown in Table 2. All the catalysts showed 100% selectivity and 2-ethyl-2-butenal was observed as the only product. The most active catalyst in terms of the mass of the used catalyst was Amberlyst-15, giving by far the highest conversion. Surprisingly, the second active catalyst was hydrotalcite with base properties, because carbon dioxide is known to inhibit the performance of base catalysts due to its weak acidic properties [1]. Also other acidic catalysts showed a reasonable catalytic performance considering that the number of acidic sites is much lower compared to Amberlyst-15.

Fig. 4 Aldol reaction with butanal to 2-ethyl-2-hexenal as an example

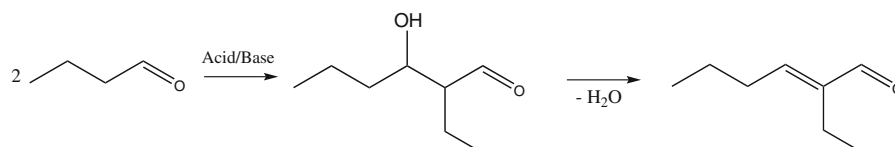


Table 2 Aldol reaction of butanal over different catalysts in $scCO_2$

Catalyst	Conv. (%)	Select. (%)	Reaction rate (mol/(g _{cat} h))	TOF (h ⁻¹)
Amberlyst-15	51	100	5.1	1087
Hydrotalcite ^a	14	100	1.4	–
HZSM-5 (15)	13	100	1.3	311
γ -Al ₂ O ₃	11	100	1.1	585
10% TSA/SiO ₂	9	100	0.9	2432
MCM-41	9	100	0.9	1154

^a Basic catalyst

Conditions: substrate 0.02 mol, $m_{cat} = 0.1$ g, temp. 100 °C, $m_{CO_2} = 10$ g, total pressure 180 bar, reaction time 120 min

Table 3 Aldol reaction of different saturated aldehydes over Amberlyst-15 catalyst in $scCO_2$

Substrate	Conversion (%)	Selectivity (%)	Reaction rate (mol/(g _{cat} h))	TOF (h ⁻¹)
Propanal	84	100	8.4	1789
Butanal	51	100	5.1	1087
Pentanal	31	99	3.1	652
Hexanal	21	98	2.1	454
3-Methylbutanal	10	99	1.0	209

Conditions: substrate 0.02 mol, $m_{cat} = 0.1$ g, temp. 100 °C, $m_{CO_2} = 10$ g, total pressure 180 bar, reaction time 120 min

However, when the catalysts were compared in terms of their turnover frequencies it turned out that Amberlyst-15 was not the most active sample. Thus, the TOF of the 10%TSA/SiO₂ sample was almost 2.4 times higher and the TOF of MCM-41 was very similar to that of Amberlyst-15. Therefore, TSA showed some potential as a possible active and selective catalyst for the process, especially at lower temperatures near the critical point of carbon dioxide.

As Amberlyst-15 turned out to be the most active catalyst for the aldol condensation of butanal it was also tested in the reactions with other saturated aldehydes under identical conditions (Table 3). Even for hexanal with the highest molecular weight only one phase was observed at the end of the reaction, which means that the dissolution power due to the sufficient density of carbon dioxide was able to maintain the system in one phase.

The table shows that the rate of the aldol condensation decreases with the complexity of the reactant structure. The

selectivity becomes also worse, but to a significantly less degree. This decrease in rate may be explained by the increased steric hindrance but also the formation of intermediates on the active site, which block it for further reaction.

In a next step, a number of different TSA supported catalysts were prepared. These samples were tested in the aldol condensation of butanal under the same conditions as in the case of Amberlyst-15. Two types of carriers were used—silica oxide with the BET surface area of 91 m²/g and mesostructured MCM-41 with the surface area of 980 m²/g. Reaction rates and TOF numbers were calculated (cf. Table 4).

The results show that higher loading of the acid gives higher magnitudes of conversion, but not to the same extent. It can be explained by the fact that higher concentrations of TSA cause strong agglomeration of the particles on the support surface. Higher surface area provides smaller particles while the acid loading maintains the

same. This can indirectly be seen from the catalyst performance of two samples with the same loading of TSA but on different carriers: 40%TSA/MCM-41 gives an almost doubled conversion compared to the 40%TSA/SiO₂ catalyst.

Seki et al. [17] suggested in an earlier work that the “one-pot” conversion of 2-butenal, i.e. hydrogenation and aldol reactions (Fig. 5), could take place on the active [Pd-H]⁺ site. In principle, similar processes should be possible on the TSA entities due to their chemical structure and pseudo-liquid behaviour [25, 28]. To check this idea 40%TSA/MCM-41 catalyst was tested in hydrogenation reaction with 2-butenal. The sample showed catalytic activity in the “one-pot” process, even though the yield of the aldol product was very small.

It turned out that this reaction is feasible even without classical hydrogenation catalysts (Pd, Pt, etc.). A number of other catalysts were tested in the reaction with 2-butenal as well. The results are shown in Tables 4 and 5.

The selectivity of the first (hydrogenation) step towards saturated butanal was 100%, i.e. no hydrogenation of the carbonyl bond was found. All the reactions were carried out in one single phase.

The hydrogenation ability of TSA supports the concept that the overall “one-pot” process can take place on one active site, without migration of intermediates from a hydrogenation site to an acidic one and back. However, the literature search showed that there are quite a number of papers devoted to the hydrogenation catalysts on tungstosilicic acid basis. All of them use noble metals as doping, e.g. Cu, Pd, Pt, Ni, etc. [29, 30] or use of additional substances as hydrogenation agents, such as NaBH₄ or

Table 4 Conversion, selectivity and TOFs of butanal aldol reaction and the properties of the tested tungstosilicic acid catalysts

Catalyst	Conv. (%)	Select. (%)	Reaction rate (mol/(g _{cat} h))	TOF (h ⁻¹)
10% TSA/SiO ₂	9	100	0.9	2432
20% TSA/SiO ₂	11	99	1.1	1111
40% TSA/SiO ₂	13	99	1.3	560
40% TSA/MCM-41	27	99	2.7	745

Conditions: substrate 0.02 mol, m_{cat} = 0.1 g, temp. 100 °C, m_{CO₂} = 10 g, total pressure 180 bar, reaction time 120 min

Fig. 5 The “one-pot” synthesis of 2-ethyl-2-hexenal from 2-butenal

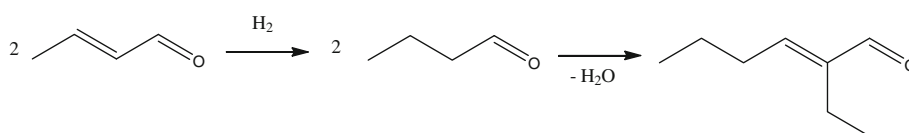


Table 5 Selective hydrogenation and consequent aldol reaction of 2-butenal to 2-ethyl-2-hexenal over different catalysts

Catalyst	Conversion ^a (%)	Yield of the butanal (%)	Yield of the 2-ethyl-hexenal (%)	Reaction rate (mol/(g _{cat} h))
40%TSA/MCM-41	46	43.8	1.1 ^b	4.6
0.8%Pd/11%WO ₃ /ZrO ₂	27	25.2	0.9	2.7
11%WO ₃ /ZrO ₂	26	25.4	0.3	2.6
TSA/carbon	4	4.0	–	4.0

Conditions: substrate 1.64 mL (0.02 mol), catalyst 0.1 g, temperature 100 °C, time 120 min, hydrogen 20 bar, m_{CO₂} = 10 g, total pressure 140 bar, batch reactor

^a In all cases the selectivity of hydrogenation step towards butanal was 100%

^b A number of further unidentified products

hydrosyne [31, 32]. There are hardly any reports on the direct use of heteropolyacids as hydrogenation catalysts and their role in the process, despite the fact that they are widely used as a component of hydrogenation catalysts.

Navalikhina et al. [33] proposed a possible hydrogenation mechanism for hydrogenation reactions over a nickel catalyst modified by heteropoly compounds. The mechanism includes the adsorption of hydrogen from the reaction medium on Ni particles, and its migration via a spillover mechanism to the heteropoly material, whereas the reaction substrate is mainly adsorbed on the heteropoly compound. They also reported that the heterolytic H₂ dissociation and its subsequent spillover do occur on the vacancies of Keggin's anions of the heteropoly material. Therefore, the hydrogen consumed by the material can react with the unsaturated substrate on the catalyst surface. However, this is significant only at elevated temperatures when the heteropoly compounds lose water, thereby forming the vacancies.

The present preliminary results indicate that palladium particles may not be required in the reaction. This is further substantiated by the “one-pot” synthesis of 2-ethyl-2-hexenal from 2-butenal over 0.8%Pd/11%WO₃/ZrO₂ and 11%WO₃/ZrO₂. These two catalysts showed very similar activity and selectivity. This similarity could be explained by the fact that the WO₃ species as well as Pd on the catalyst surface can hydrogenate the substrate as it is reported by Tauster et al. [34]. They also showed in a screening study that hydrogenation on WO₃ species is occurring according to the Eley–Rideal mechanism in contrast with the Langmuir–Hinshelwood mechanism of hydrogenation on palladium particles. It is also possible, that TSA hydrogenation activity is similar to that of WO₃ due to the fact that they both contain octahedral W^{VI}O₆ [28].

The yield of 2-ethyl-hexenal or 2-ethyl-hexanal in the experiments reported here is much lower than in previous continuous-flow processes [16–18]. This may be due to the fact that the hydrogenation is occurring in the first part of the reactor and the aldol condensation in the second part of the reactor. As the results in Tables 1, 2 and 3 clearly demonstrate, the aldol condensation occurs rapidly on butanal so that a longer reaction time may be beneficial for this purpose.

Due to its complex structure and special synthesis procedure, it would be beneficial to another carrier for TSA instead of MCM-41. That could be activated carbon with very high surface area. However, the experimental results showed that much smaller conversion was obtained with TSA/Carbon catalyst. This could be because of the fact that large molecules of TSA simply blocked the narrow pores of the charcoal. Despite the fact that carbon support has a huge surface area of 950 m²/g, it has very narrow pores

(<1 nm). Hence, other high surface area supports should be used in future.

4 Conclusion and Outlook

In this preliminary study a number of active catalysts for the aldol reaction of saturated aldehydes in supercritical carbon dioxide have been found during a first screening of basic and acidic catalyst materials. In fact, both acidic and basic catalyst materials are active in this reaction. Particularly, tungstosilicic acid based catalysts have a great potential, and further efforts should be made in this direction considering that a whole class of supported heteropolyacids is known in literature. Surprisingly, the TSA based catalysts do not only catalyse the aldol reaction, but they can also hydrogenate C=C double bonds with high selectivity. This makes TSA supported bifunctional heterogeneous catalysts also interesting for the selective hydrogenation of unsaturated aldehydes towards saturated aldehydes and subsequent aldol reaction of the latter in supercritical CO₂.

Apart from the heterogeneous catalysts also the use of supercritical carbon dioxide as a reaction medium provides a number of opportunities to optimise the aldol reaction. The experiments here were performed under single phase conditions, which probably have lead to beneficial mass and heat transfer properties. In addition, it allows to minimise waste and facilitates the separation step afterwards. Presently, advanced association models, e.g. PC-SAFT or CPA [35], which can describe scCO₂ and polar hydrogen bonding compounds (e.g. aldols with hydroxyl functional groups) are used to calculate the phase equilibria and thereby rationally optimize the reaction conditions.

Further investigations will be devoted to screening new types of materials, optimising the preparation method of TSA supported catalysts and optimising the reaction conditions in different reactor types. Benzonitrile-TPD will be of importance to further reveal the surface acidity of the TSA catalysts. More extensive characterization studies such as EXAFS will be necessary to investigate the catalyst structure. It is also crucial to elucidate the real reaction mechanism using both ex situ and in situ catalyst characterisation techniques.

Acknowledgments We are very grateful to Zeolyst and Sven Kureti (KIT), for providing the catalyst samples, the Danish Research Council (FTP-proposal “Exploring new catalytic reactions in supercritical carbon dioxide as innovative and non-flammable reaction medium”) for financial support of the project, to Center of Electron Nanoscopy (CEN), DTU for assistance with TEM, Wolfgang Kleist for characterization, Matthias Beier for his help during the experiments, and to Georgios Kontogeorgis (DTU) concerning optimization of reaction conditions by calculation of phase equilibria. ANKA at KIT and HASYLAB at DESY, Hamburg, are gratefully

acknowledged for beamtime and DANSCAT and the EU (Contract RIII3-CT-2004-506008) for financial support of the synchrotron radiation experiments.

References

1. Baiker A (1999) *Chem Rev* 99:453
2. Jessop PG, Leitner W (1999) *Chemical synthesis using supercritical fluids*. Wiley-VCH, Weinheim
3. Grunwaldt J-D, Wandeler R, Baiker A (2003) *Catal Rev Sci Eng* 45:1
4. Licence P, Ke J, Sokolova M, Ross SK, Poliakov M (2003) *Green Chem* 5:99
5. Green MM, Wittcoff HA (2003) *Organic chemical principles and industrial practice*. Wiley-VCH, Weinheim
6. Kelly GJ, King F, Kett M (2002) *Green Chem* 4:392
7. Mestres R (2004) *Green Chem* 6:583
8. Figueras F, Lopez J (2001) In: Sheldon RA, van Bekkum H (eds) *Fine chemicals through heterogeneous catalysis*. Wiley-VCH, Weinheim, p 327
9. Matsui K, Kawanami H (2004) *Stud Surf Sci Catal* 153:363
10. Matsui K, Kawanami H, Ikushima Y (2003) *Chem Commun* 19:2502
11. Kirk-Othmer (1991) *Encyclopaedia of chemical technology*, 4th edn, vol. 1. Wiley-VCH, New York, p 911
12. Maki T, Yokoyama T, Sumino Y (1988) *Jpn Patent* 63,68,538, Mitsubishi Chemical Industries Co., Ltd, Japan
13. Olson KD (1978) U.S. Patent 4,704,478, Union Carbide Corp, Houston
14. Chen PY, Chu SJ, Chen CC, Chang NS, Lin WC, Chaung TK (1991) U.S. Patent 5,059,724 Industrial Technology Research Institute, Taiwan
15. Chen YZ, Hwang CM, Liaw CW (1996) *Appl Catal A* 145:231
16. Seki T, Grunwaldt J-D, Baiker A (2007) *Chem Commun* 34:3562
17. Seki T, Grunwaldt J-D, van Vegten N, Baiker A (2008) *Adv Synth Catal* 350:691
18. Stevens JG, Bourne RA, Poliakov M (2009) *Green Chem* 11:409
19. Grunwaldt J-D, Baiker A (2005) *Phys Chem Chem Phys* 7:3526
20. Reichle W (1985) *J Catal* 94:547
21. Ravel B, Newville M (2005) *J Synchrotron Rad* 12:537
22. Carriazo D, Domingo C, Martin C, Rives V (2008) *J Solid State Chem* 181:2046
23. Kamiya Y, Ooka Y, Obara C, Ohnishi R, Fujita T, Kurata Y, Tsuji K, Nakajyo T, Okuhara T (2007) *J Mol Catal A* 262:77
24. Kuang W, Rives A, Fournier M, Hubaut R (2003) *Appl Catal A* 250:221
25. Kamiya Y, Okuhara T, Misono M, Miyaji A, Tsuji K, Nakajo T (2008) *Catal Surv Asia* 12:101
26. Miyaji A, Echizen T, Nagata K, Yoshinaga Y, Okuhara T (2003) *J Mol Catal A* 201:145
27. Newman AD, Brown DR, Siril P, Lee AF, Wilson K (2006) *Phys Chem Chem Phys* 8:2893
28. Regalbutto J (2007) *Catalyst preparation: science and engineering*. CRC Press, Boca Raton
29. Huang L, Zhu Y, Zheng H, Ding G, Li Y (2009) *Catal Lett* 131:312
30. Hubaut R, Rives A, Kuang W, Fournier M (2005) *Top Catal* 4:101
31. Joshi MV, Narasimhan CS (1989) *J Catal* 120:282
32. Joshi MV, Vaidya S, Pandey R, Mukesh D (1999) *J Catal* 183:102
33. Navalikhina MD, Krylov OV (2001) *Kinet Catal* 42:264
34. Tauster SJ, Sinfelt JH (1970) *J Phys Chem* 74:3831
35. van Solms N, Kouskoumvekaki IA, Michelsen ML, Kontogeorgis GM (2006) *Fluid Phase Equilib* 241:344



Fluid phase equilibria of the reaction mixture during the selective hydrogenation of 2-butenal in dense carbon dioxide

Nikolai E. Musko^{a,b,d}, Anker Degn Jensen^b, Alfons Baiker^c, Georgios M. Kontogeorgis^{a,*}, Jan-Dierk Grunwaldt^{d,**}

^a Department of Chemical and Biochemical Engineering, Centre for Energy Resources Engineering (CERE), Technical University of Denmark, DK-2800 Kgs. Lyngby, Denmark

^b Department of Chemical and Biochemical Engineering, Combustion and Harmful Emission Control Centre (CHEC), Technical University of Denmark, DK-2800 Kgs. Lyngby, Denmark

^c Institute for Chemical and Bioengineering, Department of Chemistry and Applied Biosciences, ETH Zurich, Hönggerberg, HCI, CH 8093 Zurich, Switzerland

^d Institute for Chemical Technology and Polymer Chemistry (ITCP) and Institute of Catalysis Research and Technology (IKFT), Karlsruhe Institute of Technology (KIT), D-76131 Karlsruhe, Germany

ARTICLE INFO

Article history:

Received 21 May 2012

Received in revised form 15 July 2012

Accepted 19 July 2012

Available online 27 July 2012

Keywords:

CO₂-2-butenal VLE

Supercritical CO₂

Selective hydrogenation

Equations of state

CPA

ABSTRACT

Knowledge of the phase behaviour and composition is of paramount importance for understanding multiphase reactions. We have investigated the effect of the phase behaviour in the palladium-catalysed selective hydrogenation of 2-butenal to saturated butanal in dense carbon dioxide. The reactions were performed using a 5 wt% Pd on activated carbon in custom-designed high pressure autoclaves at 323 K. The Cubic-Plus-Association (CPA) equation of state was employed to model the phase behaviour of the experimentally studied systems. CPA binary interaction parameters were estimated based on the experimental vapour–liquid or liquid–liquid equilibria data available in the literature. No experimental data for the CO₂-2-butenal binary system were available in the literature; therefore, the bubble points of this mixture of varying composition at three different temperatures were measured in a high-pressure view cell. The results of the catalytic experiments showed that small amounts of carbon dioxide added to the system significantly decrease the conversion, whereas at higher loadings of CO₂ the reaction rate gradually increases reaching a maximum. The CPA calculations revealed that this maximum is achieved in the so-called “expanded liquid” region, which is located near the critical point of the reacting mixture. It was also found that in this point the hydrogen concentration achieved its maximum in the CO₂-expanded phase. Furthermore, the pressure – temperature regions where the multicomponent reaction system exists in one single phase and in multiphase were calculated.

© 2012 Elsevier B.V. All rights reserved.

1. Introduction

Hydrogenation reactions in general are widely used in the chemical industry [1]. Particularly, the selective hydrogenation of α,β -unsaturated aldehydes has been extensively studied over the past decades, because the products – saturated aldehydes and α,β -unsaturated alcohols – have many applications, especially in the synthesis of various fine chemicals [2]. The scope of the present study comprises the selective hydrogenation of 2-butenal to butanal (Scheme 1). Recent findings on bifunctional catalysts have shown that it is the first step of the “one-pot” synthesis with the consecutive second step of the aldol reaction of the saturated aldehydes [3]. The present study is planned to be extended to those

systems as well, and some exploration in that direction has already been done [4–6].

In molecules of α,β -unsaturated aldehydes with two types of double bonds, C=C and C=O, the former unsaturated bond is thermodynamically more prone to hydrogenation than the latter. However, depending on the catalyst used in the process one or the other product can be selectively produced. Thus, platinum catalysts doped with different additives favours mainly C=O hydrogenation [7–15], whereas palladium catalysts are typically used for C=C hydrogenation. For example, using a 10 wt% Pd/C catalyst, 2-butenal was easily hydrogenated into butanal with almost 100% selectivity [16]. Also over 1 wt% Pd/Amberlyst-15 and 1 wt% Pd/C in carbon dioxide as reaction medium selective hydrogenation of the double bond was found [3]. Similarly, the C=C double bond in 2-hexenal is selectively converted with hydrogen on a 1 wt% Pd/Amberlyst-15 catalyst [17].

Heterogeneous catalysis combined with the use of dense and/or supercritical carbon dioxide provides additional opportunities to optimise and intensify the process [18–21]. This is particularly

* Corresponding author. Tel.: +45 45252859.

** Corresponding author. Tel.: +49 721 60842120.

E-mail addresses: gk@kt.dtu.dk (G.M. Kontogeorgis), grunwaldt@kit.edu (J.-D. Grunwaldt).

List of symbols

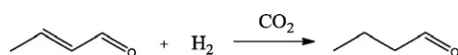
a_0	CPA fluid specific parameter
b	CPA fluid specific parameter
c_1	CPA fluid specific parameter
$g, g(\rho)$	radial distribution function
k_{ij}	binary interaction parameter
n	number of experimental points
P	pressure
P^{sat}	vapour pressure
R	gas constant
T	temperature
T_c	critical temperature
T_r	reduced temperature
V^{liq}	liquid volume
x, y	mole fraction
X_{A_i}	fraction of free sites A belonging to molecule i

Greek letters

α_0	fluid specific parameter in CPA
$\beta_{A_i B_j}$	association volume for the hydrogen bond between sites A and B belonging in molecules i and j , respectively
$\Delta^{A_i B_j}$	association strength between two sites A and B belonging in molecules i and j , respectively

interesting for gas–liquid reactions like selective hydrogenation [22,23]. Thus, it has been shown that the reaction rate of the selective hydrogenation of 2-butenal to butanal is higher in supercritical fluids than in conventional liquid phase with or without addition of a solvent [3,16,17]. Burgener *et al.* [24] studied the hydrogenation of citral in supercritical CO₂ and conventional solvents in continuous and batch reactors. It was shown that the reaction rate and selectivity were greatly influenced by the type of the reactor, solvent, total pressure, and feed composition. In many cases both conversion and selectivity in CO₂ were higher than those in conventional solvents, and both depended on the CO₂ pressure, whereas hydrogen pressure mainly accelerated the reaction rate [24]. An interesting trend was observed when different H₂: feed ratios were used. The highest conversion was observed when the system was changing from single phase to two phases at a moderate H₂ concentration. The authors claimed that these changes might be attributed to the changes in the phase behaviour of the reaction mixture. All aforementioned reactions have been performed in carbon dioxide media but the phase behaviour during the reaction progress with its changing composition was not studied systematically. Note, however, that the phase behaviour for a number of other systems has been investigated experimentally [25].

Phase behaviour plays an important role in chemical reactions in dense and/or supercritical carbon dioxide media. It is very demanding to study it experimentally, especially *in situ* during the reaction, however theoretical thermodynamic calculations may be very useful in this regard. A large number of thermodynamic models have been developed in order to predict many thermodynamic properties of mixtures, including their phase behaviour with satisfactory accuracy [26]. The challenge for applying them to catalysis is to provide examples that demonstrate that they are capable of predicting multicomponent mixtures at varying composition, as occurring during reaction.



Scheme 1. Selective hydrogenation of 2-butenal in dense carbon dioxide.

For this purpose, an advanced thermodynamic model, the Cubic-Plus-Association (CPA) equation of state [27], is used in the present study. CPA is one of the models that takes into account strong cross-association between components, i.e. hydrogen bonding; and it has been proven to be a powerful tool for predicting various properties of complex multicomponent systems at elevated temperatures and pressures [28,29]. The CPA equation of state consists of two parts – the Soave–Redlich–Kwong (SRK) equation of state and an association term based on Wertheim's first order thermodynamic perturbation theory [30]. In the case when no hydrogen-bonding components are present in the mixture, the association term vanishes and CPA reduces to the SRK functionality.

In the present reaction, all the components comprising the reaction mixture – 2-butenal, hydrogen, butanal and carbon dioxide – are non-associating, i.e. they do not form hydrogen bonds between themselves and/or each other. For such a simple system the original Soave–Redlich–Kwong equation of state might be used [31], instead of CPA. However, the original SRK uses critical temperature T_c , critical pressure P_c , and acentric factor ω as pure fluid parameters. On the other hand, the estimation of pure fluid parameters for CPA is based on experimental vapour pressure and liquid density data, which means that the temperature dependency of those important properties is captured by the model. Therefore, CPA gives better results when describing vapour pressure dependencies with temperature.

In order to account for intermolecular interactions one interaction parameter k_{ij} is typically used in the model. It is estimated on the basis of experimental vapour–liquid, liquid–liquid or vapour–liquid–liquid equilibria data (VLE, LLE or VLLE) for the binary mixtures of the components comprising the reaction system. In many cases such data are available in the literature for binary systems; however, no experimental data were found for the CO₂–2-butenal binary system. Therefore, the bubble point pressures of the CO₂–2-butenal binary mixture of various compositions at the different temperatures were measured experimentally. Based on the obtained data the binary interaction parameter of CPA for this system was estimated.

In summary, the present study aims at the following aspects: (1) the elucidation of the influence of the carbon dioxide amount on the catalyst performance, (2) the measurement of the phase equilibrium of the CO₂–2-butenal binary mixture, and finally, (3) the application of the CPA equation of state and the parameters obtained for predicting the phase equilibrium of the multicomponent reaction systems.

2. Experimental

2.1. Catalyst preparation

A 5 wt% Pd/C catalyst was prepared using the incipient wetness impregnation technique as follows. 0.1282 g of [Pd(NH₃)₄]Cl₂ (Sigma–Aldrich) as a precursor was dissolved in 1.69 ml of deionised water – the amount required for the complete impregnation of 0.988 g of activated carbon (Sigma–Aldrich, ground fraction 125–250 μm). The sample was dried at room temperature overnight, then in an oven at 373 K for 24 h, and subsequently activated in nitrogen flow containing 10 vol% of hydrogen at 383 K for 2 h. The final catalyst sample was stored in dry atmosphere.

2.2. Catalyst characterisation

The specific surface areas of the as-prepared 5 wt% Pd/C catalyst was determined using BET isotherms recorded on a BEL Japan surface area analyser at a nitrogen adsorption temperature of 77 K. The specific surface of the sample was measured to be 994 m²/g.

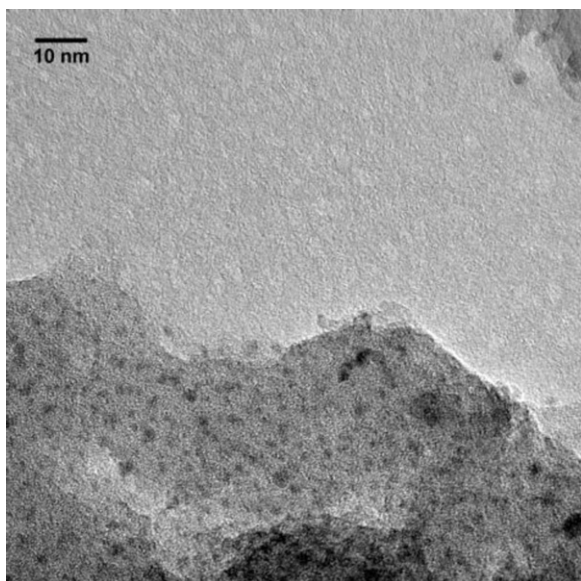


Fig. 1. Typical TEM image of 5 wt% Pd/C catalyst.

The as-prepared catalyst was analysed using X-ray diffraction (Bruker D8-Advance Diffractometer with a Cu $K\alpha$ -Anode source, $\lambda = 1.54$ nm, angle range 20 – 80° 2θ). The obtained diffractograms did not reveal any significant reflections, which indicates that the palladium particles are well dispersed and fairly small.

In order to support this finding, the transmission electron microscopy images (TEM) were obtained on a FEI Technai TEM operating at 200 kV (Centre of Electron Nanoscopy, DTU). A typical TEM image is depicted in Fig. 1. It can be seen that the palladium particles are evenly distributed on the carbon surface, and the average particle size falls below 4 nm.

Temperature-programmed reduction (TPR) of the impregnated catalyst was performed as follows: 500 mg of the fresh sample was placed into a quartz tube (10 mm in diameter) heated in flowing N_2 (air liquid, 50 ml/min) to 393 K, and held for 10 min. The tube was then cooled in flowing nitrogen to room temperature, N_2 was replaced by the carrier gas, and the TPR run was started using the following conditions: carrier gas 5 vol% H_2 in N_2 (air liquid) with a flow rate of 50 ml/min; initial temperature 308 K; ramp rate 5 K/min; and final temperature 433 K. The concentration of hydrogen was detected with a GC-14A chromatograph (Shimadzu GmbH). The TPR experiments indicate that the palladium constituent of the catalyst was reduced to metallic palladium in the temperature range 363 and 383 K.

2.3. Catalytic hydrogenation of 2-butenal

The catalyst performance was tested in the selective hydrogenation of 2-butenal using homemade stainless steel autoclaves with magnetic stirring bars ($T_{\max} = 250^\circ C$, $P_{\max} = 200$ bar, inner volume ~ 125 ml). Before use, the reactors were thoroughly washed with organic solvents and dried with compressed air. Required amounts of the catalyst and 2-butenal were loaded into the autoclaves which then were tightly closed. After that, the reactors were carefully flushed with hydrogen several times and pressurised up to the desired pressure. Hydrogen was supplied directly from the hydrogen cylinder via an interconnected reduction valve. As a next step, carbon dioxide was added using a CO_2 -compressor (NWA, PM-101, Loerrach, Germany), and its amount was measured by weighing the autoclaves before and after loading. Pressure and temperature were monitored with installed manometers and thermocouples, respectively.

After the reaction, the autoclaves were quickly cooled down to room temperature in a water bath, slowly and carefully depressurised, and opened.

Samples of the reaction mixture were taken out, diluted with toluene and analysed employing a gas chromatograph (Shimadzu, GC 2010+, polar column), which had been previously calibrated for the reactant and possible products.

All catalytic experiments were performed at least twice. The conversion of 2-butenal in two identical experiments by maximum deviated by 7% relative.

2.4. Phase behaviour measurements

Phase behaviour was visually monitored in a high pressure view cell (15–65 ml, SITEC, Switzerland) with a sapphire window (26 mm diameter). The pressure was adjusted by changing the volume of the cell by means of a screw-type manual pump. The set up principle is based on the so-called synthetic method [32], where the phase transition is directly observed through the window without taking samples. The flow chart and the set up description can be found in Ref. [33–35]. Temperature and pressure were monitored with a thermocouple and a Dynisco pressure sensor, respectively. Stirring was performed by a magnetic stirrer with a stirring bar placed inside the cell. Temperature was controlled by means of an oil-containing heating jacket connected to a thermo/cryostat.

Before every experiment the view cell was thoroughly cleaned with acetone and CO_2 , dried with an air jet, and left open heated up to 323 K in the air for a minimum of 2 h. After cooling it down to room temperature, the desired amount of 2-butenal (Aldrich, 99.8%+) was loaded into the cell. Its mass was calculated by weighing the syringe before and after loading. After charging the cell with the liquid, it was closed, tightened, and flushed slowly and carefully with gaseous CO_2 in order to substitute the air. CO_2 was added using a CO_2 -compressor (NWA, PM-101, Loerrach, Germany), and its quantity was measured by a mass flow transmitter (Rheonik Messgeraete GmbH, Germany) at a constant pressure of 100 bar, which was controlled by means of an interconnected reduction valve. The view cell was further heated up to a desired temperature and pressurised to a pressure higher than the expected bubble point pressure. At this stage the cell was left for equilibrating for at least 2 h. A first rough estimation of the bubble point was made by stepwise depressurising the system (4–6 bar). After the first bubbles appeared in the top part of the cell, it was pressurised again and left for equilibration. Small stepwise pressure drop (0.2–1 bar) with subsequent equilibration after each step was applied to determine the bubble point pressure of the specific system. Since the first bubble of gas phase usually appeared in the highest point of the cell, the latter was slightly tilted to make this point more visible. The pressure at which the first bubble of the second phase appeared was noted. All the experimental points were measured at least three times. The difference between these points was generally less than 0.2–0.4 bar, which was within the accuracy range of the pressure gauge. The temperature was measured with a precision of 0.5 K.

3. Experimental results

3.1. Catalyst performance

A series of catalytic experiments were carried out in order to investigate the influence of the carbon dioxide content on the catalytic performance. Blind tests without a catalyst were also performed, and no detectable catalytic activity was observed. The results are presented in Table 1.

The results showed that the conversion, and corresponding turnover frequency (TOF) reached a minimum when the amount

Table 1
Selective hydrogenation of 2-butenal to butanal over 5 wt% Pd/C catalyst.

Amount of CO ₂ , g	Mole ratio CO ₂ :2-butenal	Total pressure, bar	Conversion, %	TOF, h ⁻¹ ^a
0	0.0:1	22	34.3	730
4	2.3:1	34	27.6	580
10	5.7:1	50	10.7	230
28	15.9:1	70	14.6	310
34	19.3:1	98	17.1	360
45	25.6:1	111	20.2	430
60	34.1:1	126	39.1	840
70	39.8:1	138	39.7	840
82	46.6:1	150	26.6	560
92	52.3:1	185	24.6	520

Conditions: Substrate 0.04 mol, H₂:2-butenal molar ratio 2.5:1 (corresponding to a pressure of 20 bar at room temperature), $m_{\text{cat}} = 0.01$ g, temp = 323.2 K, reaction time 60 min.

^a TOF [h⁻¹] = $(n_{\text{sub}} \times \text{Conv.}) / ((m_{\text{cat}} \times \text{wt}_{\text{Pd}}) / (M_{\text{rPd}} \times t))$, where n_{sub} – amount of 2-butenal, mol; Conv. – conversion of 2-butenal, %; m_{cat} – catalyst mass, g; wt_{Pd} – palladium loading, wt%; M_{rPd} – molecular weight of Pd, g/mol; t – time, h.

of carbon dioxide approached 10 g, i.e. when the mole ratio CO₂:2-butenal was 5.7:1. When this ratio was increased, the conversion also went up reaching a maximum of almost 40% at a mole ratio CO₂: substrate of 35–40:1. The total pressure of the reaction system, however, was almost linearly dependent on the amount of CO₂ used in the reaction. Note that in the present case the turnover frequency was referred to the total number of Pd atoms: in reality only the surface palladium atoms or even special sites will contribute to the reaction.

3.2. Phase behaviour measurements

The bubble point pressures for the CO₂–2-butenal binary mixture at four different compositions were measured at three different temperatures using the aforementioned setup and experimental procedure. The results are presented in Table 2.

4. Modelling with the CPA equation of state

Modelling of the reaction mixture, also during the progress of the reaction, was based here on the CPA EoS which combines the classical Soave–Redlich–Kwong (SRK) equation of state with an advanced association term [27]. The CPA EoS can be expressed for mixtures in terms of pressure P as follows [26]:

$$P = \frac{RT}{v_m - b} - \frac{a_0 [1 + c_1 (1 - \sqrt{T_r})]^2}{v_m (v_m + b)} - \frac{1}{2} \frac{RT}{v_m} \left(1 + \rho \frac{\partial \ln g}{\partial \rho} \right) \sum_i x_i \sum_{A_i} (1 - X_{A_i}) \quad (1)$$

The key element in the association term is X_{A_i} – the fraction of sites type A on molecule i that do not form hydrogen bonds with other active sites. It is related to the association strength $\Delta^{A_i B_j}$ between two sites belonging to two different molecules, e.g. site A

Table 2
Experimental bubble point pressures for CO₂–2-butenal.

CO ₂ mole fraction	Pressure, bar		
	313.2 K	331.9 K	350.2 K
0.3899	28.8	38.2	48.4
0.4580	34.9	46.5	59.2
0.5429	41.5	55.2	70.3
0.7081	57.4	77.6	98.8

on molecule i and site B on molecule j . This parameter is determined from:

$$X_{A_i} = \frac{1}{1 + \rho \sum_j x_j \sum_B B_j x_{B_j} \Delta^{A_i B_j}} \quad (2)$$

The association strength $\Delta^{A_i B_j}$, in its turn, can be expressed as:

$$\Delta^{A_i B_j} = g(\rho) \left[\exp \left(\frac{\varepsilon^{A_i B_j}}{RT} \right) - 1 \right] b_{ij} \beta^{A_i B_j} \quad (3)$$

where $g(\rho) = 1/1 - 1.9(b\rho/4)$ – the radial distribution function, while $b_{ij} = (b_i + b_j)/2$. b_i is the temperature independent co-volume parameter of the component i , and ρ is the molar density. $T_r = T/T_c$ is the reduced temperature, and T_c is the experimental critical temperature.

In the expression for the association term (Eq. (3)), the parameters $\varepsilon^{A_i B_j}$ and $\beta^{A_i B_j}$ are called the association energy and association volume, respectively. These two parameters are only used for associating components, and together with the three additional parameters from the SRK part (a_0 , b , c_1) are the five pure fluid parameters of the CPA model.

When the CPA is used for mixtures, the conventional mixing rules are employed in the physical term (SRK) for the energy and co-volume parameters. The geometric mean rule is used for the energy parameter a_{ij} . The interaction parameter k_{ij} is the only binary adjustable parameter of CPA:

$$a = \sum_i \sum_j x_i x_j a_{ij}, \text{ where } a_{ij} = \sqrt{a_i a_j} (1 - k_{ij}) \quad (4)$$

$$b = \sum_i x_i b_i \quad (5)$$

4.1. Pure fluids

The CPA pure fluid parameters (a_0 , b , c_1) were estimated using saturated liquid density V^{liq} and vapour pressure P^{sat} data from DIPPR [36] or, when it was possible, they were obtained from the literature (Table 3). Due to the fact that all the components are non-associating, the association energy and volume ($\varepsilon^{A_i B_j}$ and $\beta^{A_i B_j}$) are equal to zero. The pure fluid parameters are presented in Table 3.

4.2. Binary mixtures

The reaction mixture consists of four components (CO₂, hydrogen, 2-butenal, and butanal) therefore, six interaction parameters are required for the six binaries occurring in the system. As it was previously mentioned, for estimating k_{ij} parameters some experimental data are required.

Unfortunately, the experimental data were not available for all the binaries, specifically, for the binaries with 2-butenal no data were found in the literature. However, due to the strong similarities between the structure of 2-butenal and butanal, the following assumptions were made: (1) the k_{ij} for the hydrogen–2-butenal binary was assumed to be equal to that of hydrogen–butanal, and (2) for the 2-butenal–butanal system k_{ij} was set to zero. The binary interaction parameters are presented in Table 4.

The CPA model describes quite satisfactorily the phase behaviour of the CO₂–hydrogen binary mixture, however, slight deviations between the model predictions and experimental data are observed at higher hydrogen concentrations, as shown in Fig. 2.

For the CO₂–butanal binary mixture a temperature independent k_{ij} parameter was estimated based on the experimental VLE data. The first attempt to measure and predict the phase behaviour of this system was made by da Silva et al. [37]. In their work the authors used the SRK and Peng–Robinson (PR) equations of state, in both cases employing the quadratic mixing rules with two

Table 3
CPA parameters for pure fluids.

T_c , K	a_0 , L ² bar mol ⁻²	b , L mol ⁻¹	c_1	%AAD ^a in P^{sat}	%AAD in V^{liq}	Ref.
Carbon dioxide ($T_m - 0.9T_c$) 304.2	3.5079	0.0272	0.7602	0.2	0.8	[47]
Hydrogen ($0.5T_c - 0.9T_c$) 33.19	0.2664	0.0194	0.0474	1.6	4.4	This work
2-Butenal ($0.4T_c - 0.9T_c$) 565.0	18.9939	0.0728	0.8140	4.8	1.9	This work
Butanal ($0.4T_c - 0.9T_c$) 537.2	16.6777	0.0758	0.8803	2.2	0.8	This work

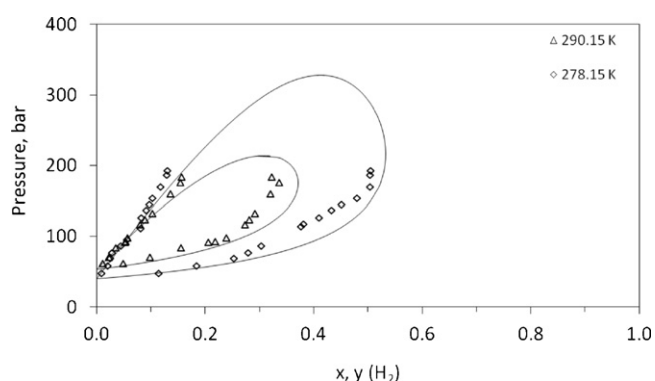
^a %AAD = $\frac{1}{n} \sum_i \left| \frac{X_i^{cal} - X_i^{exp}}{X_i^{exp}} \right| \times 100$, where X stands for P^{sat} or V^{liq} and n is the number of experimental data points.

Table 4
CPA binary interaction parameters for binary mixtures. All k_{ij} are independent of temperature.

System	Temperature range, K	k_{ij}	%AAD in P	%AAD in y_1	Data ref.
CO ₂ -H ₂	278.15–290.15	-0.0323	6.9	17.9	[48]
CO ₂ -butanal	303.2–313.2	-0.2859	10.0	0.6	[37]
CO ₂ -2-butenal	313.2–350.2	-0.0180	1.4	– ^a	This work
H ₂ -butanal	293.15–393.15	-0.0436	7.3	– ^a	[49]
H ₂ -2-butenal	–	-0.0436 ^b	–	–	No lit. data
2-Butenal-butanal	–	0	–	–	No lit. data

^a Calculations based on experimental P - x - T data, therefore, %AAD in y_1 were not estimated.

^b The interaction parameter for this binary mixture is set equal to the interaction parameter of the H₂-butanal binary.

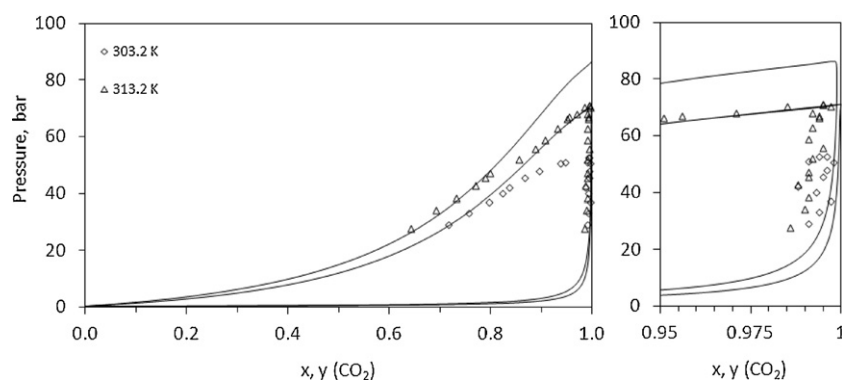
**Fig. 2.** Hydrogen-CO₂ VLE. Experimental data (points) at different temperatures and CPA calculations (lines) with a temperature independent $k_{ij} = -0.0323$.

adjustable parameters, i.e. k_{ij} for the energy parameter and l_{ij} for the co-volume. The authors report that the employed equations of state quite accurately described the experimental data. However, at higher concentrations of carbon dioxide in the mixture (0.9–1.0

CO₂ molar fraction) a large difference between the model prediction and experimental data is observed. This might be due to the fact that the experimental data in this range are not accurate enough. One of the sets of data was measured at a temperature of 303.2 K, which is very close to the critical temperature of pure CO₂ (304.2 K [36]). This means that at high concentrations of CO₂ the vapour pressure of the mixtures should be close to its critical pressure (73.83 bar [36]), however, it is nearly 20 bar lower than that. Moreover, the second data set was measured at 313.2 K, which is 9 K higher than the critical point of CO₂, but the vapour pressures of the mixtures with a significant excess of CO₂ are still lower than its critical pressure.

Note, however, that the CPA model predictions account for this behaviour and show reasonable vapour pressures for the CO₂-rich mixtures. This is due to the fact that the CPA pure fluid parameters are fitted to the pure compound vapour pressure. In the present work only one adjustable parameter k_{ij} is considered for the CO₂-butanal binary, as shown in Fig. 3.

The temperature independent binary interaction parameter was estimated for the CO₂-2-butenal system based on the P - x - T experimental data obtained in the present study. The CPA model

**Fig. 3.** CO₂-butanal VLE. Experimental data (points) at different temperatures and CPA calculations (lines) with a temperature independent $k_{ij} = -0.2859$. On the right: carbon dioxide-butanal VLE in the CO₂-rich region.

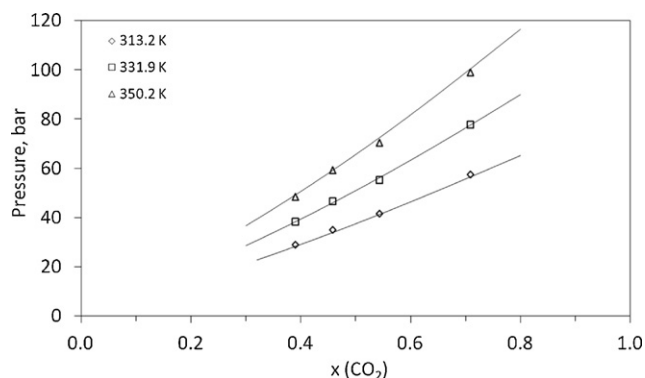


Fig. 4. CO₂–2-butenal VLE. Experimental data (points) at different temperatures and CPA calculations (lines) with a temperature independent $k_{ij} = -0.0180$.

predictions are in good agreement with the bubble point pressures of the binary mixtures of different composition at three different temperatures, as shown in Fig. 4.

The phase behaviour of CO₂–2-butenal resembles that of the CO₂–butanal binary mixture. However, the vapour pressures of the CO₂ binaries with butanal are lower than those with 2-butenal at the same composition. This might be explained by the fact that 2-butenal is more polar than butanal, dipole moment 3.66 versus 2.72 D, respectively [36]. Carbon dioxide, in turn, is a non-polar compound, and therefore, less polar components, such as butanal, are more soluble in it, which explains the lower vapour pressures of binary mixtures.

The k_{ij} parameter for the hydrogen–butanal system was estimated using available P – x – T data at different temperatures. The H₂–butanal mixture had been previously investigated by Ke et al. [38], where the authors used the Peng–Robinson equation of state which required a temperature dependent k_{ij} . However, due to its small value they set it to zero in their further calculations. When using the CPA model one temperature independent parameter is sufficient, as shown in Fig. 5. Again, due to the similarity of CPA with SRK for non-associating components, this improvement is attributed to the inclusion of vapour pressure data in the pure compound parameter estimation.

4.3. CPA predictions for the multicomponent reaction system

The catalytic results have shown that the conversion of 2-butenal is dependent on the amount of CO₂ loaded into the reactor (Table 1). There are multiple effects caused by the addition of CO₂ to the system. Firstly, the more carbon dioxide is used in a batch autoclave the higher the reaction pressure. The partial pressures of the reacting components, however, do not change and, therefore, the thermodynamic equilibrium is not affected by the increasing pressure, as seen in Scheme 1. What possibly happens is that the amount

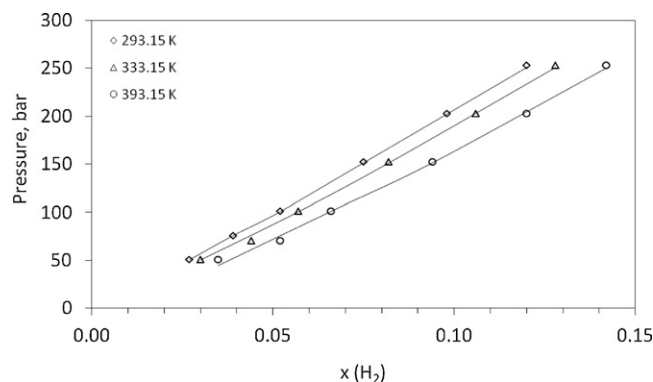


Fig. 5. Hydrogen–butanal VLE. Experimental data (points) at different temperatures and CPA calculations (lines) with a temperature independent interaction parameter $k_{ij} = -0.0436$.

of CO₂ determines the number and composition of the phases co-existing in the reactor as well as the dissolution power of hydrogen in the CO₂–expanded liquid reactant phase. The liquid (or more general, the denser phase) is of particular interest, because it is in direct contact with the solid catalyst at the bottom of the autoclave and, therefore, the reaction occurs in this dense fluid. In order to determine the initial concentrations of the components in the 2-butenal hydrogenation reaction, the CPA equation of state together with the binary interaction parameters estimated in the present work were used. The concentrations of the components and the number of phases present in the reactor before reaction are presented in Table 5 and underline the presence of a CO₂–expanded reactant phase. The amount of CO₂ increases with pressure, whereas for hydrogen in only increases between 70 and 138 bar.

Table 5 shows that in most cases the reaction started at biphasic conditions and only when a large excess of CO₂ was used, the reaction ran in the single phase regime.

However, at this point another question arises, i.e. whether the number of phases changes as the reaction proceeds. In this regard, P – T regions where the multicomponent reaction mixture exists in one or two phases depending on the conversion were calculated with CPA. It was assumed that the mole ratio of the components in the initial mixture was CO₂:H₂:2-butenal = 25:2.5:1. No conversion, 20, 40, 60, 80% and full conversion were considered. The corresponding compositions of the mixtures are presented in Table 6, and the obtained P – T diagrams are shown in Fig. 6. According to this figure and the phase behaviour calculations, if the mentioned above initial reaction mixture starts to react, for instance, at 313 K and 175 bar, it means that before the reaction ($t = 0$) it exists in one single phase, and it will stay in one phase even after all 2-butenal has converted. If the reaction occurs under the same conditions but at a pressure in the system of around 130 bar, the predictions imply that the initial system is bi-phasic, however,

Table 5
Phase composition of the reaction mixture before reaction.

T, K	P, bar	Feed composition, mol			Number of phases	Composition of the liquid (dense) phase, mole fraction		
		CO ₂	H ₂	2-Butenal		CO ₂	H ₂	2-Butenal
323	22	0.00	0.1	0.04	2	0.000	0.007	0.993
323	34	0.09	0.1	0.04	2	0.178	0.006	0.816
323	50	0.23	0.1	0.04	2	0.367	0.006	0.627
323	70	0.64	0.1	0.04	2	0.604	0.006	0.390
323	98	0.77	0.1	0.04	2	0.770	0.014	0.216
323	111	1.02	0.1	0.04	2	0.817	0.021	0.162
323	126	1.36	0.1	0.04	2	0.911	0.043	0.045
323	138	1.59	0.1	0.04	1	0.919	0.057	0.024
323	150	1.86	0.1	0.04	1	0.930	0.050	0.020
323	185	2.09	0.1	0.04	1	0.937	0.045	0.018

Table 6

Composition of a reaction mixture with a ratio CO₂:H₂:2-butenal:butanal at different conversion.

Mixture	Conversion, %	Composition of the reaction mixture, mol			
		CO ₂	H ₂	2-Butenal	Butanal
1	0	25	2.5	1.0	0
2	20	25	2.3	0.8	0.2
3	40	25	2.1	0.6	0.4
4	60	25	1.9	0.4	0.6
5	80	25	1.7	0.2	0.8
6	100	25	1.5	0.0	1.0

as the reaction proceeds, at some point the phase transition will occur and the system will become mono-phasic. Finally, if the reaction pressure is 90 bar, the reaction will begin in the two phase region and it will stay like this even after all substrate has reacted.

5. Discussion

The results of the catalytic studies (Table 1) show that the presence of small amounts of carbon dioxide in the reacting system deteriorates catalytic performance; however, higher amounts of carbon dioxide added to the system leads to higher conversion. As mentioned above, this might be due to the concentration and phase behaviour effects arising when more CO₂ is added to the system. The calculations performed with CPA show that the amount of CO₂ used in the reaction determines the number of phases, their composition and total pressure in the reaction, as shown in Table 5.

Most of the time, the reactions occurred in the biphasic region. This means that the initial reaction kinetics was determined by the initial concentrations of the components in the liquid phase, which is in direct contact with the catalyst. The reaction pathway in the biphasic region might be easily impeded by mass transfer limitations, i.e. diffusion of the components (particularly hydrogen) from the gas phase to the liquid and further to the catalyst surface. Under single phase conditions, the concentration of all the components was constant in the whole volume of the reaction mixture due to intense stirring, therefore, possible external mass transfer limitations were minimised. However, as it was shown by the calculations the maximum catalyst activity was observed at a CO₂:2-butenal ratio near the critical point of the reaction mixture, where the phase transition occurred. Further dilution of the system with CO₂ caused a decrease of catalytic activity. In other words, even though the reaction conditions were in favour of higher conversion, i.e. minimised mass transfer effects, the opposite was observed.

A similar observation was made by Burgener et al. [24], where they found that at higher hydrogen concentrations the

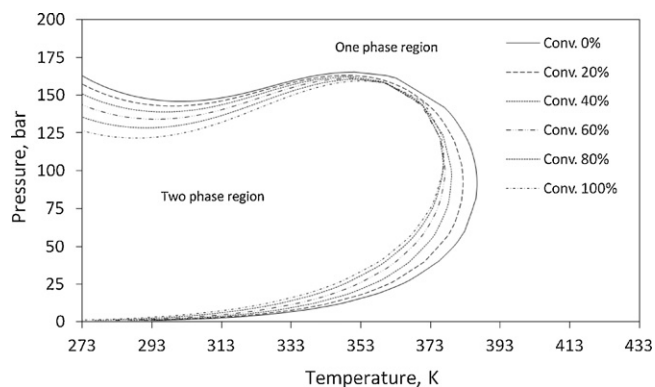


Fig. 6. CPA predictions of the bubble and dew point curves for the reaction mixtures during the selective hydrogenation of 2-butenal in carbon dioxide. The composition of every mixture is shown in Table 6.

catalytic performance decreased, which was against the expectation from reaction thermodynamics and kinetics. A significant change occurred when the system moved to an “expanded liquid” where maximal conversion was obtained. Unlike in the present study, this phase transition occurred due to the fact that hydrogen decreased the dissolution power of carbon dioxide, and as a consequence, the one phase system split into two phases. Furthermore, in an earlier study by Tschan et al. [39], the authors investigated the selective semi-hydrogenation of propargyl alcohol in supercritical carbon dioxide. They concluded that in the two phase region excessive amounts of hydrogen are required in order to maintain a sufficient supply through the liquid layer to the catalyst surface, whereas when working in a single phase lower hydrogen concentrations are needed for the selective semi-hydrogenation of propargyl alcohol due to the minimised mass transport limitations. In both studies the concentrations of hydrogen in the reaction phase was speculated to be crucial.

In the present study, thermodynamic calculations were used to provide insight into the behaviour during the hydrogenation of 2-butenal. Table 5 suggests that the concentration of 2-butenal gradually decreased when more CO₂ was added to the system, whereas the concentration of hydrogen was more or less stable at the very beginning and after a certain point it started to rise to the point where the phase transition occurred, as shown in Fig. 7. At this point the concentration of hydrogen in the dense layer was maximal, and then it started to decrease gradually. The maximum concentration of hydrogen coincides with the maximum catalytic activity. Interestingly, only C=C-hydrogenation and not carbonyl hydrogenation was observed despite the group of Arai and co-workers [40,41] have shown that there is a strong interaction between CO₂ and unsaturated aldehydes such as cinnamaldehyde, which affects the selectivity. Therefore, due to the fact that the concentration of 2-butenal was decreasing at the beginning while the concentration of hydrogen in the liquid layer was constant the reaction rate was decreasing as well. After the point where the concentration of hydrogen started to increase, the reaction rate increased as well. These observations are in line with the conclusions for the abovementioned reactions studied by Burgener et al. [24] and Tschan et al. [39]. Fig. 7 further shows that in the one phase region the concentration of hydrogen decreases while the concentration of the substrate stays almost unchanged; thereby possibly explaining the decrease in the catalytic activity. Furthermore, the excessive amounts of carbon dioxide at high reaction pressures may

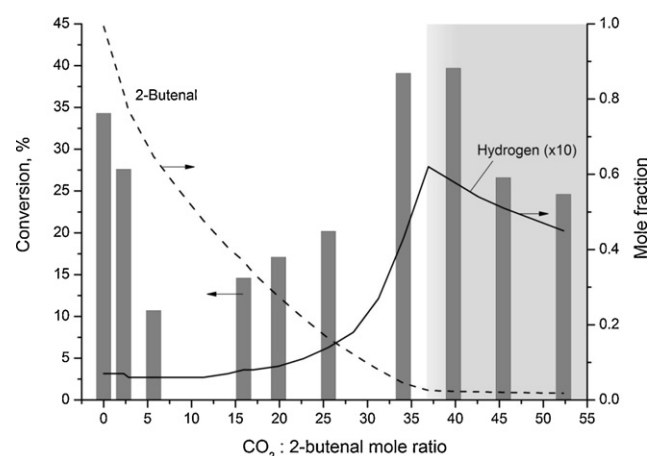


Fig. 7. Mole fractions (CPA lines) of hydrogen and 2-butenal in the liquid (dense) phase which is in contact with the catalyst and conversion of 2-butenal (bars) depending on the initial CO₂:2-butenal mole ratio. Conditions: 2-butenal 0.04 mol, H₂:2-butenal mole ratio 2.5:1, $m_{\text{cat}} = 0.01$ g, $T = 323.2$ K, reaction time 60 min. Shaded area – one phase region.

cause its strong adsorption on the catalyst surface, which competes with the adsorption of hydrogen and 2-butenal. In addition, both Zhao et al. [42] and Burgener et al. [43] found reaction of CO₂ and hydrogen under single phase conditions on noble metal particles.

Further CPA calculations of the *P*–*T* regions of co-existing phases (Fig. 6) showed that the system phase transition at a constant temperature and elevated pressures decreases towards lower pressures as the reaction proceeds. This means that if the initial reaction mixture (at *t* = 0) was in a single phase it stayed in one phase even after all the 2-butenal had reacted. However, depending on the composition, *T* and *P*, in some cases the reaction may begin in the two phase region, but at a certain conversion the phase transition may occur and the system will become single phase. These changes of the phase behaviour as a result of concentration changes during reaction have to be considered for proper interpretation of reaction kinetics and the CPA calculations proved to be an elegant tool for this task.

Usually, carbon dioxide is considered as an inert reaction medium, however, some recent findings revealed that under certain conditions, i.e. in the presence of hydrogen and noble metals already at relatively low temperatures, CO₂ can react with hydrogen in the so-called reverse water–gas shift reaction and form carbon monoxide and water [43,44]. The former acts as catalyst poison especially for low coordinated metal sites [45], and thereby sometimes changes the catalyst selectivity [46]. Despite poisoning by CO might be the case in the present study, this is hardly the main reason because of the too strong drop in conversion when excessively large amounts of CO₂ were used. As it was pointed out by Burgener et al. [43], the reverse water–gas shift reaction takes place in many hydrogenation reactions and under hydrogenation conditions metal surfaces are partially covered with CO, however, this effect is mostly restricted to low coordinated Pt-sites.

Another type of intermolecular interactions can play an important role when reactions are performed in scCO₂. Carbon dioxide, possessing electron-accepting properties, can easily interact with other functional groups in organic molecules, such as aldehydes, ketones, esters, etc. Such interactions and their pressure dependency have been studied using high-pressure FT-infrared spectroscopy [40,41]. It was found that CO₂ is capable of activating of carbonyl groups in organic aldehydes and this effect is different for saturated and unsaturated ones [41]. Thus, in the hydrogenation of benzaldehyde the conversion into benzyl alcohol is merely decreasing with increasing CO₂ pressure due to dilution of the system, whereas for cinnamaldehyde conversion reaches a maximum. The authors attribute it to the activation of C=O bond in cinnamaldehyde by CO₂ at low pressures, and at elevated pressures this effect disappears and conversion decreases due to the dilution of the system. Despite in the present study another type of hydrogenation is relevant, i.e. C=C bond saturation, the presence of intermolecular forces between CO₂ and aldehydes is indirectly indicated by binary interaction parameters *k*_{ij} (Table 4), which is attributed to the non-ideality of the binary systems. The significance of such interactions is that they determine the phase behaviour of the system, which in turn determines the catalyst performance as it was discussed above.

6. Conclusion

The influence of the phase behaviour on the palladium-catalysed selective hydrogenation of 2-butenal to butanal was investigated. For this purpose the CPA equation of state was successfully used and directly provided a correlation between the concentrations of the reactants in the fluid phase and the reaction rate. The interaction parameters for three binaries were estimated using

experimental data from the literature. The binary mixture carbon dioxide–2-butenal was experimentally studied in order to find the bubble point pressures at different temperatures. Based on this experimental data the binary interaction parameter was obtained.

The CPA model is shown to be a powerful tool allowing thermodynamic calculations with high precision and accuracy. Using CPA the number of co-existing phases was predicted, and the concentrations of the reacting components in coexisting phases were calculated. These data are very important and useful for further kinetic studies where knowledge of concentrations in individual phases is a key element.

Furthermore, calculations using CPA gave insight into the phase behaviour during the reaction, showing that the pressures and temperatures at which a one phase region exists are decreasing as the reaction proceeds.

The catalytic studies showed that maximum conversion was achieved when the reaction mixture changed from one-phase to the two-phase regions, near the critical point of the system. The concentrations of the components in the reaction mixture, calculated with CPA, were shown to cause such behaviour.

Acknowledgements

The authors are grateful for financial support from the Technical University of Denmark (DTU), The Danish Research Council for Technology and Production Sciences, Institute of Catalysis Research and Technology (IKFT) at Karlsruhe Institute of Technology (KIT), where all the catalytic experiments were performed, and also ETH Zurich, Institute for Chemical and Bioengineering, Department of Chemistry and Applied Biosciences, where the phase behaviour measurements were carried out. Centre for Electron Nanoscopy (DTU-CEN) is acknowledged for providing TEM images. Furthermore, Dr. Wolfgang Kleist, Dr. Loubna Gharnati, and Dr. Matthias J. Beier are acknowledged for their help and support in building-up experimental setups and performing the experiments. Dr. Ioannis Tsivintzelis is acknowledged for his help with the thermodynamic calculations. Many calculations presented in this study were made using SPECS software – a program for phase equilibrium calculations developed at the Center for Energy Resources Engineering (CERE), Department of Chemical and Biochemical Engineering, Technical University of Denmark.

References

- [1] B. Chen, U. Dingerdissen, J.G.E. Krauter, H.G.J.L. Rotgerink, K. Mobus, D.J. Ostgard, P. Panster, T.H. Riermeier, S. Seebald, T. Tacke, H. Trauthwein, *Appl. Catal. A* 280 (2005) 17–46.
- [2] P. Gallezot, D. Richard, *Catal. Rev.: Sci. Eng.* 40 (1998) 81–126.
- [3] T. Seki, J.D. Grunwaldt, A. Baiker, *Chem. Commun.* (2007) 3562–3564.
- [4] N.E. Musko, J.D. Grunwaldt, *Top. Catal.* 54 (2011) 1115–1123.
- [5] J.G. Stevens, R.A. Bourne, M. Poliakoff, *Green Chem.* 11 (2009) 409–416.
- [6] K. Matsui, H. Kawanami, Y. Ikushima, H. Hayashi, *Chem. Commun.* (2003) 2502–2503.
- [7] L. Tian, Q.Y. Yang, Z. Jiang, Y. Zhu, Y. Pei, M.H. Qiao, K.N. Fan, *Chem. Commun.* 47 (2011) 6168–6170.
- [8] E. Gebauer-Henke, J. Farbotko, R. Touroude, J. Rynkowski, *Kinet. Catal.* 49 (2008) 574–580.
- [9] A.M. Ruppert, T. Paryjczak, *Appl. Catal. A* 320 (2007) 80–90.
- [10] B.A. Riguetto, C.E.C. Rodrigues, M.A. Morales, E. Baggio-Saitovitch, L. Gengembre, E. Payen, C.M.P. Marques, J.M.C. Bueno, *Appl. Catal. A* 318 (2007) 70–78.
- [11] J.C.S. Wu, T.S. Cheng, C.L. Lai, *Appl. Catal. A* 314 (2006) 233–239.
- [12] W.X. Tu, H.F. Liu, *Chin. J. Polym. Sci.* 23 (2005) 487–495.
- [13] F. Ammari, J. Lamotte, R. Touroude, *J. Catal.* 221 (2004) 32–42.
- [14] M. Abid, G. Ehret, R. Touroude, *Appl. Catal. A* 217 (2001) 219–229.
- [15] B.M. Bhanage, Y. Ikushima, M. Shirai, M. Arai, *Catal. Lett.* 62 (1999) 175–177.
- [16] F. Zhao, Y. Ikushima, M. Chatterjee, M. Shirai, M. Arai, *Green Chem.* 5 (2003) 76–79.
- [17] T. Seki, J.D. Grunwaldt, N. van Vegten, A. Baiker, *Adv. Synth. Catal.* 350 (2008) 691–705.
- [18] A. Baiker, *Chem. Rev.* 99 (1999) 453–473.

- [19] W. Leitner, P.G. Jessop, *Chemical Synthesis Using Supercritical Fluids*, Wiley-VCH, 1999.
- [20] C.A. Eckert, D. Bush, J.S. Brown, C.L. Liotta, *Ind. Eng. Chem. Res.* 39 (2000) 4615–4621.
- [21] X. Han, M. Poliakov, *Chem. Soc. Rev.* 41 (2012) 1428–1436.
- [22] T. Seki, J.D. Grunwaldt, A. Baiker, *Ind. Eng. Chem. Res.* 47 (2008) 4561–4585.
- [23] J.R. Hyde, P. Licence, D. Carter, M. Poliakov, *Appl. Catal. A* 222 (2001) 119–131.
- [24] M. Burgener, R. Furrer, T. Mallat, A. Baiker, *Appl. Catal. A* 268 (2004) 1–8.
- [25] J.D. Grunwaldt, R. Wandeler, A. Baiker, *Catal. Rev.: Sci. Eng.* 45 (2003) 1–96.
- [26] G.M. Kontogeorgis, G.K. Folas, *Thermodynamic Models for Industrial Applications: From Classical And Advanced Mixing Rules to Association Theories*, Wiley, 2010.
- [27] G.M. Kontogeorgis, E.C. Voutsas, I.V. Yakoumis, D.P. Tassios, *Ind. Eng. Chem. Res.* 35 (1996) 4310–4318.
- [28] G.M. Kontogeorgis, M.L. Michelsen, G.K. Folas, S. Derawi, N. von Solms, E.H. Stenby, *Ind. Eng. Chem. Res.* 45 (2006) 4855–4868.
- [29] G.M. Kontogeorgis, M.L. Michelsen, G.K. Folas, S. Derawi, N. von Solms, E.H. Stenby, *Ind. Eng. Chem. Res.* 45 (2006) 4869–4878.
- [30] M.S. Wertheim, *J. Stat. Phys.* 42 (1986) 477–492.
- [31] G. Soave, *Chem. Eng. Sci.* 27 (1972) 1197–1203.
- [32] R. Dohrn, S. Peper, J.M.S. Fonseca, *Fluid Phase Equilib.* 288 (2010) 1–54.
- [33] C. Crampon, G. Charbit, E. Neau, *J. Supercrit. Fluids* 16 (1999) 11–20.
- [34] I. Tsivintzelis, M.J. Beier, J.D. Grunwaldt, A. Baiker, G.M. Kontogeorgis, *Fluid Phase Equilib.* 302 (2011) 83–92.
- [35] R. Wandeler, N. Kunzle, M.S. Schneider, T. Mallat, A. Baiker, *J. Catal.* 200 (2001) 377–388.
- [36] D. DIADEM, *The DIPPR Information and Data Evaluation Manager for the Design Institute for Physical Properties*, 2006, Version 1.1.0.
- [37] M.V. da Silva, D. Barbosa, *Ind. Eng. Chem. Res.* 39 (2000) 4427–4430.
- [38] J. Ke, B.X. Han, M.W. George, H.K. Yan, M. Poliakov, *J. Am. Chem. Soc.* 123 (2001) 3661–3670.
- [39] R. Tschan, R. Wandeler, M.S. Schneider, M. Burgener, M.M. Schubert, A. Baiker, *Appl. Catal. A* 223 (2002) 173–185.
- [40] F. Zhao, S. Fujita, S. Akihara, M. Arai, *J. Phys. Chem. A* 109 (2005) 4419–4424.
- [41] Y. Akiyama, S. Fujita, H. Senboku, C.M. Rayner, S.A. Brough, M. Arai, *J. Supercrit. Fluids* 46 (2008) 197–205.
- [42] F. Zhao, Y. Ikushima, M. Arai, *J. Catal.* 224 (2004) 479–483.
- [43] M. Burgener, D. Ferri, J.-D. Grunwaldt, T. Mallat, A. Baiker, *J. Phys. Chem. B* 109 (2005) 16794–16800.
- [44] D. Ferri, T. Buergi, A. Baiker, *Phys. Chem. Chem. Phys.* 4 (2002) 2667–2672.
- [45] B. Minder, T. Mallat, K.H. Pickel, K. Steiner, A. Baiker, *Catal. Lett.* 34 (1995) 1–9.
- [46] S. Ichikawa, M. Tada, Y. Iwasawa, T. Ikariya, *Chem. Commun.* (2005) 924–926.
- [47] I. Tsivintzelis, G.M. Kontogeorgis, M.L. Michelsen, E.H. Stenby, *Fluid Phase Equilib.* 306 (2011) 38–56.
- [48] K. Bezahtak, G.B. Combes, F. Dehghani, N.R. Foster, D.L. Tomasko, *J. Chem. Eng. Data* 47 (2002) 161–168.
- [49] I.I. Vasileva, A.A. Naumova, A.A. Polyakov, T.N. Tyvina, V.V. Fokina, *J. Appl. Chem.-USSR*. 62 (1989) 1755–1757.